V. Faye McNeill
Parisa A. Ariya   *Editors*

Atmospheric and Aerosol Chemistry

**339
Topics in Current Chemistry**

Aims and Scope

The series Topics in Current Chemistry presents critical reviews of the present and future trends in modern chemical research. The scope of coverage includes all areas of chemical science including the interfaces with related disciplines such as biology, medicine and materials science.

The goal of each thematic volume is to give the non-specialist reader, whether at the university or in industry, a comprehensive overview of an area where new insights are emerging that are of interest to larger scientific audience.

Thus each review within the volume critically surveys one aspect of that topic and places it within the context of the volume as a whole. The most significant developments of the last 5 to 10 years should be presented. A description of the laboratory procedures involved is often useful to the reader. The coverage should not be exhaustive in data, but should rather be conceptual, concentrating on the methodological thinking that will allow the non-specialist reader to understand the information presented.

Discussion of possible future research directions in the area is welcome.

Review articles for the individual volumes are invited by the volume editors.

Readership: research chemists at universities or in industry, graduate students.

V. Faye McNeill · Parisa A. Ariya
Editors

Atmospheric and Aerosol Chemistry

With contributions by

M. Ammann · P.A. Ariya · T. Bartels-Rausch · B. D'Anna ·
D.J. Donaldson · N.M. Donahue · N. Eltouny · V. Faye ·
C. George · D. Heard · H. Herrmann · E.D. Hudson ·
V. Kanthasamy · G. Kos · J.H. Kroll · V.F. McNeill ·
R. Mortazavi · I. Riipinen · A.L. Robinson · N. Sareen ·
A.N. Schwier · J. Sun · D. Stone · E.R. Trump · V. Vaida ·
C. Weller · L. Whalley · C. Wilde

Springer

Editors
V. Faye McNeill
Department of Chemical Engineering
Columbia University
New York
USA

Parisa A. Ariya
Department of Chemistry and
   Department of Atmospheric and
   Oceanic Sciences
McGill University
Montreal
Québec
Canada

Printed on acid-free paper

Preface

Understanding and mitigating the effects of human activities on air quality and the earth's climate are among the most significant challenges facing mankind today and for future generations. A detailed understanding of the mechanisms of atmospheric chemistry, and the physical and chemical processes leading to aerosol and cloud formation, is necessary for accurate predictions of future air quality and climate. Steps towards mitigation of pollutants at the source set the stage for smart policy decisions. Some of the field's leaders in atmospheric chemistry, in both the gas and the aerosol phases, provide insights in this volume of *Topics in Current Chemistry*.

Sunlight, and specifically its ability to break several chemical bonds, is the major driving force of atmospheric chemistry, normally through generation of reactive radicals. In their chapter "Emerging Areas in Atmospheric Photochemistry," George and co-authors review new concepts in long-wavelength photochemistry in the gas phase, in condensed phases, and at environmental interfaces.

Isoprene emissions are the highest among all non-methane hydrocarbons. Their chemistry is critical for predicting atmospheric oxidant levels as well as organic aerosol loadings. Heard et al. in their chapter "New Insights into the Tropospheric Oxidation of Isoprene: Combining Field Measurements, Laboratory Studies, Chemical Modelling, and Quantum Theory" review recent advances in our understanding of the chemistry of isoprene in remote areas (i.e., regions of low NO_x) driven by surprising observations in the field.

Understanding aerosol volatility, i.e., the partitioning of chemical species between the gas and particulate phases, is important in order to determine atmospheric aerosol loadings accurately. The volatility of organic aerosol species evolves throughout the aerosol's lifetime due to chemical "aging" in the oxidizing environment of the atmosphere. Likewise, the phase of an organic species influences the rate and mechanisms of oxidative aging. In their chapter, Donahue and coauthors review the principles behind the linkages between "Volatility and Aging of Atmospheric Organic Aerosol."

One of the major predicaments of evaluation of the physical–chemical transformations of chemicals in the earth's atmosphere is their characterization at very low

detection limits. Bio-organic chemicals are ubiquitous in the earth's atmosphere and at air–snow interfaces. Besides impacts on the oxidative potential of the atmosphere, aerosol–cloud interactions, and radiation, airborne biological substances play various roles in the transmission of disease in humans and in ecosystems, and are linked to bio-terrorism. Ariya et al. explore existing techniques and methods applicable to the physical characterization of bio-organic matter, and which provide information on gases, liquids, and aerosols in the atmosphere and at snow–air interfaces. They evaluate their strengths and weaknesses, and foresee future directions in the domain.

Atmospheric aerosol particles serve an important role in establishing the climate and in the hydrological cycle as nuclei in the formation of cloud droplets. The relationship between an aerosol particle's chemical composition and its ability to serve as a cloud condensation nucleus (CCN) is complex. Organic material, a ubiquitous component of tropospheric aerosols, is typically more hydrophobic and less hygroscopic, and therefore less CCN active, than inorganic salts. However, many common aerosol organics are amphiphilic and therefore surface-active. Surface-active organics can lower aerosol surface tension, thereby enhancing CCN activation. An organic surface film can also act as a kinetic barrier for uptake of water or reactive gases to the aerosol, or serve as a nucleus for freezing in aqueous droplets. In their chapter, McNeill et al. review the sources and impacts of "Surface-Active Organics in Atmospheric Aerosols."

New York, NY   V. Faye McNeill
Montreal, QC   Parisa A. Ariya

Contents

Emerging Areas in Atmospheric Photochemistry

**Christian George, Barbara D'Anna, Hartmut Herrmann, Christian Weller,
Veronica Vaida, D.J. Donaldson, Thorsten Bartels-Rausch,
and Markus Ammann**

Abstract Sunlight is a major driving force of atmospheric processes. A detailed
knowledge of atmospheric photochemistry is therefore required in order to under-
stand atmospheric chemistry and climate. Considerable progress has been made in
this field in recent decades. This contribution will highlight a set of new and
emerging ideas (and will therefore not provide a complete review of the field)
mainly dealing with long wavelength photochemistry both in the gas phase and on a
wide range of environmental surfaces. Besides this, some interesting bulk photo-
chemistry processes are discussed. Altogether these processes have the potential to
introduce new chemical pathways into tropospheric chemistry and may impact
atmospheric radical formation.

Keywords Cloud chemistry · Dust · Heterogeneous chemistry · Ice photochemistry ·
Organic aerosols · Urban grime · Vibrational overtone absorption

C. George (✉) and B. D'Anna
Université de Lyon, Lyon 69626, France

CNRS, UMR5256, IRCELYON, Institut de recherches sur la catalyse et l'environnement de Lyon,
Villeurbanne 69626, France
e-mail: christian.george@ircelyon.univ-lyon1.fr

H. Herrmann and C. Weller
Leibniz-Institut für Troposphärenforschung (IfT), Chemistry Department, Permoserstr. 15,
04318 Leipzig, Germany

V. Vaida
Department of Chemistry and Biochemistry and CIRES, University of Colorado, Boulder,
CO 80309, USA

D.J. Donaldson
Department of Chemistry, University of Toronto, 80 St. George Street, Toronto, ON,
Canada M5S 3H6

T. Bartels-Rausch and M. Ammann
Laboratory of Radiochemistry and Environmental Chemistry, Paul Scherrer Institute, Villigen,
Switzerland

Contents

1 Introduction

From a chemical perspective, the atmosphere may be described as a giant, fairly well-mixed photochemical reactor, in which most of the processes are initiated by sunlight. As the light source in this context, the sun may be considered as a spherical blackbody emitter at $T \sim 5{,}770$ K outside the atmosphere. One of the most important photochemical processes in the atmosphere is the generation of free radicals (such as the hydroxyl radical, OH) through the UV photolysis of precursors such as ozone or carbonyl compounds. These reactions have been the focus of numerous studies and will not be covered here [1]. The present contribution will deal mainly with reactions which may occur at longer wavelengths than those initiated by direct photolysis, such as vibrational overtone initiated processes and photosensitized reactions. As illustrated in Fig. 1, visible light photons are significantly more abundant in the atmosphere than UV photons, since several atmospheric constituents (such as O_2 and O_3) absorb UV strongly, and thus filter out the short wavelength light emitted by the sun. Nevertheless, a few important UV-triggered processes, for example reactions of non-conventional precursors in aqueous systems, will also be discussed as the authors regard this as an emerging field in atmospheric photochemistry.

An atmospheric photochemical reaction starts with the absorption of a photon by an atmospheric molecule at an appropriate wavelength of available light, producing an excited electronic or vibrational state. Typically, absorption of a photon by a singlet ground state (S_0) will initially produce primarily a singlet excited state (S_1), because the transition from a singlet to a triplet state (i.e., a transition in which electron unpairing takes place with a changing spin) is spin-forbidden and may only take place with a very low probability [2]. However, a triplet state of lower energy
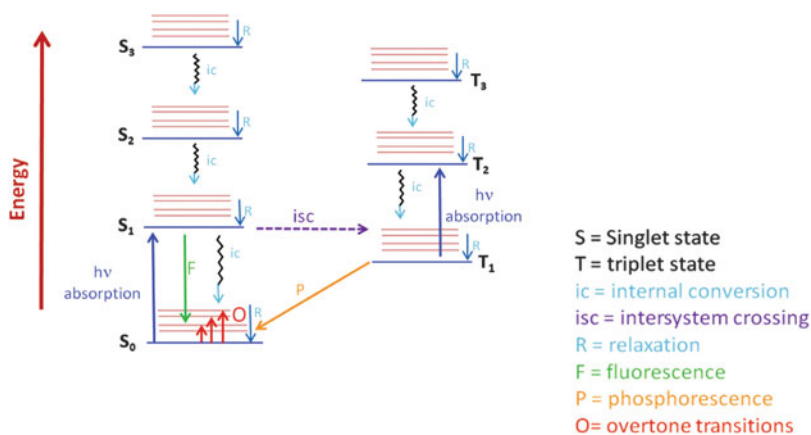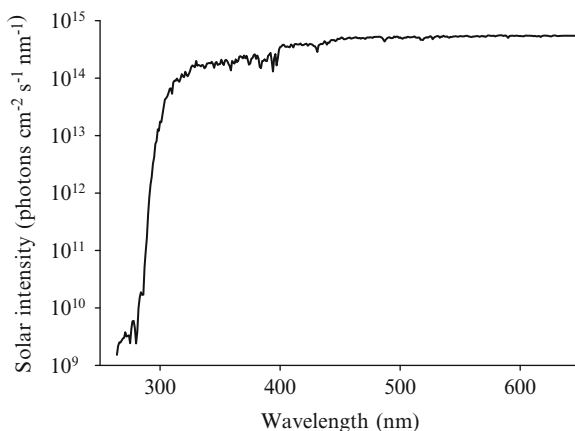
Fig. 2 Schematic Jablonski diagram

may be created by intersystem crossing (induced by spin-orbit coupling). In general, the energy absorbed during the electronic transition can be dissipated by a variety of photochemical and photophysical processes, such as fluorescence, collisional deactivation, collisional or collisionless transition to a lower electronic state, or chemical reaction (dissociation or rearrangement). Radiationless transitions may connect the excited electronic state prepared by photon absorption with the ground state as shown in Fig. 2. In such instances, the system is prepared in its ground electronic state with large excess of thermal energy or in another configuration favorable to photochemical product formation. In contrast, vibrational overtone excitation initiated by red light prepares the system "cold," in its ground electronic state, with sufficient vibrational energy for reaction but little or no excess vibrational or thermal excitation. Several of these energy transfer pathways are illustrated in the Jablonski diagram in Fig. 2.

Photodissociation leads to bond breaking and is of central importance in atmospheric chemistry for free radical production. Photodissociation is well studied for electronic transitions, and this will not be reviewed here. Direct excitation of vibrationally excited states, which have sufficient energy to dissociate, can occur with visible solar radiation; this process is discussed below.

Energy transfer between two molecules is also an important deactivation pathway for excited states, allowing photosensitized reactions to take place. Such a process can be simply described as

$$D + h\nu \rightarrow D^* \tag{1}$$

$$D^* + A \rightarrow D + A^* \tag{2}$$

where the excited molecule D* transfers its energy to A, producing the excited state A*. The sequence of (1) and (2) is described as photosensitization of A by the photosensitizer D. In another way of looking at this, D* has been quenched by A. Energy transfers are named as a function of the spin multiplicity of the excited states of D* and A*:

$$\text{singlet-singlet energy transfer: } {}^1D^* + {}^1A \rightarrow {}^1D + {}^1A^* \tag{3}$$

$$\text{triplet-triplet energy transfer: } {}^3D^* + {}^1A \rightarrow {}^1D + {}^3A^* \tag{4}$$
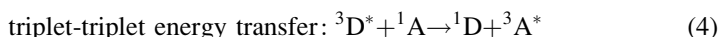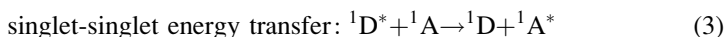
Such processes have been the focus of many studies, especially in liquid phases. The triplet–triplet process is interesting as it allows excitation of the triplet state of the molecule A that would otherwise be inaccessible (for instance due to a poor intersystem crossing $S_1 \rightarrow T_1$). This then may increase the yield of a reaction but also initiate specific reactions. If the energy required to excite the initial state ${}^1D^*$ (prior to its transition to the triplet state) is lower than the excitation energy of ${}^1A^*$, then photosensitized reactions of ${}^3A^*$ become possible at longer wavelengths [3].

Let us illustrate this chemistry with an example. Benzophenone is a well-known photosensitizer, which will phosphoresce at low temperature (77 K) after excitation in the range 360–370 nm. This phosphorescence of benzophenone is quenched by adding a polyaromatic hydrocarbon (PAH) such as naphthalene; phosphorescence is then observed from this species even though it has no absorption band around 360–370 nm. Such observations clearly describe the activation at wavelengths otherwise transparent for a given medium. This sequence of processes can be described as follows:

$(C_6H_5)_2CO + h\nu \rightarrow {}^1(C_6H_5)_2CO^*$	Light absorption by the photosensitizer
${}^1(C_6H_5)_2CO^* \rightarrow {}^3(C_6H_5)_2CO^*$	Intersystem crossing producing the triplet state
${}^3(C_6H_5)_2CO^* + {}^3PAH \rightarrow {}^1(C_6H_5)_2CO + {}^3PAH^*$	Triplet–triplet energy transfer to the added PAH
${}^3PAH^* \rightarrow {}^1PAH + h\nu$	Deactivation of the triplet state – here by a photophysical process such as phosphorescence

In this example, the triplet state of benzophenone is quenched by the added PAH. However oxygen is also known to be an effective triplet state quencher:

$$D^*(T_1) + {}^3O_2 \rightarrow D(S_0) + {}^1O_2 \tag{5}$$
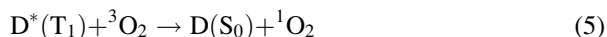
where, despite quenching of $D^*(T_1)$, reactive singlet oxygen is produced by energy transfer to the ground state triplet state of oxygen.

Light absorption by a molecule (R) promotes an electron to a higher energy level, and this may affect the redox properties of this molecule. For example, this molecule may become a better electron donor (reducing agent) in its excited state as compared to its ground sate. In contrast, the electron vacancy created by the electronic transition might exhibit better electron acceptor properties and thereby be a better oxidizing agent. These two features, known as photoinduced electron transfer, can be described in the case of R reacting with the molecule M as follows:

$R + h\nu \rightarrow R^*$	Light absorption by R
$R^* + M \rightarrow R^{\bullet+} + M^{\bullet-}$	R acts as electron donor and is oxidized
$R^* + M \rightarrow R^{\bullet-} + M^{\bullet+}$	R acts as electron acceptor and is reduced

As mentioned above, photoinduced electron transfer occurs via electron exchange interactions, which require overlap of the electronic densities of both molecules R and M, and is therefore a process occurring over short distances.

While the above examples are often used to describe homogeneous organic photochemistry, there are processes that are specific to heterogeneous processes involving solid oxides (such as those found in mineral dust), i.e., heterogeneous photocatalysis [4, 5]. Heterogeneous photocatalysis has been reported in gas and liquid phases (aqueous and organic). Classically, the overall process can be broken down into five independent steps:

1. Transfer of the reactants in gas or liquid phase to the surface
2. Adsorption of at least one of the reactants
3. Reaction in the adsorbed phase
4. Desorption of the product(s)
5. Removal of the products from the interface region

While these steps are common to all heterogeneous processes (such as the uptake of a gas by a liquid droplet or heterogeneous catalysis), step 3 is where the photocatalytic nature of certain metal oxides plays a role. In fact, when a semiconductor catalyst (SC), such as a metal oxide (TiO_2, ZnO, ZrO_2, CeO_2,...) or sulfide (CdS, ZnS,...), is illuminated with photons carrying energy equal or in excess of its band gap, absorption of light promotes one electron into the conduction band, creating an electron–hole pair (Fig. 3) similar to photoinduced electron transfer. The oxide may transfer its electron to any adsorbed electron acceptor (thereby promoting its reduction), while the hole (or the electron vacancy) may accept an electron from an adsorbed donor (promoting its oxidation).

In the case of an oxide exposed to ambient air, adsorbed oxygen (O_2) will act as the dominant electron acceptor and produce the highly reactive superoxide radical anion (O_2^-). Simultaneously, adsorbed water will be oxidized to hydroxyl radicals
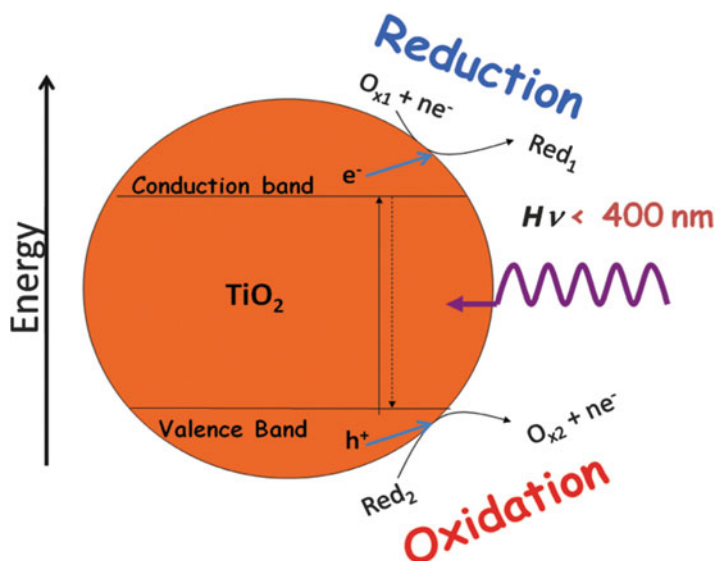
Fig. 3 Schematic of a photocatalytic process. When illuminated with light of energy higher than the band gap, electron–hole pairs are created in a semiconductor, thus allowing chemical reactions on its surface

(OH). Hence the surface of such an illuminated oxide will be highly reactive toward a series of organic (and adsorbed) compounds such as volatile organic compounds (VOCs) often encountered in atmospheric chemistry.

Both photosensitized reactions and heterogeneous photocatalysis have been the focus of many studies and reviews for the degradation of organic and inorganic species in natural terrestrial surface water. This review will discuss their potential importance in the atmosphere for two distinct cases – photochemistry of mineral dust (which contains oxides able to initiate photocatalysis) and organic or carbonaceous aerosols (which contain aromatic compounds or humic like substances able to act as photosensitizers). Additionally, direct photochemistry of unconventional precursors, i.e., iron-dicarboxylic acid anionic complexes, will also be dealt with.

2 Vibrationally Excited Photochemical Processes in the Gas Phase

Like all photolysis reactions, those initiated by vibrational overtone absorption are analyzed as first-order kinetic processes with a photochemical rate, J, which depends upon the absorption coefficient $\sigma(\lambda)$ of the absorbing compound, the

quantum yield (that is, the ratio of dissociation events to the number of photons absorbed for the dissociation $\varphi(\lambda)$), and the available photon flux $I(\lambda)$:

$$J = \int_{\lambda} \sigma(\lambda)\varphi(\lambda)I(\lambda)\mathrm{d}\lambda \tag{6}$$

In the Earth's atmosphere, visible light ($\lambda > 400$ nm) is present to some extent at all altitudes and solar zenith angles. Although such radiation may be sufficiently energetic to rupture weaker chemical bonds, it is generally not in the correct wavelength range to induce electronic transitions of the chemical compounds present in the atmosphere. However, in polyatomic molecules containing O–H, C–H, and N–H groups, the small mass of the hydrogen atom means that X–H stretching frequencies are considerably higher than those of other vibrational modes. In the absorption spectrum this feature and the generally large anharmonicities associated with such X–H stretches give rise to the appearance of overtone transitions with appreciable intensity [6]. Of particular atmospheric importance are the OH stretching overtones of alcohols, organic acids, and peroxy-compounds which, for the most part, are transparent to the ultraviolet wavelengths present in the lower atmosphere. Such species are emitted directly into the troposphere, but are also products of atmospheric oxidation reactions initiated by the OH radical.

The OH stretching frequency lies in the range 3,600–3,000 cm^{-1} and the anharmonicity is approximately 85 cm^{-1} [7–10]. The light hydrogen oscillator and the large anharmonicity value give rise to higher overtone transitions (generally by the $v = 3$ level) becoming sufficiently separated from the rest of the molecular vibrations to be treated by the "local mode" approximation [11], in which each X–H vibration is taken to be an independent anharmonic oscillator. Spectroscopically, the latter condition means that overtone absorptions are well separated from other absorptions, as shown for the case of nitric acid in Fig. 4.

The energies accessed by OH vibrational overtone transitions above $v_{OH} = 3$ or so are sufficient to initiate reactions. However, the challenge of initiating reaction by vibrational overtone excitation lies in the low cross section of vibrational overtone transitions, which are typically three to six orders of magnitude lower in intensity at chemically relevant regions compared to electronic transitions in the ultraviolet. Intensities of vibrational overtone transitions generally decrease by an order of magnitude with each quantum of excitation [12]. Nevertheless, under conditions in which ultraviolet photochemistry is limited due to the lack of appropriate light and/or molecular absorptions, such overtone-initiated chemistry may play an important role in the atmosphere [13–16]. As mentioned above, alcohols, organic acids, and peroxy-compounds all possess OH stretching overtone transitions in the visible spectral region.

What distinguishes vibrational overtone initiated chemistry from that driven by electronic excitation is that the chemistry takes place exclusively in the ground electronic state. In general, following absorption of a photon, chemistry is in competition with energy dissipation; in the lower atmosphere this is often driven
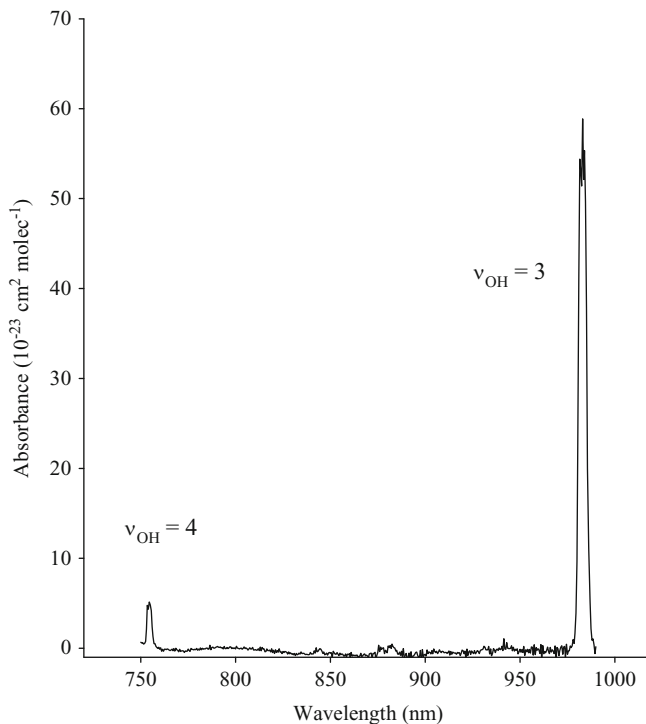
Fig. 4 Absorption spectrum of gas phase nitric acid in the near IR region, showing the overtone transitions to the $v = 3$ and $v = 4$ levels of the OH stretch. Adapted from Fig. 1 of [7]

by collisional energy loss. Electronic transitions of atmospherically important molecules such as NO_2 and O_3 access dissociative states with very short lifetimes compared to the collisional time. By contrast, overtone chemistry requires energy flow away from the initially excited mode (i.e., the OH stretch vibration) into adjacent regions of the molecule. This intramolecular vibrational redistribution (IVR) process takes place on the time scale of many vibrational periods, setting a limit for the effectiveness of chemistry, depending on local temperature and pressure. The efficiency of such processes is higher at high altitude where low pressure limits the efficiency of collisional deactivation.

2.1 Bond Cleavage Reactions

This type of process has been studied reasonably extensively for systems in which an OH moiety is adjacent to a weak bond, such as O–O or O–N. Vibrational overtone transitions to states with 3–6 quanta of OH stretch occur in the near-infrared to visible region of the spectrum and deliver sufficient energy to break the

adjacent weak bond in several atmospherically important molecules, such as the O–O bond in peroxy-compounds such as HOOH [17–20] or the N–O bond in HNO_x type compounds (HONO, $HONO_2$, HO_2NO_2) [19, 21–24]. These compounds are very important sequestering agents for NO_2 (which forms ozone through photolysis to NO + O and recombination of the O-atom with O_2) and OH (the primary agent for oxidation reactions in the troposphere). Therefore, understanding their formation and destruction reactions is critical to being able to predict air quality and the oxidative ability of the lower atmosphere.

In nitric acid ($HONO_2$), for example, initial excitation of an OH stretching motion at $v_{OH} \geq 5$ accesses energies above the dissociation limit to OH + NO_2 [19]. In the absence of collisional de-excitation, this energy will "flow" from the initially excited vibration throughout the molecule, via IVR. During this equilibration process, sufficient energy may be deposited in motion along the N–O dissociation co-ordinate to induce bond cleavage. An upper limit to the enhancement due to vibrational overtone pumping of the photolysis rate of HNO_3 has been calculated based on vibrational overtone cross sections [19, 21–24] with an assumed quantum yield of 1. At 20 km altitude and at about $92°$ zenith angle the calculated enhancement for the photolysis rate of HNO_3 is about 30%.

In the well-studied case of hydrogen peroxide, H_2O_2, overtone levels of the OH stretch may be excited at energies exceeding the O–O bond dissociation energy of about 215 kJ mol^{-1}. Reaction occurs by energy flow from the initially excited OH stretch local mode to the weak O–O bond to give the OH radical. Simulations of the dynamics following overtone excitation have shown that the initial step in the dissociation is a rapid coupling of the OH stretching and OOH bending modes. This type of coupling seems to allow flow of energy out of the OH moiety and into the weak bond. Similar reaction mechanisms were used to explain dissociation following vibrational overtone pumping in other, similar compounds.

In the case of HO_2NO_2 (peroxynitric acid or PNA) the thermochemical dissociation limit is reached at energies somewhat below the $v = 3$ level of the OH stretch. Thermally-assisted dissociation becomes possible from the $v = 2$ level as well, depending upon the temperature. This process has been shown to occur in laboratory measurements, using action spectra of HO_2 formation as a function of the excitation wavelength of PNA [23, 25]. These measurements show temperature-dependent formation of HO_2 from the $v = 2$ level of OH stretch, and a smaller but temperature-invariant formation efficiency from the $v = 3$ level. Inclusion of overtone-initiated dissociation of PNA from OH stretching vibrational levels $v \geq 2$ in atmospheric models has shown this process to be an important source for HO_x in the free troposphere and lower stratosphere [26–30]. Reaction with HO_x radicals is a dominant sink in photochemical loss cycles of ozone in the lower stratosphere. The vibrational overtone process is calculated to produce a 20–60% increase in HO_x at high latitudes in the spring, leading to a greater sensitivity of ozone to atmospheric perturbations such as increased water vapor.

The postulated mechanism for energy flow from the OH to the weak bond by IVR in examples where a weak bond ruptures following overtone excitation appears to be more complicated in HONO and $HONO_2$. Gerber and co-workers [22] have

carried out dynamical simulations of the molecular motion following overtone excitation and find that IVR to the N–O bond is not the only important process taking place. Intramolecular hopping of the hydrogen atom from one oxygen atom to another also occurs on very fast time scales. Interestingly, this H atom hopping occurs at energies well below the bond dissociation energy for the O–H bond, so the process is a concerted reaction where one O–H bond breaks while another is being generated.

2.2   Rearrangement Followed by Dissociation

In addition to direct bond cleavage, molecules with a high degree of internal excitation may undergo rearrangements followed by dissociation to molecular products. This is the idea behind the well-known phenomenon of thermal (unimolecular) decomposition. It is similar in initiation to the bond cleavage process described above, with the important distinction that such "concerted" chemistry may occur at energies lower than an individual bond dissociation energy. For example, malonic acid undergoes thermally-induced decarboxylation at relatively low temperatures [31]; this chemistry may also be induced by OH stretching overtone excitation [32]. Similarly, sulfuric acid has been predicted to undergo a unimolecular dehydration reaction to form SO_3 and H_2O following excitation to $v \geq 4$ of an OH stretching vibration [33]. This level corresponds to energies well below the weakest individual bond in the acid. The decomposition of H_2SO_4 is also known to occur thermally but at very high temperatures [34].

Sulfuric acid is one of the main constituents of atmospheric aerosols, of enormous interest because of the large and as yet not completely understood effect these aerosols have on the planet's climate. Sulfate aerosols form at low altitude in the troposphere and the cool stratosphere and evaporate as they ascend towards the warm stratopause. Modeling studies led to the conclusion that sunlight-initiated chemistry of H_2SO_4 must occur at high altitude to explain measured stratospheric SO_2 concentrations [35]. Although the lowest electronic transitions are not accessible to the available solar radiation [36], several OH vibrational overtone transitions do absorb in the actinic region and are therefore available to activate this molecule [33, 37]. Below 70 km the relevant photodissociation mechanism for H_2SO_4 is initiated by absorption of red light by OH vibrational overtones, specifically by $v_{OH} = 4$ and 5 [38–40].

The possibility of vibrational overtone initiated dehydration of sulfuric acid to $SO_3 + H_2O$ has been investigated by spectroscopic [37, 41, 42] and theoretical [38, 43, 44] methods. Dynamical simulations of the dehydration reaction find two mechanisms to be operative in this reaction: a fast loss of H_2O initiated by hydrogen atom hopping, similar to that found following nitric acid excitation, and a slower dissociation, occurring after full or partial IVR [43, 45]. Based on these mechanisms and rates, the dehydration of sulfuric acid is very effective under conditions of the upper stratosphere and mesosphere [46]. The rate of dehydration thus obtained is

sufficient to explain atmospheric observations of the SO_2 vertical profile and the formation of large concentrations of cloud condensation nuclei at the top of the aerosol layer in polar spring or in mid-latitude air of recent polar origin [39, 40]. In this example, no alternative photochemical process is available in the stratosphere, since the electronically excited states of H_2SO_4 are at very high energy [33, 37]. Sunlight-initiated reactions of sulfuric acid will be important beyond the Earth's atmosphere, notably on Venus where sulfuric acid clouds are known to exist [47].

Concerted photoreactions initiated by OH vibrational overtone excitation have also been proposed to occur in organic acids and their reaction mechanisms and rates have recently been investigated by theoretical and spectroscopic methods [10, 42, 48]. The early time dynamics of vibrationally excited pyruvic and glyoxylic acids have been studied by a combination of "on-the-fly" dynamics simulations and cavity ringdown spectroscopy [48–50]. These combined studies concluded that decarboxylation of the ketoacids occurs on sub-picosecond time scales following OH overtone excitation. A strong correlation between structure and reactivity was observed: conformers that possess intramolecular hydrogen bonded structures react on excitation of the third and fourth OH overtone by hydrogen atom chattering, while nearly isoenergetic conformers of *trans* geometry do not react by a fast process. The "chattering" mechanism involves rapid hydrogen atom exchanges between donor and acceptor oxygen atoms. In contrast with hydrogen atom "tunneling," chattering is a classically allowed process occurring above any exchange barrier. Chattering proceeds on a time scale set by the vibrational frequency and is consequently much faster than the tunneling motion [51].

The examples discussed above illustrate the utility of vibrational overtone excitation by red sunlight in atmospheric photochemistry. The low absorption cross-section of vibrational overtones limits the importance of such light-initiated chemistry. However, when reactive electronic states are high in energy (as is the case with most alcohols and acids) or when UV radiation is suppressed at high solar zenith angles, vibrational overtone initiated photochemistry has been used to explain discrepancies between measurements and model results.

3 Aerosol Photochemistry

3.1 *Organic Aerosols*

Organic material comprises a large fraction of the sub-micron aerosol mass ranging from 20% to 50% in continental mid-latitudes and up to 90% in tropical forested areas [52–54]. Significant amounts of carbonaceous aerosols are also observed in the upper troposphere [55]. Organic particles may have a direct radiative forcing through scattering and absorption of solar and infrared radiation and an indirect radiative forcing by affecting cloud formation and by inducing changes in cloud properties [56]. Organic aerosols are also related to health effects due partly to the

presence of toxic compounds, such as polycyclic aromatic hydrocarbons (PAHs), which are known for their carcinogenic and mutagenic potency to humans and animals [57–59].

Chemical reactions proceeding at the surface or within the bulk of aerosol particles can influence atmospheric gas phase chemistry as well as the properties of the particles themselves, including their effects on climate and human health. So far, the atmospheric chemistry community has mostly considered heterogeneous or multiphase reactions under dark conditions between reactive atmospheric gas phase oxidants and organic compounds known to be present in the particulate phase. Many laboratory studies have used oxidation of PAHs and/or soot [60–87], oleic acid, and other organic compounds as proxy systems to understand mechanisms and kinetics of these reactions and to assess their significance [88–90].

This focus on dark reactions has ignored the fact that organic sub-micron aerosols absorbing near-UV and visible light are ubiquitous in the atmosphere, including soot as the most extreme example. Enhanced UV absorption features were observed, for instance, in remote areas as well as in polluted environments [41, 91–95]. Reference [91] showed strong spectral dependence of the light absorption by organic aerosols in the UV. Similar absorption attributed to organics has been reported in several other measurements (e.g., [41, 94–102]). Sources of this absorbing material in organic aerosols may include the resuspension of soil-derived material by wind erosion or combustion processes such as biomass burning or fossil fuel combustion [91, 103–107]. Laboratory studies have noted the formation of solar light absorbing material following a few hours of oxidation in the condensed phase. These studies have mostly concentrated on bulk solutions, with only a few observing reaction in the aerosol phase directly (e.g., [92, 108–114]). During processing, initially non-absorbing organic compounds are converted into compounds that display significant absorption in the UV and even visible regions. The presence of such light absorbing material in particles may enable photo-induced and/or photo-sensitized processes. While a significant body of literature exists on photo-induced charge and/or energy transfer in organic molecules of relevance in terrestrial water chemistry, biochemistry, and water waste treatment [115–117], relatively little work exists in the field of atmospheric aerosols, where only a few groups have investigated the chemistry of the light-absorbing organic material present in aerosols [118–123].

Stemmler et al. [124] used humic acid aerosols as a proxy for HULIS (HUmic-LIke Substances) to study the photo-induced conversion of NO_2 into HONO, which was previously observed on various organic condensed films [125–128]. The light-induced process was able to release more HONO than was obtained under dark conditions, similar to what was observed for other organic substrates. The amount of the enhancement is not dramatic: even if the whole organic aerosol was composed of humic acids, for typical aerosol surface concentrations of 100 μm^2 cm^{-3} for rural and 1,000 μm^2 cm^{-3} for urban conditions, only 1.2 and 17 pptv h^{-1} of HONO would be formed on aerosol surfaces in rural and urban environments, respectively. These values represent upper limits as in reality rural and urban continental aerosol is composed only of 20–50 mass % of organic matter. On the

other hand, HONO production reported for daytime at ground and over forested or rural sites is up to 170–500 ppt h^{-1} [127] or in urban environments up to 2 ppb h^{-1}. Stemmler et al. [124] suggested that photochemical HONO formation on organic aerosol is unlikely to be an important contributor to the HONO formation observed in the boundary layer. In exceptionally highly polluted areas, such as in biomass burning plumes or in mega-cities, environmentally relevant HONO photo formation rates on organic aerosol may occur.

Similar light-induced production of HONO upon exposure to NO_2 has been observed on soot [129]. The source strengths estimated for atmospheric conditions are comparable to those for humic acids. The process therefore represents only a small source of HONO in the gas phase. However, Monge et al. demonstrated that HONO production on soot does not cease quickly due to deactivation of reactive species under irradiation as it does under dark conditions, and so soot may act as a photoactive substrate over its entire life cycle in the atmosphere.

The need for investigating the role of organic aerosols as a possible sink for ozone has been suggested in the past by Jacob et al. [130], since this type of particle has a sufficient source strength and potentially a high enough reactivity to provide a significant sink for ozone in the continental boundary layer. The photo-reactivity of ozone with humic acid aerosol was investigated by D'Anna and co-authors [131]. The authors concluded that the light-induced process is not able to affect gas phase concentrations of ozone in the troposphere. Nevertheless, the amount of ozone reacted may be significant for aerosol aging [131] because OH radical is produced upon electron transfer from the organic substrate to ozone [132].

Because significant differences exist between terrestrial aquatic humic acids (such as those used in most laboratory experiments on HULIS) and aerosol humic-like substances (lower aromaticity, lower molecular weight, and better droplet activation ability) [133], the photo-induced reactivity of genuine atmospheric HULIS extracts with gas phase ozone was investigated by the same group (Fig. 5) [134]. The authors used HULIS collected from winter filters in Chamonix, which are strongly influenced by local emission of residential wood burning. The experimental results indicate a much higher photo-induced uptake of ozone on films prepared with such HULIS extracts than with films of humic acids. TOC (Total Organic Carbon) analysis of the extract before and after photo-treatment showed a reduction of the total amount of carbon; emission of VOCs and CO was interpreted to be a consequence of ozonation [135], photolysis [136–138], and a combination of both processes [131]. Functional group analysis suggested the formation of carbonyl and carboxylic groups under the combined action of light and ozone [134].

As in the case of NO_2, soot particles also exhibit photoenhanced O_3 uptake, in both the UVA and the visible wavelength ranges [139]. While under dark conditions over long times O_3 shows only very low reactivity, the study by Zelenay et al. [139] demonstrates that rates of O_3 uptake are orders of magnitude higher under light than under dark conditions. Surprisingly, this enhanced oxidation was accompanied by an increase in the contact angle of water, i.e., the surface became less hydrophilic. X-Ray absorption spectroscopy revealed a reduction in oxygenated organic components upon irradiation, suggestive of decarboxylation processes and
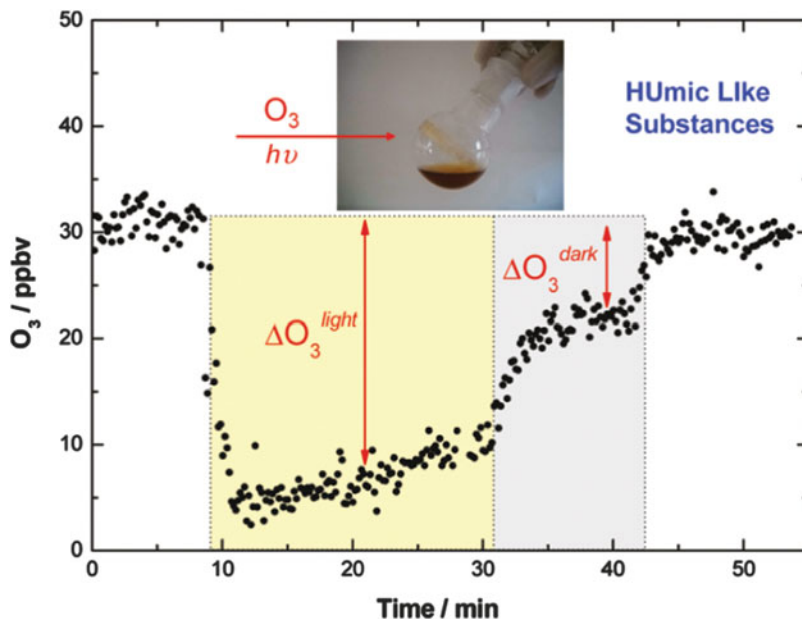
Fig. 5 Evolution of the O_3 gas phase mixing ratio (*black dots*) as a function of time after contact with a film made of HULIS extracted from organic aerosols collected in the winter season at Chamonix, France (*photo*). An ozone reduction of approximately 25 ppbv is observed during UVA irradiation

evaporation of highly oxidized small OVOC and CO_2. This demonstrates that indirect photochemistry affects the subtle feedbacks among oxidation, photochemistry, and hydroscopic properties (and thus climatic effects) of particles.

While the experiments related to photosensitized processes reviewed above were concerned with inorganic oxidants from the gas phase, the question arises as to whether comparable processes would occur with organic acceptors. Rouviere et al. [140] noted significant light induced degradation of succinic acid in deliquesced ammonium sulfate particles in the presence of small amounts of benzophenone. This effect was also confirmed by experiments in aqueous solution showing efficient triplet quenching by succinic acid. This has led to the idea that photosensitized processes may play a role in secondary organic aerosol (SOA) formation. Recently, Monge and co-authors [141] proposed that heterogeneous reactions activated by light lead to fast uptake of non-condensable VOCs at the surface of particles when traces of a photosensitizer were in the aerosol seeds. Seed particles containing succinic acid and only traces of humic acids showed a rapid diameter growth when irradiated with near-UV light in the presence of a terpene. An enhanced effect was reported when traces of nitrate were added to the seed particles, while no growth was observed, under the same experimental conditions, if the seed particles contained only carboxylic acids. Replacing air by pure N_2 (containing traces of O_2 up to 50 ppmv) drastically reduced the photo-induced particle growth,
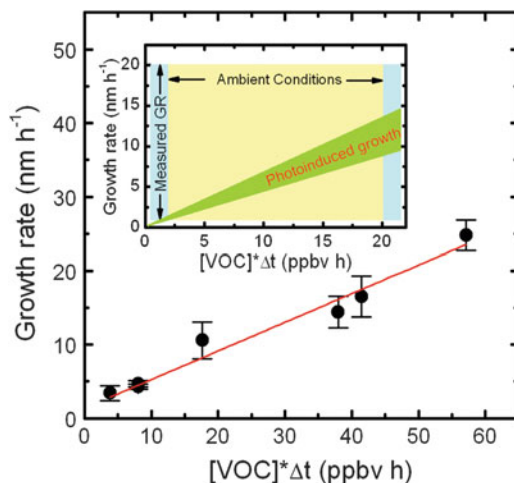
Fig. 6 Experimental results from an aerosol flow tube experiment using humic acid/succinic acid/NH_4NO_3 (1:10:1 by weight) as seed particles exposed to 320 ppbv of limonene and to UV-A light. The residence time of the aerosol in the flowtube is 9.7 min. Calculated growth rate values as a function of the product between limonene concentration and residence time in the flow tube. These values are calculated by considering the photoenhanced growth (GR = $\Delta D_m/\Delta t$) vs VOCs concentration per exposure time. Values are evaluated for solar irradiance. The *inset* shows growth rate (GR) values given by the photoinduced process compared to the literature GRs values (1–20 nm h^{-1}). Ambient conditions are assumed to vary from 0.2 ppbv to 2 ppbv of limonene and exposure to solar irradiance for 10 h, in the 300–420 nm (near-UV) wavelength range

suggesting that O_2 is involved in the reaction mechanism, a role well known from previous studies on DOM- and humic-containing waters [142–144]. Figure 6 shows how the particle growth rate depends upon the product between limonene concentration and residence time in the aerosol flow tube for typical solar irradiance. Ambient conditions are assumed to vary from 0.2 to 2 ppbv of limonene; the exposure to solar irradiance is approximated to 10 h per day in the 300–420 nm (near-UV) wavelength range. Therefore the experimentally determined growth rate values matched field observations, suggesting that this photochemical process can provide a new and unaccounted pathway for atmospheric particle growth and should be considered by models [141]. These laboratory results represent a radical change from the traditional view of gas phase oxidation of VOCs by atmospheric oxidants leading to SOA formation.

3.2 Mineral Dust

Estimates of emissions of mineral dust into the atmosphere presently lie around 1,500–2,000 Tg per annum [145] making mineral dust an important component of the coarse fraction of atmospheric aerosol and explaining its significant impact on

several atmospheric processes including radiative forcing and the modification of photochemical cycles. The direct radiative forcing effect (due to scattering and absorption of incoming solar radiation) is accompanied by an indirect effect as clay and silica particles are effective condensation and ice nuclei [146, 147], which can ultimately affect cloud structure and precipitation patterns [148]. The indirect effect will be modified by the physical state of the mineral dust particles, which will be influenced by chemical ageing during atmospheric transport.

Uptake of several trace gases (such as N_2O_5, NO_x, HNO_3, SO_x, O_3) on mineral dust particles and their surrogates has recently received attention [149–155]. Of particular importance is the conversion of SO_2 into sulfates and of NO_x and NO_y into nitrates on dust particles during transport [156, 157]. Model studies have confirmed that the nitrate content is consistent with the uptake of reactive NO_y trace gases (such as HNO_3) [158]. The overall impact of NO_y-mineral aerosol interactions on tropospheric photochemical cycles has been assessed in combined aerosol/gas phase models [158–161]. They potentially impact mineral dust hydroscopic and optical properties, they change the gas phase composition (NO_y/NO_x ratio and ozone concentrations), and they establish a transport route of nitrate and sulfate to regions far from the sources (i.e., nitrogen fertilization of oceans) [162, 163]. The accuracy of the simulations is severely impacted by a lack of high quality laboratory data describing trace gas/dust interactions. As this section is focussing on dust photochemistry, the reader is referred to recent reviews on dust heterogeneous chemistry [164] for more information about the uptake of various gases on dust surfaces.

As dust particles are mobilised by strong winds and therefore eroded from the ground, their composition reflects the chemical composition of crustal materials from which they are produced. As the Earth's crust is dominated by silicon and aluminum oxides, the latter are also dominantly present in uplifted particles. Indeed, several studies focusing on the chemical (elemental) composition of dust originating from various locations around the world have demonstrated that mineral dust is approximately 60% SiO_2 and 10–15% Al_2O_3 (by weight) [165]. Beside these major elements, some other oxides are found. The percentages of these other oxides, namely Fe_2O_3, MgO, CaO, and TiO_2, are slightly more variable and dependent on source location. For instance, titanium dioxide is found in dust particles at mass mixing ratios ranging from 0.1% to 10% depending on the exact location from where the particles were uplifted [166].

Both titanium and iron oxides are known semiconductors used as photochemical sources of radicals (see Sect. 1). In aqueous solutions, iron oxides are used to induce the so-called Fenton or photo-Fenton reactions [167] (see section on bulk phase chemistry). Pure TiO_2 is used in a variety of remediation processes due to its photocatalytic properties. The exposure of TiO_2 to light with wavelengths below 400 nm leads to an electron hole pair. Each of these can reach the surface and react with adsorbed species to form OH, O_2^-, or singlet oxygen. These free-radicals are very efficient oxidizers of organic and inorganic matter. For instance, pure TiO_2 has been demonstrated in a number of studies to be an effective photocatalyst for NO_2 reduction [168–170]. Similar reactions also occur with other inorganic compounds such as ozone and sulfur oxides with synergistic effects being active if these
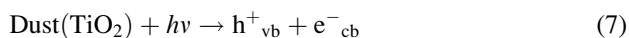
compounds are present in combination [171]. Accordingly, the TiO_2 contained in mineral dust could induce photochemical reactions that were not considered so far. In turn, this could drastically modify the chemistry of the dust particles and their potential impact on the tropospheric composition. As a consequence, there is a recent but growing interest in studies focussing on photochemical transformation at the air-dust interface. Several surface photochemical mechanisms are currently being discussed in the literature, i.e., surface photolysis and photo-assisted reactions.

The photolysis of nitrate on surfaces is especially important as it could lead to the renoxification of the atmosphere, whereby nitrate (or nitric acid) becomes a source of NO_x and thus mineral dust would not be a permanent sink for gaseous nitrogen oxides. uptake of several gases, i.e., NO_2 [126, 172, 173], O_3 [174], and HCHO [175], while [176] presented similar conclusion for the surface photooxidation of SO_2.

The striking features in all cases are that under illumination (1) the uptake of these gases is enhanced by more than one order of magnitude as compared to data obtained in the dark and (2) the reaction is sustained as long as light is available (while in the dark most surfaces are passivated in short time scales).

Let us focus on the case of nitrogen dioxide (NO_2) [126, 172, 173, 177], which is generally thought to be only very poorly reactive on a large variety of solid surfaces at room temperature and low gas phase concentrations. (We note that high concentrations may lead to the formation of N_2O_4 which, in turn, is known to be quite reactive on various surfaces [178].) However, once a dust surface is irradiated, in the range 300–400 nm and under conditions where gas phase photochemistry was shown to be minor (typically by the use of short reaction times), a very rapid chemical conversion of NO_2 is observed. Not only is the uptake rate drastically accelerated but it also appears that the uptake rate is catalytic in the sense that the uptake rate does not depend on time, i.e., no surface saturation has been observed on these synthetic samples over hours (even at NO_2 concentrations as large as 300 ppb). The uptake coefficients (normalized to the BET surface area) were observed to be close to 10^{-6}, up to two orders of magnitude larger than without light. Gustafsson et al. [179, 180] derived the uptake rate of NO_2 onto pure TiO_2 to be ca. 8×10^{-3}. Such photoenhancements were observed over a large range of dust surfaces including synthetic surrogates and samples originating from Mauritania, Algeria, Morocco, Tunisia, and Arizona (Arizona Test Dust, ATD); see Fig. 7. While the uptake in the dark was always very small, a photoenhanced uptake of NO_2 was observed on all samples with an enhancement factor ranging from 8 to 15.

The photocatalytic action of TiO_2 (and other semiconductors) is initiated by the photo-production of excess electrons in the conduction band (e^-_{cb}) and holes in the valence band (h^+_{vb}). The electron reduces the oxygen or the nitrogen dioxide while the hole oxidizes water vapor. The associated reactions mechanism could be [5]

$$Dust(TiO_2) + h\nu \rightarrow h^+_{vb} + e^-_{cb} \tag{7}$$

$$h^+_{vb} + H_2O \rightarrow OH + H^+ \tag{8}$$

$$e^-_{cb} + O_2 \rightarrow O_2^- \tag{9}$$
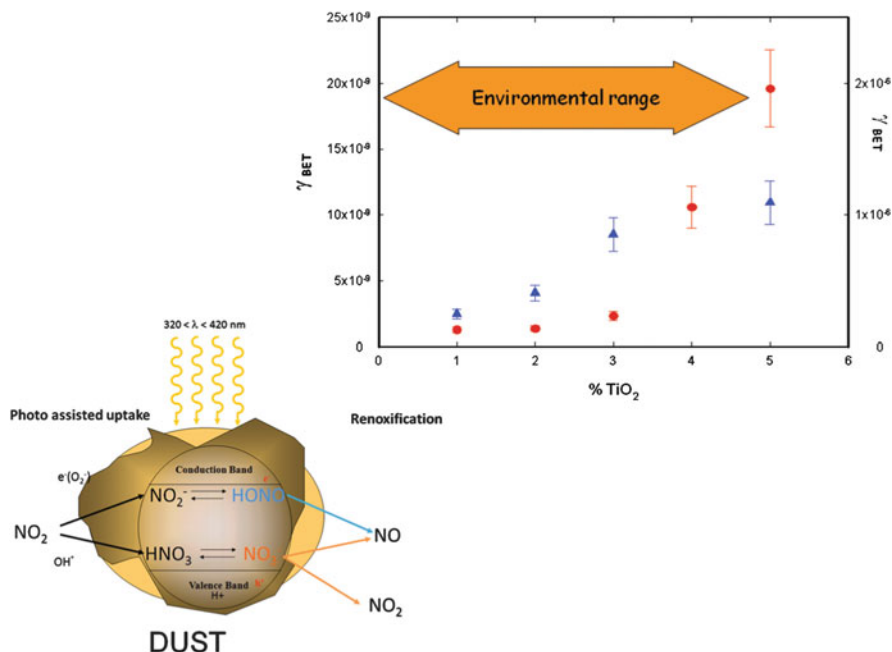
Fig. 7 Schematic representation of the conversion of NO_2 into HONO on UV-A (300–420 nm) irradiated mineral dust, illustrating the chemistry initiated by the photoinduced electron and hole, respectively. Dependence of the uptake coefficient (based on the BET surface) as a function of the TiO_2 content of synthetic dust

where OH and the electrons or O_2^-, respectively, can react with nitrogen dioxide according to

$$NO_2 + OH \rightarrow HNO_3 \tag{10}$$

$$NO_2 + O_2^- (or\ e^-_{cb}) \rightarrow NO_2^- + O_2 \tag{11}$$
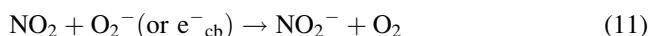
It must be emphasized that these reactions are just a subset of a large number of possible reactions changing the final yield of each product. Depending on the acidity of the surface, the production of nitrite anions is linked to that of gaseous nitrous acid (HONO), known to be a very important source of hydroxyl radicals. HONO was observed from irradiated samples, but with varying yields. On synthetic dust surfaces (i.e., 1 wt% TiO_2 in SiO_2) HONO was produced with an average yield of 33% while, for an authentic Saharan sample, the yield was about 80%. This indicates that surface acidity, microstructure, and other factors finally control surface chemistry and the release of HONO.

It is well known that nitrate anions are formed as a consequence of the photocatalytic oxidation of NO_2 on UV-illuminated TiO_2 surfaces [181–186].

In addition, on the dust surface, nitrate anions were observed to be the only product formed during the photoconversion of NO_2. The formation of nitrate on dust particles is typically considered as a sink for atmospheric NO_y (such as HNO_3). However, if dust is photochemically or photocatalytically active, surface nitrate will photoreact according to

$$NO_3^- + h^+{}_{vb} \rightarrow NO_3 \tag{12}$$

$$NO_3 + hv \rightarrow NO + O_2 \tag{13}$$

$$NO_3 + hv \rightarrow NO_2 + O \tag{14}$$

The photocatalytic action of TiO_2 is again initiated by the photo-production of excess electrons in its conduction band ($e^-{}_{cb}$) and holes in its valence band ($h^+{}_{vb}$). The nitrate ion adsorbed at the oxide surface can react with the holes in the valence band to form a nitrate radical. The nitrate radical (NO_3), which absorbs strongly in the visible, can subsequently be photolyzed (occurring at longer wavelength compared to the anion) and form NO_2 and NO through reactions (13) and (14), respectively, as observed by Ndour et al., leading to a potential renoxification process of the atmosphere [177]. These processes are then in competition with surface photolysis as described by Grassian and co-workers [176, 187–189].

The latter two reactions above produce atomic and molecular oxygen that may lead to the formation of ozone at the surface. Monge et al. [129] investigated this chemical route by exposing a mix of TiO_2/KNO_3 50 wt% to near-UV irradiation (300–420 nm) using synthetic air or pure N_2 as carrier gases with 30% RH under atmospheric pressure and room temperature. The formation of ozone was indeed observed and explained by reactions (7) to (14) followed by a surface recombination:

$$O^\bullet + O_2 + M \rightarrow O_3 + M \tag{15}$$

Although O_3 has recently been proved to decompose on illuminated TiO_2 surfaces [174], its formation is observed when TiO_2 treated surfaces are exposed to NO_x under illumination. Charge transfer reactions take place at the surface of TiO_2, producing nitrate radicals from the corresponding anions. The photochemistry of the NO_3 radical leads to O_3 formation, enhancing the oxidizing power of these surfaces.

Recent laboratory work has shown that the uptake and photooxidation of organics on TiO_2-containing mineral dust proxies can be an efficient process [190]. n-Propyl and isopropyl alcohols were efficiently oxidized to propionaldehyde and acetone, respectively, after uptake to photoactive dust in a Knudsen cell reactor when the dust substrate was exposed to actinic radiation. The presence of trace amounts of O_2 in the reactor enhanced the production of oxidized product. These observations are consistent with the general mechanism for TiO_2 photoactivity, as shown below for isopropanol:
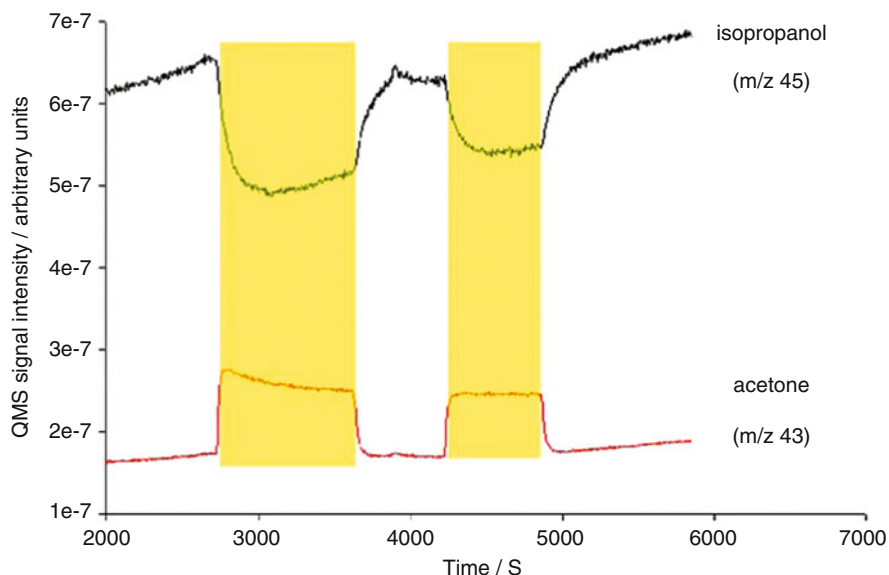
Fig. 8 Photoenhanced uptake of propanol and the corresponding production of acetone on an illuminated TiO_2 dust sample in the presence of 0.7 Pa of $O_2(g)$

$$h^+_{vb} + (CH_3)_2CHOH \rightarrow\rightarrow (CH_3)_2CO \tag{16}$$

$$\{>TiOH^\bullet\}^+ + (CH_3)_2CHOH \rightarrow\rightarrow (CH_3)_2CO \tag{17}$$

$$O_2^{-\bullet} + (CH_3)_2CHOH \rightarrow\rightarrow (CH_3)_2CO \tag{18}$$
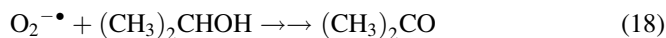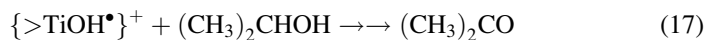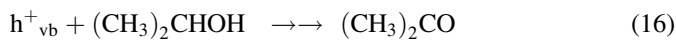
Figure 8 displays the photoenhanced uptake of propanol and the corresponding production of acetone on an illuminated TiO_2 dust sample in the presence of 0.7 Pa of $O_2(g)$.

4 Tropospheric Aqueous Phase Bulk Photochemistry

4.1 Introduction

Atmospheric particles very often contain water when they occur as deliquesced aerosol particles, haze, fog, cloud droplets, or even rain droplets (hydrometeors). It has been suggested before that the atmospheric aqueous bulk phase in these systems might also host a lively and important photochemistry which, up to now, has mostly been described insofar as hydroxyl (OH) radicals are generated by the photolysis of nitrate, nitrite, hydrogen peroxide [191–198], and iron-hydroxyl complexes [199]. These processes have been treated in recent overviews such as [200, 201].

Photosensitization has been studied not only in connection with interfaces but also for bulk phase aqueous environmental systems [202].

Iron is the most abundant metal in the Earth's crust and is always identified as a component in tropospheric particle systems, either aqueous or dry [167]. It has been known for a long time that iron forms chelate complexes very efficiently and that oxalate forms complexes with Fe(III). These can be regarded as being very stable from their complex stability constants but they also exhibit a considerable potential for light absorption in the actinic range of the spectrum. Iron-oxalato-complexes have been characterized with regard to their photochemical activity by the measurement of their effective quantum yields for the formation of Fe(II) [203, 204]. As a consequence of this chemistry the formation of iron-oxalate complexes is included in the series of CAPRAM (Chemical Aqueous Phase Radical Mechanism) schemes for atmospheric aqueous phase chemistry [205]. Leaving these very important photochemical sink processes out of any description of tropospheric aqueous phase chemistry results in a dramatic overestimation of aqueous phase oxalate formation and, as a consequence, gives rise to misleading interpretations. Below, we discuss the molecular mechanisms underlying bulk aqueous phase photochemistry of the iron-oxalato-complexes and present an introduction to the study of other Fe(III) complex systems. There are strong interactions among the photochemically generated radical species formed in complex photolysis reactions. We further discuss the possible impacts of extending the iron complex photochemistry treatment in tropospheric chemistry simulations. Such impacts include, for example, the formation of Fe(II) in aqueous phase photochemical redox-cycling and the degradation of dissolved organics which may be "activated" by complexation to iron centers.

4.2 Ferrioxalate Photochemistry

Ferrioxalate complexes are thought to hold a major portion of Fe(III) in atmospheric waters [167]. Although such complexes are widely used as chemical actinometers [206] and have been the subject of numerous experimental investigations [207–218], the exact primary step in ferrioxalate photochemistry is still controversial. Two different versions of the ferrioxalate reaction mechanism have been proposed following the excitation of the complex [219]. One possibility is an intramolecular electron transfer from the oxalate ligand to the center ion Fe(III) and the formation of a long lived radical complex (19) or the formation of a $C_2O_4^{\bullet-}$ radical (20) [213, 215]:

$$\left[Fe^{(III)}(C_2O_4)_3\right]^{3-} + h\nu \rightarrow \left[Fe^{(II)}(C_2O_4^{\bullet})(C_2O_4)_2\right]^{3-} \quad \text{or} \tag{19}$$

$$\rightarrow \left[Fe^{(II)}(C_2O_4)_2\right]^{2-} + C_2O_4^{\bullet-} \tag{20}$$
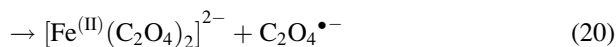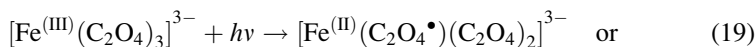
The $C_2O_4^{\bullet-}$ radical will then decarboxylate instantly and form CO_2 and $CO_2^{\bullet-}$ [220]:

Fig. 9 Photolysis of Fe(III)-oxalato complex in the atmospheric aqueous phase, including subsequent reactions and possible interactions with the gas phase

$[Fe^{III}(C_2O_4)_3]^{3-} + h\nu \rightarrow [Fe^{III}(C_2O_4)_3]^{3-*}$

$[Fe^{III}(C_2O_4)_3]^{3-*} \rightarrow [Fe^{III}(C_2O_4)_2]^- + 2\,CO_2^{\cdot-}$

$[Fe^{III}(C_2O_4)_2]^- + 2\,CO_2^{\cdot-} \rightarrow [Fe^{II}(C_2O_4)_2]^{2-} + CO_2^{\cdot-} + CO_2$

$CO_2^{\cdot-} + O_2 \rightarrow CO_2 + O_2^{\cdot-} \qquad O_2^{\cdot-} + H^+ \rightleftharpoons HO_2^{\cdot} \quad (pKa = 4.8)$

$HO_2^{\cdot} \quad \dashleftarrow \quad HO_2^{\cdot} + HO_2^{\cdot} \rightarrow H_2O_2 + O_2 \qquad H_2O_2 + h\nu \rightarrow 2\,\cdot OH$

$H_2O_2 \quad \dashleftarrow \quad H_2O_2 + Fe^{2+} \rightarrow \cdot OH + OH^- + Fe^{3+} \text{ (Fenton-reaction)}$

$\cdot OH \quad \dashleftarrow$

Gas Phase   **Aqueous Phase**

$$C_2O_4^{\cdot-} \rightarrow CO_2^{\cdot-} + CO_2 \quad k_{1st} = 2 \times 10^6 \text{ s}^{-1} \tag{21}$$
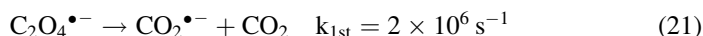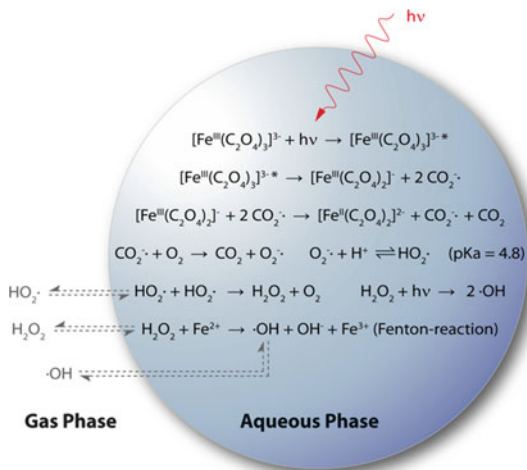
Another option is the sequential cleavage of the Fe(III)–O bond between iron and one oxalate ligand and its C–C bond which produces a biradical complex or two $CO_2^{\cdot-}$ radicals [211, 216, 221]:

$$[Fe^{(III)}(C_2O_4)_3]^{3-} + h\nu \rightarrow [Fe^{(III)}(CO_2^\bullet)_2(C_2O_4)_2]^{3-} \quad \text{or} \tag{22}$$

$$\rightarrow [Fe^{(III)}(C_2O_4)_2]^- + 2CO_2^{\cdot-} \tag{23}$$
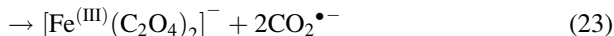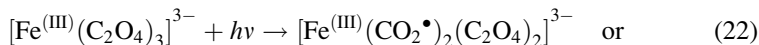
The different proposed mechanisms were presented by two research groups; [219, 222, 223], both groups presenting experimental evidence for their findings. Thus, it might be possible that both reaction mechanisms take place simultaneously depending on parameters such as mono-, bis-, or tris-oxalato coordination, excitation wavelength, or excitation energy. In atmospheric aqueous phases chemistry it is of importance which mechanism holds; that is, whether one Fe(II) and one $CO_2^{\cdot-}$ or two $CO_2^{\cdot-}$ radicals are produced. $CO_2^{\cdot-}$ is capable of producing Fe(II) via secondary reactions with parent Fe(III)-oxalato complexes but can also react with other electron acceptors such as O_2 which are likely to compete in more or less dilute atmospheric aqueous media (Fig. 9). Regardless of the exact reaction mechanism, the ferrioxalate system can produce Fe(II) quantum yields larger than unity because of the secondary Fe-reduction by the $CO_2^{\cdot-}$ radical formed.

Figure 9 illustrates the complicated interactions of iron-oxalato complex photochemistry with radical chemistry and the chemistry of organic substances. The main impacts of iron complex photochemistry are ultimately (1) breaking of C–C bonds and thus degradation of the ligand (oxalate) and (2) formation of radicals
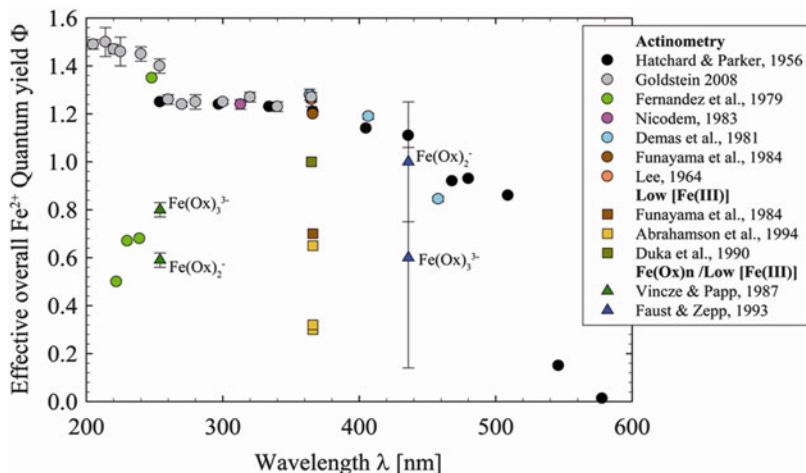
Fig. 10 Overview of Fe^{2+} quantum yield measurements in argon saturated solutions for the ferrioxalate system, Actinometry: specified actinometry conditions, high initial Fe, [Fe(III)] = 0.006–0.15 M, 0.05 M H_2SO_4, see Hatchard and Parker [206] for details; low [Fe(III)]: lower initial Fe(III) concentrations than actinometry conditions, Fe(Ox)n: individual complexes

which can lead to turnover of substances present in the droplets or deliquesced particles.

A prerequisite to simulate the impact of iron complex photochemistry in atmospheric aqueous systems is the characterization of its efficiency. Figure 10 presents an overview of quantum yield measurements in the ferrioxalate system as a function of wavelength.

At first glance, the results appear quite scattered. The values obtained under conditions of chemical ferrioxalate actinometry represent the upper boundary of the reported values, which mostly agree with each other. Between 250 and 350 nm the quantum yields are fairly constant around $\Phi \sim 1.25$. Ferrioxalate actinometry is performed under standardized conditions using millimolar concentrations of ferrioxalate (and above millimolar at $\lambda \geq 436$ nm) and an acidic pH (0.05 M H_2SO_4) of about 1.2 [206]. Other measurements have been carried out at lower initial Fe(III) concentrations as well as different Fe(III) to oxalate ratios and different pH values; these mostly result in lower Fe(II)-quantum yields. Some investigations discriminating between individual complexes of Fe(III) and oxalate have been performed, while others did not provide an analysis of the individual complexes and are thus valid only for their respective complex-mixtures. However, all measurements with initial Fe(III) concentrations below millimolar result in lower quantum yields. It is therefore desirable to characterize systemically any possible effects of initial Fe(III) complex concentration, speciation, and other experimental conditions on the ferrioxalate quantum yield to be able to interpret reported differences.

At initial Fe(III) concentrations higher than 2×10^{-4} M, quantum yields of $\Phi \sim 1.25$ are obtained using 308-nm laser flash photolysis, in agreement with the

values measured under actinometry conditions [204]. At lower initial Fe(III) concentrations the measured quantum yields begin to decrease down to approximately half of the maximum value. This phenomenon can be explained by a kinetic effect of the concentration decrease on the secondary reactions involved in Fe(II) formation. The recombination of $CO_2^{\bullet-}$ radicals to form oxalate becomes more favored at more dilute conditions whereas the secondary reduction of unphotolyzed Fe(III) species by $CO_2^{\bullet-}$ becomes less effective at lower Fe(III) concentrations. These findings can explain the discrepancies between measured ferrioxalate quantum yields (Fig. 10) and should be considered when ferrioxalate photochemistry takes place at sub-millimolar initial concentrations.

4.3 Photochemistry of Fe(III) Polycarboxylate Complexes

As discussed above, the first step in photochemical reactions of Fe(III) carboxylate complexes has been thought to involve ligand to metal charge transfer [224, 225] as a concerted inner sphere electron transfer, and the subsequent separation of the photofragments into the bulk solution. It can be written in simplified form as

$$[\text{Fe}^{(\text{III})}(\text{OOC-R})]^* \rightarrow \text{Fe}^{2+} + \text{R-COO}^\bullet \tag{24}$$
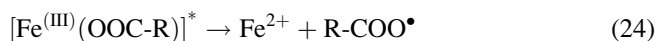
where R-COO$^-$ is the carboxylate ligand and R-COO$^\bullet$ is the primary organic radical formed. Recently, investigations of the primary photochemical steps in polycarboxylate complex photochemistry have been carried out using time resolved transient spectroscopy. These investigations report the formation of long lived radical complexes (25) with lifetimes in the millisecond range as the main reaction path (90–98% of photoactivated complexes) whereas (24) only accounts for 2–10% decay of photoactivated complexes [226–230]:

$$[\text{Fe}^{(\text{III})}(\text{OOC-R})]^* \rightarrow [\text{Fe}^{(\text{II})}(^\bullet\text{COO-R})] \tag{25}$$

$$[\text{Fe}^{(\text{II})}(^\bullet\text{OOC-R})] \rightarrow \text{Fe}^{2+} + {}^\bullet\text{OOC-R} \tag{26}$$

However, it could be argued that, despite the discovery of the new transient, the net chemical products are identical with those in (24). Possible reactions of the long lived radical complex are poorly characterized but they will most likely influence the quantum yield and product formation depending on the reaction conditions and available reaction partners. In laboratory systems such reactions could involve dissolved O_2, other Fe(III) species, or back-electron transfer; reaction paths in the atmospheric aqueous phase would be less restricted.

After the radical complex decays, R-COO$^\bullet$ will decarboxylate instantaneously ($k_{R27} \sim 10^9$–10^{12} s^{-1}) [231–233]:
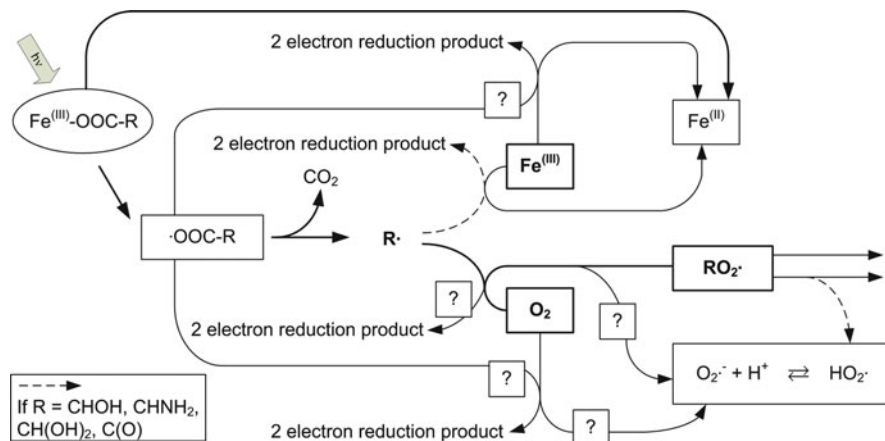
Fig. 11 Scheme of Fe(III) complex photochemistry, modified after [203], 2 electron reduction can only occur in case of hydroxyl, amino, diol, or keto substitution at the radical bearing C-atom; questionable and rather improbable reaction paths have been marked with ?, see text for discussion

$$R\text{-}COO^\bullet \rightarrow R^\bullet + CO_2 \tag{27}$$

followed by the rapid reaction of the alkyl radical $R^\bullet$ with dissolved oxygen, forming a peroxyl radical with $k_{R28} \sim 2 \times 10^9 \, M^{-1} \, s^{-1}$ [234]:

$$R^\bullet + O_2 \rightarrow RO_2^\bullet \tag{28}$$

Subsequent reactions of $R^\bullet$ and $RO_2^\bullet$ can be specific depending on the type of ligand and its substitution. The scheme in Fig. 11 presents a critical evaluation of possible reactions following complex photolysis proposed by Faust and Zepp (1993). The main channels are electron transfer reactions of the alkyl radical $R^\bullet$ with Fe(III) species and the formation of peroxyl radicals $RO_2^\bullet$.

It should be noted that the formation of peroxyl radicals seems to be the most favourable path, because dissolved O_2 is present in concentrations of around 3×10^{-4} M at atmospheric pressure and (28) is usually fast ($k_{R28} \sim 2 \times 10^9$ $M^{-1} \, s^{-1}$ [234]). Furthermore, an electron transfer reaction of the alkyl radical $R^\bullet$ with Fe(III) or O_2 seems to be feasible only if there is a hydroxyl, amino, diol, or keto substitution on the radical bearing C atom [235, 236]. Unfortunately, the pathway of an electron transfer reaction of the alkyl radical $R^\bullet$ with O_2 forming $O_2^{\bullet-}$ has been postulated as a general pathway following Fe(III)-organic complex photolysis by a number of authors [167, 224, 237–241]. This is overly simplified and can be misleading, since a mechanism can only be explained in the case of hydroxyl-, amino-, diol-, or keto-substitution. It has to be emphasized that the peroxyl radical formation is expected to be a major reaction route after Fe(III) organic complex photolysis other than oxalate for the above-mentioned reasons.
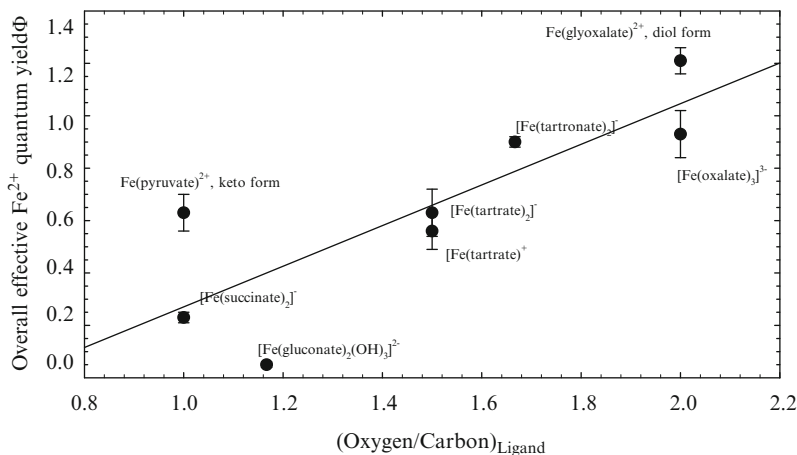
Fig. 12 Measured overall Fe^{2+} quantum yields of Fe(III) complexes as function of oxygen to carbon ratio of the ligand (308 nm single flash photolysis, Ar saturated solutions)

Peroxyl radical formation has been suggested, for example, in the photolysis of Fe (III) acetate [242] and Fe(III) malate [243]. According to the known pathways of peroxyl radical chemistry in solution [234], formation of H_2O_2, $HO_2^{\bullet}$, and stable organic end products will occur. Consequently, $O_2^{\bullet -}$ can be produced indirectly via $HO_2^{\bullet}$ elimination in some cases.

Fe^{2+} quantum yield measurements of several other atmospherically relevant Fe(III) carboxylate complexes have been performed for excimer laser flash photolysis [204, 227] and Hg(Xe) lamp photolysis [203, 235, 244, 245]. Different experimental types of quantum yield determinations have been listed. Quantum yields labelled with ΦFe(II) Ar are Fe(II) quantum yield measurements in argon saturated solution, while those labeled ΦFe(II) O_2 pertain to Fe(II) quantum yield measurement in solutions saturated with atmospheric oxygen. For ΦFe(III) the initial Fe(III) complex disappearance upon photolysis was measured. In the case of Φmalonate the amount of the malonate ligand that was photochemically decomposed was measured, leading to a ligand disappearance quantum yield. The range of measured quantum yields among the different carboxylate ligand complexes with Fe^{3+} shows a large variability with measured Fe^{2+} quantum yields from 0.021 to 1.21 at the chosen reference wavelength 308 nm (Fig. 12).

Obviously, the choice of ligand seems to affect the measured quantum yields. A trend of increasing overall Fe(III) quantum yields of Fe(III) complexes with increasing oxygen to carbon ratio of the ligands is seen among the investigated complexes (Fig. 12).

Oxygen can be present in three different binding modes in the carboxylates considered here: the carboxylate, hydroxyl, and keto groups. Additionally, the keto-form can be hydrated, forming a gem-diol with two hydroxyl groups at one carbon atom. Oxygen substitution is thought to affect the photoreactivity in two ways. The first is via inductive effects causing better ligand-to-metal charge transfer (LMCT) in the primary reaction step, as explained for glyoxalate and

pyruvate above. It is presumed that the increased electron density through the oxygen lone electron pairs of the -OH, -C(O)-, or -CH(OH)$_2$ groups can be inductively propagated to the neighboring -COO$^-$ group, thus facilitating the LMCT. Second, the influence can occur via the presence of an oxygen containing group on the C-atom next to the LMCT-involved carboxylate group, which enables a two electron oxidation product of the ligand. Ligand fragments, which are able to undergo a two electron oxidation after decarboxylation, are those of tartronate and tartrate (both $^\bullet$CHOH-R), pyruvate ($^\bullet$C(O)-R), and glyoxalate ($^\bullet$CH(OH)$_2$). The unpaired electron can be transferred to parent Fe(III) complexes and thus increase the Fe(II) yield. Additionally, the peroxyl radicals formed from ligand fragments of tartronate, tartrate, and glyoxalate can undergo an HO$_2^\bullet$ elimination, which can further cause secondary Fe(II) production.

Fe(III) complexes having a primary organic fragment after decarboxylation with $^\bullet$CH$_2$-R structure (such as complexes of malonate, succinate, and glutarate) all display significantly lower quantum yields compared to the more oxygenated compounds discussed above (Fig. 12). With the $^\bullet$CH$_2$-R structure, a second electron oxidation step of the ligand is not possible; instead the fragments can only decay through peroxyl radical formation and subsequent recombination. Thus no relevant secondary Fe(II) production occurs in systems with $^\bullet$CH$_2$-R structure, and observed quantum yields are accordingly low. An additional factor causing low Fe(II) quantum yields in the case of malonate is the reported quenching mechanism with a free ligand that causes reoxidation of Fe(II) [245]. Quenching was also reported for Cu(II) malonate photolysis, but not for Cu(II) complexes with succinate and glutarate [246].

In the presence of dissolved O$_2$, peroxyl radicals RO$_2^\bullet$ can form in the reaction of photochemically produced alkyl radicals R$^\bullet$. Generally, oxygen has the effect of decreasing the quantum yield (Table 1). This is usually attributed to the secondary production of oxidants such as H$_2$O$_2$, O$_2^{\bullet-}$/HO$_2^\bullet$, and RO$_2^\bullet$ [203, 230]. The radical species O$_2^{\bullet-}$/HO$_2^\bullet$ can act as both oxidizing and reducing agents. According to a kinetic reaction simulation of the Fe(III) glyoxalate system, the measured effects of lower quantum yields in the presence of dissolved O$_2$ could not be reproduced with the simulation, despite using sensitivity test runs focusing on reaction paths that are sensitive to O$_2$ [204]. Consequently, the O$_2$ effect cannot be kinetically simulated and thus our knowledge about Fe(III) photochemical processes is not complete in this respect. The causes of a quantum yield decrease seem to be complex and therefore the O$_2$ effect has to be considered separately for each system.

4.4 Atmospheric Chemistry Simulation with Extended Fe(III) Complex Photochemistry in CAPRAM

The binding of Fe in different complex species is determined by the amount of potential ligands present, their respective stability constants and the pH. Due to the high stability constants and being a major fraction of organic compounds in the atmospheric liquid phase, mono- and dicarboxylic acids are among the most

Table 1 Summary of quantum yield measurements from Fe(III) carboxylate complex photolysis at different wavelengths using laser flash or continuous Hg(Xe) lamp irradiation

Ligand/complex	Experiment type	Flash photolysis 308 nm	Flash photolysis 355 nm[a]	Lamp photolysis 365/366 nm	Lamp photolysis 436 nm
Oxalate					
$[Fe(OOCCOO)_2]^-$	$\Phi_{Fe(II)}$ Ar	[b]			**1.40 ± 0.40** ; 1.00 ± 0.25[c]
$[Fe(OOCCOO)_3]^{3-}$	$\Phi_{Fe(II)}$ Ar	**0.93 ± 0.09**			**1.00 ± 0.20** ; 0.60 ± 0.46[c]
Malonate					
$[Fe(OOCCH_2COO)_2]^-$	$\Phi_{malonate}$			0.036 ± 0.005[d] ; 0.027[c]	
	$\Phi_{Fe(II)}$ Ar			0.0074 ± 0.0008[d]	
Tartronate					
$[Fe(OOCCHOHCOO)_2]^-$	$\Phi_{Fe(II)}$ Ar	**0.90 ± 0.02**		0.50[e]	
Succinate					
$[Fe(OOC(CH_2)_2COO)_2]^-$	$\Phi_{Fe(II)}$ Ar	**0.23 ± 0.02**		0.13[f]	
Tartrate					
$Fe(OOC(CHOH)_2COO)^+$	$\Phi_{Fe(III)}$		0.47		
	$\Phi_{Fe(II)}$ O$_2$		0.40		
	$\Phi_{Fe(II)}$ Ar	**0.56 ± 0.07**	0.44	0.42[e] ; 0.40 (pH 2.7)[f]	
$[Fe(OOC(CHOH)_2COO)_2]^-$	$\Phi_{Fe(II)}$ Ar	**0.63 ± 0.09**		0.58 (pH 4)[f]	
Pyruvate					
$FeOOCCOCH_3^{2+}$	$\Phi_{Fe(III)}$		0.53		
	$\Phi_{Fe(II)}$ O$_2$	**0.47 ± 0.07**	0.46		
	$\Phi_{Fe(II)}$ Ar	**0.63 ± 0.07**	1.00		
Glyoxalate					
$FeOOCC(OH)_2^{2+}$	$\Phi_{Fe(III)}$		0.70		
	$\Phi_{Fe(II)}$ O$_2$	**0.76 ± 0.05**	0.80		
	$\Phi_{Fe(II)}$ Ar	**1.21 ± 0.05**	1.05	0.97[e]	
Gluconate					
$[Fe(HOCH_2(CHOH)_4COO)_2(OH)_3]^{2-}$	$\Phi_{Fe(II)}$ Ar	**0.05 ± 0.01**			

$\Phi_{Fe(II)}$ Ar is Fe(II) quantum yield measurement in Ar saturated solution, $\Phi_{Fe(II)}$ O$_2$ is Fe(II) quantum yield measurement in atmospheric oxygen saturated solution, $\Phi_{Fe(III)}$ is initial Fe(III) complex disappearance quantum yield, $\Phi_{malonate}$ is ligand disappearance quantum yield

Bold values: [204]

[a] [227]

[b] Not determined due to experimental limitations

[c] [203]

[d] [245], 300–366 nm integral

[e] [244]

[f] [235]

Fig. 13 Fe(III) speciation in cloud water and wet particles when included in the chemical aqueous phase radical mechanism (CAPRAM) to simulate aqueous tropospheric chemistry
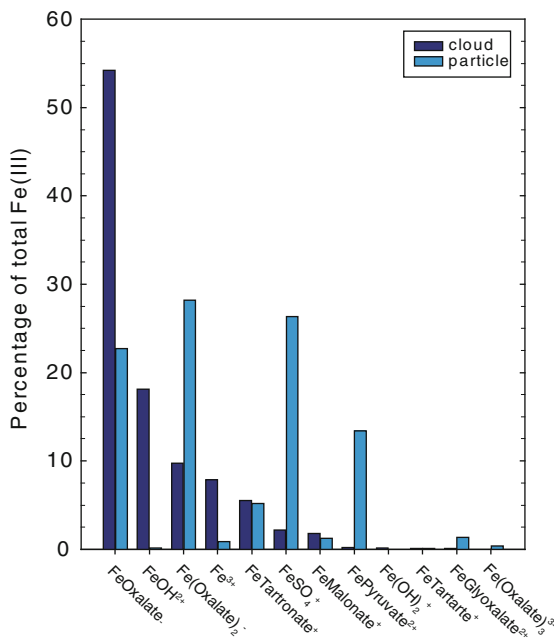
important ligands for Fe to be considered [167, 247]. Realistic speciation calculations have been performed using a set of iron complex reactions based on kinetics implemented in the CAPRAM [248], which contains organic chemistry up to C4 compounds.

The major fraction of Fe(III) is bound in carboxylate complexes, mainly with oxalate, and a smaller fraction in inorganic complexes with hydroxide and sulfate in both scenarios, cloud and deliquesced particles (Fig. 13). After oxalate, complexes with tartronate, pyruvate, malonate, and glyoxalate altogether constitute a significant portion of the total soluble Fe(III). It is important to distinguish cloud and particle periods because the differences in pH (pH$_{cloud}$ = 3.2, pH$_{particle}$ = 1.2) and liquid water content (LWC) lead to a largely different Fe(III) species distribution. Other calculations with an equilibrium speciation model show that complexes with tartrate, lactate, and malate may also be able to compete with the aforementioned carboxylates when their concentrations approach the upper limit that has been reported for cloud water or ambient particles. Since oxalate complexes constitute the largest fraction of bound Fe(III), their photochemistry is especially interesting.

Iron complex photolysis is one of the processes that produce reduced iron (Fe(II)) in a highly oxidizing environment like the atmospheric aqueous phase. There are numerous other processes such as reactions with HO$_x$ species or Cu(I)/Cu(II) which can reduce or oxidize iron in the troposphere. These reactions can take place simultaneously and cause iron to undergo a so-called redox-cycling [167]. Because of the large number of complex interactions in the atmospheric chemistry of the transition metal iron, it is useful to utilize models to assess the impact of the complex iron photochemistry.

Fig. 14 Simulated concentration time profiles for the Fe(III) ligands pyruvate and oxalate, summation of all forms of the respective ligand (free mono- or di-anion, free acid and ligand bound in Fe(III)-complexes), light blue stripes indicate cloud periods, in between are wet particle periods
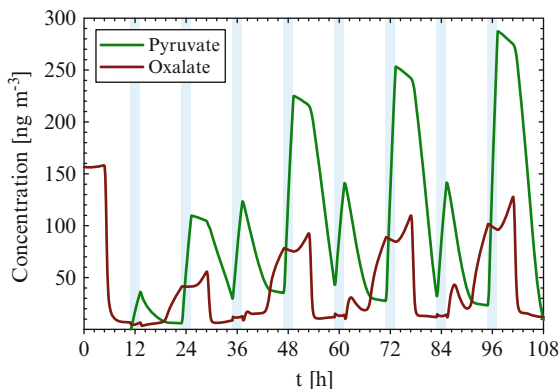
Photolysis reactions of Fe(III) complexes with malonate, tartronate, succinate, tartrate, and glyoxalate were implemented in CAPRAM; Tilgner and Herrmann [248]) as "extended Fe-carboxylate photochemistry." The former version of CAPRAM contained only Fe-sulfato, Fe-hydroxyl, and Fe-oxalato complex photochemistry. CAPRAM as part of the SPectral Aerosol Cloud Chemistry Interaction Model (SPACCIM [249]) has been applied in a 4.5-day non-permanent cloud simulation including 8 cloud passages between deliquescent particle periods. Fe (III) complex photolysis represented a small contribution to oxidant formation, where 1.3% of the total $O_2^{\bullet-}/HO_2^\bullet$ aqueous phase daytime sources in the model could be directly attributed to complex photolysis. Because Fe(III) complex photolysis can only occur during the daytime, only the daytime source fluxes have been considered. For this comparison, the daytime flux values of each reaction channel contributing to $O_2^{\bullet-}/HO_2^\bullet$ production were averaged over the entire simulation time of 108 h and added to give the 100% reference. $O_2^{\bullet-}/HO_2^\bullet$ contributing channels for the aqueous phase are in situ decay reactions of peroxyl radicals formed via oxidation processes, but the largest source is phase transfer from the gas phase. The contribution of Fe(III) complex photoreduction to the average Fe(II) formation flux over the total simulation time was 7% from Fe(III) oxalato complex photolysis, and 1% from additionally implemented other Fe(III) carboxylato photolysis reactions. Additional sources of reduced iron were reactions with $O_2^{\bullet-}/HO_2^\bullet$ and reactions with copper. The Fe(III) complex photolysis reactions can be a major sink for the carboxylate species besides radical reactions of OH, NO_3, or SO_4^-. Almost the entire oxalate in the simulation is depleted through Fe(III) complex photolysis, whereas 40% of the simulated pyruvate was degraded via complex photolysis and the remaining 60% via radical reactions. Percentage values here refer to averaged sink fluxes over the total simulation time.

Figure 14 shows simulated concentration time profiles for the Fe(III) ligands pyruvate and oxalate, which have mostly lower concentrations during the daytime, when the photochemistry as described here is active. Thus, it has to be emphasized that Fe(III) complex photolysis reactions can be a major sink for the carboxylate species besides radical reactions, and it is crucial not to neglect these reactions when the fate of carboxylic acids in the atmospheric aqueous phase is considered.

5 Photochemistry Associated with Ice

Ice is an abundant material found in the environment in the form of ice particles in the atmosphere, sea ice on oceans, and snow and glaciers on the continents. The surface of ice in each of these compartments is more or less continuously exposed to the atmosphere. Thus potentially a continuous exchange in both directions of atmospheric trace gases with these ice surfaces exists. The general role of environmental and atmospheric ices in affecting the oxidative capacity of the atmosphere, the biogeochemistry of short and long-lived organic pollutants, the cycling of halogen gases, and the nitrogen oxide cycle has been reviewed recently [250–253]. Those parts of environmental ice that are in direct contact with the atmosphere and thus the most relevant parts also experience irradiation by the sun. The illuminated, or photic, zone in snow packs in alpine or polar environments constitutes a significant fraction of those parts of snow or firn that exchange with the overlying air [254–256]. Similar arguments may hold for sea ice. The vanishingly small absorption cross section for water in the visible and near UV regions of the spectrum means that photochemistry in ice is governed by the presence of chromophoric material there. One example of processes induced by chromophoric material in snow is illustrated in Fig. 15 showing the emission of HONO from snow containing humic material exposed to NO_2 and UVA light, which will be discussed further below.

Ice itself is a high temperature material in the sense that under environmental conditions it is close to its melting point. The relatively weak hydrogen bonds which are the basis for the crystalline solid (hexagonal Ih ice) allow the surface to become disordered in response to the broken symmetry near the surface [258]. This disordered layer is a general surface phenomenon of solid matter and also referred to as surface premelting or quasi-liquid layer (QLL) [259] and involves the top few nanometers near the surface. This layer may present a particular environment for adsorbing trace gases, which may exist there with a local environment different from that in a liquid or solid solution. Atmospheric ice particles nucleate from solution droplets or on refractory material so that most of them remain with some solutes left as solution pockets in equilibrium with ice or attached dust or carbonaceous material [260]. Those solution pockets must not be confused with the QLL as they are considered a thermodynamically stable phase [261]. This microstructure determines the specific environment for photochemical processes with ice in the atmosphere, but also with snow derived from this ice. Once precipitated, snow continuously changes its microstructure through metamorphosis [262–264] that may lead again to relocation of associated material. The snow structure is also crucial to determine the depths to which radiation reaches in the actinic wavelength region [265]. Sea ice presents a polycrystalline structure with the solutes present within a brine solution in cracks, veins, and triple junctions, or also on the surface [266–269], out of which frost flowers may grow [270].

In the following paragraphs we will summarize the recent developments in understanding direct and indirect photochemical processes in the "light" of this
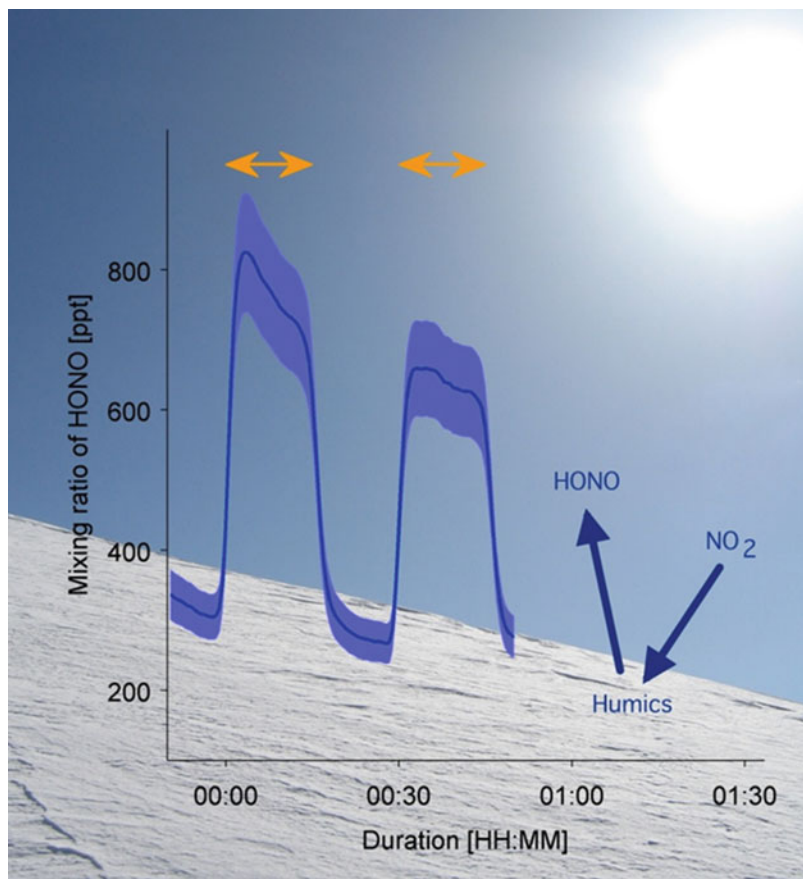
Fig. 15 Evolution of the HONO gas phase mixing ratio (*solid line*) with time after contact of NO_2 with humic acid doped ice. Two consecutive irradiation periods in the visible range (*orange arrows*) in the presence of NO_2 in the gas phase are shown. The *shaded area* illustrates the accuracy of the HONO measurement. Time zero denotes the beginning of the (first) irradiation period [257]

structural picture of ice in the environment [367]. The examples include organic and inorganic chromophores as far as they are implicated in the chemistry of atmospherically relevant gases.

The general significance of photochemical processes in snowpacks has been reviewed by Grannas et al. [251]. Evidence has emerged that many insoluble and soluble organic compounds are associated with ice in snow that may be responsible for a wealth of direct and indirect photochemical processes [271]. While many direct photolytic processes have been considered in the past [251], indirect processes, especially those involving organic chromophores, have only been recognized in this context recently. As an example, Rowland et al. [255] demonstrate that organic and inorganic chromophores induce photochemical degradation

of aldrin and dieldrin in frozen aqueous solutions. They also argue that the specific arrangement of soluble chromophores and the hydrophobic target leads to distinctly different degradation behavior compared to that in solution.

Almost all laboratory studies of ice photochemistry have used illuminated bulk ice samples, with reagents frozen in solution. Often it is assumed that the reagents are excluded together and uniformly to the ice surface region in contact with the overlying atmosphere. Various thermodynamic formulations have been used to estimate the concentrations of the excluded reagents [272, 273], but such approaches seem to be deficient in some cases [274]. Nevertheless, photolytic kinetics experiments have generally, but not always, found similar loss rates for species frozen from solution as in the liquid phase [192, 251, 275–277].

Recently it has become possible to test the assumption that photochemistry of compounds present at the air-ice interface, whether through exclusion during freezing or following deposition from the gas phase, is well described by the corresponding solution-phase process. Donaldson and co-workers have used glancing-angle laser fluorescence and Raman spectroscopy to probe chemical processes at the condensed phase-air interface of water and ice surfaces [93, 278–280]. They report that at least in the case of aromatic organic compounds, photolysis on "pure" ice surfaces is significantly faster than on liquid surfaces or that occurring within the ice matrix. This is a true surface effect, as demonstrated by experiments in which the photolysis rate is seen to be directly related to the surface/volume ratio of the ice [281]. Another study altered the surface properties of the air-ice interface, by freezing salt solutions such that an increasing amount of a "quasi-brine-layer" was present at the interface [281]. The photolysis rate of an aromatic test molecule at the air interface became slower as that interface became more "liquid-like" on a microscopic level, until it became identical with the rate seen on a liquid surface. This result also showed that increased light scattering at the ice vs liquid surfaces (or within the ice matrix) is not responsible for the enhanced photolysis rates.

One possible reason for this rate enhancement, at least in some instances, is a change in absorption cross sections and/or photolysis quantum yields due to self-association at the interface. This effect has been documented for aromatic compounds both spectroscopically and by simulations [278, 282, 283], and is a consequence of the different hydrogen bonding environment present at the air-ice interface compared to the liquid surface. In the case of benzene in particular, the self association gives rise to a significant red-shift in the absorption spectrum [279], such that benzene present at the air-ice interface may absorb available solar radiation in the lower atmosphere. This opens the possibility of a previously unconsidered fate for several aromatic pollutants present in snow- and ice-covered regions.

The majority of the examples mentioned above are concerned with oxidative degradation processes. Bartels-Rausch et al. [257] have shown that organic chromophores in ice can also reduce atmospheric gases. Humic acid was demonstrated to reduce nitrogen dioxide to gaseous nitrous acid, and this reaction was further found to be significantly enhanced by visible light. It was argued that organic sensitizers, such as benzophenone, receive an electron from a donor, such

as phenols, upon irradiation and pass this electron to NO_2 [127, 128, 202]. Both benzophenone and phenols represent typical building blocks of humic matter and have also been identified in polar surface snow [251]. Recent HONO emission measurements at Barrow, Alaska indeed indicated that this process is responsible for light induced HONO production during the day [284]. Bartels-Rausch et al. [257] further showed that the rate of HONO production scales linearly with increasing humic acid content in the ice and that extrapolations of the rate meet rates previously found for pure humic acid films and in aqueous aerosol particles. From this they concluded that the general chemistry in ice and in water is identical. Interestingly, this correlation was found to be valid only for small concentrations of humic acid in ice; at higher concentrations the rate of HONO production stagnated. It was concluded that at high concentrations part of the organic material in the ice matrix is no longer accessible to the gaseous NO_2 due to specific agglomeration or displacements in the ice matrix.

Another example of an environmentally relevant species that is strongly involved in redox-cycling is mercury. Mercury is a globally distributed pollutant, and as such is also found in snow and sea ice. Input to the surface snow comes preliminarily from atmospheric deposition [253, 285]. Ocean currents transport most mercury found in sea ice [286]. What makes mercury especially interesting from a chemical point of view is that its environmental fate is largely given by its oxidation state [253, 285]. Elemental mercury, Hg(0), is highly volatile and has a negligible affinity to surfaces such as snow or ice [287]. Divalent mercury, Hg(II), is highly water-soluble and the main oxidation state present in snow and ice. The precise balance between Hg(0) in the gas phase and Hg(II) in the surface snow is not static. For example, during spring episodes so-called Mercury Depletion Events (MDE) occur where Hg(0) is almost completely removed from the air. These events are driven through gas phase chemistry, which converts Hg(0) to Hg(II) that subsequently becomes bound to particles and/or ground snow. Halogen emissions from surface snow are currently thought to trigger those gas phase chemical cycles. Snow may thus act as a reservoir in which mercury is accumulated during winter. In spring this sequestered mercury may be released to the aquatic environment during snowmelt [288] from which it may enter the food chain [289]. Field studies have, however, shown that the Hg(II) initially trapped in the surface snow can be reemitted as Hg(0) to the atmosphere and that this emission is enhanced by solar radiation [290]. This light-driven emission of mercury from the snow thus lowers the overall net transfer of atmospheric mercury to the aquatic environment. Only the fraction of mercury that is buried in the snow below the photolytic zone is inert to photochemistry and can be permanently stored.

The detailed mechanisms and rates of the underlying redox chemistry in ice and snow are still open. In a recent laboratory study, Bartels-Rausch et al. [291] could show that the light-driven emission of Hg(0) from an ice matrix is significantly enhanced in the presence of organic chromophores (Fig. 16). That the photolytic reduction of mercury is enhanced in the presence of organics is well established for the aqueous phase [292]. There, two mechanisms seem to operate simultaneously [293]. Organics easily form complexes with mercuric ions and light absorption of
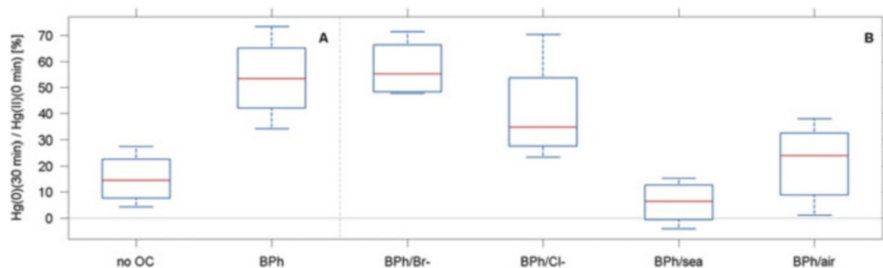
Fig. 16 The effect of organic chromophores, halogens, and oxygen on the light-driven release of elemental mercury from ice films. Results are given relative to the initial concentration of mercuric ions in the ice after 30 min irradiation at 258 K. The solution to freeze the ice films was always doped with Hg(II) (6×10^{-8} M) and additionally contained the following compounds as indicated: "no OC" denotes experiments of pure HgO solutions; "BPh" 6×10^{-7} M benzophenone in unbuffered solutions at pH 7 (of the molten ice film); "BPh/Br$^-$" 6×10^{-7} M benzophenone and 5×10^{-8} M bromide; "BPh/Cl$^-$" 7×10^{-8} M chloride; "BPh/sea" 0.5 M chloride, 1 mM bromide; "BPh/air" 6×10^{-7} M benzophenone in the ice – 20% oxygen was present in the carrier gas stream. In each box, the central mark is the median, the edges of the boxes are the 25th and 75th percentiles, and the whiskers extend to the most extreme data points [291]

these complexes can lead to intramolecular redox reactions [294]. Also, the organics can adsorb light and transfer electrons, or energy, intermolecularly, similar to the chemistry described above for nitrogen oxides. In either case, Bartels-Rausch et al. [291] argued that the reduction of Hg(II) to Hg(0) in ice most likely proceeds via Hg(I) as intermediate. They observed that the presence of chloride and of oxygen significantly lowers the photoreactivity of the mercury-organics mixtures in ice, whereas the presence of bromide had little influence. This observation is in line with the oxidation capacity of oxygen and of the halogens in irradiated aqueous solutions [292, 295]. This preservation of mercury in the snow might partially explain the higher mercury concentrations in halogen-rich snow on sea ice as compared to more off-shore samples [253].

Turning our attention to inorganic chromophores, one of the most relevant is certainly H_2O_2. H_2O_2 is ubiquitously present in environmental snow and ice and is an important photolytic OH source [179]. While estimates based on photochemistry in solution indicate a relatively short photolytic lifetime [195], Beine and Anastasio [254] suggest that when H_2O_2 is dissolved in crystalline ice the apparent lifetime becomes significantly longer because cage recombination may occur, while when adsorbed in a QLL or dissolved in a brine, OH may escape as in solution. This is therefore an example where a trace gas may become a solute in crystalline ice, leading to an extended photolytic lifetime.

Of similar photochemical importance as H_2O_2 is nitrate, which absorbs light above 290 nm. The ubiquitous presence of nitrate in environmental ices is well documented for cirrus ice particles [296, 297] as well as permanent and perennial snow packs [298–301]. In aqueous solution, photolysis of nitrate ion leads to either OH and NO_2 or $O(^3P)$ and nitrite ion, with typically significantly higher quantum yields for the first pathway [197, 200]. In the upper troposphere, it is currently thought that uptake of HNO_3 to ice makes it ineffective as a photolytic source of

NO_X as it is in the gas phase, in spite of the fact that the nature of nitrate at the ice surface is not well established. Recent spectroscopic experiments indicate that nitrate exists at the ice surface in solvated form with a local environment similar to that in concentrated solution [302]. Still, this does not rule out a reduced solvent cage compared to dilute nitrate solution that would allow NO_2 to escape, more likely due to recombination being suppressed, as has been suggested based on quantum yield measurements for frozen nitrate solutions [192]. Since in snow the nitrate anion is often co-located with other ions, e.g., halogenide ions, in a brine solution, ion specific effects may lead to enhancement of nitrate ions at the aqueous brine-air interface. Such effects have been shown to lead to enhanced nitrate photolysis rates in aqueous solution [303, 304]. In some contrast to the case of H_2O_2, the particular environment in snow or ice makes photolysis of nitrate more efficient than in solution. Such effects would help to explain the significant cycling of NO_X mediated by nitrate photolysis in polar snow [276, 298, 305–308].

Halogens have not been discussed so far. Halogens are important atmospheric players in stratospheric and tropospheric ozone depletion. In the stratosphere direct photolysis leads to ozone depletion. In surface ice, snow halogens can be activated and released to overlying air, where they foster ozone depletion. In snow or ice the most prevalent condensed phase halogen compounds do not absorb the available light of the solar spectrum. Potentially, interhalogen complexes such as Br_2I^- and BrI_2^- might absorb in the visible wavelengths [309] yet their existence at the low halogen concentrations in typical snow samples is questionable. It might be proposed that the light-induced reaction with excited organic chromophores might be of higher relevance, similar to the chemistry observed in aqueous solutions [295]. This chemistry can interfere with light-driven redox reactions, as discussed above for mercury where halogens can foster the back-reaction of the photochemistry. Additionally, halogens might form complexes with metallic ions such as mercury. Those complexes typically absorb at longer wavelength than the isolated species; mercury-iodine complexes for example absorb at wavelengths above 300 nm [310]. Indirect photochemical processes involving halogen compounds associated with ice have the potential to release Br_2, BrCl or halogenated VOCs that are in turn strongly implicated in gas phase photochemical cycles of the air mass in contact with ice or snow.

In summary, atmospherically relevant photochemistry with environmental ices is initiated by a range of organic and inorganic chromophores. In a wealth of secondary energy transfer and redox processes species of atmospheric relevance may be reduced or oxidized. Recent developments in the field have indicated the role of the specific arrangement of chromophores and reaction partners as well as their molecular level local environment in ice cloud particles, sea ice, or snow packs that will require further attention in the future. Photochemical processes in ice continue to be an important issue in the cycling of major and trace constituents as highlighted in this chapter. They are also linked to albedo changes of the frozen parts of the Earth's surface and thus to the radiative budget of the atmosphere [311]. Furthermore, photochemical processes are important ingredients in the way trace constituents are incorporated into ice archives from which past climates are reconstructed [308].

6 Photochemical processes on natural and built ground surfaces

In the preceding sections we addressed long-wavelength photoassisted reactions as overtone processes and heterogeneous reactions on aerosols (photosensitized and photocatalyzed) or on ice. However, the condensed material initiating these reactions can also (and maybe even predominately) be found on the continental natural or affected ground surface, such as soil, vegetation covered by plant degradation products, and within films coating urban surfaces (such as roads and buildings).

Of special interest are the films on the ground in densely populated and urban areas, also called 'urban grime', whose chemical composition partly resembles that of urban atmospheric aerosols [312–314] but whose chemistry is still almost unknown. In this section, we first turn our attention to urban grime and soil surfaces.

In the past decade or so, extensive work by Diamond and co-workers [312–317] has shown that exposed outdoor surfaces in urban areas rapidly become coated with a complex mixture of chemical compounds ("urban surface film"), most readily encountered as "window grime." This film grows via accretion from the atmosphere and is removed by rain wash-off, or revolatilization processes, yielding an (estimated) steady-state thickness of several tens to hundreds of nanometers. Chemical analysis of these films has been carried out both in a "broad brush" approach [312, 313], which identified the compound classes present, and by more detailed studies [315–317] that determined the specific compounds within these classes.

Interestingly, organics make up only 5–10 mass % of the films; most of the identified mass is nitrate (~7%), sulfate (~8%), and various metals (18%). The organic fraction contains a wide array of natural and anthropogenic chemicals including carbohydrates and aliphatic and aromatic compounds [313–321]. PAHs account for approximately 20% of the organic mass of "urban grime" [313, 314]. Sources of PAHs are incomplete fossil fuel combustion [322], wood burning [323], and industrial processes [324]. Some of these PAHs are reported to have carcinogenic and mutagenic properties [312, 325, 326]; those bearing five aromatic rings or more are predominantly adsorbed onto particulate matter [1] and therefore their lifetime and fate are strongly influenced by heterogeneous oxidative processes [73, 76, 78, 80, 81, 84, 85, 328–341]. Raja and Valsaraj showed that particle bound naphthalene and phenanthrene degrade much faster than in the gas phase [338].

Inorganic compounds represent the major mass fraction of "urban grime." Metals, sulfates and nitrates have been identified as the main components [314, 342]. Deposited nitrate ions can further undergo direct photolysis affecting the atmosphere through the release of volatile and reactive nitrogen compounds to the gas phase [276, 298, 305–308, 342, 343]. However, as shown above, the heterogeneous loss of gas phase molecules at surfaces containing photoreactive compounds may be significantly enhanced under illumination [344–346]. Soot, pyrene, and humic acids promote the photoenhanced heterogeneous removal of NO_2 producing both NO and HONO [124, 347, 348].

In one study [349] nitric acid was deposited from the gas phase onto films prepared to mimic the organic fraction of urban grime [73]. Using acridine,

Fig. 17 Fluorescence of acridine in organic film before exposure to gas phase nitric acid (*circles*); following exposure to gas phase acid (*triangles*); and following 90 min of irradiation with actinic light (*squares*)
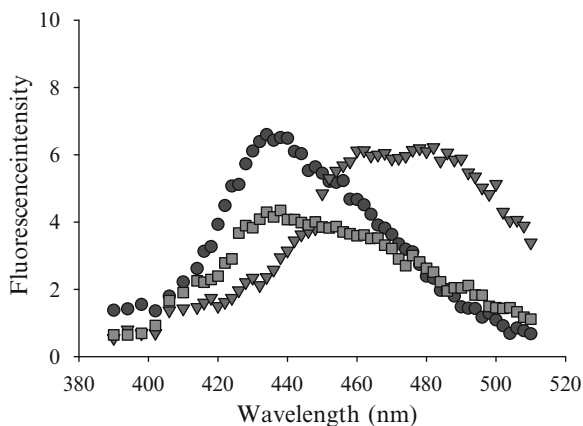
a pH-sensitive fluorescent probe, acidification of the film upon exposure to $HNO_3(g)$ was observed, indicating that the acid was taken up by the organic film and remained there in (at least partially) dissociated form. Illumination of this acidified film using the output of a Xe lamp, filtered optically to simulate actinic radiation on the Earth's surface, caused the pH to increase, eventually returning to its original value (i.e., that which it displayed before acidification). Figure 17 displays these changes in the emission spectrum. At the same time, the concentration of nitrate anion also diminished, as measured by ion chromatography. Given the known photochemistry of nitrate anion in water and ice [192, 197, 350–352], and other arguments presented in Handley et al. [349], we proposed that these observations indicate that the nitrate anion in organic films could photochemically generate NO_2 and HONO, which are then released to the gas phase.

This could have important atmospheric consequences. Because the primary pathway for removal of inorganic nitrate (nitric acid or ammonium nitrate) from the atmosphere is by wet (i.e., uptake by water droplets) or dry deposition, followed by rainout/wash off to the ground, this photochemical reduction of NO_3^- provides a mechanism to recycle nitrate back to the gas phase as "active" nitrogen oxides (HONO, NO_2, or NO). These observations are finally "similar" to the renoxification processes on dust discussed above.

Ammar et al. [353] studied the heterogeneous reaction between gaseous NO_2 and solid pyrene/KNO_3 films, used as a proxy of "urban grime." The uptake coefficients measured under near-UV irradiation (300–420 nm) were between 7- and 15-fold higher than the uptake under dark conditions, highlighting again a strong photo enhancement (Fig. 18). The gaseous products that were identified were NO and HONO. The HONO yield was as high as 36% depending on the composition of the film.

If extrapolated to the solar spectral irradiance at the Earth's surface under near-UV irradiation, the uptake coefficient (at 50 ppbv of NO_2) becomes $\gamma = (8.8 \pm 0.5) \times 10^{-6}$. Such data can be used to estimate the HONO source flux from these urban surfaces as 130 pptv h^{-1} just by assuming that only 1% of a street-canyon surface with 10 m street width and 20 m building height is covered by
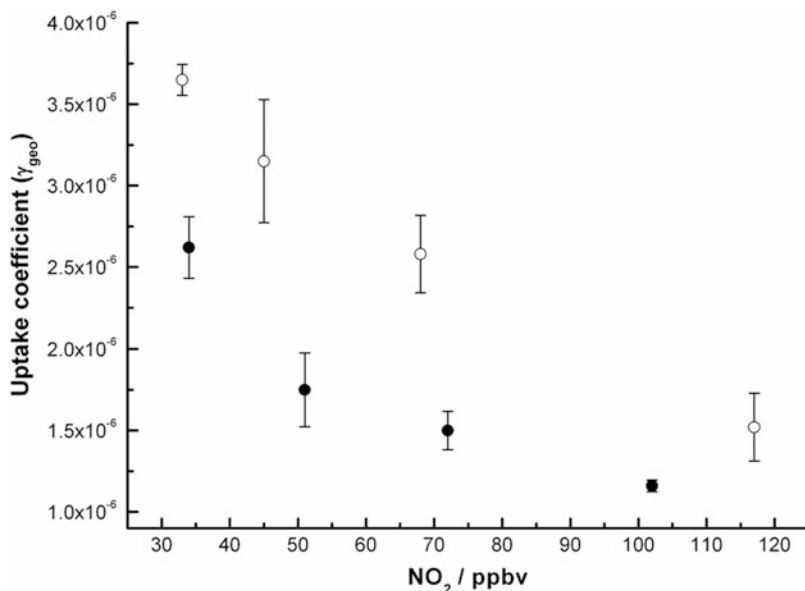
Fig. 18 Steady-state uptake coefficients for the heterogeneous reaction of NO_2 with pyrene films (*empty circles*) and pyrene/nitrate films (*filled circles*) under irradiation as a function of the initial NO_2 concentration. *Errors bar* are 1σ precision

pyrene/nitrate films (it is important to emphasize that this is potentially a quite conservative assumption).

To explain the photoenhanced conversion of NO_2 on pyrene (Py) films into HONO, NO, NO_2^-, and traces of 1-nitropyrene, the following mechanism was suggested:

$$Py \xrightarrow{h\nu} Py^* \tag{29}$$

$$Py^* + NO_2 \rightarrow [Py^+ + NO_2^-] \tag{30}$$

$$[Py^+ + NO_2^-] \rightarrow Py' + NO_2^- \tag{31}$$

$$[Py^+ + NO_2^-] \rightarrow PyNO_2 \tag{32}$$

$$NO_2^- + H^+ \rightleftarrows HONO \tag{33}$$

$$NO_2^- \xrightarrow{h\nu} NO + O^- \tag{34}$$
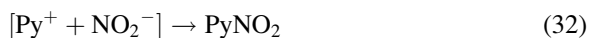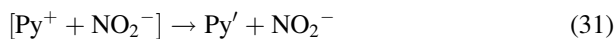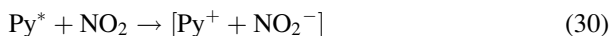
As discussed previously [347, 348], the heterogeneous reaction may proceed via electron transfer from electronically excited states of the PAH (in this specific case pyrene (Py^*)) to NO_2. As indicated in (5), HONO is formed by the acid–base

reaction involving NO_2^-. Miet et al. [337] have suggested HONO formation in the mechanism to explain 1-nitropyrene production. The photo-stability of NO_2^- on the film was tested by Ammar et al. and emission of HONO and NO was indeed observed, implying reactions (5)–(6) [353]. Similar conclusions about the mechanism were also drawn by Sosedova et al. [89], who identified both direct and indirect pathways of HONO formation from exposure of phenolic and polyphenolic compounds to NO_2 and light. HONO was also formed through photolysis of nitrophenols formed as intermediates.

The main conclusion from these observations is that "dirty" urban surfaces may contribute to urban air pollution and promote photochemical pollution.

We finally turn our attention to the natural soil. Soil on Earth is considered to be the layered deposits of parent rock weathering and erosion, which is composed of a large range of organic and mineral components. The relative abundance of these two classes of components varies from pure mineral to almost entirely organic soils. Within the context of atmospheric sciences, soil plays a tremendous role in the biogeochemical cycles of carbon and nitrogen. Soil covers a large fraction of the continental ground surfaces on Earth. Soil is composed of a significant fraction of chromophoric material and is exposed to sunlight for significant periods of time. It is therefore not surprising that the interaction of UV and visible radiation with the biogeochemical cycles has received considerable attention [354]. Such interactions have been investigated mainly in terms of direct and indirect effects of UV radiation on metabolic and abiotic processes that affect carbon sequestration or nutrient cycling. Relatively little attention has been given to direct photochemical processes that would affect deposition to or emission from soil of species implicated in atmospheric chemistry. A few studies have addressed the impact of UV on the net efflux of carbon dioxide and methane [355, 356]. Following up on previous knowledge on the implications of soil processes in the context of the carbon budget, Derendorp et al. [357] specifically determined C2 to C5 hydrocarbon emission rates from irradiated leaf litter. Emission of these saturated and unsaturated hydrocarbons was clearly linked to UV irradiation and the presence of oxygen, providing some evidence for reactive oxygen species inducing lipid peroxidation processes. Degradation of vegetation, and especially lignin, a major structural compound of vegetation, leads to both light absorbing and redox active aromatic compounds as constituents of humic material [358, 359] that are implicated in the production of singlet oxygen, superoxide, or phenoxy type radicals [360]. These in turn are important promoters in the degradation and photobleaching of plant litter itself. However, the radical induced degradation processes also lead to emission of volatile products, such as those observed by Derendorp et al. mentioned above, and also of CO_2 [361] or CO [362, 363]. Some of these emitted species may be directly involved in the photooxidation capacity of the troposphere. This is especially true for the photolytic OH precursors like aldehydes or ketones. Such species have been known to be emitted from degrading plant material [364]. D'Anna et al. [131] observed the emission of several small aldehydes and ketones from humic acid as a result of direct and indirect (sensitized) photochemical processes in the UV and visible wavelengths. The implication to atmospheric chemistry is twofold: these

OVOC species contribute to the atmospheric OH budget. On the other hand, D'Anna et al. also observed a strongly enhanced reaction of humic and fulvic acids with O_3 and suggested that this may be a non-negligible contribution to the overall O_3 deposition to soil. A similar interaction has been discovered by Stemmler et al. [128]. They observed that soil dust or macroscopic soil layers emit nitrous acid (HONO) when exposed to nitrogen dioxide and light (both UV and visible) that showed similar behavior to that observed in similar experiments with humic acids. They suggested that the reaction is due to photosensitized electron transfer from the donating humic acid moieties to nitrogen dioxide. Such a process was suggested before based on similar experiments with mixtures of aromatic ketones and phenolic species [127], which are considered building blocks of humic matter. A third example is the mercury cycle in which photoreduction or photooxidation of Hg(II) and Hg(0), respectively, through radiation induced redox activity of humic material [365, 366], may play an important role in the bioavailability of this toxic compound.

7 Summary and Outlook

The topics discussed in this chapter demonstrate the existence of a wide range of photo-assisted processes in the troposphere not considered in atmospheric models to date. These processes occur through various mechanisms on a wide range of surfaces (including aerosols, urban grime, soil, liquid water, and ice), in aqueous bulk solutions, and in the gas phase (through long wavelength overtone processes).

These sunlight driven processes have only recently been recognized as addressing emerging issues in atmospheric chemistry and so there are still significant gaps in our knowledge limiting our ability to quantify and predict their atmospheric importance. Radical generation may occur in the bulk phase of aqueous particles and thus change reactive radical budgets. However, an important emerging issue is the production of radicals at interfaces; this process may significantly change our understanding of tropospheric heterogeneous chemistry because radicals being formed in such interfacial processes can either increase the gross reactivity of the surface or desorb and become active in the gas phase. Experiments to quantify this radical production under a wider range of chemical composition and conditions are now needed. Excitation of vibrational overtone transitions by red light, followed by molecular dissociation, represents another example of "non-classical" atmospheric photochemistry which may exert a significant influence on radical budgets.

Optical properties of aerosols are currently the focus of many studies aiming to characterize their potential impact on the Earth's albedo and therefore on climate change. However, light-absorbing chemical constituents of aerosols may also change the physico-chemical properties of the particles. The current conceptual view is that trace gases are taken up by aerosols depending on their volatility, the latter being altered by gas phase oxidation processes. If light-absorbing species

present within (or at the surface of) aerosols also act as photosensitizers (which is still an open question), then maybe one should consider the aerosols as being surrounded by reactive oxidizing species or radicals that will certainly alter the phase partitioning of impinging trace gases. If true, this implies that surface reactions are a general phenomenon during daytime in the atmosphere. Additionally, the bulk of particles is probably also chemically very active because of conventional radical chemistry together with species resulting from "new photochemistry." How important may the overall photo-induced chemistry be in terms of coupling air pollution and climate change?

The general sense behind the illustrative examples presented here is that photo-assisted processes are potentially accelerating reactions that would otherwise be too slow to be of any importance, as shown in the case of NO_2 and some organics reacting on dust. But how general is that statement? Do we need to revisit dust chemistry in the upper troposphere? Does this chemistry have the potential to affect the budget of long lived species?

The forecasted impact of climate change is huge and naturally attracts attention. However, air pollution is still an acute issue in the ever growing urban environment, where little attention has been given to the built environment in terms of sinks of pollutants. Given that the surface area of the built environment is by far larger than that exposed by aerosols, we may ask the question whether such surfaces and the urban grime found upon them may be key players in air pollution that have previously been ignored.

Clearly, enhanced radical production through the range of photochemical mechanisms discussed in this chapter could have a significant impact on atmospheric chemistry. Assessing the full extent by which they influence the atmosphere will certainly require further research. We look forward to a new era of atmospheric photochemistry; one which recognizes that the full solar spectrum should be considered as important to the chemistry which affects us all.

References

1. Finlayson-Pitts BJ, Pitts JN (2000) Chemistry of the upper and lower atmosphere: theory, experiments, and applications. Academic, San Diego
2. Calvert JG, Pitts JN (1966) Photochemistry. Wiley, New York
3. Braun AM, Maurette M-Trs, Oliveros E (1986) Technologie photochimique. Presses Polytechniques Romandes
4. Herrmann JM (1999) Catal Today 53:115
5. Hoffmann MR, Martin ST, Choi W, Bahnemann DW (1995) Chem Rev 95:69
6. Lane JR, Kjaergaard HG (2010) J Chem Phys 132. doi:174304 10.1063/1.3408192
7. Donaldson DJ, Orlando JJ, Amann S, Tyndall GS, Proos RJ, Henry BR, Vaida V (1998) J Phys Chem A 102:5171. doi:10.1021/jp980811d
8. Havey DK, Vaida V (2004) J Mol Spectrosc 228:152. doi:10.1016/j.jms.2004.07.015
9. Phillips JA, Orlando JJ, Tyndall GS, Vaida V (1998) Chem Phys Lett 296:377. doi:10.1016/s0009-2614(98)01045-8

10. Plath KL, Axson JL, Nelson GC, Takahashi K, Skodje RT, Vaida V (2009) React Kinet Catal Lett 96:209. doi:10.1007/s11144-009-5528-2
11. Henry BR (1977) Acc Chem Res 10:207
12. Crim FF (1984) Annu Rev Phys Chem 35:657
13. Donaldson DJ, George C, Vaida V (2010) Environ Sci Technol 44:5321. doi:10.1021/es903680v
14. Donaldson DJ, Tuck AF, Vaida V (2003) Chem Rev 103:4717. doi:10.1021/cr0206519
15. Vaida V (2009) J Phys Chem A 113:5. doi:10.1021/jp806365r
16. Vaida V, Feierabend KJ, Rontu N, Takahashi K (2008) Int J Photoenergy. doi:138091 10.1155/2008/138091
17. Matthews J, Fry JL, Roehl CM (2008) J Chem Phys 128: Article 184306
18. Rizzo TR, Hayden CC, Crim FF (1984) J Chem Phys 81:4501. doi:10.1063/1.447419
19. Sinha A, Vanderwal RL, Crim FF (1990) J Chem Phys 92:401. doi:10.1063/1.458442
20. Homitsky SC, Dragulin SM, Haynes LM, Hsieh S (2004) J Phys Chem A 108:9492. doi:10.1021/jp0474551
21. Matthews J, Sinha A (2005) J Chem Phys 122. doi:104313 10.1063/1.1858437
22. Miller Y, Chaban GM, Finlayson-Pitts BJ, Gerber RB (2006) J Phys Chem A 110:5342
23. Zhang H, Roehl CM, Sander SP (2000) J Geophys Res Atmos 105:14593
24. Brown SS, Wilson RW, Ravishankara AR (2000) J Phys Chem A 104:4976. doi:10.1021/jp000439d
25. Stark H, Brown SS, Burkholder JB, Aldener M, Riffault V, Gierczak T, Ravishankara AR (2008) J Phys Chem A 112:9296
26. Donaldson DJ, Frost GJ, Rosenlof KH, Tuck AF, Vaida V (1997) Geophys Res Lett 24:2651. doi:10.1029/97gl02663
27. Donaldson DJ, Tuck AF, Vaida V (2000) Phys Chem Earth Part C 25:223. doi:10.1016/s1464-1917(00)00009-x
28. Murphy JG, Thornton JA, Wooldridge PJ, Day DA, Rosen RS, Cantrell C, Shetter RE, Lefer B, Cohen RC (2004) Atmos Chem Phys 4:377
29. Salawitch RJ, Wennberg PO, Toon GC (2002) Geophys Res Lett 29: Article 1762
30. Wennberg PO, Salawitch RJ, Donaldson DJ, Hanisco TF, Lanzendorf EJ, Perkins KK, Lloyd SA, Vaida V, Gao RS, Hintsa EJ, Cohen RC, Swartz WH, Kusterer TL, Anderson DE (1999) Geophys Res Lett 26:1373. doi:10.1029/1999gl900255
31. Hall GA (1949) J Am Chem Soc 71:2691. doi:10.1021/ja01176a027
32. Staikova M, Oh M, Donaldson DJ (2005) J Phys Chem A 109:597. doi:10.1021/jp046141v
33. Vaida V, Kjaergaard HG, Hintze PE, Donaldson DJ (2003) Science 299:1566
34. Brutti S, Bencivenni L, Barbarossa V, Sau S, De Maria G (2006) J Chem Thermodyn 38:1292. doi:10.1016/j.jct.2006.02.009
35. Mills MJ, Toon OB, Solomon S (1999) Geophys Res Lett 26:1133. doi:10.1029/1999gl900187
36. Lane JR, Kjaergaard HG (2008) J Phys Chem A 112:4958. doi:10.1021/jp710863r
37. Hintze PE, Kjaergaard HG, Vaida V, Burkholder JB (2003) J Phys Chem A 107:1112. doi:10.1021/jp0263626
38. Kjaergaard HG, Lane JR, Garden AL, Schofield DP, Robinson TW, Mills MJ, (2008) Atmospheric photolysis of sulphuric acid. In: Goodsite, Michael E, Johnson, Matthew S (Eds.), Advances in Quantum Chemistry: Applications of Theoretical Methods to Atmospheric Science, Vol. 55. Elsevier, pp. 137–158. Chapter 8.
39. Mills MJ, Toon OB, Thomas GE (2005) J Geophys Res 110:D24208
40. Mills MJ, Toon OB, Vaida V, Hintze PH, Kjaergaard HG, Schofield DP, Robinson TW (2005) J Geophys Res Atmos 110:D08201
41. Hecobian A, Zhang X, Zheng M, Frank N, Edgerton ES, Weber RJ (2010) Atmos Chem Phys 10:5965. doi:10.5194/acp-10-5965-2010
42. Feierabend KJ, Havey DK, Brown SS, Vaida V (2006) Chem Phys Lett 420:438. doi:10.1016/j.cplett.01.013
43. Miller Y, Chaban GM, Gerber RB (2005) J Phys Chem A 109:6565. doi:10.1021/jp058110l
44. Yosa J, Meuwly M (2011) J Phys Chem A 115:14350

45. Miller Y, Gerber RB (2006) J Am Chem Soc 128:9594. doi:Ja062890 10.1021/ja062890+
46. Miller Y, Gerber RB, Vaida V (2007) Geophys Res Lett 34. doi:L16820 10.1029/2007gl030529
47. Zhang X, Liang MC, Montmessin F, Bertaux JL, Parkinson C, Yung YL (2010) Nat Geosci 3:834. doi:10.1038/ngeo989
48. Dunn ME, Shields GC, Takahashi K, Skodje RT, Vaida V (2008) J Phys Chem A 112:10226. doi:10.1021/jp805746t
49. Takahashi K, Plath KL, Axson JL, Nelson GC, Skodje RT, Vaida V (2010) J Phys Chem A 132. doi:10.1021/094305
50. Takahashi K, Plath KL, Skodje RT, Vaida V (2008) J Phys Chem A 112:7321. doi:10.1021/jp803225c
51. Skodje RT (1991) J Chem Phys 95:7234. doi:10.1063/1.461401
52. Kanakidou M, Seinfeld JH, Pandis SN, Barnes I, Dentener FJ, Facchini MC, Van Dingenen R, Ervens B, Nenes A, Nielsen CJ, Swietlicki E, Putaud JP, Balkanski Y, Fuzzi S, Horth J, Moortgat GK, Winterhalter R, Myhre CEL, Tsigaridis K, Vignati E, Stephanou EG, Wilson J (2005) Atmos Chem Phys 5:1053
53. Murphy DM, Cziczo DJ, Froyd KD, Hudson PK, Matthew BM, Middlebrook AM, Peltier RE, Sullivan A, Thomson DS, Weber RJ (2006) J Geophys Res Atmos 111:15. doi:D23s32 10.1029/2006jd007340
54. Zhang Q, Jimenez JL, Canagaratna MR, Allan JD, Coe H, Ulbrich I, Alfarra MR, Takami A, Middlebrook AM, Sun YL, Dzepina K, Dunlea E, Docherty K, DeCarlo PF, Salcedo D, Onasch T, Jayne JT, Miyoshi T, Shimono A, Hatakeyama S, Takegawa N, Kondo Y, Schneider J, Drewnick F, Borrmann S, Weimer S, Demerjian K, Williams P, Bower K, Bahreini R, Cottrell L, Griffin RJ, Rautiainen J, Sun JY, Zhang YM, Worsnop DR (2007) Geophys Res Lett 34:6. doi:L13801 10.1029/2007gl029979
55. Froyd KD, Murphy DM, Sanford TJ, Thomson DS, Wilson JC, Pfister L, Lait L (2009) Atmos Chem Phys 9:4363
56. IPCC (2007) Climate change 2007 - the physical science basis: contribution of working group I to the fourth assessment report of the IPCC. Cambridge University Press, Cambridge, UK
57. IARC (1983) IARC Monogr Eval Carcinog Risk Chem Hum 32:1
58. IARC (1987) IARC Monogr Eval Carcinog Risks Hum Suppl 7:1
59. Donaldson K, Li XY, MacNee W (1998) J Aerosol Sci 29:553
60. Akhter MS, Chughtai AR, Smith DM (1984) J Phys Chem 88:5334
61. Al-Abadleh HA, Grassian VH (2000) J Phys Chem A 104:11926
62. Alcala-Jornod C, van den Bergh H, Rossi MJ (2000) Phys Chem Chem Phys 2:5584
63. Ammann M, Kalberer M, Jost DT, Tobler L, Rossler E, Piguet D, Gäggeler HW, Baltensperger U (1998) Nature 395:157
64. Arens F, Gutzwiller L, Baltensperger U, Gäggeler HW, Ammann M (2001) Environ Sci Technol 35:2191
65. Arens F, Gutzwiller L, Gäggeler HW, Ammann M (2002) Phys Chem Chem Phys 4:3684. doi:10.1039/b201713j
66. Aubin DG, Abbatt JPD (2007) J Phys Chem A 111:6263. doi:10.1021/jp068884h
67. Daly HM, Horn AB (2009) Phys Chem Chem Phys 11:1069. doi:10.1039/b815400g
68. Esteve W, Budzinski H, Villenave E (2004) Atmos Environ 38:6063. doi:10.1016/j.atmosenv.2004.05.059
69. Esteve W, Budzinski H, Villenave E (2006) Atmos Environ 40:201
70. Fan ZH, Kamens RM, Zhang JB, Hu JX (1996) Environ Sci Technol 30:2821
71. Gerecke A, Thielmann A, Gutzwiller L, Rossi MJ (1998) Geophys Res Lett 25:2453
72. Gross S, Bertram AK (2008) J Phys Chem A 112:3104
73. Kahan TF, Kwamena NOA, Donaldson DJ (2006) Atmos Environ 40:3448
74. Kalberer M, Ammann M, Arens F, Gäggeler HW, Baltensperger U (1999) J Geophys Res Atmos 104:13825
75. Karagulian F, Rossi MJ (2007) J Phys Chem A 111:1914. doi:10.1021/jp0670891

76. Kwamena NOA, Clarke JP, Kahan TF, Diamond ML, Donaldson DJ (2007) Atmos Environ 41:37. doi:10.1016/j.atmosenv.2006.08.016
77. Kwamena N-OA, Thornton JA, Abbatt JPD (2004) J Phys Chem A 108:11626
78. Mak J, Gross S, Bertram AK (2007) Geophys Res Lett 34. doi:L10804 10.1029/2006gl029756
79. Mmereki BT, Chaudhuri SR, Donaldson DJ (2003) J Phys Chem A 107:2264
80. Mmereki BT, Donaldson DJ, Gilman JB, Eliason TL, Vaida V (2004) Atmos Environ 38:6091
81. Perraudin E, Budzinski H, Villenave E (2005) Atmos Environ 39:6557. doi:10.1016/j.atmosenv.2005.07.037
82. Perraudin E, Budzinskia H, Villenave E (2007) J Atmos Chem 56:57
83. Pltts JN, Sweetman JA, Zlellnska B, Atklnson R, Wlner AM, Harger WP (1985) Environ Sci Technol 19:1115
84. Pöschl U, Letzel T, Schauer C, Niessner R (2001) J Phys Chem A 105:4029
85. Prince AP, Wade JL, Grassian VH, Kleiber PD, Young MA (2002) Atmos Environ 36:5729
86. Stadler D, Rossi MJ (2000) Phys Chem Chem Phys 2:5420
87. Wang HM, Hasegawa K, Kagaya S (2000) Chemosphere 41:1479
88. Arens F, Gutzwiller L, Gäggeler HW, Ammann M (2002) Phys Chem Chem Phys 4:3684
89. Sosedova Y, Rouviere A, Bartels-Rausch T, Ammann M (2011) Photochem Photobiol Sci 10:1680. doi:10.1039/c1pp 05113j
90. Sosedova Y, Rouviere A, Gäggeler HW, Ammann M (2009) J Phys Chem A 113:10979. doi:10.1021/jp9050462
91. Kirchstetter TW, Novakov T, Hobbs PV (2004) J Geophys Res Atmos 109. doi:D21208 10.1029/2004jd004999
92. Bones DL, Henricksen DK, Mang SA, Gonsior M, Bateman AP, Nguyen TB, Cooper WJ, Nizkorodov SA (2010) J Geophys Res Atmos 115:14. doi:D05203 10.1029/2009jd012864
93. Cappa CD, Che DL, Kessler SH, Kroll JH, Wilson KR (2011) J Geophys Res Atmos 116:12. doi:D15204 10.1029/2011jd015918
94. Martins JV, Artaxo P, Kaufman YJ, Castanho AD, Remer LA (2009) Geophys Res Lett 36. doi:L13810 10.1029/2009gl037435
95. Park K, Chow JC, Watson JG, Trimble DL, Doraiswamy P, Arnott WP, Stroud KR, Bowers K, Bode R, Petzold A, Hansen ADA (2006) J Air Waste Manag Assoc 56:474
96. Alexander DTL, Crozier PA, Anderson JR (2008) Science (Washington, DC) 21:833. doi:10.1126/science.1155296
97. Barnard JC, Volkamer R, Kassianov EI (2008) Atmos Chem Phys 8:6665
98. Chen Y, Bond TC (2010) Atmos Chem Phys 10:1773
99. Russell PB, Bergstrom RW, Shinozuka Y, Clarke AD, DeCarlo PF, Jimenez JL, Livingston JM, Redemann J, Dubovik O, Strawa A (2010) Atmos Chem Phys 10:1155
100. Soto-Garcia LL, Andreae MO, Andreae TW, Artaxo P, Maenhaut W, Kirchstetter T, Novakov T, Chow JC, Mayol-Bracero OL (2011) Atmos Chem Phys 11:4425. doi:10.5194/acp-11-4425-2011
101. Sun HL, Biedermann L, Bond TC (2007) Geophys Res Lett 34:5. doi:L17813 10.1029/2007gl029797
102. Zhang XL, Lin YH, Surratt JD, Zotter P, Prevot ASH, Weber RJ (2011) Geophys Res Lett 38:4. doi:L21810 10.1029/2011gl049385
103. Decesari S, Facchini MC, Matta E, Mircea M, Fuzzi S, Chughtai AR, Smith DM (2002) Atmos Environ 36:1827
104. Gonzalez-Perez JA, Gonzalez-Vila FJ, Almendros G, Knicker H (2004) Environ Int 30:855
105. Hoffer A, Kiss G, Blazso M, Gelencser A (2004) Geophys Res Lett 31. doi:L06115 10.1029/2003gl018962
106. Holmes BJ, Petrucci GA (2006) Environ Sci Technol 40:4983
107. Mayol-Bracero OL, Guyon P, Graham B, Roberts G, Andreae MO, Decesari S, Facchini MC, Fuzzi S, Artaxo P (2002) J Geophys Res Atmos 107:LBA59/1
108. Chang JL, Thompson JE (2009) Atmos Environ 44:541. doi:10.1016/j.atmosenv.2009.10.042

109. Galloway MM, Chhabra PS, Chan AWH, Surratt JD, Flagan RC, Seinfeld JH, Keutsch FN (2009) Atmos Chem Phys 9:3331
110. Gelencser A, Hoffer A, Kiss G, Tombacz E, Kurdi R, Bencze L (2003) J Atmos Chem 45:25. doi:10.1023/a:1024060428172
111. Nguyen TB, Lee PB, Updyke KM, Bones DL, Laskin J, Laskin A, Nizkorodov SA (2012) J Geophys Res Atmos 117. doi:10.1029/2011JD016944
112. Noziere B, Dziedzic P, Cordova A (2007) Geophys Res Lett 34:5. doi:L21812 10.1029/2007gl031300
113. Nozière B, Esteve W (2005) Geophys Res Lett 32. doi:L03812 10.1029/2004gl021942
114. Rincon AG, Guzman MI, Hoffmann MR, Colussi AJ (2009) J Phys Chem A 113:10512. doi:10.1021/jp904644n
115. Canonica S, Hellrung B, Wirz J (2000) J Phys Chem A 104:1226
116. Canonica S, Kohn T, Mac M, Real FJ, Wirz J, Von Gunten U (2005) Environ Sci Technol 39:9182
117. Giese B, Napp M, Jacques O, Boudebous H, Taylor AM, Wirz J (2005) Angew Chem Int Ed 44:4073
118. Baduel C, Voisin D, Jaffrezo JL (2010) Atmos Chem Phys 10:4085. doi:10.5194/acp-10-4085-2010
119. Bateman AP, Nizkorodov SA, Laskin J, Laskin A (2011) Phys Chem Chem Phys 13:12199. doi:10.1039/c1cp20526a
120. Net S, Nieto-Gligorovski L, Gligorovski S, Temime-Rousell B, Barbati S, Lazarou YG, Wortham H (2009) Atmos Environ 43:1683
121. Yu Y, Ezell MJ, Zelenyuk A, Imre D, Alexander L, Ortega J, Thomas JL, Gogna K, Tobias DJ, D'Anna B, Harmon CW, Johnson SN, Finlayson-Pitts BJ (2008) Phys Chem Chem Phys 10:3063. doi:10.1039/b719495a
122. Rincon AG, Guzman MI, Hoffmann MR, Colussi AJ (2010) J Phys Chem Lett 1:368. doi:10.1021/jz900186e
123. Shapiro EL, Szprengiel J, Sareen N, Jen CN, Giordano MR, McNeill VF (2009) Atmos Chem Phys 9:2289
124. Stemmler K, Ndour M, Elshorbany Y, Kleffmann J, D'Anna B, George C, Bohn B, Ammann M (2007) Atmos Chem Phys 7:4237
125. Ammann M, Rössler E, Strekowski R, George C (2005) Phys Chem Chem Phys 7:2513
126. Ndour M, D'Anna B, George C, Ka O, Balkanski Y, Kleffmann J, Stemmler K, Ammann M (2008) Geophys Res Lett 35:5. doi:L05812 10.1029/2007gl032006
127. George C, Strekowski RS, Kleffmann J, Stemmler K, Ammann M (2005) Faraday Discuss 130:195. doi:10.1039/b417888m
128. Stemmler K, Ammann M, Donders C, Kleffmann J, George C (2006) Nature 440:195. doi:10.1038/nature04603
129. Monge ME, D'Anna B, Mazri L, Giroir-Fendler A, Ammann M, Donaldson DJ, George C (2010) Proc Natl Acad Sci. doi:10.1073/pnas.0908341107
130. Aymoz G, Jaffrezo JL, Jacob V, Colomb A, George C (2004) Atmos Chem Phys 4:2499
131. D'Anna B, Jammoul A, George C, Stemmler K, Fahrni S, Ammann M, Wisthaler A (2009) J Geophys Res Atmos 114. doi:D12301 10.1029/2008jd011237
132. Staehelin J, Hoigne J (1983) Vom Wasser 61:337
133. Graber ER, Rudich Y (2006) Atmos Chem Phys 6:729
134. Baduel C, Monge ME, Voisin D, Jaffrezo JL, George C, El Haddad I, Marchand N, D'Anna B (2011) Environ Sci Technol 45:5238. doi:10.1021/es200587z
135. Miao HF, Tao WY (2008) J Chem Technol Biotechnol 83:336. doi:10.1002/jctb.1816
136. Allard B, Boren H, Pettersson C, Zhang G (1994) Environ Int 20:97. doi:10.1016/0160-4120(94)90072-8
137. Corin N, Backlund P, Kulovaara M (1996) Chemosphere 33:245. doi:10.1016/0045-6535(96)00167-1
138. Dahlen J, Bertilsson S, Pettersson C (1996) Environ Int 22:501. doi:10.1016/0160-4120(96)00038-4

139. Zelenay V, Monge ME, D'Anna B, George C, Styler SA, Huthwelker T, Ammann M (2011) J Geophys Res 116. doi:D11301 10.1029/2010jd015500
140. Rouvière A, DeCarlo PF, Schlierf A, Favez O, D'Anna B, George C, Prévôt A, Ammann M (2009) Geochim Cosmochim Acta 73:A1125
141. Monge ME, Rosenørn T, Favez O, Müller M, Adler G, Riziq AA, Rudich Y, Herrmann H, George C, D'Anna B (2012) Proc Natl Acad Sci www.pnas.org/cgi/doi/10.1073/pnas.1120593109,109, 6840-6844.
142. Aguer JP, Richard C (1996) J Photochem Photobiol A Chem 93:193
143. Baxter RM, Carey JH (1983) Nature 306:575. doi:10.1038/306575a0
144. Latch DE, McNeill K (2006) Science 311:1743. doi:10.1126/science.1121636
145. Tegen I, Lacis AA (1996) J Geophys Res 101:19237
146. Sassen K, DeMott PJ, Prospero JM, Poellot MR (2003) Geophys Res Lett 30. doi:10.1029/2003gl017371
147. Ansmann A, Mattis I, Muller D, Wandinger U, Radlach M, Althausen D, Damoah R (2005) J Geophys Res Atmos 110. doi:10.1029/2004jd005000
148. Twomey SA, Piepgrass M, Wolfe TL (1984) Tellus Ser B Chem Phys Meteorol 36:356
149. Chang RYW, Sullivan RC, Abbatt JPD (2005) Geophys Res Lett 32:L14815/1
150. Hanisch F, Crowley JN (2003) Phys Chem Chem Phys 5:883
151. Seisel S, Keil T, Lian Y, Zellner R (2006) Int J Chem Kinet 38:242
152. Underwood GM, Li P, Al-Abadleh H, Grassian VH (2001) J Phys Chem A 105:6609
153. Usher CR, Al-Hosney H, Carlos-Cuellar S, Grassian VH (2002) J Geophys Res 107:ACH16/1
154. Vlasenko A, Huthwelker T, Gäggeler HW, Ammann M (2009) Phys Chem Chem Phys 11:7921. doi:10.1039/b904290n
155. Vlasenko A, Sjogren S, Weingartner E, Stemmler K, Gäggeler HW, Ammann M (2006) Atmos Chem Phys 6:2147
156. Falkovich AH, Schkolnik G, Ganor E, Rudich Y (2004) J Geophys Res 109. doi:D02208 10.1029/2003jd003919
157. Sullivan RC, Guazzotti SA, Sodeman DA, Prather KA (2007) Atmos Chem Phys 7:1213
158. Dentener FJ, Carmichael GR, Zhang Y, Lelieveld J, Crutzen PJ (1996) J Geophys Res 101:22869
159. Bauer SE, Balkanski Y, Schulz M, Hauglustaine DA, Dentener F (2004) J Geophys Res 109: D02304/1
160. Phadnis MJ, Carmichael GR (2000) J Atmos Chem 36:285. doi:10.1023/a:1006391626069
161. Song CH, Carmichael GR (2001) J Geophys Res Atmos 106:18131. doi:10.1029/2000jd900352
162. Savoie DL, Prospero JM, Saltzman ES (1989) J Geophys Res 94:5069. doi:10.1029/JD094iD04p05069
163. Baker AR, Kelly SD, Biswas KF, Witt M, Jickells TD (2003) Geophys Res Lett 30. doi:2296 10.1029/2003gl018518
164. Usher CR, Michel AE, Grassian VH (2003) Chem Rev 103:4883
165. Linke C, Moehler O, Veres A, Mohacsi A, Bozoki Z, Szabo G, Schnaiter M (2006) Atmos Chem Phys 6:3315
166. Hanisch F, Crowley JN (2001) J Phys Chem A 105:3096
167. Deguillaume L, Leriche M, Desboeufs K, Mailhot G, George C, Chaumerliac N (2005) Chem Rev 105:3388. doi:10.1021/cr040649c
168. Yumoto H, Matsudo S, Akashi K (2002) Vacuum 65:509
169. Gustafsson RJ, Orlov A, Griffiths PT, Cox RA, Lambert RM (2006) Chem Commun (Cambridge, UK) 3936
170. Langridge JM, Gustafsson RJ, Griffiths PT, Cox RA, Lambert RM, Jones RL (2009) Atmos Environ 43:5128. doi:10.1016/j.atmosenv.2009.06.046
171. Linsebigler AL, Lu GQ, Yates JT (1995) Chem Rev 95:735. doi:10.1021/cr00035a013

172. George C, Ndour M, Balkanski Y, Ka O (2007) In: Mellouki A, Ravishankara AR (eds) Regional climate variability and its impacts in the Mediterranean area. Springer, Dordrecht, p 219
173. Ndour M, Nicolas M, D'Anna B, Ka O, George C (2009) Phys Chem Chem Phys 11:1312. doi:10.1039/b806441e
174. Nicolas M, Ndour M, Ka O, D'Anna B, George C (2009) Environ Sci Technol 43:7437. doi:10.1021/es901569d
175. Sassine M, Burel L, D'Anna B, George C (2010) Atmos Environ 44:5468. doi:10.1016/j.atmosenv.2009.07.044
176. Rubasinghege G, Elzey S, Baltrusaitis J, Jayaweera PM, Grassian VH (2010) J Phys Chem Lett 1:1729. doi:10.1021/jz100371d
177. Ndour M, Conchon P, D'Anna B, Ka O, George C (2009) Geophys Res Lett 36:4. doi:L05816 10.1029/2008gl036662
178. Crowley JN, Ammann M, Cox RA, Hynes RG, Jenkin ME, Mellouki A, Rossi MJ, Troe J, Wallington TJ (2010) Atmos Chem Phys 10:9059. doi:10.5194/acp-10-9059-2010
179. Anastasio C, Galbavy ES, Hutterli MA, Burkhart JF, Friel DK (2007) Atmos Environ 41:5110. doi:10.1016/j.atmosenv.2006.12.011
180. Gustafsson RJ, Orlov A, Griffiths PT, Cox RA, Lambert RM (2006) Chem Commun 3936
181. Beaumont SK, Gustafsson RJ, Lambert RM (2009) Chemphyschem 10:331
182. Dalton JS, Janes PA, Jones NG, Nicholson JA, Hallam KR, Allen GC (2002) Environ Pollut 120:415
183. Usher CR, Grassian VH (2001) Abstracts of papers, 222nd ACS National Meeting, Chicago, IL, United States, August 26–30, 2001: PHYS
184. Ibusuki T, Takeuchi K (1994) J Mol Catal 88:93
185. Lin YM, Tseng YH, Huang JH, Chao CC, Chen CC, Wang I (2006) Environ Sci Technol 40:1616. doi:10.1021/es051007p
186. Ohko Y, Nakamura Y, Fukuda A, Matsuzawa S, Takeuchi K (2008) J Phys Chem C 112:10502. doi:10.1021/jp802959c
187. Chen HH, Navea JG, Young MA, Grassian VH (2011) J Phys Chem A 115:490. doi:10.1021/jp110164j
188. Chen HH, Stanier CO, Young MA, Grassian VH (2011) J Phys Chem A 115:11979. doi:10.1021/jp208164v
189. Meland B, Kleiber PD, Grassian VH, Young MA (2011) J Quant Spectrosc Radiat Transfer 112:1108. doi:10.1016/j.jqsrt.2010.12.002
190. Styler SA, Donaldson DJ (2011) Environ Sci Technol 45:10004. doi:10.1021/es202263q
191. Bones DL, Phillips LF (2009) Phys Chem Chem Phys 11:5392
192. Chu L, Anastasio C (2003) J Phys Chem A 107:9594
193. Fischer M, Warneck P (1996) J Phys Chem 100:18749
194. France JL, King MD, Lee-Taylor J (2007) Atmos Environ 41:5502
195. Goldstein S, Rabani J (2007) J Am Chem Soc 129:10597
196. Vaughan PP, Blough NV (1998) Environ Sci Technol 32:2947
197. Zellner R, Exner M, Herrmann H (1990) J Atmos Chem 10:411
198. Karagulian F, Dilbeck CW, Finlayson-Pitts BJ (2008) J Am Chem Soc 130:11272. doi:10.1021/ja8041965
199. Benkelberg HJ, Warneck P (1995) J Phys Chem 99:5214
200. Herrmann H (2007) Phys Chem Chem Phys 9:3935
201. Herrmann H, Hoffmann D, Schaefer T, Brauer P, Tilgner A (2010) Chemphyschem 11:3796
202. Canonica S, Jans U, Stemmler K, Hoigné J (1995) Environ Sci Technol 29:1822
203. Faust BC, Zepp RG (1993) Environ Sci Technol 27:2517
204. Weller C, Herrmann H (2012) submitted to the "Journal of Photochemistry and Photobiology A: Chemistry"
205. Herrmann H, Tilgner A, Barzaghi P, Majdik Z, Gligorovski S, Poulain L, Monod A (2005) Atmos Environ 39:4351

206. Hatchard CG, Parker CA (1956) Proc R Soc Lond A Math Phys Sci 235:518
207. Cooper GD, Degraff BA (1971) J Phys Chem 75:2897
208. Cooper GD, Degraff BA (1972) J Phys Chem 76:2618
209. Doetschman DC, Dwyer DW, Trojan KL (1989) Chem Phys 129:285
210. Ingram DJE, Hodgson WG, Parker CA, Rees WT (1955) Nature 176:1227
211. Jamieson RA, Perone SP (1972) J Phys Chem 76:830
212. Loginov AV, Katenin SB, Voyakin IV, Shagisultanova GA (1986) Sov J Coord Chem 12:1621
213. Nadtochenko V, Kiwi J (1996) J Photochem Photobiol A Chem 99:145
214. Parker CA (1954) Trans Faraday Soc 50:1213
215. Parker CA, Hatchard CG (1959) J Phys Chem 63:22
216. Patterson JIH, Perone SP (1973) J Phys Chem 77:2437
217. Rehorek D, Benedix M, Thomas P (1977) Inorg Chim Acta 25:L100
218. Rehorek D, Grikos H, Billing R (1990) Z Chem 30:378
219. Pozdnyakov IP, Kel OV, Plyusnin VF, Grivin VP, Bazhin NM (2008) J Phys Chem A 112:8316
220. Mulazzani QG, Dangelantonio M, Venturi M, Hoffman MZ, Rodgers MAJ (1986) J Phys Chem 90:5347
221. Chen J, Zhang H, Tomov IV, Wolfsherg M, Ding XL, Rentzepis PM (2007) J Phys Chem A 111:9326
222. Chen J, Dvornikov AS, Rentzepis PM (2009) J Phys Chem A 113:8818
223. Pozdnyakov IP, Kel OV, Plyusnin VF, Grivin VP, Bazhin NM (2009) J Phys Chem A 113:8820
224. Ciesla P, Kocot P, Mytych P, Stasicka Z (2004) J Mol Catal A Chem 224:17
225. Horváth O, Stevenson KL (1993) Charge transfer photochemistry of coordination compounds. VCH, New York
226. Feng W, Nansheng D, Glebov EM, Pozdnyakov IP, Grivin VP, Plyusnin VF, Bazhin NM (2007) Russ Chem Bull 56:900
227. Glebov EM, Pozdnyakov IP, Grivin VP, Plyusnin VF, Zhang X, Wu F, Deng N (2011) Photochem Photobiol Sci 10:425
228. Plyusnin VF, Pozdnyakov IP, Glebov EM, Grivin VP, Bazhin NM (2009) In: Bahadir AM, Duca G (eds) The role of ecological chemistry in pollution research and sustainable development. Springer, Berlin, p 65
229. Pozdnyakov IP, Glebov EM, Plyusnin VF, Grivin VP, Bunduki E, Goryacheva NV, Gladki V, Duka GG (2009) High Energy Chem (Translation of Khimiya Vysokikh Energii) 43:406
230. Zhang X, Gong Y, Wu F, Deng N, Pozdnyakov IP, Glebov EM, Grivin VP, Plyusnin VF, Bazhin NM (2009) Russ Chem Bull 58:1828
231. Abel B, Assmann J, Buback M, Grimm C, Kling M, Schmatz S, Schroeder J, Witte T (2003) J Phys Chem A 107:9499
232. Bockman TM, Hubig SM, Kochi JK (1997) J Org Chem 62:2210
233. Hilborn JW, Pincock JA (1991) J Am Chem Soc 113:2683
234. von Sonntag C, Schuchmann HP (1991) Angew Chem 30:1255
235. Abrahamson HB, Rezvani AB, Brushmiller JG (1994) Inorg Chim Acta 226:117
236. Voelker BM, Morel FMM, Sulzberger B (1997) Environ Sci Technol 31:1004
237. Kuo DTF, Kirka DW, Jiaa CQ (2006) J Sulfur Chem 27:461
238. Wang L, Zhang CB, Wu F, Deng NS (2006) J Coord Chem 59:803
239. Zuo YG, Hoigne J (1992) Environ Sci Technol 26:1014
240. Zuo YG, Hoigne J (1994) Atmos Environ 28:1231
241. Zuo YG, Zhan J (2005) Atmos Environ 39:27
242. Pehkonen SO, Siefert R, Erel Y, Webb S, Hoffmann MR (1993) Environ Sci Technol 27:2056
243. Franch MI, Ayllon JA, Peral J, Domenech X (2004) Appl Catal B 50:89
244. Duka GG, Batyr DG, Romanchuk LS, Sychev AY (1990) Sov J Coord Chem 16:93
245. Wang Z, Chen X, Ji H, Ma W, Chen C, Zhao J (2010) Environ Sci Technol 44:263

246. Sun LH, Wu CH, Faust BC (1998) J Phys Chem A 102:8664
247. Okochi H, Brimblecombe P (2002) Scientific World 2:767. doi:10.1100/tsw.2002.132
248. Tilgner A, Herrmann H (2010) Atmos Environ 44:5415. doi:10.1016/j.atmosenv.2010.07.050
249. Wolke R, Sehili AM, Simmel M, Knoth O, Tilgner A, Herrmann H (2005) Atmos Environ 39:4375
250. Domine F, Albert M, Huthwelker T, Jacobi HW, Kokhanovsky AA, Lehning M, Picard G, Simpson WR (2008) Atmos Chem Phys 8:171
251. Grannas AM, Jones AE, Dibb J, Ammann M, Anastasio C, Beine HJ, Bergin M, Bottenheim J, Boxe CS, Carver G, Chen G, Crawford JH, Domine F, Frey MM, Guzman MI, Heard DE, Helmig D, Hoffmann MR, Honrath RE, Huey LG, Hutterli M, Jacobi HW, Klan P, Lefer B, McConnell J, Plane J, Sander R, Savarino J, Shepson PB, Simpson WR, Sodeau JR, von Glasow R, Weller R, Wolff EW, Zhu T (2007) Atmos Chem Phys 7:4329
252. Simpson WR, von Glasow R, Riedel K, Anderson P, Ariya P, Bottenheim J, Burrows J, Carpenter LJ, Friess U, Goodsite ME, Heard D, Hutterli M, Jacobi HW, Kaleschke L, Neff B, Plane J, Platt U, Richter A, Roscoe H, Sander R, Shepson P, Sodeau J, Steffen A, Wagner T, Wolff E (2007) Atmos Chem Phys 7:4375
253. Steffen A, Douglas T, Amyot M, Ariya P, Aspmo K, Berg T, Bottenheim J, Brooks S, Cobbett F, Dastoor A, Dommergue A, Ebinghaus R, Ferrari C, Gardfeldt K, Goodsite ME, Lean D, Poulain AJ, Scherz C, Skov H, Sommar J, Temme C (2008) Atmos Chem Phys 8:1445
254. Beine H, Anastasio C (2011) J Geophys Res Atmos 116. doi:D14302 10.1029/2010jd015531
255. Rowland GA, Bausch AR, Grannas AM (2011) Environ Pollut 159:1076. doi:10.1016/j.envpol.2011.02.026
256. Rowland GA, Grannas AM (2011) Cold Reg Sci Technol 66:75. doi:10.1016/j.coldregions.2011.01.009
257. Bartels-Rausch T, Brigante M, Elshorbany YF, Ammann M, D'Anna B, George C, Stemmler K, Ndour M, Kleffmann J (2010) Atmos Environ 44:5443. doi:10.1016/j.atmosenv.2009.12.025
258. Huthwelker T, Ammann M, Peter T (2006) Chem Rev 106:1375
259. Henson BF, Robinson JM (2004) Phys Rev Lett 92. doi:246107 10.1103/PhysRevLett.92.246107
260. Ebert M, Worringen A, Benker N, Mertes S, Weingartner E, Weinbruch S (2011) Atmos Chem Phys 11:2805. doi:10.5194/acp-11-2805-2011
261. Kuo MH, Moussa SG, McNeill VF (2011) Atmos Chem Phys 11:9971
262. Kerbrat M, Pinzer B, Huthwelker T, Gäggeler HW, Ammann M, Schneebeli M (2008) Atmos Chem Phys 8:1261
263. Pinzer BR, Schneebeli M (2009) Geophys Res Lett 36. doi:L23503 10.1029/2009gl039618
264. Schneebeli M, Sokratov SA (2004) Hydrol Processes 18:3655
265. Kaempfer TU, Hopkins MA, Perovich DK (2007) J Geophys Res Atmos 112. doi:D24113 10.1029/2006jd008239
266. Maus S, Muller S, Buttner J, Brütsch S, Huthwelker T, Schwikowski M, Enzmann F, Vahatolo A (2011) Ann Glaciol 52:301
267. Stedmon CA, Thomas DN, Papadimitriou S, Granskog MA, Dieckmann GS (2011) J Geophys Res Biogeosci 116. doi:G0302710.1029/2011jg001716
268. Tepavitcharova S, Todorov T, Rabadjieva D, Dassenakis M, Paraskevopoulou V (2011) Environ Monit Assess 180:217. doi:10.1007/s10661-010-1783-y
269. Wells AJ, Wettlaufer JS, Orszag SA (2011) Geophys Res Lett 38. doi:L04501 10.1029/2010gl046288
270. Obbard RW, Roscoe HK, Wolff EW, Atkinson HM (2009) J Geophys Res 114
271. Beine H, Anastasio C, Esposito G, Patten K, Wilkening E, Domine F, Voisin D, Barret M, Houdier S, Hall S (2011) J Geophys Res 116:D00R05
272. Boxe CS, Saiz-Lopez A (2008) Atmos Chem Phys 8:4855
273. Cho H, Shepson PB, Barrie LA, Cowin JP, Zaveri R (2002) J Phys Chem B 106:11226
274. Wren SN, Donaldson DJ (2011) J Phys Chem Lett 2:1967. doi:10.1021/jz2007484

275. Chu L, Anastasio C (2007) Environ Sci Technol 41:3626. doi:10.1021/es062731q
276. Jacobi HW, Annor T, Quansah E (2006) J Photochem Photobiol A Chem 179:330. doi:10.1016/j.jphotochem.2005.09.001
277. Ram K, Anastasio C (2009) Atmos Environ 43:2252. doi:10.1016/j.atmosenv.2009.01.044
278. Kahan TF, Donaldson DJ (2007) J Phys Chem A 111:1277. doi:10.1021/jp066660t
279. Kahan TF, Donaldson DJ (2010) Environ Sci Technol 44:3819. doi:10.1021/es100448h
280. Wren SN, Donaldson DJ (2010) Phys Chem Chem Phys 12:2648. doi:10.1039/b922254e
281. Kahan TF, Zhao R, Jumaa KB, Donaldson DJ (2010) Environ Sci Technol 44:1302. doi:10.1021/es9031612
282. Ardura D, Kahan TF, Donaldson DJ (2009) J Phys Chem A 113:7353. doi:10.1021/jp811385m
283. Heger D, Nachtigallova D, Surman F, Krausko J, Magyarova B, Brumovsky M, Rubes M, Gladich I, Klan P (2011) J Phys Chem A 115:11412. doi:10.1021/jp205627a
284. Villena G, Wiesen P, Cantrell CA, Flocke F, Fried A, Hall SR, Hornbrook RS, Knapp D, Kosciuch E, Mauldin RL III, McGrath JA, Montzka D, Richter D, Ullmann K, Walega J, Weibring P, Weinheimer A, Staebler RM, Liao J, Huey LG, Kleffmann J (2011) J Geophys Res 116:D00R07
285. Durnford D, Dastoor A (2011) J Geophys Res 116. doi:10.1029/2010JD014809
286. Chaulk A, Stern GA, Armstrong D, Barber DG, Wang F (2011) Environ Sci Technol 45:1866. doi:10.1021/es103434c
287. Bartels-Rausch T, Huthwelker T, Jöri M, Gäggeler HW, Ammann M (2008) Environ Res Lett 045009
288. Mann E, Meyer T, Mitchell CPJ, Wania F (2011) J Environ Monit 13:2695. doi:10.1039/c1em10297d
289. Larose C, Dommergue Al, Marusczak N, Coves J, Ferrari CP, Schneider D (2011) Environ Sci Technol 110222143737064. doi:10.1021/es103016x
290. Lalonde J, Poulain A, Amyot M (2002) Environ Sci Technol 36:174
291. Bartels-Rausch T, Krysztofiak G, Bernhard A, Schläppi M, Schwikowski M, Ammann M (2011) Chemosphere 82:199. doi:10.1016/j.chemosphere.2010.10.020
292. Zhang H (2006) Recent Dev Mercury Sci 37. doi:10.1007/430_015
293. Si L, Ariya PA (2008) Environ Sci Technol 42:5150. doi:10.1021/es800552z
294. Gardfeldt K, Jonsson M (2003) J Phys Chem A 107:4478. doi:10.1021/jp0275342
295. Jammoul A, Dumas S, D'Anna B, George C (2009) Atmos Chem Phys 9:4229
296. Popp PJ, Gao RS, Marcy TP, Fahey DW, Hudson PK, Thompson TL, Karcher B, Ridley BA, Weinheimer AJ, Knapp DJ, Montzka DD, Baumgardner D, Garrett TJ, Weinstock EM, Smith JB, Sayres DS, Pittman JV, Dhaniyala S, Bui TP, Mahoney MJ (2004) J Geophys Res Atmos 109
297. Voigt C, Karcher B, Schlager H, Schiller C, Kramer M, de Reus M, Vossing H, Borrmann S, Mitev V (2007) Atmos Chem Phys 7:3373
298. Frey MM, Savarino J, Morin S, Erbland J, Martins JMF (2009) Atmos Chem Phys 9:8681
299. Helmig D, Seok B, Williams MW, Hueber J, Sanford R Jr (2009) Biogeochemistry 95:115. doi:10.1007/s10533-009-9312-1
300. Hiltbrunner E, Schwikowski M, Korner C (2005) Atmos Environ 39:2249. doi:10.1016/j.atmosenv.2004.12.037
301. Schwikowski M, Brutsch S, Gaggeler HW, Schotterer U (1999) J Geophys Res Atmos 104:13709. doi:10.1029/1998jd100112
302. Krepelova A, Newberg J, Huthwelker T, Bluhm H, Ammann M (2010) Phys Chem Chem Phys 12:8870
303. Richards NK, Wingen LM, Callahan KM, Nishino N, Kleinman MT, Tobias DJ, Finlayson-Pitts BJ (2011) J Phys Chem A 115:5810
304. Wingen LM, Moskun AC, Johnson SN, Thomas JL, Roeselova M, Tobias DJ, Kleinman MT, Finlayson-Pitts BJ (2008) Phys Chem Chem Phys 10:5668
305. Bock J, Jacobi H-W (2011) J Phys Chem A 114:1790. doi:10.1021/jp909205e

306. Jacobi H-W, Hilker B (2007) J Photochem Photobiol A Chem 185:371. doi:10.1016/j.jphotochem.2006.06.039
307. Morin S, Savarino J, Frey MM, Domine F, Jacobi HW, Kaleschke L, Martins JMF (2009) J Geophys Res Atmos 114. doi:D05303 10.1029/2008jd010696
308. Morin S, Savarino J, Frey MM, Yan N, Bekki S, Bottenheim JW, Martins JMF (2008) Science 322:730. doi:10.1126/science.1161910
309. O'Sullivan D, Sodeau JR (2010) J Phys Chem A 114:12208. doi:10.1021/jp104910p
310. Kunkely H, Horvath O, Vogler A (1997) Coord Chem Rev 159:85. doi:10.1016/S0010-8545(96)01307-0
311. France JL, King MD, Lee-Taylor J, Beine HJ, Ianniello A, Domine F, MacArthur A (2011) J Geophys Res Earth Surf 116:16. doi:F04013 10.1029/2011jf002019
312. Hakura A, Shimada H, Nakajima M, Sui H, Kitamoto S, Suzuki S, Satoh T (2005) Mutagenesis 20:217. doi:10.1093/mutage/gei029
313. Simpson AJ, Lam B, Diamond ML, Donaldson DJ, Lefebvre BA, Moser AQ, Williams AJ, Larin NI, Kvasha MP (2006) Chemosphere 63:142
314. Lam B, Diamond ML, Simpson AJ, Makar PA, Truong J, Hernandez-Martinez NA (2005) Atmos Environ 39:6578
315. Butt CM, Diamond ML, Truong J, Ikonomou MG, Helm PA, Stern GA (2004) Environ Sci Technol 38:3514
316. Diamond ML, Gingrich SE, Fertuck K, McCarry BE, Stern GA, Billeck B, Grift B, Brooker D, Yager TD (2000) Environ Sci Technol 34:2900
317. Gingrich SE, Diamond ML (2001) Environ Sci Technol 35:4031
318. Butt CM, Diamond ML, Truong J, Ikonomou MG, Helm PA, Stern GA (2004) Environ Sci Technol 38:3514. doi:10.1021/es0498282
319. Hodge EM, Diamond ML, McCarry BE, Stern GA, Harper PA (2003) Arch Environ Contam Toxicol 44:421. doi:10.1007/s00244-002-1272-6
320. Liu Q-T, Chen R, McCarry BE, Diamond ML, Bahavar B (2003) Environ Sci Technol 37:2340. doi:10.1021/es020848i
321. Liu Q-T, Diamond ML, Gingrich SE, Ondov JM, Maciejczyk P, Stern GA (2003) Environ Pollut 122:51
322. Marr LC, Kirchstetter TW, Harley RA, Miguel AH, Hering SV, Hammond SK (1999) Environ Sci Technol 33:3091. doi:10.1021/es981227l
323. Kleeman MJ, Robert MA, Riddle SG, Fine PM, Hays MD, Schauer JJ, Hannigan MP (2008) Atmos Environ 42:3059
324. Yang H-H, Lee W-J, Chen S-J, Lai S-O (1998) J Hazard Mater 60:159
325. Atkinson R, Arey J (1994) Environ Health Perspect 102:117
326. Durant JL, Lafleur AL, Plummer EF, Taghizadeh K, Busby WF, Thilly WG (1998) Environ Sci Technol 32:1894. doi:10.1021/es9706965
327. Gross S, Bertram AK (2008) J Phys Chem A 112:3104. doi:10.1021/jp7107544
328. Kahan TF, Donaldson DJ (2008) Environ Res Lett 3:6. doi:045006 10.1088/1748-9326/3/4/045006
329. Kong L, Ferry JL (2004) J Photochem Photobiol A 162:415
330. Kwamena NOA, Abbatt JPD (2008) Atmos Environ 42:8309. doi:10.1016/j.atmosenv.2008.07.037
331. Kwamena NOA, Staikova MG, Donaldson DJ, George IJ, Abbatt JPD (2007) J Phys Chem A 111:11050. doi:10.1021/jp075300i
332. Kwamena N-OA, Earp ME, Young CJ, Abbatt JPD (2006) J Phys Chem A 110:3638. doi:10.1021/jp056125d
333. Kwamena N-OA, Thornton JA, Abbatt JPD (2004) J Phys Chem A 108:11626. doi:10.1021/jp046161x
334. McCabe J, Abbatt JPD (2009) J Phys Chem C 113:2120. doi:10.1021/jp806771q
335. Miet K, Le Menach K, Flaud PM, Budzinski H, Villenave E (2009) Atmos Environ 43:837. doi:10.1016/j.atmosenv.2008.10.041

336. Nielsen T (1984) Environ Sci Technol 18:157
337. Pryor WA, Gleicher GJ, Cosgrove JP, Church DF (1984) J Org Chem 49:5189. doi:10.1021/jo00200a035
338. Raja S, Valsaraj KT (2005) J Air Waste Manage Assoc 55:1345
339. Ridd JH (1998) Acta Chem Scand 52:11
340. Zhang Y, Yang B, Meng J, Gao S, Dong X, Shu J (2010) Atmos Environ 44:697
341. Wang XF, Zhang YP, Chen H, Yang X, Chen JM, Geng FH (2009) Environ Sci Technol 43:3061. doi:10.1021/es8020155
342. Honrath RE, Peterson MC, Guo S, Dibb JE, Shepson PB, Campbell B (1999) Geophys Res Lett 26:695
343. Jacobi H-W, Hilker B (2007) J Photochem Photobiol A 185:371
344. Jammoul A, Gligorovski S, George C, D'Anna B (2008) J Phys Chem A 112:1268. doi:10.1021/jp074348t
345. Reeser DI, Jammoul A, Clifford D, Brigante M, D'Anna B, George C, Donaldson DJ (2008) J Phys Chem C 113:2071. doi:10.1021/jp805167d
346. Styler SA, Brigante M, D'Anna B, George C, Donaldson DJ (2009) Phys Chem Chem Phys 11:7876. doi:10.1039/b904180j
347. Brigante M, Cazoir D, D'Anna B, George C, Donaldson DJ (2008) J Phys Chem A 112:9503. doi:10.1021/jp802324g
348. Monge ME, D'Anna B, Mazri L, Giroir-Fendler A, Ammann M, Donaldson DJ, George C (2010) Proc Natl Acad Sci USA 107:6605
349. Handley SR, Clifford D, Donaldson DJ (2007) Environ Sci Technol 41:3898
350. Bartels-Rausch T, Donaldson DJ (2006) Atmos Chem Phys Discuss 6:10713
351. Vione D, Maurino V, Minero C, Pelizzetti E, Harrison MAJ, Olariu RI, Arsene C (2006) Chem Soc Rev 35:441
352. Warneck P, Wurzinger C (1988) J Phys Chem 92:6278
353. Ammar R, Monge ME, George C, D'Anna B (2010) Chemphyschem 11:3956. doi:10.1002/cphc.201000540
354. Zepp RG, Erickson DJ III, Paul ND, Sulzberger B (2007) Photochem Photobiol Sci 6:286
355. Niemi R, Martikainen PJ, Silvola J, Wulff A, Turtola S, Holopainen T (2002) Glob Chang Biol 8:361. doi:10.1046/j.1354-1013.2002.00478.x
356. Rinnan R, Impio M, Silvola J, Holopainen T, Martikainen PJ (2003) Oecologia 137:475. doi:10.1007/s00442-003-1366-5
357. Derendorp L, Holzinger R, Röckmann T (2011) Environ Chem 8:602. doi:http://dx.doi.org/10.1071/EN11024
358. Gallet C, Keller C (1999) Soil Biol Biochem 31:1151
359. Del Vecchio R, Blough NV (2004) Environ Sci Technol 38:3885
360. McNally AM, Moody EC, McNeill K (2005) Photochem Photobiol Sci 4:268
361. Brandt LA, Bohnet C, King JY (2009) J Geophys Res 114:G02004
362. Schade GW, Hofmann MR, Crutzen PJ (1999) Tellus B 51:889
363. Tarr MA, Miller WL, Zepp RG (1995) J Geophys Res 100:11403
364. Warneke C, Karl T, Judmaier H, Hansel A, Jordan A, Lindinger W, Crutzen PJ (1999) Global Biogeochem Cycles 13:9
365. Lalonde JD, Amyot M, Orvoine J, Morel FMM, Auclair JC, Ariya PA (2004) Environ Sci Technol 38:508. doi:10.1021/es034394g
366. Siciliano SD, O'Driscoll NJ, Tordon R, Hill J, Beauchamp S, Lean DRS (2005) Environ Sci Technol 39:1071. doi:10.1021/es048707z
367. McNeill VF, Grannas AM, Abbatt JPD, Ammann M, Ariya P, Bartels-Rausch T, Dominé F, Donaldson DJ, Guzman MI, Heger D, Kahan TF, Klán P, Masclin S, Toubin C, Voisin D (2012) Atmos. Chem. Phys. 12:9653

New Insights into the Tropospheric Oxidation of Isoprene: Combining Field Measurements, Laboratory Studies, Chemical Modelling and Quantum Theory

Lisa Whalley, Daniel Stone, and Dwayne Heard

Abstract In this chapter we discuss some of the recent work directed at further understanding the chemistry of our atmosphere in regions of low NO_x, such as forests, where there are considerable emissions of biogenic volatile organic compounds, for example reactive hydrocarbons such as isoprene. Recent field measurements have revealed some surprising results, for example that OH concentrations are measured to be considerably higher than can be understood using current chemical mechanisms. It has also not proven possible to reconcile field measurements of other species, such as oxygenated VOCs, or emission fluxes of isoprene, using current mechanisms. Several complementary approaches have been brought to bear on formulating a solution to this problem, namely field studies using state-of-the-art instrumentation, chamber studies to isolate sub-sections of the chemistry, laboratory studies to measure rate coefficients, product branching ratios and photochemical yields, the development of ever more detailed chemical mechanisms, and high quality ab initio quantum theory to calculate the energy landscape for relevant reactions and to enable the rates of formation of products and intermediates for previously unknown and unstudied reactions to be predicted. The last few years have seen significant activity in this area, with several contrasting postulates put forward to explain the experimental findings, and here we attempt to synthesise the evidence and ideas.

L. Whalley and D. Heard (✉)
School of Chemistry, University of Leeds, Leeds LS2 9JT, UK

National Centre for Atmospheric Science, University of Leeds, Leeds LS2 9JT, UK
e-mail: D.E.Heard@leeds.ac.uk

D. Stone
School of Chemistry, University of Leeds, Leeds LS2 9JT, UK

Contents

1   Introduction

The composition of the atmosphere is changing, with wide-ranging implications for air quality and climate change. The future well-being of our atmosphere relies on a detailed understanding of the chemistry responsible for the oxidation of man-made and natural emissions. Photo-oxidation in the troposphere is highly complex, and is initiated by short lived radical species, in the daytime dominated by the hydroxyl radical, OH, and at night by the nitrate radical, NO$_3$, or ozone. Chemical oxidation cycles remove primary emitted trace species which are directly harmful to humans or to the wider environment. The international societal response to deteriorating air quality and the changing climate is guided by the predictions of numerical models which make assumptions about both emission scenarios in the future for trace gases and aerosols from natural and human activity, and global weather patterns which disperse and mix these emissions. An integral part of any air quality or climate model is a chemical mechanism which describes the degradation of all emissions into a wide range of secondary products by reaction with oxidants, for example OH, NO$_3$, O$_3$ and Cl atoms, as well as by photochemical degradation by sunlight or removal by physical deposition. Some chemical schemes are very large, containing thousands of individual chemical species and tens of thousands of individual chemical reactions which eventually generate carbon dioxide and water vapour, and along the way a richness of chemical functionality emerges. Many of the secondary products produced by atmospheric photo-oxidation are also directly harmful, for example O$_3$, NO$_2$, acids and multifunctional species. Some species are relatively nonvolatile and partition to the aqueous phase to create secondary organic aerosol (SOA) which contributes a significant fraction of tropospheric aerosol, with associated impacts on climate and human health.

It is the realm of laboratory chemical kinetics to measure the rate constants of individual chemical reactions and the yields of products from different reaction channels, under relevant conditions of temperature and pressure, for all processes required to describe adequately chemical oxidation in a given environment. Although very extensive chemical kinetics databases exist for gas phase and heterogeneous reactions, for example from the IUPAC sub-committee for gas kinetic data evaluation [1] (also http://www.iupac-kinetic.ch.cam.ac.uk/), and the JPL kinetics data evaluation panel [2] (also http://jpldataeval.jpl.nasa.gov), and which are used frequently by numerical modellers, there are many gaps, and often the relevant chemistry may be completely missing. Sometimes it is not possible to isolate an individual chemical reaction to study, and process studies in chambers under relevant atmospheric conditions are used to extract kinetic data indirectly. For some reactions it is not possible to synthesise the necessary reagents, and structural–activity relationships (SAR) are used to estimate rate constants using known data from similar molecules and established additivity rules. Estimating the yield of products is more difficult via this method, and theoretical methods utilizing advances in ab initio quantum mechanics have proven extremely useful to predict the likely course of a reaction through calculation of energy barriers to reaction.

Field measurements of atmospheric composition provide crucial data with which to test how complete and accurate chemical mechanisms are within atmospheric models. In the atmosphere, concentrations of trace gases are dependent on the rate of their chemical production and loss, as well as physical transport into or away from the measurement volume. In order to separate chemistry from transport processes, it is useful to measure a species whose chemical lifetime is short, such that transport plays no direct role in controlling its abundance. Free radicals are examples of such species. In steady-state, the abundance of OH is determined by equating the rate of its production and loss, as its rate of loss is directly proportional the concentration of OH. Therefore in order to calculate the abundance of OH it is necessary to measure as wide a range as possible of OH sources and sinks at the same location. Of course, good model-to-measurement agreement for OH may occur fortuitously if missing OH sources counterbalance missing OH sinks in the model. In such cases field measurements have not provided an adequate test of the level of understanding of the underlying chemistry. A common example of missing sinks are some of the many thousands of volatile organic compounds (VOCs) which exist in urban air and which react with OH, and are either directly emitted or generated as reaction intermediates.

Although there are many examples of comparisons between modelled and measured OH, and other radicals, there are relatively few in environments with significant emissions of biogenic volatile organic compounds (BVOCs) at locations which are significantly removed from pollution sources where levels of nitrogen oxides are very low. Chemical mechanisms have been developed for the oxidative degradation of a select few BVOCs, but these schemes are complex, with often only the rate constant of OH with the parent BVOC and the initial branching to primary products well established. The ensuing chemistry involving reactive intermediates and further reactions or photochemistry is often written down, but with relatively little experimental evidence to support the postulated mechanism.

In this chapter we examine the mechanism for the OH initiated oxidation of isoprene under low NO_x levels (NO < 50 ppt). At higher NO_x levels, although it is likely that there are still processes that are missing within atmospheric models (e.g. [3]), isoprene oxidation chemistry is simplified somewhat by the loss of the isoprene-derived peroxy radicals being dominated by reaction with NO. Under low NO_x conditions the fate of these peroxy radicals is much less certain. New insights into the isoprene mechanism have been derived using a combination of:

1. Field measurements of the concentrations of isoprene (and fluxes), OH and HO_2 radicals, and isoprene secondary oxidation products and comparison to calculations of a variety of models, from zero dimensional box models to global three dimensional models.
2. Laboratory studies to study the oxidation of isoprene under carefully controlled conditions, in particular using atmospheric simulation chambers, in order to confirm the presence of reaction products and the rates of competing channels.
3. Theoretical methods using quantum mechanics and chemical rate theory to calculate the multidimensional potential energy surface upon which the reaction of isoprene and OH occurs, and the rates of different reaction pathways under relevant conditions, and the incorporation of these calculated kinetic data into a range of models for comparison with field data.

2 Model and Measurement Comparisons in High Isoprene Low NO_x Regions

A number of field campaigns in regions characterised by high concentrations of isoprene (and sometimes other biogenic species) and low concentrations of NO_x ($NO_x = NO + NO_2$) have highlighted considerable differences between observed and modelled concentrations of OH and HO_2 radicals [4–14]. Appreciable HO_x ($HO_x = OH + HO_2$) concentrations have been observed in the presence of high biogenic emissions that cannot be reconciled with chemical schemes currently adopted in atmospheric models, indicating poor model representation of HO_x chemistry under high VOC and low NO_x conditions. An alternative explanation is that OH and/or HO_2 detected by laser induced fluorescence (LIF) at low pressures [15] may be biased in some way for some instruments in some types of forested environments, for example by the presence of interference under high loadings of isoprene and/or other BVOCs [16, 17].

The earliest reports of model discrepancies for OH and HO_2 under high VOC and low NO_x conditions were made following the aerosols formation from biogenic organic carbon (AEROBIC) campaign in a forested region of Greece in 1997 [5, 18]. The modelled concentrations of OH were, on average, a factor of two lower than the observations, and although the source of the discrepancy was not identified in this study, it was noted that the disagreement was most significant when NO concentrations were low [5].

The program for research on oxidants: photochemistry, emissions and transport (PROPHET) campaign in a deciduous forest in northern Michigan in 1999 also reported OH and HO_2 concentrations that were significantly higher than model calculations, with the OH observations a factor of at least six greater than the modelled concentrations at NO mixing ratios below 100 ppt [12]. This study found that reasonable agreement for OH could be obtained if the NO concentrations in the model were tripled, or the NO doubled and the isoprene halved, indicating the combination of low NO_x and high isoprene as a source of the problem [12].

The suggestion that incomplete or incorrect treatment of reactions involving organic peroxides (ROOH), either their formation via $HO_2 + RO_2$ or their photolysis to produce $RO + OH$, may be responsible for the HO_x model failure came as a result of the southern oxidant study (SOS) in Nashville, Tennessee [13]. At high NO_x concentrations the dominant fate of HO_2 and RO_2 is generally reaction with NO, resulting in production of OH, either directly (in the case of HO_2) or via the production of an alkoxy radical (RO) and its subsequent reaction with O_2 (in the case of RO_2). Any misrepresentation of $HO_2 + RO_2$ reactions, or their products, in model simulations will therefore become more apparent at low NO_x concentrations owing to the reduced importance of $HO_2 + NO$ and $RO_2 + NO$ reactions.

2.1 Recycling of OH in Isoprene Oxidation

The Guyanas atmosphere–biosphere exchange and radicals intensive experiment with the Learjet (GABRIEL) project carried out in 2005 reported the first boundary layer measurements of OH and HO_2 made over a tropical rainforest, with measurements made over the Amazon rainforest in Suriname onboard a Learjet aircraft using LIF [9]. Global models predict particularly low OH concentrations in this region due to elevated levels of isoprene which rapidly reacts with OH [19–21], but comparison with the GABRIEL dataset revealed significant differences between model predictions and observations [4, 7, 8]. Disagreements between observed and modelled OH concentrations for GABRIEL were found with both global models [4] and box models [7], with the OH concentrations simulated by the box model, constrained to the reduced Mainz isoprene mechanism (MIM), a factor of approximately 12 times lower than the observations at the highest isoprene concentrations. Use of a more explicit isoprene oxidation scheme, similar to that described by the master chemical mechanism (MCM), did little to improve the model failure [7].

The OH model discrepancy for GABRIEL was found to display a dependence on isoprene [4, 7, 8], as shown in Fig. 1. This discrepancy was similar to that observed over forested regions in North America, in the intercontinental chemical transport experiment (INTEX-A), and during the PROPHET campaign [10] (also shown in Fig. 1). The level of discrepancy between OH observed and predicted from other isoprene-rich field studies (Oxidant and Particle Photochemical Processes – OP3 and Program of Regional Integrated Experiments of Pearl River Delta region – PRIDE-PRD, discussed further below) were also consistent with this trend.

Fig. 1 Dependence of the observed to modelled ratio for OH as a function of the isoprene mixing ratio reported from PROPHET (1998), INTEX (2004), GABRIEL (2006), PRIDE-PRD (2006) and OP3-I (2008) projects (reproduced from Lu et al. [57])
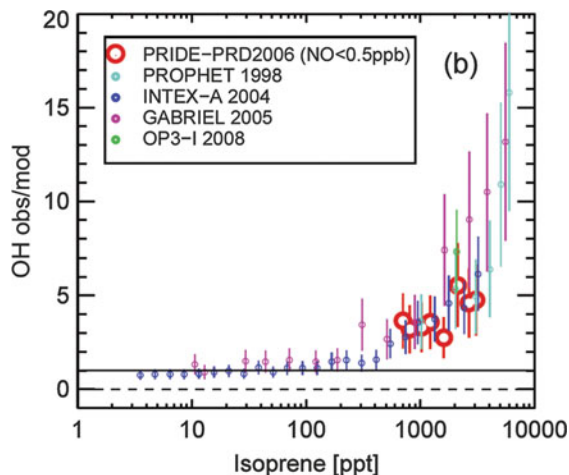
Isoprene photo-oxidation products were also found to be higher than model predictions [22], indicating the need for additional OH sources related to isoprene in order to reconcile models with measurements. This observation led to an extension of the idea that reactions involving HO_2 and RO_2 could be responsible for model failure. It was proposed that direct formation of OH in $HO_2 + RO_2$ reactions, and specifically those involving RO_2 radicals generated in isoprene oxidation ($ISOPO_2$), could improve model simulations for OH over the Amazon rainforest by providing an additional pathway for recycling of OH via HO_2 under low NO_x conditions, as shown in Fig. 2 [4, 7, 8].

Generation of OH in $HO_2 + RO_2$ reactions has been observed in several laboratory studies [23–28], and although inclusion of an OH yield in $HO_2 + ISOPO_2$ reactions in atmospheric models has enabled replication of field observations, the yields required (between 200% and 400%) are significantly higher than the laboratory data suggest for any reaction of this type. Moreover, production of OH in such reactions has thus far only been observed for RO_2 radicals containing acyl, α-carbonyl, α-hydroxy or α-alkoxy functionalities [23–28], and experiments have placed an upper limit of 6% on the OH yield from RO_2 radicals structurally similar to $ISOPO_2$ [23].

2.2 The Role of Air Mass Segregation in Simulations of HO_x Chemistry

While the production of such large amounts of OH from $HO_2 + RO_2$ reactions is unlikely, its inclusion in atmospheric models does facilitate investigation of the impact of underpredictions of OH in modelling studies. Butler et al. [4] found that increasing the OH concentration in a global 3D model European centre for medium-range weather forecasts-Hamburg/module earth submodel system
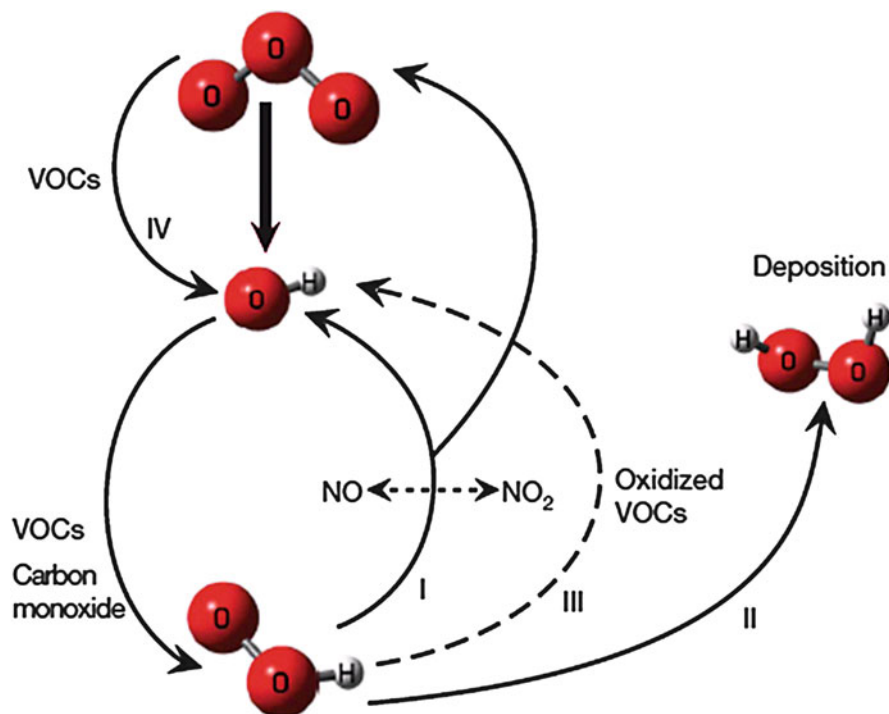
Fig. 2 Schematic to show the main processes controlling HO_x concentrations in the troposphere (reproduced from [8]). Pathway I shows the cycling of HO_2 to OH through reaction with NO; pathway II shows the production of peroxides from HO_2, leading to loss of HO_x; pathway III indicates a potential route for production of OH from reactions of HO_2 with VOC oxidation products

(ECHAM/MESSy) led to unrealistically low concentrations of isoprene. In order to achieve model agreement with observed concentrations of both OH and isoprene it was necessary not only to include the additional OH source but also to reduce the effective rate coefficient between OH and isoprene by approximately 50% [4]. The rationale behind the reduction in $k_{OH+C_5H_8}$ lies in the potential segregation of air masses containing OH from those containing isoprene, such that the two air masses do not fully mix and therefore do not react at a rate given by $k_{OH+C_5H_8}[OH][C_5H_8]$ when considering the concentrations of OH and isoprene in the two air masses.

This concept has also been investigated by Pugh et al. [29, 30] for the OP3 project which took place in Borneo in 2008, comprising both ground-based and aircraft measurements of atmospheric composition in and over rainforest and oil palm plantations [31]. Using the Cambridge tropospheric trajectory model of chemistry and transport (CiTTyCAT) atmospheric chemistry box model with MIM2 chemistry, Pugh et al. [29] demonstrated similar problems in simulating OH concentrations to those reported by Lelieveld et al. [8], with the model unable

to replicate concurrent observations of OH and isoprene whilst maintaining agreement with measurements of VOC emission fluxes.

Pugh et al. [29] included a recycling term for OH in the reaction between OH and isoprene to investigate its impact on the model simulations, but found that any improvements in the modelled OH were at the cost of model success for isoprene and other VOCs. Further analysis of the model revealed that reasonable agreement with observations could be achieved for OH and VOCs by a combination of a small recycling term in OH, variation of the deposition rates of intermediate VOC oxidation products, including methyl vinyl ketone (MVK) and methacrolein (MACR), and segregation of OH-containing and isoprene-containing air masses. Similar to the work of Butler et al. [4], Pugh et al. [29] represented the segregation of air masses containing OH from those containing isoprene by a reduction in the effective rate coefficient for the OH + isoprene reaction, with a 50% reduction required to achieve adequate model success. It was thus concluded that model success in tropical regions may be less strongly influenced by mechanistic problems in isoprene oxidation schemes than by detailed representation of physical and micrometeorological processes. This conclusion is in contrast to those of Whalley et al. [14] and Stone et al. [11], discussed below, which conclude that mechanistic changes can result in significant differences in modelled HO_x concentrations for the OP3 campaign.

The importance of boundary layer dynamics and potential segregation of oxidant-rich and VOC-rich air parcels has also been investigated using a large eddy simulation within a mixed-layer model [32]. Although the model uses a highly condensed gas phase chemistry mechanism containing only 19 reactions, the results of the study suggest that the chemistry is equally important as the dynamics in reproducing isoprene mixing ratios measured during the tropical forest and fire emissions experiment (TROFFEE) campaign in Central Amazonia in 2004.

The extent of segregation and turbulent mixing above a forest canopy has been estimated using tower-based measurements of OH, HO_2 and VOC above a deciduous forest in Germany during the emission and chemical transformation of biogenic volatile organic compounds (ECHO) campaign in conjunction with the eddy covariance method [33]. This study showed that, although inhomogeneous mixing can occur near emission sources, the degree of segregation of air masses observed was significantly less than that required to improve the model simulations for the Amazon rainforest [4] and the Borneo rainforest [29]. A reduction in the effective rate coefficient for OH + isoprene of 15% was justified by the measurements [33], in contrast to the 50% proposed by Butler et al. [4] and Pugh et al. [29].

In addition, Pugh et al. [30] conducted a model analysis of high frequency isoprene measurements, made by a proton transfer reaction-mass spectrometer (PTR-MS) instrument during the OP3 campaign in Borneo, to provide an experimentally-based estimate of the extent of segregation between OH and isoprene during OP3. To test the analysis method, Pugh et al. [30] analysed data taken during the German ECHO project and determined similar percentage segregations of OH and isoprene as reported by Dlugi et al. [33]. When applied to the OP3 dataset, Pugh et al. [30] found that the 50% reduction in the effective rate coefficient for the OH + isoprene reaction required to reconcile model discrepancies could not be justified. The results indicated that a

maximum reduction of 15% in the effective rate coefficient for reaction between OH and isoprene was more appropriate, suggesting that the chemistry may play a more significant role than expected by Pugh et al. [29].

Further evidence for a limited role of air mass segregation in explaining OH model discrepancies in tropical regions has been provided by Ouwersloot et al. [34] using a large eddy simulation model. Ouwersloot et al. [34] propose that incomplete mixing of reactive species in a turbulent boundary layer over a spatially homogeneous surface should reduce the OH + isoprene rate coefficient by no more than 10%, while spatially heterogeneous surface emissions should result in no more than a 20% reduction in OH + VOC effective rate coefficients [34]. Comparing model simulations with homogeneous surface emissions to those with heterogeneous emissions yielded differences in OH concentrations of <2% [34]. Several papers thus suggest a limited role of turbulent mixing and segregation of air masses in explaining observed OH concentrations [30, 33, 34].

3 Unidentified Sources of OH in High Isoprene Environments

The possibility for production of OH through unknown chemistry was discussed by Hofzumahaus et al. [6] as a potential explanation for model underestimates of OH in the Pearl River Delta region in China. This study demonstrated the ability of a box model to reproduce HO_2 observations whilst underestimating OH observations by a factor of up to 5, and postulated the presence of an unknown species able to convert RO_2 to HO_2 and HO_2 to OH independently of NO and without producing ozone. Although the region surrounding the Pearl River Delta is characterised by high biogenic VOC emissions, the noontime NO mixing ratios were significantly higher than those encountered during the GABRIEL and OP3 projects (~200 ppt at noon for the Pearl River Delta compared to ~20 ppt for the GABRIEL and OP3 campaigns). Nevertheless, the OH discrepancies were consistent with other field studies which encountered similarly elevated isoprene concentrations (as shown in Fig. 1), suggesting that problems with isoprene oxidation mechanisms can lead to model failures even under moderate NO_x conditions.

Further evidence for the involvement of isoprene oxidation chemistry in model failures in low to moderate NO_x regions has also come from laboratory and theoretical studies, revealing that the oxidation mechanisms currently adopted in atmospheric models provide inaccurate representations of isoprene-related photochemistry, with model discrepancies more likely to be apparent under low NO_x conditions.

3.1 Experimental Indication for OH Formation During Isoprene Oxidation

A chamber study by the California Institute of Technology (CalTech) group observed epoxide formation during the gas phase Photo-oxidation of isoprene [35], with
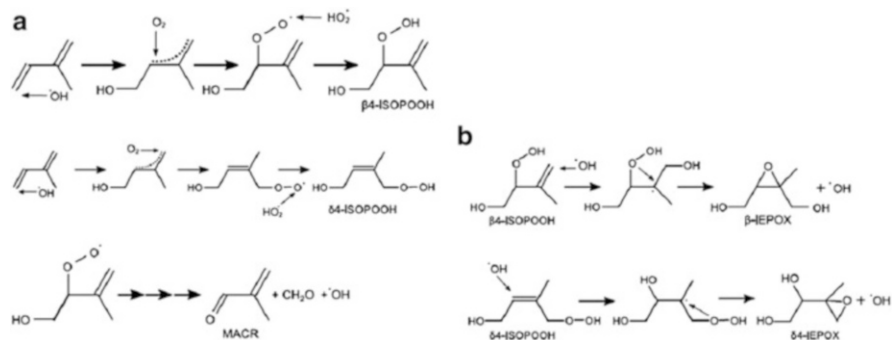
Fig. 3 (**a**) Production of peroxides (ISOPOOH) and MACR following OH-addition to isoprene in the atmosphere. (**b**) Formation of epoxides following addition of OH to isoprene peroxides (reproduced from [35])

implications for OH production and generation of SOA. The CalTech environmental chamber produces OH by photolysis of H_2O_2, resulting in low NO_x conditions (initial mixing ratios of NO_x were varied between 0.1 and 1.3 ppb), and uses a chemical ionisation mass spectrometry (CIMS) detection system to monitor stable reaction products of the OH + isoprene reaction. The experiments showed that peroxides (ISOPOOH) were formed in high yields following OH addition to isoprene and the subsequent reaction of peroxy radicals (ISOPO$_2$) with HO$_2$, with smaller reaction channels resulting in production of OH, formaldehyde and either MACR or MVK (depending on the site of the initial OH addition to isoprene). The reaction scheme depicting these processes is shown in Fig. 3a and Table 1 provides the structural formulas for abbreviations of isoprene-derived species discussed in Sects. 3.2 and 3.3.

Production of peroxides and MVK/MACR following OH-addition to isoprene has been observed in previous studies [36–38], and is included in chemical mechanisms such as the MCM [39]. Prior to the CalTech study, the ISOPOOH peroxides were expected to undergo physical loss, photolysis (yielding ISOPO alkoxy radicals and OH) or react with OH to produce a peroxy radical (in the case of the dominant ISOPOOH isomer of the four isomers in the MCM) or carbonyl species with regeneration of OH (in the case of the three remaining ISOPOOH isomers in the MCM).

However, the CalTech group showed that the reaction of ISOPOOH peroxides with OH could produce epoxides (IEPOX) in an OH neutral reaction, as shown in Fig. 3b. Although the IEPOX species are isobaric with ISOPOOH, and thus appear as a combined IEPOX + ISOPOOH CIMS signal, use of collision induced dissociation enables the production of distinct daughter ions from each compound and separation of the signals. Use of ^{18}OH also enabled separation of the IEPOX and ISOPOOH signals, since ISOPOOH requires addition of one ^{18}OH on isoprene, whereas IEPOX production involves addition of a second ^{18}OH to ISOPOOH and loss of a ^{16}OH radical. Theoretical arguments also provide

Table 1 Abbreviations and structural formulas associated with isoprene oxidation products

Isoprene oxidation products	Structural formula
β4-ISOPO$_2$	
δ4-ISOPO$_2$	
β4-ISOPOOH	
δ4-ISOPOOH	
β4-IEPOX	
δ4-IEPOX	

Table 1 (continued)

Isoprene oxidation products	Structural formula
β4-ISOPO	
δ4-ISOPO	
β4-HPALD	
δ4-HPALD	
β4-PACALD	
HALD	
MVK	
MACR	

evidence for the existence of an energetically favourable pathway producing IEPOX from ISOPOOH [35].

While the initial epoxide production from ISOPOOH is OH-neutral, and will thus have little impact on modelled OH concentrations in low NO_x environments, the discovery of IEPOX species highlights significant gaps in our understanding of isoprene oxidation chemistry. Moreover, the fate of the IEPOX species may be important in terms of understanding field observations of OH and formation of SOA. It is expected that the lifetime of IEPOX with respect to OH addition is of the order of 18–22 h, and that reactive uptake of IEPOX to aerosol surfaces and subsequent SOA formation could be important [35]. If IEPOX are involved in SOA formation then isoprene-derived carbon will be sequestered from the gas phase, potentially reducing the expected impact of isoprene on atmospheric OH concentrations.

The production of ISOPOOH, and therefore IEPOX, is dependent on the reaction of $ISOPO_2$ radicals with HO_2, and is thus expected to occur to a greater extent in low NO_x regions. However, recent theoretical studies have indicated that $ISOPO_2$ radicals may undergo unimolecular decomposition processes which do not produce ISOPOOH, but may result in regeneration of HO_x radicals [40–43].

3.2 Theoretical Indication for OH Production in Isoprene Oxidation

Density functional theory (DFT) calculations have predicted the unimolecular decomposition of β-$ISOPO_2$ radicals (the dominant $ISOPO_2$ isomers), resulting in production of OH, formaldehyde and (depending on the isomer) MVK or MACR [40]. However, the rates of decomposition are expected to be slow, and may not be sufficient to compete effectively with the bimolecular reactions of $ISOPO_2$ radicals with HO_2 and NO in all but the most remote environments [40].

Theoretical investigation of the OH-initiated oxidation of isoprene by the Leuven group has also led to the proposal of HO_x radical production following unimolecular processes in $ISOPO_2$ radicals [41–43]. An outline of the initial steps in the proposed mechanism – the Leuven isoprene mechanism (LIM) – are shown in Fig. 4.

A key feature of the mechanism is the existence of an equilibrium between the initial OH-isoprene radical adduct and the $ISOPO_2$ peroxy radical formed on addition of molecular oxygen to the adduct, leading to the greatest reaction flux through the fastest product forming pathway [42]. Under low NO_x conditions, Peeters et al. [42] propose that the fastest pathways occur through unimolecular 1,6-H shifts in two of the $ISOPO_2$ radicals, producing HO_2 and unsaturated hydroperoxy-aldehydes (HPALDs). Based on an average temperature of 303 K and concentrations of 5×10^8 cm^{-3} NO (~20 ppt), 10^9 cm^{-3} HO_2 (~40 ppt) and 10^9 cm^{-3} total RO_2, Peeters et al. [42] calculated a value of 0.025 s^{-1} for
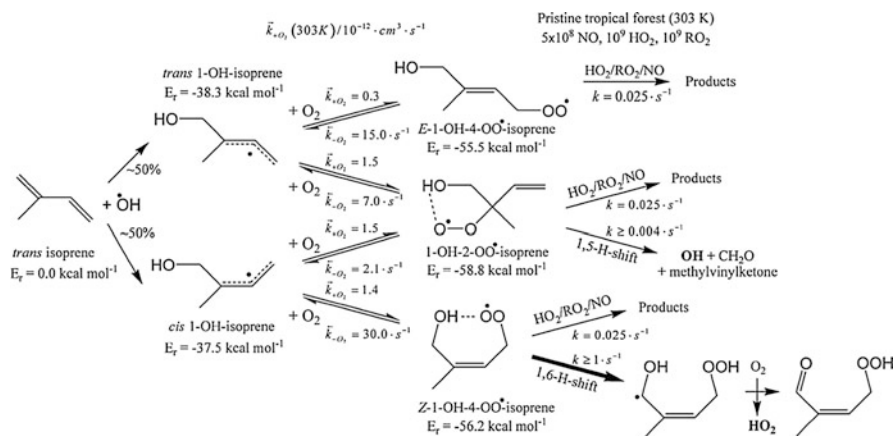
Fig. 4 Outline of the initial steps in the Leuven Isoprene Mechanism, with their predicted rates, following 1-OH addition to isoprene (reproduced from [42])

$\{k_{NO}[NO]+k_{HO_2}[HO_2]+k_{RO_2}[RO_2]\}$ (where k_x is the rate coefficient for the reaction of ISOPO$_2$ isomers with species X). In comparison, the proposed ISOPO$_2$ isomerisation processes to produce the HPALD and HO$_2$ were expected to occur with $k \geq 1$ s^{-1} for the ISOPO$_2$ isomer produced by 1-OH addition to isoprene and $k \geq 8$ s^{-1} for the ISOPO$_2$ isomer produced following 4-OH addition.

The HPALD products are thought to photolyse rapidly during the day, owing to the combination of the –OOH hydroperoxide moiety and an O=C–C=C chromophore, thereby increasing the yield of both OH and HO$_2$ [42]. Subsequent chemistry of the organic fragments of HPALD photolysis, resulting in rapid production of photolabile peroxy-acid-aldehydes (PACALDs), is also expected to increase further the OH and HO$_2$ yields [41–43]. More minor reaction pathways of the initial ISOPO$_2$ peroxy radicals, involving 1,5-H shifts, are also proposed to contribute to OH production, and the potential for similar mechanisms in the oxidation of MVK and MACR has been postulated [42] and, in the case of MACR, experimentally verified [44].

3.3 Experimental and Theoretical Evidence for OH Production Combined

Peeters and Müller [43] surveyed available experimental evidence in order to assess the strengths of the LIM, comparing the expected yields of key species in the novel mechanism against those derived from previous work. Figure 5 shows the dependence of a number of these key species (OH, HPALD, HALD, MVK and MACR) as a function of the NO mixing ratio as derived from the LIM and used in the analysis by Peeters and Müller.

Mechanisms, such as the MCM or MIM, currently adopted in atmospheric models predict relatively high concentrations of hydroxy aldehydes (HALDs),
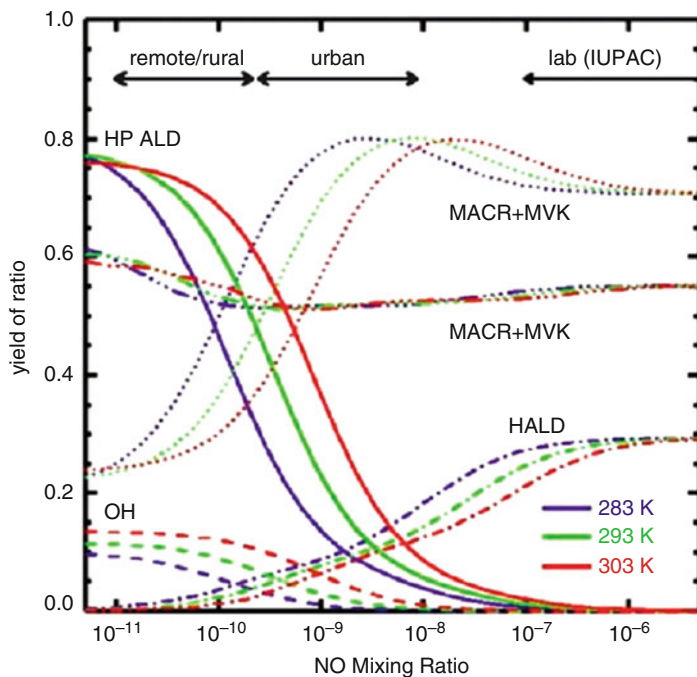
Fig. 5 Expected yields of key species in the Leuven Isoprene Mechanism as a function of the NO mixing ratio (reproduced from [43])

largely formed by hydroxy alkoxy ISOPO radicals produced in $ISOPO_2 + NO$ reactions. Such HALDs, however, have yet to be observed in the field or in laboratory studies at NO mixing ratios below 1 ppb [43]. Peeters and Müller provide an example of this in the work of Karl et al. [37], in which a MIM-based mechanism would predict HALD yields of over 40% in their photoreactor study at NO mixing ratios between 200 and 600 ppt. The LIM predicts a maximum HALD yield of 5% at 400 ppt NO, as shown in Fig. 5, and the lack of HALD observations at low NO mixing ratios is put forward in support of the LIM [43].

Peeters and Müller [43] also discussed the results of the CalTech chamber study [35] in the context of the LIM, proposing that a significant proportion of $ISOPO_2$ sinks were unaccounted for in the CalTech experiment, which could potentially be explained by the additional 1,6-H shifts predicted by the LIM.

The CalTech study observed combined [MVK + MACR] yields of approximately 12% in the absence of NO, attributable to the minor $ISOPO_2$ 1,5-H shift channels [43]. Although this yield is somewhat higher than predicted by the LIM, requiring a factor of 5 increase in the predicted 1,5-H shift rate coefficients, this increased yield does help to rectify discrepancies in MVK/MACR ratios between the LIM and field observations of Karl et al. [22] made in the Amazon rainforest.

The rate coefficients calculated for LIM by Peeters et al. [42] were stated to be lower limits, owing to a possible underestimation of the effects of tunnelling.

Peeters and Müller [43] proposed a similar argument to explain the low rates of peroxy radical isomerisation processes calculated by da Silva et al. [40], and discussed the uncertainties associated with the LIM calculations in greater detail. The probable error on the rates of peroxy radical isomerisations was reported to be of the order of a factor of 5, owing to possible errors on the calculated dissociation energies and barrier heights, and thus within the bounds of the increase required to reconcile the theory with the CalTech experiments. Moreover, calculations made using higher levels of theory indicated that the computed barrier heights for the isomerisation reactions were lower than had been initially reported, supporting the expectation that the calculated rates represent a lower limit.

Low observed yields of a product with a CIMS signal consistent with the HPALD products in the CalTech study were explained by Peeters and Müller [43] as resulting from high chamber concentrations of HO_2, making ISOPOOH peroxide formation more favourable than the unimolecular process generating the HPALDs. In addition, photolysis of HPALDs in the chamber, coupled with their reaction with OH, is expected to have led to more rapid HPALD loss ($\sim 4 \times 10^4$ s^{-1}) compared to ISOPOOH loss ($\sim 6.4 \times 10^{-5}$ s^{-1}).

Very recently the photo-oxidation of HPALDs was incorporated into a detailed chemical mechanism and embedded into a global atmospheric model which generated higher levels of OH in better agreement with field measurements in pristine forested regions [45].

Further work by the CalTech group [46] has provided more direct evidence for the formation of HPALDs in isoprene oxidation, and hence for the occurrence of rapid 1,6-H shifts in $ISOPO_2$ radicals. The experiments were designed to investigate the OH-initiated oxidation of isoprene in the chamber at concentrations of HO_2 and NO pertinent to the pristine troposphere, with NO mixing ratios ranging between 30 and 60 ppt, using photolysis of methyl nitrite (CH_3ONO) as the HO_x source. The study was conducted over a range of temperatures, with experiments also performed using fully deuterated isoprene (C_5D_8) in order to corroborate conclusions drawn from the C_5H_8 system.

The HPALD production rates were measured relative to those of H_2O_2, produced by the HO_2 self-reaction, and ISOPOOH, produced by $HO_2 + ISOPO_2$ [46]. It was therefore possible to determine the ratio of the rate coefficient for the 1,6-H shift in $ISOPO_2$ ($k_{1,6-H}$) relative to that for $HO_2 + ISOPO_2$ ($k_{HO2+ISOPO2}$), using literature recommendations for the HO_2 self-reaction rate coefficient. This method does, however, require knowledge of the CIMS sensitivity to the measured species. For H_2O_2 the sensitivity can be determined using gas phase standards, but it was necessary for HPALD and ISOPOOH sensitivities to be calculated [46].

The experimental analysis did not consider oxidation chemistry of the reaction products (H_2O_2, ISOPOOH, HPALD), introducing a potential error of <10% [46]. Photolysis of the HPALD product was expected to be negligible under the experimental conditions [46].

The results of the study provide clear evidence for the formation of HPALDs, and thus for the 1,6-H shifts in $ISOPO_2$ radicals predicted by Peeters et al. [42]. However, the rate of HPALD formation was observed to be approximately 50 times

slower than that expected by Peeters et al. [42] and Peeters and Müller [43]. Implementation of the 1,6-H shifts in ISOPO$_2$ radicals into the global 3D chemistry transport model GEOS-Chem showed that while the isomerisation reaction producing HPALDs is an important process in isoprene oxidation, constituting 7.4% of the global loss of ISOPO$_2$ radicals, the reaction is not as dominant as previously expected [46]. Recent work by the CalTech group has demonstrated that isomerisation reactions in other organic peroxy radicals can also lead to OH formation, with OH observed following a rapid 1,4-H shift in a peroxy radical derived from MACR [44]. The impact of these novel OH sources on model simulations is considered below.

4 Impacts of Additional OH Sources on Model Simulations in High Isoprene Low NO$_x$ Regions

Several studies have been conducted to assess the impact of the potential mechanistic changes in isoprene oxidation on tropospheric concentrations of OH and HO$_2$, including our own work as part of the OP3 project in Borneo [11, 14, 31].

Wolfe et al. [47] used the one-dimensional chemistry of atmosphere – forest exchange (CAFE) model – to aid understanding of measurements made during the biosphere effects on aerosols and photochemistry experiment (BEARPEX-2007) campaign in a Ponderosa pine forest in the western foothills of the Sierra Nevada Mountains in California. The chemistry scheme within the model was based on MCMv3.1, with additional chemistry to represent the formation of isoprene-derived epoxides as observed by Paulot et al. [35]. However, the model still underpredicted OH observations by a factor of 6 during particularly warm periods when VOC emissions were high [47]. During these 'hot' periods, Wolfe et al. [47] required additional OH sources, which were represented in the model by the production of OH from HO$_2$ + RO$_2$ reactions, similar to the modelling studies for the GABRIEL campaign [4, 7, 8]. Formation of epoxides in isoprene oxidation, although an important discovery in terms of our understanding of isoprene chemistry, thus appears to do little to rectify model discrepancies for OH.

This result has also been observed in a number of other modelling studies [11, 47–49]. Stavrakou et al. [49] used the intermediate model of global evolution of species IMAGESv2 global chemistry transport model to investigate the impacts of several of the previously described proposed mechanisms for OH recycling in isoprene oxidation. The model used chemistry based on the MIM2 [50], with simulations to assess the impacts of the artificial recycling scheme used by Lelieveld et al. [8] and Wolfe et al. [47], the formation of isoprene epoxides and the occurrence of ISOPO$_2$ 1,6-H shifts in the LIM. It was found that the LIM had the greatest potential for increasing modelled HO$_x$ concentrations over densely vegetated areas in the tropics and at mid-latitudes, with increases in OH concentrations by a factor of 4 compared to the MIM2. In comparison, inclusion

of epoxide forming chemistry gave increases in OH by a factor of only 1.25. As described by Stavrakou et al. [49] and Peeters and Müller [43], inclusion of the LIM in the IMAGESv2 model replicated average boundary layer observations of OH and HO_2 during the GABRIEL and INTEX campaigns to within 30%.

Archibald et al. [48] also investigated the impacts of OH formation from HO_2 + RO_2 reactions, epoxide chemistry, and 1,5-H and 1,6-H shifts in $ISOPO_2$ radicals, using a zero-dimensional model with chemistry based on the MCMv3.1. Inclusion of OH-producing channels in HO_2 + RO_2 reactions in which OH formation is expected to occur gave increases in OH concentrations of 7%, compared to a 16% increase on consideration of the epoxide chemistry and 330% for the 1,5-H and 1,6-H shifts in $ISOPO_2$.

Implementation of a modified version of CRIv2-R5 chemistry scheme [51] within the UK meteorological office three-dimensional Lagrangian global model (STOCHEM) indicated that use of the LIM resulted in significant elevations in modelled OH concentrations over rainforested regions in the Amazon and in Borneo, and concluded that the LIM had the greatest potential for increasing modelled OH concentrations. It was noted, however, that it was likely that some degree of parameter refinement and optimisation within the scheme would be necessary before the mechanism could be fully reconciled with atmospheric observations and other laboratory data.

While arguments to explain some of the apparent discrepancies between laboratory data and the LIM may have been put forward by Peeters and Müller [43], it would appear that there are outstanding issues in modelling HO_x observations with the mechanism as it currently stands. In our work as part of the OP3 project in Borneo [31], measurements of OH and HO_2 were made by both ground-based instruments in the rainforest [14, 52] and by an aircraft instrument on the BAe146 NERC research aircraft [11]. Analysis of the HO_x observations and detailed chemical modelling with the dynamically simple model of atmospheric chemical complexity (DSMACC) [53] for both ground and aircraft campaigns have revealed that HO_x observations in tropical regions still cannot be fully explained.

The combination of measurements of HO_x concentrations and the OH reactivity (a measure of the total OH sinks in an air mass) [52, 54] at the ground-based site enabled quantification of the total OH source in the rainforest [14]. It was found that to maintain the observed OH concentrations, given the measured reactivity, required an OH production rate ten times greater than that calculated using all measured OH sources. Model calculations were also shown to under-predict simultaneously the observed OH concentrations while over-predicting HO_2. Inclusion of an additional OH source formed as a recycled product of OH-initiated isoprene oxidation improved the model agreement for OH, but served to worsen the model failure for HO_2. In order to replicate observations of both OH and HO_2, the model required additional loss process for HO_2, or a process that converts HO_2 to OH.

OP3 aircraft measurements have also been used to test our understanding of isoprene oxidation chemistry, using the DSMACC box model to assess the ability of the various proposed oxidation mechanisms to reproduce the observed
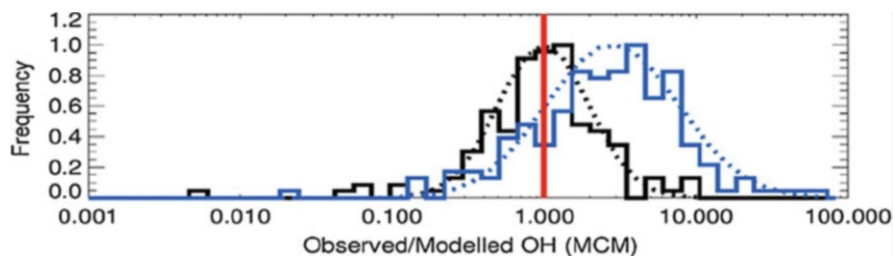
Fig. 6 Probability distribution functions of the observed to modelled ratio for OH using the MCMv3.1 for data points during the OP3 aircraft campaign with low (<15 ppt) isoprene concentrations (*black*) and high (>15 ppt) isoprene concentrations (*blue*), with Gaussian fits to the data shown by the *broken lines*. The *red line* indicates an observed to modelled ratio of 1. The plot displays the ability of the model to replicate OH observations at low isoprene concentrations, but a model failure at high isoprene concentrations (reproduced from [11])

concentrations of OH and HO_2 [11]. The base model run for the aircraft campaign, using the MCMv3.1, displayed a significant underestimate for OH in airmasses impacted by isoprene, with a mean observed to modelled ratio of $5.32^{+3.68}_{-4.43}$ compared to a ratio of $1.62^{+1.27}_{-1.24}$, for airmasses not significantly impacted by isoprene, as shown in Fig. 6 [11]. For HO_2, the model was generally able to replicate the observations, with no significant dependence of the model success on the isoprene concentration.

Table 2 shows the OP3 aircraft model results for the range of potential isoprene oxidation mechanisms and additional OH sources discussed above, including epoxide formation [35], unimolecular decomposition of isoprene peroxy radicals [41–43] and recent updates to the MCM (MCMv3.2). In keeping with the results of Whalley et al. [14], the LIM gave significant improvements to the modelled OH concentrations, but resulted in a large model overestimate for HO_2. However, the experimental findings of Crounse et al. [46], indicating a slower HPALD production rate than predicted by Peeters et al. [42] and Peeters and Müller [43], reduces the impact of the LIM and thus its potential to rectify model discrepancies for OH.

Analysis of our measurements during OP3 [11, 14] show that it is not possible to remove simultaneously the model bias in both OH and HO_2 using any of the suggestions described above. The results of this field campaign show that, despite significant recent advances in our understanding of isoprene oxidation chemistry, there are still considerable gaps in our knowledge. Similar conclusions have been drawn from field studies in anthropogenically influenced regions under high isoprene loadings [6, 55–58], indicating that uncertainties in the isoprene oxidation mechanism are important not only under pristine forest conditions (NO < 50 ppt), but also at moderate NO_x levels (several hundred ppt) in populated areas where ozone production and air quality predictions could be biased. Lu et al. found that the LIM mechanism was unable to reconcile fully OH observed during PRIDE [57] and CAREBeijing2006 (Campaigns of Air Quality Research in Beijing and Surrounding Region 2006) [58], particularly if the reduced isomerisation rate determined by

Table 2 Mean observed to modelled ratios of OH and HO$_2$ at isoprene concentrations above and below 15 ppt for a range of mechanisms investigated by Stone et al. [11]

Mechanism	Mean [OH]$_{obs/mod}$, C$_5$H$_8$ < 15 ppt	Mean [OH]$_{obs/mod}$, C$_5$H$_8$ > 15 ppt	P_D	P_H	Mean [HO$_2$]$_{obs/mod}$, C$_5$H$_8$ < 15 ppt	Mean [HO$_2$]$_{obs/mod}$, C$_5$H$_8$ > 15 ppt	P_D	P_H
MCMv3.1	$1.62^{+1.27}_{-1.24}$	$5.32^{+3.68}_{-4.43}$	0	0	$0.86^{+0.32}_{-0.31}$	$1.18^{+0.30}_{-0.30}$	0	0.921
MCMv3.2	$1.62^{+1.27}_{-1.24}$	$4.51^{+3.08}_{-3.75}$	0	0	$0.83^{+0.31}_{-0.27}$	$1.05^{+0.27}_{-0.27}$	0	0.889
C$_5$H$_8$ + OH $\rightarrow$ 3OH	$1.62^{+1.27}_{-1.24}$	$1.62^{+1.25}_{-1.25}$	0.867	0.054	$0.86^{+0.32}_{-0.31}$	$0.67^{+0.30}_{-0.26}$	0	0
HO$_2$ + ISOPO$_2$ $\rightarrow$ 3OH	$1.62^{+1.27}_{-1.24}$	$1.62^{+1.11}_{-1.21}$	0.913	0.149	$0.86^{+0.32}_{-0.31}$	$0.70^{+0.21}_{-0.21}$	0	0
HO$_2$ + RO$_2$ $\rightarrow$ 0.5OH	$1.42^{+1.14}_{-1.07}$	$4.13^{+2.87}_{-3.39}$	0	0	$0.81^{+0.30}_{-0.30}$	$1.05^{+0.27}_{-0.27}$	0	0
RO$_2$ + X $\rightarrow$ HO$_2$ HO$_2$ + X $\rightarrow$ OH	$1.62^{+1.27}_{-1.24}$	$1.68^{+0.38}_{-1.49}$	0	0.001	$0.86^{+0.32}_{-0.31}$	$0.89^{+0.40}_{-0.40}$	0.002	0
Epoxide	$1.62^{+1.27}_{-1.24}$	$4.27^{+2.90}_{-3.52}$	0	0	$0.86^{+0.32}_{-0.31}$	$0.96^{+0.24}_{-0.24}$	0	0.633
da Silva	$1.62^{+1.27}_{-1.24}$	$5.19^{+4.31}_{-3.61}$	0	0	$0.86^{+0.32}_{-0.31}$	$1.17^{+0.30}_{-0.30}$	0	0.943
Peeters	$1.62^{+1.27}_{-1.24}$	$1.50^{+1.12}_{-1.14}$	0.820	0.014	$0.86^{+0.32}_{-0.31}$	$0.46^{+0.18}_{-0.19}$	0	0

Errors shown are the standard deviations in the mean. P_D refers to the probability result of a Kolmogorov–Smirnov test and refers to the probability that the distribution functions of the ratios for data points with isoprene above and below 15 ppt are statistically identical. P_H refers to the probability result of a Kruskal–Wallis test and indicates the probability that the ratios for data points with isoprene concentrations above 15 ppt are independent of the isoprene concentration. Probability values <0.001 are listed as zero (reproduced from [11])

Crounse et al. [46] was implemented; inclusion of epoxide chemistry also had little impact on the modelled OH in these studies. Inclusion of LIM led to overpredictions of HO_2 measured during PRIDE, CAREBeijing2006 and HOxCOMP [55–58] similar to findings from OP3.

Archibald et al. [59] investigated the impact of HO_x recycling in isoprene oxidation on modelling of past, present and future atmospheres using the UKCA global chemistry climate model. The study showed the potential for substantial changes to our estimates of global methane lifetimes as a result of developments in our understanding of isoprene chemistry. The changes to OH concentrations owing to changes to the descriptions of isoprene chemistry result in an 11% reduction in the global methane lifetime and a 9% increase in the global ozone burden by 2100. The representation of isoprene chemistry in atmospheric models thus has important consequences for predictions of future climate change scenarios.

The role of isoprene chemistry in controlling atmospheric composition and climate, and the influence of temperature and land use change on isoprene emissions, should not be underestimated. The field observations of OH in isoprene-rich, NO_x-poor environments discussed above indicate that isoprene has a considerably smaller effect on OH concentrations than chemistry models predict. This conclusion, based on direct measurements of OH and comparison with model predictions, is also supported by observations of other atmospheric species undertaken in VOC rich NO_x poor environments. Discrepancies between isoprene concentration measurements and model predictions when constrained to isoprene emission inventories have been reported, as have discrepancies between model predictions of isoprene oxidation product concentrations and those measured. Large model underestimates of OH reactivity and SOA formation under isoprene-rich conditions also point towards significant uncertainties in the OH-initiated isoprene oxidation mechanism.

5 Isoprene Emission Rates and Mixing Ratios and Comparisons with Model Predictions

Emission inventories of natural VOCs on regional and global scales have been available since the late 1970s. Many of the regional and global early inventories [60–62] suffered from considerable weaknesses owing to lack of available/relevant data including accurate estimates of global vegetation coverage, VOC emissions from different sources, how emissions change with changes in drivers such as temperature and light intensity and how these drivers change [63]. With these weaknesses in mind, considerable effort was put into generating a more robust global emission inventory on a $1° \times 1°$ grid for use in global chemistry and transport models. The global emissions inventory activity (GEIA) developed a model of isoprene and other VOC emissions [63] and a regional biogenic emissions model [biogenic emissions inventory system (BEIS)] developed in the 1980s [64] was updated [65]. The model of emissions of gases and aerosols from nature
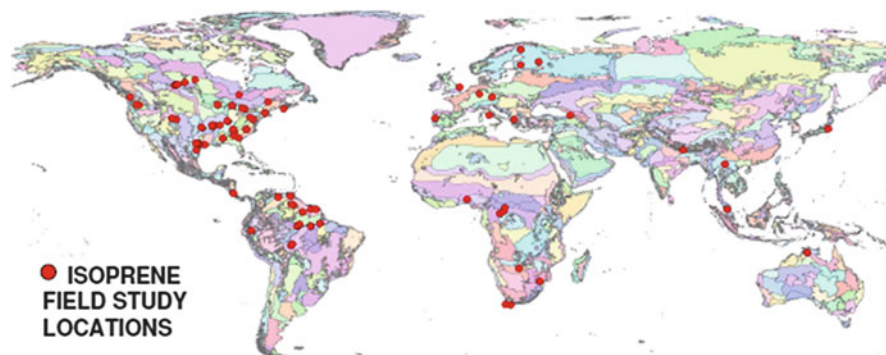
Fig. 7 Geographical distribution of ecoregions identified in Olson et al. [138] and the locations of ~90 isoprene field experiments used to develop isoprene emission factors (reproduced from [66])

(MEGAN) was developed to replace GEIA and BEIS in 2006 [66]. The isoprene emission rates recommended in the mid-1990s [63, 65] were greater by more than a factor of two than those previously used in the early regional air quality and global transport models [60–62, 64]. Global emission estimates of isoprene were of the order of 570 Tg year^{-1} and were derived primarily from enclosure measurement studies which assigned leaf level emission factors to many global ecosystems; other ecosystems that were unmeasured were assigned default values. In the GEIA and BEIS inventories only 3 of the 20 publications used to determine emissions included studies conducted in tropical regions. In addition to this, emission activity algorithms describing the response of isoprene emissions to temperature and light were based on investigations of temperate plants rather than tropical measurements [63].

Since the 1990s, thousands of isoprene emission rate measurements using enclosure techniques have been conducted (Fig. 7) and are incorporated into the most recent global emission inventories [66]. These are often extrapolated to canopy scale using canopy environment models. Measurements conducted in tropical regions are now much more abundant [67–72] and direct measurements of above-canopy fluxes have become more widespread, enabling parameterisation of emissions on an eco-system scale, e.g. [73, 74], which is particularly advantageous in tropical landscapes where eco-system species are extremely diverse. With much improved constraints, MEGAN estimates a global isoprene emission of ~600 Tg year^{-1}. In many cases, when employed in chemistry and transport models and global atmospheric chemistry models, these isoprene emission rates result in unrealistically high concentrations of isoprene and ozone in the boundary layer [75, 76]. Scaling factors have been introduced in many instances which uniformly reduce emissions by 20% or more or, in some cases, reduce emissions in selected landscapes by up to a factor of 3 [77]. The intergovernmental panel on climate change (IPCC) recommends a 56% reduction in global isoprene emission rates as recommended by Guenther et al. [63] to allow models to replicate observations of

CO and isoprene concentrations [78]. Favourable comparisons between canopy-scale emissions based on leaf-level emission measurements and above-canopy flux measurements scaled up (or down) with a canopy environment model have been made, however. Spirig et al. [79] found that above-canopy fluxes of isoprene measured using eddy covariance and PTR-MS during the ECHO campaign, which took place in a European deciduous forest, provided a top-down estimate of isoprene emission rates at the leaf level comparable to cuvette measurements made at the site. Similarly, Kuhn et al. [80], measuring isoprene and monoterpene fluxes in a tropical forest in the Central Amazon basin, found that the observed VOC fluxes were in good agreement with simulations using a single-column chemistry and climate model (SCM). Comparison of the biogenic emission model, MEGAN, with flux measurements made in the Amazon basin during TROFFEE were also found to agree with each other within associated model and measurement uncertainties [81].

Discrepancies between flux observations and emission models have been reported; these differences tend to relate to the use of inappropriate base emission rates (BER) (rate at which plants emit isoprene under a set of standard conditions; $T = 30°C$; photosynthetically active radiation $= 1,000$ µmol m^{-2} s^{-1}) within emission models, however. Langford et al. (2010) report isoprene and mono-terpene flux observations made during OP3. Comparison of the observations with emissions estimated by the MEGAN model demonstrated that large discrepancies could arise if default isoprene BER – based on measurements (Fig. 7, Table 3) made over the Amazon rainforest where the emission factors are largely derived from – were used, with model isoprene emissions being four times greater than those observed. The modelled to measured flux agreement could be improved considerably, however, if the model was constrained to typical photosynthetically active radiation (PAR) and temperature variables measured at the Borneo station [82]. Hewitt et al. [83] have recently demonstrated that BER for isoprene is not necessarily constant and instead is under circadian control and can vary throughout the day. Assuming a constant BER led to an overestimation in the isoprene flux relative to those observed during OP3 [83]. These direct flux observations and comparison to emission models suggest that emissions inventories do not necessarily overestimate isoprene emission rates; rather, other model factors such as deposition of isoprene oxidation products, oxidation schemes employed or the factors controlling isoprene emissions may contribute to poor model performance [66].

It must be noted that, although the examples given above demonstrate good agreement between modelled emissions rates and directly measured isoprene fluxes, many of these models overestimate VOC mixing ratios [76, 77]. For example, Kuhn et al. [80] observed the vertical gradients of isoprene and isoprene oxidation products; comparison between model and observations led Kuhn and co-workers to suggest that the oxidation capacity was much higher than that assumed by the model. A simple chemical kinetics study utilising the ratio of (MVK + MACR)/isoprene estimated an [OH] of ~8×10^6 molecule cm^{-3}, an order of magnitude higher than predictions made by the model employed. This high [OH]

Table 3 Isoprene and monoterpene flux measurements from tropical forests and typical monoterpene: isoprene ratio (units in mg C $m^{-2} h^{-1}$; reproduced from Langford et al. 2010 [82]). See Langford et al. [82] for details of the references cited in this table

Location	Season	Method	Isoprene	∑Monoterpene	Ratio	References
Borneo SE Asia	L wet	vDEC	0.48 ± 0.72	0.13 ± 0.19	0.27	Langford et al. (this study)
Borneo SE Asia	E dry	vDEC	1.04 ± 1.3	0.25 ± 0.33	0.24	Langford et al. (this study)
Malaysia SE Asia	Dry	LL	1.1	–	–	Saito et al. (2008)
Amazon, Brazil	E dry	MB	2.7	0.24	0.23	Zimmerman et al. (1998)
Amazon, Peru	E dry	MLG	7.2	0.45	0.06	Helmig et al. (1998)
Amazon, Brazil	L wet	EC, REA	2.1	0.23	0.11	Rinne et al. (2002)
Amazon, Brazil	L dry	vDEC	7.3 ± 2.7	1.5 ± 1.1	0.21	Karl et al. [81]
Amazon, Brazil	L dry	MLG	10.2 ± 3.5	2.2 ± 0.7	0.22	Karl et al. [81]
Amazon, Brazil	L dry	MLV	11.0 ± 0.9	3.9 ± 1.1	0.35	Karl et al. [81]
Amazon, Brazil	E dry	REA	2.1 ± 1.6	0.39 ± 0.43	0.19	Kuhn et al. [80]
Amazon, Brazil	E dry	SLG	3.4 ± 3.6	0.38 ± 0.58	0.11	Kuhn et al. [80]
Amazon, Brazil	–	REA	1.1	0.2	0.18	Stefani et al. (2000)
Amazon, Brazil	–	BM	1.9	0.16	0.08	Greenberg et al. (2004)
Amazon, Brazil	–	BM	4.7	0.20	0.04	Greenberg et al. (2004)
Amazon, Brazil	–	BM	8.6	0.54	0.06	Greenberg et al. (2004)
Amazon, Brazil	Dry	EC	0.4–1.5	–	–	Muller et al. (2008)
Amazon, Brazil	Wet	EC	0.1–0.3	–	–	Muller et al. (2008)
French Guyana Suriname	Dry	CBL	6.1	–	–	Eerdekens et al. (2009)
Costa Rica	Wet	REA	2.2	–	–	Geron et al. (2002)
Costa Rica	Dry	DEC	2.2	0.29	0.13	Karl et al. [74]
Congo, Africa	–	A-REA	0.9	–	–	Greenberg et al. (1999)
Congo, Africa	–	LL	0.8–1	–	–	Klinger et al. (1998)
Congo, Africa	–	REA	0.46–1.4	–	–	Serca et al. (2001)

EC eddy convariance, *vDEC* virtual disjunct eddy convariance, *DEC* disjunct eddy convariance, *(A)-REA* (airborne) relaxed eddy accumulation, *SLG* surface layer gradient, *MB* mass budget, *MLG* mixed layer gradient, *MLV* mixed layer variance, *LL* leaf level extrapolation, *BM* box modelling, *CBL* convective boundary layer budgeting

estimate was also supported by a simple budget analysis, which assumes that the isoprene mixing ratio is in steady state with the chemical boundary layer and, hence, the amount of isoprene emitted and entrained (F_{ISO}) is balanced by the

amount chemically degraded by oxidants such as OH and O_3 at a particular boundary layer height (z_i). The respective flux-to-lifetime relationship can be described as

$$F_{ISO} = (k_{OH(ISO)} \times [OH] + k_{O_3(ISO)} \times [O_3]) \times [ISO] \times z_i. \tag{1}$$

Solving (1) for OH, Kuhn and co-workers estimate an OH radical concentration of ~4.5×10^6 molecule cm^{-3} using mean observations of isoprene mixing ratios and fluxes determined using mixed layer gradient measurements. These elevated OH concentration estimates support the recent, direct, OH concentration measurements made over Suriname [8]. Increasing the modelled OH concentration was suggested to remedy isoprene emissions with the observed isoprene concentrations [80]. Similarly, Karl et al. [81] found during a study conducted during the dry season in the Amazon that OH modelled in the boundary layer using a photochemical box model was significantly lower than that calculated using the mixed layer budget analysis. Karl et al. [81] hypothesised that reactive sesquiterpenes present at 1% of the isoprene concentration could produce sufficient OH radicals by ozonolysis (assuming an OH yield of one) that could largely reconcile the differences in the OH predicted by a zero dimensional detailed chemical box model and estimates based on the budget analysis.

Pugh et al. [29], using a box model to simulate the atmospheric boundary layer over the Borneo rainforest, constrained to the measured VOC fluxes [82], found that the model, rather than overpredict isoprene (as is the case with many of the earlier emission constrained models), was able to simulate concentrations well, but underpredicted the measured OH concentration (by two to three times) and over-predicted the concentrations of isoprene oxidation products of MVK and MACR considerably (five to ten times) (consistent with findings by Kuhn et al. [80] and Karl et al. [81]). Increasing the dry deposition velocity of the MVK and MACR improved the modelled to measured agreement for these species and brought the modelled OH into better agreement with observations due to a reduction in the modelled OH sink. Pugh et al. [29] found that increasing OH in the model only served to reduce the modelled isoprene concentration, with modelled isoprene concentrations dropping below those observed. Increasing the isoprene emissions (to greater than observed) to rectify the model underestimation only resulted in a further re-suppression of OH [29]; Butler et al. [4] report similar findings from model measurement comparisons undertaken as part of the GABRIEL project. As discussed in Sect. 2.2, Pugh et al. found that a 50% segregation between OH and isoprene was able to reconcile inconsistencies between measurements, although in a later paper Pugh et al. [30] determined the degree of segregation explicitly for observations conducted during OP3 and concluded that the segregation was not >15%. These findings highlight that, despite an accurate representation of isoprene emissions, observations of isoprene, isoprene oxidation products and OH cannot be fully reconciled, suggesting that there are still gaps in our understanding of isoprene oxidation chemistry.

5.1 Isoprene Emissions Inferred from Satellite Measurements of HCHO

Global and regional biogenic emissions, determined using bottom-up methods which rely on as yet relatively sparse in-situ concentration data (Fig. 7) and/or flux measurements extrapolated to regional or continental scales using satellite-derived land cover, have large associated uncertainties. For example, the annual global isoprene emission estimated with MEGAN ranges from 500 to 750 Tg isoprene depending on driving variables such as temperature, solar radiation, leaf index area and plant functional type [66]. A promising, alternative approach for assessing global emission inventories and developing global isoprene emission maps is to use a top-down approach based on satellite measurements of isoprene oxidation products such as formaldehyde (HCHO). The success of this technique to predict global isoprene emissions accurately relies heavily on an accurate description of isoprene oxidation leading to the formation of HCHO and upon the OH concentration, however. The principal sink of isoprene is oxidation by the OH radical; underestimating OH concentrations will directly affect isoprene and HCHO concentrations. The method assumes that the HCHO column, Ω (molecule cm^{-2}), observed by satellites, and the sum of HCHO precursor emissions at steady state in the absence of horizontal transport can be linearly related by

$$\Omega = \frac{1}{k_{\mathrm{HCHO}}} \sum_i Y_i E_i \tag{2}$$

where k_{HCHO} is the first order loss of HCHO from oxidation and photolysis applied to the column, E_i is the emission of VOC species i and Y_i is the HCHO yield from species i. For isoprene the conversion time to HCHO may be as little as 1 h and the lifetime of HCHO is of the order of a few hours during the daytime. For reactive VOCs, such as isoprene, which produce HCHO promptly, transport away from the point of emission can be considered minimal and, as such, any variability in the HCHO column can be assumed to be largely caused by variability in isoprene oxidation rather than transport into and out of the HCHO column. Fu et al. [84] compared observed HCHO columns from the global ozone monitoring experiment (GOME) satellite with those simulated using the Goddard Earth Observing System chemical transport model (GEOS-Chem) constrained to biogenic emissions determined using MEGAN [66]. Isoprene emissions from east and south Asia inferred from the satellite measurements were 53 ± 30 Tg year^{-1} and compared well, on average, with MEGAN predictions of 56 Tg year^{-1} for the region. MEGAN was found to underestimate isoprene emissions by a factor of 3 for Chinese mixed forests and croplands and overestimate emissions from tropical vegetation. Using a similar approach, Millet et al. [85] studied the spatial distribution of HCHO over North America, using HCHO column measurements taken from the ozone monitoring instrument (OMI), and compared to the bottom-up MEGAN emission inventory. Although spatially consistent, OMI-derived isoprene emissions were

found to be between 4% and 25% lower than those predicted by MEGAN on average. Shim et al. [86] used the GEOS-Chem chemical transport model driven by the GEIA biogenic emissions database to conduct a global inversion of GOME HCHO column data. The estimated global isoprene annual emissions were higher at mid-latitudes and lower in the tropics when compared to the GEIA inventory. Barkley et al. [87] comparing isoprene emissions derived from HCHO GOME columns and those derived from the MEGAN inventory found that over South America MEGAN predicted much higher isoprene emissions than GOME; this positive bias was found to be larger in the dry season than the wet season. The mean [OH] from MEGAN and GOME simulations conducted by Barkley et al. [87] were approximately 1.2–4.5 lower than values observed over the tropical rainforest in Suriname during the GABRIEL project. Underestimating the OH oxidation in the GOME model will in turn lead to an underestimation of isoprene inferred from the observed HCHO column. Additional OH recycled during isoprene oxidation could help to resolve quantitatively MEGAN and GOME isoprene emission estimates [87].

6 Isoprene Oxidation Products

Observations of other isoprene oxidation products such as MVK, MACR and hydroxyacetone in a number of field studies and comparison with model predictions also point towards large uncertainties in isoprene oxidation schemes currently employed. Observed oxygenated volatile organic carbon (OVOC) mixing ratios are determined by a balance of their production (largely dominated by photochemistry) and loss rates (which include reactive loss, dry deposition and vertical mixing). Pugh et al. [29], for example, found that the model scheme used to assess chemistry during the OP3 project that took place in the Borneo rainforest greatly overestimated the sum of MVK and MACR measured and suggested that the dry deposition rate of these OVOC could be larger than assumed by the model. Karl et al. [22], comparing observations of MVK + MACR and hydroxyacetone (measured using PTR-MS) during the Amazonian aerosol characterisation experiment (AMAZE-08) with model predictions, report a factor of 10 underprediction in the hydroxyacetone/(MVK + MACR) ratio, implying a missing source of hydroxyacetone in the model. Karl et al. [22] also reanalysed data from five other field campaigns and found that during all of them, hydroxyacetone mixing ratios were significantly higher than what would be expected from model predictions which assume that the major source of hydroxyacetone is an oxidation product of MACR. Theoretical studies have proposed a primary source of hydroxyacetone direct from isoprene [88], and laboratory studies have demonstrated a fast secondary production which is currently not included in atmospheric chemistry models [3]. Karl et al. [22] implemented the additional hydroxyacetone pathway proposed by Paulot et al. [3] extended to low NO_x conditions in model runs and found that the mechanism reproduced well the MVK/MACR ratio observed during

the AMAZE campaign; the modelled hydroxyacetone/(MVK + MACR) ratio obtained from the Paulot mechanism was within 50% of observations, suggesting that fast secondary production could explain 50% of the observed hydroxyacetone/(MVK + MACR) ratio. The remaining 50% may be related to the primary production mechanism as suggested by [88]. Karl et al. [22] also assessed the performance of the recently proposed Leuven mechanism in reproducing the AMAZE OVOC observations. This mechanism was found to predict an MVK/MACR ratio of ~10; observed ratios were typically ~1.34 (measured by GC-MS). The Leuven mechanism also significantly underestimated the sum of MVK and MACR to isoprene ratio. The yields of MVK, MACR and hydroxyacetone are highly sensitive to the rate of decomposition of the 1,6-H shift reactions which are proposed to be rapid in the Leuven mechanism (Fig. 4). Karl et al. [22] found that to reconcile the mechanism of Leuven with the observed OVOC ratios during the AMAZE campaign would require the 1,6-H shift reactions decomposition rate and the reverse reaction rates of the Z-1-OH-4-OO* and Z-4-OH-1-OO* peroxy radicals to be reduced (consistent with the experimental results of Crounse et al. [46]). Such an adjustment would lead to a corresponding reduction in the overall HO_x yield from the Leuven mechanism, with an approximate yield of 0.1 HO_2 and 0.12 OH radicals, just 33% of the original.

7   OH Reactivity

If, as suggested by Karl et al. [22], the rate of formation of isoprene oxidation products are underestimated, due to uncertainties in the isoprene oxidation method employed in models, this will undoubtedly impact the oxidative capacity and OH reactivity determined by models due to reaction of these OVOCs with OH. Although the direct radiative forcing of these species is small, their indirect effect on the lifetime of species such as CH_4 and their role in the formation of organic aerosol and tropospheric ozone have an important influence on climate as well as local and regional air quality [89]. Observations of the total OH reactivity have been made in a variety of chemical environments [52, 54, 90–101]. In most studies the observed reactivity is underestimated by models constrained to the measured OH sink species; this discrepancy is often greatest in regions of high biogenic activity [52]. Much of this discrepancy may be caused by unmeasured VOCs using standard observation techniques such as gas chromatography [102]. Chung et al. [103] found that as much as 45% of the total non-methane organic carbon was unmeasured during observations in the Los Angeles basin. The discrepancy increased as the air mass aged, suggesting that the missing organic fraction was made up largely by oxidation products of primarily emitted VOCs. In contrast to this, Di Carlo et al. [90] found that the oxidation products of the VOCs observed in a mid-latitude mixed hardwood forest accounted for <2% of the calculated OH reactivity and instead suggested that unmeasured primarily emitted biogenic
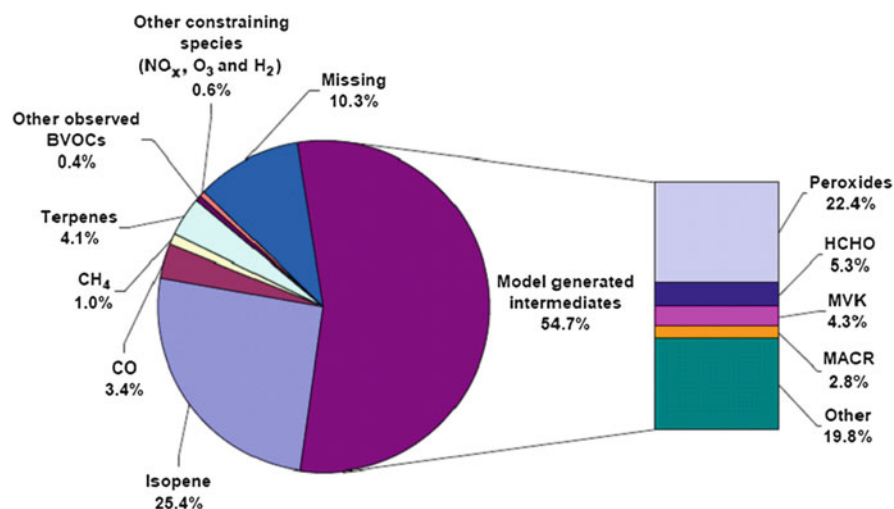
Fig. 8 Pie-chart showing the contributions to OH reactivity calculated using a zero-dimensional box model constrained to the Master Chemical Mechanism for comparison with observations of OH reactivity made during the OP3 campaign in the Borneo rainforest

VOCs such as terpenes could account for the missing reactivity. Di Carlo et al. [90] relied on a heavily lumped model, however.

Sinha et al., [100] determined during measurements taken in Suriname, within the canopy at a height of approximately about 35 m, an average OH reactivity of ~53 s^{-1} with a peak OH reactivity of 72 ± 18 s^{-1}. The calculated OH reactivity determined from concentration measurements of acetone, acetaldehyde, isoprene, MVK and MACR made up just 35% of the measured OH sink; the limited dataset, however, prevented any strong conclusions on the likely missing sink species. Edwards et al. [52] assessed the measured OH reactivity observed in the Borneo rainforest using a zero dimensional model based upon MCM chemistry and found that the model was particularly sensitive to concentrations of unconstrained oxidation products of the observed BVOCs, in particular isoprenal hydroperoxides, carbonyls and alcohols, highlighting the importance of these species in the chemistry controlling oxidation in this environment. This importance of isoprene oxidation products as a major sink for tropical OH has been suggested previously by Warneke and Gouw [104], where measured concentrations of MVK, MACR and isoprenal peroxides above the Amazon rainforest resulted in large reductions in OH concentrations within a photochemical box model. Edwards et al. [52] demonstrate from direct measurements of OH and OH reactivity within a tropical rainforest that as much as 55% of the observed OH loss is potentially through reaction with unmeasured oxidation products of primary BVOCs. This work highlights the importance of an accurate description of the isoprene degradation mechanism within models to understand ultimately the fate of the oxidised isoprene products and their impact on the oxidising capacity (Figs. 8 and 9).
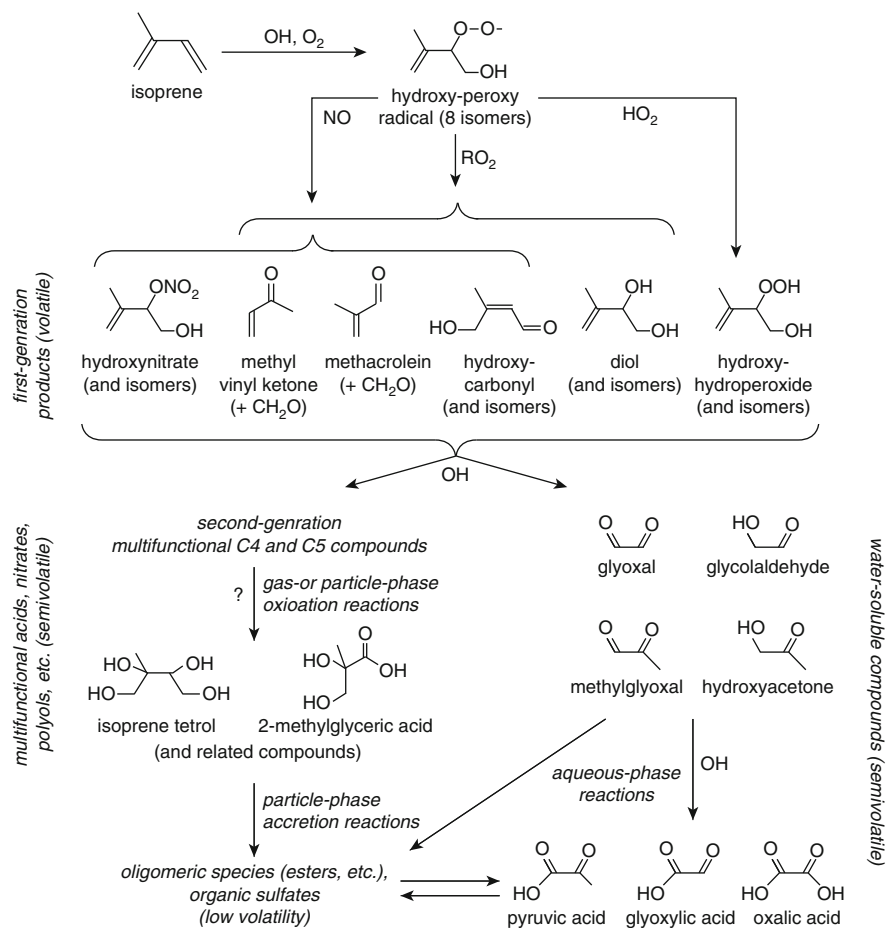
Fig. 9 Oxidation pathways leading to isoprene SOA (reproduced from [137])

8 SOA Formation from Isoprene

The oxygenated products of isoprene may contribute to SOA formation and, as such, any uncertainty in the isoprene oxidation mechanism will impact model predictions of SOA. Atmospheric models consistently underpredict organic aerosol mass in both the boundary layer and aloft [105–111]. This underprediction is not present in model predictions of black (elemental) carbon, leading to the conclusion that this bias is due to an underprediction in SOA specifically. Although isoprene is one of the most abundant hydrocarbons emitted into the atmosphere, second only to methane [63], in the early 1990s it was concluded that isoprene did not form SOA through gas-phase oxidation owing to the assumption that SOA only forms when condensable products reach concentrations exceeding their saturation vapour pressure [112]. In support of

this, early chamber studies only observed SOA formation from isoprene at concentrations much greater than ambient levels [113–115]. Kiendler-Scharr suggests that the presence of isoprene may actually suppress SOA formation from mono-terpene oxidation [116] owing to the scavenging of OH by isoprene (and the assumed lack of SOA formation from isoprene oxidation). In contrast, offline field measurements of organic aerosol in forested areas indicated that isoprene did play a part in SOA formation [117–123]. Claeys et al. [118] detected considerable quantities of methyl tetrols which have the isoprene skeleton in organic aerosols from the Amazon rainforest. The authors estimated that the photo-oxidation of isoprene may result in the global production of 2 Tg year^{-1} of the polyols, a significant fraction of the total IPCC estimate of SOA from biogenic sources of 8–40 Tg year^{-1}. Laboratory studies have now demonstrated that absorption into condensed-phase organics could provide a mechanism for SOA formation from gas-phase species at concentrations below their saturation vapour pressure [115, 124]. In 2003 Limbeck and co-workers proposed that isoprene, by direct reaction with acidic particles, was able to contribute to the formation of humic-like substances that make up 20–50% of the water-soluble organic aerosols in urban and rural European air [125]. The most recent results from laboratory and chamber studies indicate that isoprene oxidation can form SOA even in the absence of a strong seed aerosol [126–128], albeit over longer timescales [129]. Isoprene derived SOA species (e.g. epoxides, tetrols and organosulphates) have now been measured in chamber studies [35, 123, 130–132] and observed in the offline field samples. Kiendler-Scharr et al. [133], by introduction of fully deuterated isoprene into plant chambers containing non-isoprene emitting poplars, determined an aerosol mass yield from isoprene of ~2.3%. Online SOA field observations made, for example, using aerosol mass spectrometry, which provide higher time-resolved data and permit comparison to gas-phase isoprene oxidation products and fast changing oxidant concentrations, have recently been reported. During OP3, Robinson et al. [134] observed that up to 15% by mass of the sub-micron organic aerosol was observed as methyl furan in the aerosol mass spectrum (AMS) and was assigned to be representative of isoprene SOA owing to the simultaneous observation of gas-phase isoprene oxidation products of MVK and MACR. Froyd et al. [135], using online particle analysis by laser mass spectrometry (PALMS), also observed isoprene-derived SOA in the form of IEPOX-derived organosulphates, a second generation oxidation product of isoprene. From this study it was estimated that IEPOX contributed >0.4% to tropospheric aerosol mass in the remote tropics and up to 20% in regions downwind of isoprene sources [135].

The distribution of isoprene oxidation products depends upon the fate of the RO_2 radicals formed. Upon reaction with NO, MVK and MACR and hydroxynitrates may form; conversely, under low NO_x conditions hydroxyhydroperoxides form by reaction of RO_2 with HO_2. SOA yields under low NO_x conditions tend to be higher than under higher NO_x scenarios (~3% yield vs 1–2% yield at higher NO_x concentrations) [128], suggesting that further reactions of the hydroxyhydroperoxides can lead to lower volatility products. Surratt and Kroll and co-workers have found that the oxidation of MACR generates SOA with very similar chemical

composition to SOA formed from isoprene, suggesting that MACR is an important intermediate in the formation of SOA from isoprene [128, 131]. Henze and Seinfeld [136] demonstrated that inclusion of an SOA source from isoprene increased the SOA yield in global model simulations considerably but the increase alone was not sufficient to reconcile observations made during the ACE-Asia campaign [106]. Currently a single-step process for SOA formation from isoprene is assumed within most atmospheric models used to estimate SOA formation [137]. The kinetic study by Ng et al. [129], however, highlighted the multi-oxidation nature of SOA formation from isoprene as it was found that most of the aerosol formation observed only occurred after most of the isoprene was consumed. Carlton and co-workers [137] suggest that modelling SOA formation from the individual isoprene products may better reflect the multi-step nature of isoprene oxidation and SOA formation, but an improved understanding of the chemical mechanisms involved in isoprene oxidation is needed before this can be implemented.

9   Summary

Uncertainties in the isoprene oxidation mechanism impacts much of the work currently being pursued in the atmospheric community. Discrepancies in the modelled-to-measured OH concentration in isoprene rich environments can lead to overestimations of the methane lifetime and reduction in the rate of VOC degradation predicted by global models. Global or regional models currently able to reproduce isoprene observations likely underestimate the flux of BVOCs into the atmosphere; this underestimation will impact processes associated with their oxidation, for example, the formation of OVOCs, which can impact OH reactivity predictions and also SOA production, both of which are currently consistently underpredicted by atmospheric models in isoprene-rich environments. As carbonaceous aerosol strongly influences air quality and climate change, the accurate mechanism by which isoprene is oxidised to secondary gas-phase species and ultimately to SOA becomes increasingly sought.

Although earlier modelling studies often reduced isoprene emissions to reconcile the modelled isoprene mixing ratio with those observed, a number of observations of canopy scale fluxes have been reported which support the magnitude of isoprene emissions estimated by MEGAN. Perhaps as a consequence of this, the focus in more recent years has turned to the uncertainties associated with the isoprene oxidation mechanism itself rather than the estimated emissions. A number of alternative oxidation schemes have been proposed, some of which are able to reconcile the modelled OH radical concentration with observations (at times), for example the Leuven mechanism. It has been highlighted by recent laboratory studies, however, that the actual amount of OH recycled during isoprene oxidation may be lower than the Leuven mechanism predicts, and currently there does not seem to be one mechanism that can fully satisfy all field and laboratory based observations to date.

Uncertainty in the rate of deposition of isoprene oxidation products has also been suggested as a potential source of error in models. Increasing the rate of deposition of these species which act as important OH sinks could certainly extend the lifetime of OH and increase radical concentrations. There is no consensus in the current literature on how fast this deposition should be. Furthermore, increasing the deposition would only increase the discrepancy between OH reactivity observations and predictions. Although a bias in the measurement technique for OH could explain the large discrepancy between the direct OH observations and model predictions, this would not help to resolve the inconsistencies between observations and model predictions of the ratio of isoprene to its oxidation products, and also the disagreement between isoprene emission estimates based on satellite retrievals of HCHO columns and those predicted by the most recent emissions inventories. These discrepancies could certainly be improved, if not resolved, if mechanisms which generated more OH were implemented in atmospheric chemistry models [80, 81, 87] supporting the direct observations of OH.

References

1. Atkinson R, Baulch DL, Cox RA, Crowley JN, Hampson RF, Hynes RG, Jenkin ME, Rossi MJ, Troe J (2004) Evaluated kinetic and photochemical data for atmospheric chemistry: volume I – gas phase reactions of O_x, HO_x, NO_x and SO_x species. Atmos Chem Phys 4:1461–1738

2. Sander, S. P., J. Abbatt, J. R. Barker, J. B. Burkholder, R. R. Friedl, D. M. Golden, R. E. Huie, C. E. Kolb, M. J. Kurylo, G.K. Moortgat, V. L. Orkin and P. H. Wine "Chemical Kinetics and Photochemical Data for Use in Atmospheric Studies, Evaluation No. 17," JPL Publication 10-6, Jet Propulsion Laboratory, Pasadena, 2011 http://jpldataeval.jpl.nasa.gov.

3. Paulot F, Crounse JD, Kjaerdaard HG, Kroll JH, Seinfeld JH, Wennberg PO (2009) Isoprene photooxidation: new insights into the production of acids and organic nitrates. Atmos Chem Phys 9:1479–1501

4. Butler TM, Taraborrelli D, Brühl C, Fischer H, Harder H, Martinez M, Williams J, Lawrence MG, Lelieveld J (2008) Improved simulation of isoprene oxidation chemistry with the ECHAM5/MESSy chemistry-climate model: lessons from the GABRIEL airborne field campaign. Atmos Chem Phys 8:4529–4546

5. Carslaw N, Creasey DJ, Harrison D, Heard DE, Hunter MC, Jacobs PJ, Jenkin ME, Lee JD, Lewis AC, Pilling MJ, Saunders SM, Seakins PW (2001) OH and HO_2 radical chemistry in a forested region of north-western Greece. Atmos Environ 35:4725–4737

6. Hofzumahaus A, Rohrer F, Lu K, Bohn B, Brauers T, Chang CC, Fuchs H, Holland F, Kita K, Kondo Y, Li X, Lou S, Shao M, Zeng L, Wahner A, Zhang Y (2009) Amplified trace gas removal in the troposphere. Science 324:1702–1704

7. Kubistin D, Harder H, Martinez M, Rudolf M, Sander R, Bozem H, Eerdekens G, Fischer H, Gurk C, Klupfel T, Konigstedt R, Parchatka U, Schiller CL, Stickler A, Taraborrelli D, Williams J, Lelieveld J (2010) Hydroxyl radicals in the tropical troposphere over the Suriname rainforest: comparison of measurements with the box model MECCA. Atmos Chem Phys 10:9705–9728. doi:10.5194/acp-10-9705-2010

8. Lelieveld J, Butler TM, Crowley JN, Dillon TJ, Fischer H, Ganzeveld L, Harder H, Lawrence MG, Martinez M, Taraborrelli D, Williams J (2008) Atmospheric oxidation capacity sustained by a tropical forest. Nature 452:737–740

9. Martinez M, Harder H, Kubistin D, Rudolf M, Bozem H, Eerdekens G, Fischer H, Klupfel T, Gurk C, Konigstedt R, Parchatka U, Schiller CL, Stickler A, Williams J, Lelieveld J (2010) Hydroxyl radicals in the tropical troposphere over the Suriname rainforest: airborne measurements. Atmos Chem Phys 10:3759–3773. doi:10.5194/acp-10-3759

10. Ren X, Olson JR, Crawford J, Brune WH, Mao J, Long RB, Chen Z, Chen G, Avery MA, Sachse GW, Barrick JD, Diskin GS, Huey G, Fried A, Cohen RC, Heikes B, Wennberg PO, Singh HB, Blake D, Shetter R (2008) HO_x chemistry during INTEX-A 2004: observations, model calculation and comparison with previous studies. J Geophys Res Atmos 113:D05310

11. Stone D, Evans MJ, Edwards PM, Commane R, Ingham T, Rickard AR, Brookes DM, Hopkins J, Leigh RJ, Lewis AC, Monks PS, Oram D, Reeves CE, Stewart D, Heard DE (2011) Isoprene oxidation mechanisms: measurements and modelling of OH and HO(2) over a South-East Asian tropical rainforest during the OP3 field campaign. Atmos Chem Phys 11:6749–6771

12. Tan D, Faloona I, Simpas JB, Brune W, Shepson PB, Couch TL, Sumner AL, Carroll MA, Thornberry T, Apel E, Riemer D, Stockwell W (2001) HOx budgets in a deciduous forest: results from the PROPHET summer 1998 campaign. J Geophys Res Atmos 106: 24407–24427

13. Thornton JA, Wooldridge PJ, Cohen RC, Martinez M, Harder H, Brune WH, Williams EJ, Roberts JM, Fehsenfeld FC, Hall SR, Shetter RE, Wert BP, Fried A (2002) Ozone production rates as a function of NOx abundances and HOx production rates in the Nashville urban plume. J Geophys Res Atmos 107:4146

14. Whalley LK, Edwards PM, Furneaux KL, Goddard A, Ingham T, Evans MJ, Stone D, Hopkins JR, Jones CE, Karunaharan A, Lee JD, Lewis AC, Monks PS, Moller S, Heard DE (2011) Quantifying the magnitude of a missing hydroxyl radical source in a tropical rainforest. Atmos Chem Phys 11:7223–7233

15. Heard DE, Pilling MJ (2003) Measurement of OH and HO_2 in the troposphere. Chem Rev 103:5163–5198

16. Fuchs H, Bohn B, Hofzumahaus A, Holland F, Lu KD, Nehr S, Rohrer F, Wahner A (2010) Detection of HO_2 by laser-induced fluorescence: calibration and interferences from RO_2 radicals. Atmos Meas Tech 4:1209–1225

17. Mao J, Ren X, Brune W, Van Duin DM, Cohen RC, Park JH, Goldstein A, Paulot F, Beaver MR, Crounse JD, Wennberg PO, DiGangi JP, Henry SB, Keutsch FN, Park C, Schade GW, Wolfe GM, Thornton JA (2012) Insights into hydroxyl measurements and atmospheric oxidation in a California forest. Atmos Chem Phys Discuss 12:6715–6744

18. Creasey DJ, Heard DE, Lee JD (2001) OH and HO_2 measurements in a forested region of north-western Greece. Atmos Environ 35:4713–4724

19. Lelieveld J, Peters W, Dentener F, Krol MC (2002) Stability of tropospheric hydroxyl chemistry. J Geophys Res Atmos 107:4715

20. Lelieveld J, Dentener F, Peters W, Krol MC (2004) On the role of hydroxyl radicals in the self cleansing capacity of the troposphere. Atmos Chem Phys 4:2337–2344

21. Wang YH, Jacob DJ, Logan JA (1998) Global simulation of tropospheric O-3-NOx-hydrocarbon chemistry. 3. Origin of tropospheric ozone and effects of nonmethane hydrocarbons. J Geophys Res Atmos 103:10757–10767

22. Karl T, Guenther A, Turnipseed A, Tyndall G, Artaxo P, Martin S (2009) Rapid formation of isoprene photo-oxidation products observed in Amazonia. Atmos Chem Phys 9:7753–7767

23. Dillon TJ, Crowley JN (2008) Direct detection of OH formation in the reactions of HO_2 with $CH_3C(O)O_2$ and other substituted peroxy radicals. Atmos Chem Phys 8:4877–4889

24. Hasson AS, Tyndall GS, Orlando JJ (2004) A product yield study of the reaction of HO_2 radicals with ethyl peroxy ($C_2H_5O_2$), acetyl peroxy ($CH_3C(O)O_2$), and acetonyl peroxy ($CH_3C(O)CH_2O_2$) radicals. J Phys Chem A 108:5979–5989

25. Jenkin ME, Hurley MD, Wallington TJ (2007) Investigation of the radical product channel of the $CH_3C(O)O_2$ + HO_2 reaction in the gas phase. Phys Chem Chem Phys 9:3149–3162

26. Jenkin ME, Hurley MD, Wallington TJ (2008) Investigation of the radical product channel of the $CH_3C(O)$ CH_2O_2 + HO_2 reaction in the gas phase. Phys Chem Chem Phys 10:4274–4280

27. Jenkin ME, Hurley MA, Wallington TJ (2010) Investigation of the radical product channel of the $CH_3OCH_2O_2$ + HO_2 reaction in the gas phase. J Phys Chem A 114:408–416

28. Le Crane JP, Rayez MT, Rayez JC, Villenave E (2006) A reinvestigation of the kinetics and the mechanism of the $CH3C(O)O-2$ + HO_2 reaction using both experimental and theoretical approaches. Phys Chem Chem Phys 8:2163–2171

29. Pugh T, MacKenzie AR, Hewitt CN, Langford B, Edwards PM, Furneaux KL, Heard DE, Hopkins J, Jones CE, Karunaharan A, Lee JD, Mills G, Misztal P, Moller S, Monks PS, Whalley LK (2010) Simulating atmospheric composition over a South-East Asian tropical rainforest: performance of a chemistry box model. Atmos Chem Phys 10:279–298

30. Pugh TAM, MacKenzie AR, Langford B, Nemitz E, Misztal PK, Hewitt CN (2011) The influence of small-scale variations in isoprene concentrations on atmospheric chemistry over a tropical rainforest. Atmos Chem Phys 11:4121–4134

31. Hewitt CN, Lee JD, MacKenzie AR, Barkley MP, Carslaw N, Carver GD, Chappell NA, Coe H, Collier C, Commane R, Davies F, Davison B, Di Carlo P, Di Marco CF, Dorsey JR, Edwards PM, Evans MJ, Fowler D, Furneaux KL, Gallagher M, Guenther A, Heard DE, Helfter C, Hopkins J, Ingham T, Irwin M, Jones C, Karunaharan A, Langford B, Lewis AC, Lim SF, MacDonald SM, Mahajan AS, Malpass S, McFiggans G, Mills G, Misztal P, Moller S, Monks PS, Nemitz E, Nicolas-Perea V, Oetjen H, Oram DE, Palmer PI, Phillips GJ, Pike R, Plane JMC, Pugh T, Pyle JA, Reeves CE, Robinson NH, Stewart D, Stone D, Whalley LK, Yin X (2010) Overview: oxidant and particle photochemical processes above a south-east Asian tropical rainforest (the OP3 project): introduction, rationale, location characteristics and tools. Atmos Chem Phys 10:169–199

32. de Arellano JV-G, Patton EG, Karl T, van den Dries K, Barth MC, Orlando JJ (2011) The role of boundary layer dynamics on the diurnal evolution of isoprene and the hydroxyl radical over tropical forests. J Geophys Res Atmos 116:D07304

33. Dlugi R, Berger M, Zelger M, Hofzumahaus A, Siese M, Holland F, Wisthaler A, Grabmer W, Hansel A, Koppmann R, Kramm G, Mollmann-Coers M, Knaps A (2010) Turbulent exchange and segregation of HO_x radicals and volatile organic compounds above a deciduous forest. Atmos Chem Phys 10:6215–6235

34. Ouwersloot HG, de Arellano JV-G, van Heerwaarden CC, Ganzeveld LN, Krol MC, Lelieveld J (2011) On the segregation of chemical species in a clear boundary layer over heterogeneous land surfaces. Atmos Chem Phys 11:10681–10704

35. Paulot F, Crounse JD, Kjaergaard HG, Kurten A, St Clair JM, Seinfeld JH, Wennberg PO (2009) Unexpected epoxide formation in the gas-phase photooxidation of isoprene. Science 325:730–733

36. Carter WPL (1996) Condensed atmospheric photooxidation mechanisms for isoprene. Atmos Environ 30:4275–4290

37. Karl M, Dorn H-P, Holland F, Koppmann R, Poppe D, Rupp L, Schaub A, Wahner A (2006) Product study of the reaction of OH radicals with isoprene in the atmosphere simulation chamber SAPHIR. J Atmos Chem 55:167–187

38. Navarro MA, Dusanter S, Hites RA, Stevens PS (2011) Radical dependence of the yields of methacrolein and methyl vinyl ketone from the OH-initiated oxidation of Isoprene under NOx-free conditions. Environ Sci Technol 45:923–929

39. Saunders S, Jenkin M, Derwent R, Pilling M (2003) Protocol for the development of the Master Chemical Mechanism, MCM v3 (part A): tropospheric degradation of non-aromatic volatile organic compounds. Atmos Chem Phys 3:161–180

40. Da Silva G, Graham C, Wang Z-F (2010) Unimolecular beta-hydroxyperoxy radical decomposition with OH recycling in the photochemical oxidation of isoprene. Environ Sci Technol 44:250–256

41. Nguyen TL, Vereecken L, Peeters J (2010) HO(x) regeneration in the oxidation of isoprene III: theoretical study of the key isomerisation of the Z-delta-hydroxy-peroxy isoprene radicals. Chemphyschem 11:3996–4001

42. Peeters J, Nguyen TL, Vereecken L (2009) HO_x radical regeneration in the oxidation of isoprene. Phys Chem Chem Phys 11:5935–5939

43. Peeters J, Müller J-F (2010) HO(x) radical regeneration in isoprene oxidation via peroxy radical isomerisations. II. Experimental evidence and global impact. Phys Chem Chem Phys 12:14227–14235

44. Crounse JD, Knap HC, Ørnsø KB, Jørgensen S, Paulot F, Kjaerdaard HG, Wennberg PO (2012) Atmospheric fate of methacrolein 1 peroxy radical isomerization following addition of OH and O_2. J Phys Chem A 116(24):5756–5762

45. Taraborrelli D, Lawrence MG, Crowley JN, Dillon TJ, Gromov S, Groß CBM, Vereecken L, Lelieveld J (2012) Hydroxyl radical buffered by isoprene oxidation over tropical forests. Nat Geosci 5:190–193

46. Crounse JD, Paulot F, Kjaergaard HG, Wennberg PO (2011) Peroxy radical isomerization in the oxidation of isoprene. Phys Chem Chem Phys 13:13607–13613

47. Wolfe GM, Thornton JA, Bouvier-Brown NC, Goldstein AH, Park JH, McKay M, Matross DM, Mao J, Brune WH, LaFranchi BW, Browne EC, Min KE, Wooldridge PJ, Cohen RC, Crounse JD, Faloona IC, Gilman JB, Kuster WC, de Gouw JA, Huisman A, Keutsch FN (2011) The Chemistry of Atmosphere-Forest Exchange (CAFE) model – part 2: application to BEARPEX-2007 observations. Atmos Chem Phys 11:1269–1294

48. Archibald AT, Cooke MC, Utembe SR, Shallcross DE, Derwent RG, Jenkin ME (2010) Impacts of mechanistic changes on HO_x formation and recycling in the oxidation of isoprene. Atmos Chem Phys 10:8097–8118

49. Stavrakou T, Peeters J, Müller JF (2010) Improved global modelling of HO(x) recycling in isoprene oxidation: evaluation against the GABRIEL and INTEX-A aircraft campaign measurements. Atmos Chem Phys 10:9863–9878

50. Taraborrelli D, Lawrence MG, Butler TM, Sander R, Lelieveld J (2009) Mainz Isoprene Mechanism 2 (MIM2): an isoprene oxidation mechanism for regional and global atmospheric modelling. Atmos Chem Phys 9:2751–2777

51. Watson LA, Shallcross DE, Utembe SR, Jenkin ME (2008) A Common Representative Intermediates (CRI) mechanism for VOC degradation. Part 2: gas phase mechanism reduction. Atmos Environ 42:7196–7204

52. Edwards PM, Evans MJ, Stone D, Whalley LK, Furneaux KL, Hopkins J, Jones CE, Lewis AC, Heard DE (2011) Understanding missing OH sinks in a South East Asian tropical rainforest, Eos Transactions AGU, Fall Meeting Supplement 2011, Abstract B53A-06.

53. Emmerson KM, Evans MJ (2009) Comparison of tropospheric gas-phase chemistry schemes for use within global models. Atmos Chem Phys 9:1831–1845

54. Ingham T, Goddard A, Whalley LK, Furneaux KL, Edwards PM, Seal CP, Self DE, Johnson GP, Read KA, Lee JD, Heard DE (2009) A flow-tube based laser-induced fluorescence instrument to measure OH reactivity in the troposphere. Atmos Meas Tech 2:465–477

55. Elshorbany YF, Kleffmann J, Hofzumahaus A, Kurtenbach R, Wiesen P, Brauers T, Bohn B, Dorn HP, Fuchs H, Holland F, Rohrer F, Tillmann R, Wegener R, Wahner A, Kanaya Y, Yoshino A, Nishida S, Kajii Y, Martinez M, Kubistin D, Harder H, Lelieveld J, Elste T, Plass-Duelmer C, Stange G, Berresheim H, Schurath U (2012) HOx budgets during HOxComp: a case study of HO_x chemistry under NO_x-limited conditions. J Geophys Res Atmos 117: D03307

56. Kanaya Y, Hofzumahaus A, Dorn HP, Brauers T, Fuchs H, Holland F, Rohrer F, Bohn B, Tillmann R, Wegener R, Wahner A, Kajii Y, Miyamoto K, Nishida S, Watanabe K, Yoshino A, Kubistin D, Martinez M, Rudolf M, Harder H, Berresheim H, Elste T, Plass-Duelmer C, Stange G, Kleffmann J, Elshorbany Y, Schurath U (2012) Comparisons of observed and modeled OH and HO_2 concentrations during the ambient measurement period of the HO(x) Comp field campaign. Atmos Chem Phys 12:2567–2585

57. Lu K, Rohrer F, Holland F, Fuchs H, Bohn B, Brauers T, Chang CC, Haeseler R, Hu M, Kita K, Kondo Y, Li X, Lou S, Nehr S, Shao M, Zeng L, Wahner A, Zhang Y, Hofzumahaus A

(2012) Observations and modelling of OH and HO_2 concentrations in the Pearl River Delta 2006: a missing OH source in a VOC rich atmosphere. Atmos Chem Phys 12:1541–1569

58. Lu K, Hofzumahaus A, Holland F, Bohn B, Brauers T, Fuchs H, Hu M, Häseler R, Kita K, Kondo Y, Li X, Lou S, Oebel A, Shao M, Zeng L, Wahner A, Zhu T, Zhang Y, Rohrer F (2012) Missing OH source in a suburban environment near Beijing: observed and modelled OH and HO_2 concentrations in summer 2006. Atmos Chem Phys Discuss 12:10879–10936

59. Archibald AT, Levine JG, Abraham NL, Cooke MC, Edwards PM, Heard DE, Jenkin ME, Karunaharan A, Pike RC, Monks PS, Shallcross DE, Telford PJ, Whalley LK, Pyle JA (2011) Impacts of HO_x regeneration and recycling in the oxidation of isoprene: consequences for the composition of past, present and future atmospheres. Geophys Res Lett 38:L05804

60. Lamb B, Guenther A, Gay D, Westberg H (1987) A national inventory of biogenic hydrocarbon emissions. Atmos Environ 21:1695–1705

61. Müller JF (1992) Geographical-distribution and seasonal-variation of surface emissions and deposition velocities of atmospheric trace gases. J Geophys Res Atmos 97:3787–3804

62. Zimmerman P (1979) Testing of hydrocarbon emissions from vegetation, leaf litter and aquatic surfaces and development of a method for compiling biogenic emissions inventories. Environmental Protection Agency, EPA-450-4-70-004

63. Guenther A et al (1995) A global model of natural volatile organic compound emissions. J Geophys Res 100:8873–8892

64. Pierce TE, Waldruff PS (1991) Pc-Beis – a personal-computer version of the biogenic emissions inventory system. J Air Waste Manage Assoc 41:937–941

65. Pierce T, Geron C, Bender L, Dennis R, Tonnesen G, Guenther A (1998) Influence of increased isoprene emissions on regional ozone modeling. J Geophys Res Atmos 103:25611–25629

66. Guenther A, Karl T, Harley P, Wiedinmyer C, Palmer PI, Geron C (2006) Estimates of global terrestrial isoprene emissions using MEGAN (Model of Emissions of Gases and Aerosols from Nature). Atmos Chem Phys 6:3181–3210

67. Guenther A, Baugh B, Brasseur G, Greenberg J, Harley P, Klinger L, Serca D, Vierling L (1999) Isoprene emission estimates and uncertainties for the Central African EXPRESSO study domain. J Geophys Res Atmos 104:30625–30639

68. Harley P, Vasconcellos P, Vierling L, Pinheiro CCD, Greenberg J, Guenther A, Klinger L, De Almeida SS, Neill D, Baker T, Phillips O, Malhi Y (2004) Variation in potential for isoprene emissions among neotropical forest sites. Glob Change Biol 10:630–650

69. Keller M, Lerdau M (1999) Isoprene emission from tropical forest canopy leaves. Global Biogeochem Cycles 13:19–29

70. Kesselmeier J, Kuhn U, Wolf A, Andreae MO, Ciccioli P, Brancaleoni E, Frattoni M, Guenther A, Greenberg J, De Castro Vasconcellos P, de Telles Oliva T, Tavares T, Artaxo P (2000) Atmospheric volatile organic compounds (VOC) at a remote tropical forest site in central Amazonia. Atmos Environ 34:4063–4072

71. Klinger LF, Li QJ, Guenther AB, Greenberg JP, Baker B, Bai JH (2002) Assessment of volatile organic compound emissions from ecosystems of China. J Geophys Res Atmos 107:4603

72. Kuhn U, Rottenberger S, Biesenthal T, Ammann C, Wolf A, Schebeske G, Oliva ST, Tavares TM, Kesselmeier J (2002) Exchange of short-chain monocarboxylic acids by vegetation at a remote tropical forest site in Amazonia. J Geophys Res 107:8069. doi:10.1029/2000jd000303

73. Karl T, Guenther A, Spirig C, Hansel A, Fall R (2004) Seasonal variation of biogenic VOC emissions above a mixed hardwood forest in northern Michigan. Geophys Res Lett 30:2186

74. Karl T, Potosnak M, Guenther A, Clark D, Walker J, Herrick JD, Geron C (2004) Exchange processes of volatile organic compounds above a tropical rain forest: implications for modeling tropospheric chemistry above dense vegetation. J Geophys Res Atmos 109:D18306

75. Houweling S, Dentener F, Lelieveld J (1998) The impact of nonmethane hydrocarbon compounds on tropospheric photochemistry. J Geophys Res Atmos 103:10673–10696

76. Poisson N, Kanakidou M, Crutzen PJ (2000) Impact of non-methane hydrocarbons on tropospheric chemistry and the oxidizing power of the global troposphere: 3-dimensional modelling results. J Atmos Chem 36:157–230

77. Bey I, Aumont B, Toupance G (2001) A modeling study of the nighttime radical chemistry in the lower continental troposphere 2. Origin and evolution of HO_x. J Geophys Res 106:9991–10001

78. Ehhalt D, Prather M (2001) Atmospheric chemistry and greenhouse gases. In: Houghton J, Ding Y, Griggs D, Noguer M, van der Linden P, Xiaosu D (eds) Climate change 2001. Cambridge University Press, Cambridge

79. Spirig C, Neftel A, Ammann C, Dommen J, Grabmer W, Thielmann A, Schaub A, Beauchamp J, Wisthaler A, Hansel A (2005) Eddy covariance flux measurements of biogenic VOCs during ECHO 2003 using proton transfer reaction mass spectrometry. Atmos Chem Phys 5:465–481

80. Kuhn U, Andreae MO, Ammann C, Araujo AC, Brancaleoni E, Ciccioli P, Dindorf T, Frattoni M, Gatti LV, Ganzeveld L, Kruijt B, Lelieveld J, Lloyd J, Meixner FX, Nobre AD, Poschl U, Spirig C, Stefani P, Thielmann A, Valentini R, Kesselmeier J (2007) Isoprene and monoterpene fluxes from Central Amazonian rainforest inferred from tower-based and airborne measurements, and implications on the atmospheric chemistry and the local carbon budget. Atmos Chem Phys 7:2855–2879

81. Karl T, Guenther A, Yokelson RJ, Greenberg J, Potosnak M, Blake DR, Artaxo P (2007) The tropical forest and fire emissions experiment: emission, chemistry, and transport of biogenic volatile organic compounds in the lower atmosphere over Amazonia. J Geophys Res Atmos 112:D18302

82. Langford B, Misztal PK, Nemitz E, Davison B, Helfter C, Pugh TAM, MacKenzie AR, Lim SF, Hewitt CN (2010) Fluxes and concentrations of volatile organic compounds from a South-East Asian tropical rainforest. Atmos Chem Phys 10:8391–8412

83. Hewitt CN, Ashworth K, Boynard A, Guenther A, Langford B, MacKenzie AR, Misztal P, Nemitz E, Owen SM, Possell M, Pugh TAM, Ryan AC, Wild O (2011) Ground-level ozone influenced by circadian control of isoprene emissions. Nature Geoscience, ngeo 4:671–674

84. Fu TM, Jacob DJ, Palmer PI, Chance K, Wang YXX, Barletta B, Blake DR, Stanton JC, Pilling MJ (2007) Space-based formaldehyde measurements as constraints on volatile organic compound emissions in east and south Asia and implications for ozone. J Geophys Res Atmos 112:D06312

85. Millet DB, Jacob DJ, Boersma KF, Fu TM, Kurosu TP, Chance K, Heald CL, Guenther A (2008) Spatial distribution of isoprene emissions from North America derived from formaldehyde column measurements by the OMI satellite sensor. J Geophys Res Atmos 113:D02307

86. Shim C, Wang YH, Choi Y, Palmer PI, Abbot DS, Chance K (2005) Constraining global isoprene emissions with Global Ozone Monitoring Experiment (GOME) formaldehyde column measurements. J Geophys Res Atmos 110:D24301

87. Barkley MP, Palmer PI, Kuhn U, Kesselmeier J, Chance K, Kurosu TP, Martin RV, Helmig D, Guenther A (2008) Net ecosystem fluxes of isoprene over tropical South America inferred from Global Ozone Monitoring Experiment (GOME) observations of HCHO columns. J Geophys Res Atmos 113:D20304

88. Dibble TS (2004) Prompt chemistry of alkenoxy radical products of the double H-atom transfer of alkoxy radicals from isoprene. J Phys Chem A 108:2208–2215

89. Solomon SD, Qin D, Manning M, Alley RB, Berntsen T, Bindoff NL, Chen Z, Chidthaisong A, Gregory JM, Hegerl GC, Heimann M, Hewitson B, Hoskins BJ, Joos F, Jouzel J, Kattsov V, Lohmann U, Matsuno T, Molina M, Nicholls N, Overpeck J, Raga G, Ramaswamy V, Ren J, Rusticucci M, Somerville R, Stocker TF, Whetton P, Wood RA, Wratt D (2007) Climate change 2007: the physical science basis. Contribution of working group I to the fourth

assessment report of the Intergovernmental Panel on Climate Change IPCC. Cambridge University Press, Cambridge

90. Di Carlo P, Brune WH, Martinez M, Harder H, Lesher R, Ren X, Thornberry T, Carroll M, Young V, Shepson P, Riemer D, Apel E, Campbell C (2004) Missing OH reactivity in a forest: evidence for unknown reactive biogenic VOCs. Sci Mag 304:722–725

91. Kovacs TA, Brune WH, Harder H, Martinez M, Simpas JB, Frost GJ, Williams E, Jobson T, Stroud C, Young V, Fried A, Wert B (2003) Direct measurements of urban OH reactivity during Nashville SOS in summer 1999. J Environ Monit 5:68–74

92. Lee JD, McFiggans G, Allan JD, Baker AR, Ball SM, Benton AK, Carpenter LJ, Commane R, Finley BD, Evans MJ, Feuntes E, Furneaux KL, Goddard A, Good N, Hamilton JF, Heard DE, Herrmann H, Hollingsworth A, Hopkins JR, Ingham T, Irwin M, Jones CE, Jones RL, Keene WC, Lawler MJ, Lehmann S, Lewis AC, Long MS, Mahajan AS, Methven J, Moller SJ, Müller K, Müller T, Niedermeier N, O'Doherty S, Oetjen H, Plane JMC, Pszenny A, Read KA, Saiz-Lopez A, Saltzmann ES, Sander R, von Glasow R, Whalley LK, Wiedensohler A, Young D (2009) Reactive Halogens in the Marine Boundary Layer (RHaMBLe): the tropical North Atlantic experiments. Atmos Chem Phys Discuss 9:21717–21783

93. Lou S, Holland F, Rohrer F, Lu K, Bohn B, Brauers T, Chang CC, Fuchs H, Haeseler R, Kita K, Kondo Y, Li X, Shao M, Zeng L, Wahner A, Zhang Y, Wang W, Hofzumahaus A (2010) Atmospheric OH reactivities in the Pearl River Delta – China in summer 2006: measurement and model results. Atmos Chem Phys 10:11243–11260

94. Mao J, Ren X, Brune WH, Olson JR, Crawford JH, Fried A, Huey LG, Cohen RC, Heikes B, Singh HB, Blake DR, Sachse GW, Diskin GS, Hall SR, Shetter RE (2009) Airborne measurement of OH reactivity during INTEX-B. Atmos Chem Phys 9:163–173

95. Mogensen D, Smolander S, Sogachev A, Zhou L, Sinha V, Guenther A, Williams J, Nieminen T, Kajos MK, Rinne J, Kulmala M, Boy M (2011) Modelling atmospheric OH-reactivity in a boreal forest ecosystem. Atmos Chem Phys 11:9709–9719

96. Ren X, Harder H, Martinez M, Lesher R, Oliger A, Shirley T, Adams J, Simpas JB, Brune WH (2003) HO$_x$ and OH reactivity observations in New York City during PMTACS-NY2001. Atmos Environ 37:3627–3637

97. Ren XR, Brune WH, Oliger A, Metcalf AR, Simpas JB, Shirley T, Schwab JJ, Bai CH, Roychowdhury U, Li YQ, Cai CX, Demerjian KL, He Y, Zhou XL, Gao HL, Hou J (2006) OH, HO$_2$, and OH reactivity during the PMTACS-NY Whiteface mountain 2002 campaign: observations and model comparison. J Geophys Res Atmos 111:D10S03

98. Sadanaga Y, Yoshino A, Kato S, Kajii Y (2005) Measurements of OH reactivity and photochemical ozone production in the urban atmosphere. Environ Sci Technol 39:8847–8852

99. Shirley TR, Brune WH, Ren X, Mao J, Lesher R, Cardenas B, Volkamer R, Molina LT, Molina MJ, Lamb B, Velasco E, Jobson T, Alexander M (2006) Atmospheric oxidation in the Mexico City Metropolitan Area (MCMA) during April 2003. Atmos Chem Phys 6:2753–2765

100. Sinha V, Williams J, Crowley JN, Lelieveld J (2008) The comparative reactivity method – a new tool to measure total OH reactivity in ambient air. Atmos Chem Phys 8:2213–2227

101. Sinha V, Williams J, Lelieveld J, Ruuskanen TM, Kajos MK, Patokoski J, Hellen H, Hakola H, Mogensen D, Boy M, Rinne J, Kulmala M (2010) OH reactivity measurements within a boreal forest: evidence for unknown reactive emissions. Environ Sci Technol 44:6614–6620

102. Lewis AC, Carslaw N, Marriott PJ, Kinghorn RM, Morrision P, Lee A, Bartle KD, Pilling MJ (2000) A larger pool of ozone-forming carbon compounds in urban atmospheres. Nature 405:778–781

103. Chung MY, Maris C, Krischke U, Meller R, Paulson SE (2003) An investigation of the relationship between total non-methane organic carbon and the sum of speciated hydrocarbons and carbonyls measured by standard GC/FID: measurements in the Los Angeles air basin. Atmos Environ 37:S159–S170

104. Warneke C, Gouw JAD (2001) Organic trace gas composition of the marine boundary layer over the northwest Indian Ocean in April 2000. Atmos Environ 35:5923–5933
105. Goldstein AH, Galbally IE (2007) Known and unexplored organic constituents in the Earth's atmosphere. Environ Sci Technol 41:1514–1521
106. Heald CL, Jacob DJ, Park RJ, Russell LM, Huebert BJ, Seinfeld JH, Liao H, Weber RJ (2005) A large organic aerosol source in the free troposphere missing from current models. Geophys Res Lett 32:L18809
107. Johnson D, Utembe SR, Jenkin ME, Derwent RG, Hayman GD, Alfarra MR, Coe H, McFiggans G (2006) Simulating regional scale secondary organic aerosol formation during the TORCH 2003 campaign in the southern UK. Atmos Chem Phys 6:403–418
108. Morris RE, McNally DE, Tesche TW, Tonnesen G, Boylan JW, Brewer P (2005) Preliminary evaluation of the community multiscale air, quality model for 2002 over the southeastern United States. J Air Waste Manage Assoc 55:1694–1708
109. Morris RE, Koo B, Guenther A, Yarwood G, McNally D, Tesche TW, Tonnesen G, Boylan J, Brewer P (2006) Model sensitivity evaluation for organic carbon using two multi-pollutant air quality models that simulate regional haze in the southeastern United States. Atmos Environ 40:4960–4972
110. Volkamer R, Jimenez JL, San Martini F, Dzepina K, Zhang Q, Salcedo D, Molina LT, Worsnop DR, Molina MJ (2006) Secondary organic aerosol formation from anthropogenic air pollution: rapid and higher than expected. Geophys Res Lett 33:L17811
111. Yu SC, Mathur R, Schere K, Kang DW, Pleim J, Young J, Tong D, Pouliot G, McKeen SA, Rao ST (2008) Evaluation of real-time PM(2.5) forecasts and process analysis for PM(2.5) formation over the eastern United States using the Eta-CMAQ forecast model during the 2004 ICARTT study. J Geophys Res Atmos 113:D06204
112. Pandis SN, Paulson SE, Seinfeld JH, Flagan RC (1991) Aerosol formation in the photooxidation of isoprene and beta-pinene. Atmos Environ A Gen Top 25:997–1008
113. Kamens RM, Gery MW, Jeffries HE, Jackson M, Cole EI (1982) Ozone-isoprene reactions – product formation and aerosol potential. Int J Chem Kinet 14:955–975
114. Miyoshi A, Hatakeyama S, Washida N (1994) Om radical-initiated photooxidation of isoprene – an estimate of global co production. J Geophys Res Atmos 99:18779–18787
115. Pankow JF (1994) An absorption-model of gas-particle partitioning of organic-compounds in the atmosphere. Atmos Environ 28:185–188
116. Kiendler-Scharr A, Wildt J, Dal Maso M, Hohaus T, Kleist E, Mentel TF, Tillmann R, Uerlings R, Schurr U, Wahner A (2009) New particle formation in forests inhibited by isoprene emissions. Nature 461:381–384
117. Chan M, Surratt JD, Claeys M, Edgerton ES, Tanner RL, Shaw SL, Zheng M, Knipping EM, Eddingsaas NC, Wennberg PO, Seinfeld JH (2010) Characterisation and quantification of isoprene-derived epoxydiolsin ambient aerosol in the southeastern United States. Environ Sci Technol 44:4590–4596
118. Claeys M, Graham B, Vas G, Wang W, Vermeylen R, Pashynska V, Cafmeyer J, Guyon P, Andreae MO, Artaxo P, Maenhaut W (2004) Formation of secondary organic aerosols through photooxidation of isoprene. Science 303:1173–1176
119. Claeys M, Wang W, Ion AC, Kourtchev I, Gelencser A, Maenhaut W (2004) Formation of secondary organic aerosols from isoprene and its gas-phase oxidation products through reaction with hydrogen peroxide. Atmos Environ 38:4093–4098
120. Ion AC, Vermeylen R, Kourtchev I, Cafmeyer J, Chi X, Gelencser A, Maenhaut W, Claeys M (2005) Polar organic compounds in rural PM2.5 aerosols from K-puszta, Hungary, during a 2003 summer field campaign: sources and diurnal variations. Atmos Chem Phys 5:1805–1814
121. Kourtchev I, Ruuskanen T, Maenhaut W, Kulmala M, Claeys M (2005) Observations of 2-methyltetrols and related photo-oxidation products of isoprene in boreal forest aerosols from Hyytiala, Finland. Atmos Chem Phys 5:2761–2770
122. Matsunaga S, Mochida M, Kawaamura K (2003) Growth of organic aerosol by biogenic semi-volatile carbonyls in the forestal atmosphere. Atmos Environ 37:2045–2050

123. Surratt JD, Gomez-Gonzalez Y, Chan AWH, Vermeylen R, Shahgholi M, Kleindienst TE, Edney EO, Offenberg JH, Lewandowski M, Jaoui M, Maenhaut W, Claeys M, Flagan RC, Seinfeld JH (2008) Organosulphate formation in biogenic secondary organic aerosol. J Phys Chem A 112:8345–8378

124. Odum JR, Hoffmann T, Bowman F, Collins D, Flagan RC, Seinfeld JH (1996) Gas/particle partitioning and secondary organic aerosol yields. Environ Sci Technol 30:2580–2585

125. Limbeck A, Kulmala M, Puxbaum H (2003) Secondary organic aerosol formation in the atmosphere via heterogeneous reaction of gaseous isoprene on acidic particles. Geophys Res Lett 30:1996

126. Dommen J, Metzger A, Duplissy J, Kalberer M, Alfarra MR, Gascho A, Weingartner E, Prevot ASH, Verheggen B, Baltensperger U (2006) Laboratory observation of oligomers in the aerosol from isoprene/NOx photooxidation. Geophys Res Lett 33:L13805

127. Kroll JH, Ng NL, Murphy SM, Flagan RC, Seinfeld JH (2005) Secondary organic aerosol formation from isoprene photooxidation under high-NOx conditions. Geophys Res Lett 32: L18808

128. Kroll JH, Ng NL, Murphy SM, Flagan RC, Seinfeld JH (2006) Secondary organic aerosol formation from isoprene photooxidation. Environ Sci Technol 40:1869–1877

129. Ng NL, Kroll JH, Keywood MD, Bahreini R, Varutbangkul V, Flagan RC, Seinfeld JH, Lee A, Goldstein AH (2006) Contribution of first- versus second-generation products to secondary organic aerosols formed in the oxidation of biogenic hydrocarbons. Environ Sci Technol 40:2283–2297

130. Kleindienst TE, Lewandowski M, Offenberg JH, Jaoui M, Edney EO (2009) The formation of secondary organic aerosol from isoprene + OH reaction in the absence of NO_x. Atmos Chem Phys 9:6541–6558

131. Surratt JD, Murphy SM, Kroll JH, Ng NL, Hildebrandt L, Sorooshian A, Szmigielski R, Vermeylen R, Maenhaut W, Claeys M, Flagan RC, Seinfeld JH (2006) Chemical composition of secondary organic aerosol formed from the photooxidation of isoprene. J Phys Chem A 110:9665–9690

132. Surratt JD, Chan AWH, Eddingsaas NC, Chan M, Loza CL, Kwan AJ, Hersey SP, Flagan RC, Wennberg PO, Seinfeld JH (2010) Atmospheric chemistry special feature: reactive intermediates revealed in secondary organic aerosol formation from isoprene. Proc Natl Acad Sci USA 107(15):6640–6645

133. Kiendler-Scharr A, Andres S, Bachner M, Behnke K, Broch S, Hofzumahaus A, Holland F, Kleist E, Mentel TF, Rubach F, Springer M, Steitz B, Tillmann R, Wahner A, Schnitzler JP, Wildt J (2012) Isoprene in poplar emissions: effects on new particle formation and OH concentrations. Atmos Chem Phys 12:1021–1030

134. Robinson NH, Hamilton JF, Allan JD, Langford B, Oram DE, Chen Q, Docherty K, Farmer DK, Jimenez JL, Ward MW, Hewitt CN, Barley MH, Jenkin ME, Rickard AR, Martin ST, McFiggans G, Coe H (2011) Evidence for a significant proportion of Secondary organic aerosol from isoprene above a maritime tropical forest. Atmos Chem Phys 11:1039–1050

135. Froyd KD, Murphy SM, Murphy DM, de Gouw JA, Eddingsaas NC, Wennberg PO (2010) Contribution of isoprene-derived organosulfates to free tropospheric aerosol mass. Proc Natl Acad Sci USA 107:21360–21365

136. Henze DK, Seinfeld JH (2006) Global secondary organic aerosol from isoprene oxidation. Geophys Res Lett 33:L09812

137. Carlton AG, Wiedinmyer C, Kroll JH (2009) A review of Secondary Organic Aerosol (SOA) formation from isoprene. Atmos Chem Phys 9:4987–5005

138. Olson JR, Crawford JH, Davis DD, Chen G, Avery MA, Barrick JDW, Sachse GW, Vay SA, Sandholm ST, Tan D, Brune WH, Faloona IC, Heikes BG, Shetter RE, Lefer BL, Singh HB, Talbot RW, Blake DR (2001) Seasonal differences in the photochemistry of the South Pacific: a comparison of observations and model results from PEM-Tropics A and B. J Geophys Res 106:32749–32766

Volatility and Aging of Atmospheric Organic Aerosol

Neil M. Donahue, Allen L. Robinson, Erica R. Trump, Ilona Riipinen, and Jesse H. Kroll

Abstract Organic-aerosol phase partitioning (volatility) and oxidative aging are inextricably linked in the atmosphere because partitioning largely controls the rates and mechanisms of aging reactions as well as the actual amount of organic aerosol. Here we discuss those linkages, describing the basic theory of partitioning thermodynamics as well as the dynamics that may limit the approach to equilibrium under some conditions. We then discuss oxidative aging in three forms: homogeneous gas-phase oxidation, heterogeneous oxidation via uptake of gas-phase oxidants, and aqueous-phase oxidation. We present general scaling arguments to constrain the relative importance of these processes in the atmosphere, compared to each other and compared to the characteristic residence time of particles in the atmosphere.

Keywords Aerosols · Atmospheric Chemistry · Multiphase Chemistry

N.M. Donahue (✉), A.L. Robinson and E.R. Trump
Carnegie Mellon University Center for Atmospheric Particle Studies, Pittsburgh, PA, USA
e-mail: nmd@andrew.cmu.edu

I. Riipinen
Department of Applied Environmental Science and Bert Bolin Centre for Climate Research, Stockholm University, Stockholm, Sweden

Carnegie Mellon University Center for Atmospheric Particle Studies, Pittsburgh, PA, USA

J.H. Kroll
Department of Civil and Environmental Engineering, Massachusetts Institute of Technology, Cambridge, MA, USA

Department of Chemical Engineering, Massachusetts Institute of Technology, Cambridge, MA, USA

Contents

1   Introduction

Until very recently organic aerosol (OA) was commonly regarded as a mixture of non-volatile, non-reactive, primary organic aerosol (POA) [1, 2] augmented with a coating of secondary organic aerosol (SOA). POA particles were regarded as relatively non-volatile composites of organic compounds emitted by individual sources, such as biomass burning [3–5], gasoline [6–8] and diesel [1, 9] vehicles, food preparation [10–13], smoking [14], and numerous other small sources. SOA was regarded as an additional coating of secondary organic compounds formed via gas-phase oxidation of volatile organic carbon (VOC) precursors. Some of these reaction products evidently had a sufficiently low vapor pressure to condense onto pre-existing particles [15, 16]. Through a decade or so of research it became clear that SOA consisted of a mixture containing a large fraction of semi-volatile organic compounds that partitioned between the vapor and condensed phases based on well-established solution thermodynamics [17, 18].

This basic picture of organic aerosol was relatively well developed by the end of the 1990s. Chemical transport models were fed by inventories for POA emissions from a wide array of sources, and those emissions were treated in a variety of microphysics modules as effectively non-volatile and often chemically inert particles [19, 20]. SOA models evolved from relatively primitive treatments that simply converted a fixed fraction of VOC emissions into equally non-volatile secondary material (for example 12% of monoterpene emissions) to more sophisticated "two-product" representations that treated the equilibrium partitioning of surrogate species based on smog-chamber experiments [21–23]. Even today some global-scale models represent SOA as a fixed non-volatile fraction of VOC emissions [24, 25].

In most model representations of OA behavior, there was little if any consideration of long-term OA aging. With the realization that some OA could serve as relatively efficient cloud condensation nuclei [26–28] and also that soluble salts

such as ammonium sulfate would condense onto even the most hydrophobic organic cores, many models added some form of ad hoc aging timescale, typically converting a "hydrophobic" organic mode into a "hydrophilic" organic mode with a fixed timescale (usually of order 2 days).

Recently this picture has been more or less turned upside down. We now recognize that most POA emissions are actually fairly volatile, while SOA (at least in the form found in the atmosphere) is not very volatile at all [29, 30]. There is some debate over the effective volatility of even "traditional" SOA formed in smog-chamber experiments (called "chamber SOA" hereafter) [31], but it is also clear that chamber SOA is often a poor match for the SOA observed in the atmosphere. At the same time, recent papers have raised questions about the physical state of OA particles. There is considerable evidence that some OA particles may exist in a glassy or semi-solid state [32–34], and there is some confusion about whether this glassy state invalidates the solution thermodynamics treatments that have been developed to date (it does not) and debate over whether the mixtures actually reach equilibrium (they may not).

Work in our groups over the past decade has focused on the hypothesis that the coupling of gas-particle partitioning and gas-phase oxidation chemistry plays a central role in the properties and evolution of organic aerosol in the atmosphere, and that a very large fraction of all organic carbon atoms found in ambient particles has been involved in gas-phase chemical reactions at some point during their stay in the atmosphere. Volatility, in other words, plays a central role in the aging of organic aerosol in the atmosphere.

This chapter will focus on the interplay between volatility and chemical aging as it relates to organic aerosol. We shall emphasize the role of gas-phase oxidation chemistry but address other mechanisms as well. That emphasis is not meant to suggest that other aging mechanisms are unimportant, but rather that this one is important. Many of those other processes are ably covered by other articles in this volume.

2 Background

Of a total flux of non-methane reduced organic compounds into the atmosphere of about 1,350 Tg year^{-1} [35, 36], only 10% or so leads to organic aerosol [25, 37]. However, less than 1% of the primary organic emissions into the atmosphere have a sufficiently low volatility to remain in the condensed phase under ambient conditions, so SOA formation must be a huge part (90% or more) of the OA story [38]. The straightforward fact is that only a small fraction of all organic compounds (by mass) in the atmosphere have what it takes to stay on or in a particle. That special property is low volatility, and most compounds acquire that low volatility via chemical transformation in the atmosphere.

It is important to develop a sense of scale for volatility. A typical OA concentration is of the order 1 μg m^{-3} (a mass fraction of 1 ppbm) and, if the molar weight of the SOA molecules averages 200 g mole^{-1}, the mole fraction of OA is roughly 100 ppt. If OA consisted of a single, pure organic compound and it had a saturation vapor pressure of 10^{-7} Torr (1.3 × 10^{-5} Pa), that compound would be 50% in the gas phase and 50% in the condensed phase at equilibrium under ambient conditions. That is a good definition of a semi-volatile constituent. Compounds with this saturation vapor pressure (over a sub-cooled liquid state) include pentacosane ($C_{25}H_{52}$, the canonical paraffin) and glucose. Those are not molecules one normally considers "semi volatile"; it is thus reasonable to expect standard intuition to be off target when considering organic aerosol. Of course, OA particles are *not* pure but rather contain thousands of different molecules, so mixing thermodynamics plays an important role as well. Furthermore, paraffin and glucose are notably viscous, so it is not necessarily surprising that viscosity effects may be important to OA behavior.

2.1   Phase Partitioning Thermodynamics

The thermodynamics of semi-volatile phase partitioning for atmospheric OA mixtures has been extensively treated in the literature [17, 18, 39, 40] and will only briefly be reviewed here. We express the effective saturation concentration $\left(C_i^*\right)$ of an organic compound by converting its saturation vapor pressure into mass concentration units and multiplying by the appropriate activity coefficient for the organic mixture (this is the inverse of the partitioning coefficient used in some formulations: $K_{p,i} = 1/C_i^*$). The general effect of a solution is to lower the equilibrium partial pressure of a species from the equilibrium vapor pressure of the pure species; if the fractional reduction in the partial pressure (the activity) is equal to the fraction in the condensed phase, the solution is ideal and Raoult's law applies. One simplifying assumption is to treat the system as a "pseudo-ideal" solution [23] in which the activity coefficients of individual compounds remain more or less constant over ambient conditions, in which case C_i^* for a given compound will remain constant as well.

The fundamental property of interest is the equilibrium fraction ξ_i of a compound in the condensed phase (vs the total in the condensed and vapor phases). With a total concentration of condensed-phase solute (often assumed to be the total concentration of organic aerosol, C_{OA}), this is given very simply by

$$\xi_i = \left(1 + C_i^*/C_{OA}\right)^{-1}. \tag{1}$$

This is a straightforward equation. It is evident that when the total OA concentration equals the saturation concentration of a constituent $(C_i^* = C_{OA})$, that constituent will be 50% in the condensed phase at equilibrium ($\xi_i = 0.5$).

Furthermore, a constituent with $C_i^* = 0.1\ C_{OA}$ will be ~90% in the condensed phase while a constituent with $C_i^* = 10\ C_{OA}$ will be only ~10% in the condensed phase. There is thus a fairly narrow range of (extremely low) volatilities spanning approximately a factor of 100 in C^*, centered around C_{OA}, where a compound will be "semi volatile." Furthermore, this range varies with the aerosol loading – at high C_{OA} of perhaps 100 μg m^{-3} found in very polluted cities (or source-dominated locations such as highway tunnels), the whole range of semi-volatiles will be shifted by a factor of 100 toward higher volatility. Also, experiments with significantly higher aerosol concentrations may not have phase partitioning consistent with the atmosphere. Until quite recently aerosol chamber experiments were performed with hundreds to thousands of micrograms per cubic meter of aerosol, resulting in phase partitioning very different from ambient conditions. Emissions measurements are still routinely performed at these unrealistic conditions.

There are at least three separate ways of treating partitioning for practical application to atmospheric aerosol. One is to run a full thermodynamic model containing an ensemble of specific molecules, while the other two are empirical.

2.1.1 Explicit Methods

Explicit methods seek to treat chemistry and thermodynamics with molecular detail, either including as complete a set of compounds as possible [41] or employing a reduced set of surrogate compounds to represent the full array of atmospheric compounds [21]. In either case the thermodynamics for this model system are treated as fully as possible, with individual vapor pressures and activity coefficients for the mixture calculated using one of several thermodynamic schemes [42–45]. A major challenge for this approach is the fact that the molecular composition of the vast majority of the OA mass is not known. However, when OA composition is known or if it can be predicted, they do allow one to assess as completely as possible the consistency of available data.

Recent studies on SOA derived from α-pinene are a good illustration of the explicit methods. Simulations of α-pinene ozonolysis using detailed chemistry from the Master Chemical Mechanism reproduce both SOA mass yields and the volatility distribution derived from chamber studies with good fidelity [46], though an earlier simulation using similar MCM chemistry but different vapor pressure estimation methods under-predicted SOA mass yields at low loading ($C_{OA} < 10$ μg m^{-3}) [47]. A tailored α-pinene oxidation mechanism also performs well in comparison with chamber experiments [48]. A generative mechanism (GECKO-A) applied to α-pinene photo-oxidation generally over-predicts SOA formation, especially under low-NO$_x$ conditions [49]. None of those simulations modeled additional condensed-phase oligomerization chemistry. While the model-measurement intercomparisons were in general good, the dual uncertainties of the chemical mechanisms and vapor pressure estimation greatly complicated

substantive intercomparisons, even when additional measurements such as oxidation state of the SOA were included [46, 49].

2.1.2 Empirical Methods

Empirical methods are based on fits of partitioning data (generally chamber observations) to identify a set of pseudo-compounds with different abundances, which can then be used to simulate the gas-particle partitioning of OA. A major challenge with this approach is whether the properties of these pseudo-compounds are constant as one extrapolates away from the conditions under which the experiment was conducted. To help minimize these errors, it is critical to condition the partitioning experiments over as much atmospherically relevant space as possible.

N-Product Models

The most widely used empirical method is the "Odum two-product model" used to interpret many chamber experiments and implemented widely in air-quality models [23, 50]. When chamber SOA formation data are fitted to a two-product model, the output parameters are two mass yield parameters and two partitioning coefficients ($K_{p,i} = 1/C_i^*$), giving a total of four free parameters. The two pseudo-species are not typically associated with any particular molecular products but rather regarded as completely empirical objects. In general they split into a "low-volatility" and a "high-volatility" product. One issue is that the recovered C^* values are highly dependent on the experimental dataset. The C^* values recovered from data fitting often coincide approximately with the range of measured C_{OA} values in the data, so the volatility of the two pseudo products depends on the concentration range of the experiments [51]. As an example, the C^* value commonly used for isoprene SOA is approximately 1 µg m^{-3} [52], while the "low-volatility" C^* value used until recently for α-pinene SOA was higher, at 15 µg m^{-3} [53, 54]. It would be surprising if SOA derived from isoprene (with five carbons) were less volatile than SOA derived from α-pinene (with ten carbons); however, because isoprene SOA experiments produce much less SOA than α-pinene SOA experiments, the empirically derived product volatilities are skewed. This can have unexpected consequences when the two systems are mixed in a model simulation, where the presence of isoprene SOA will "seed" more volatile α-pinene SOA formation. Reality is more likely to be the opposite of this.

Some of the deficiencies of the empirical two-product model can be eliminated by adding information to a multiple product model. One solution is to map products from chamber experiments onto a "carbon-number–polarity grid" based not only on the empirically observed SOA mass but also expected product properties [55]. Chemical evolution could be described on the grid, enabling a sensible description of aging.
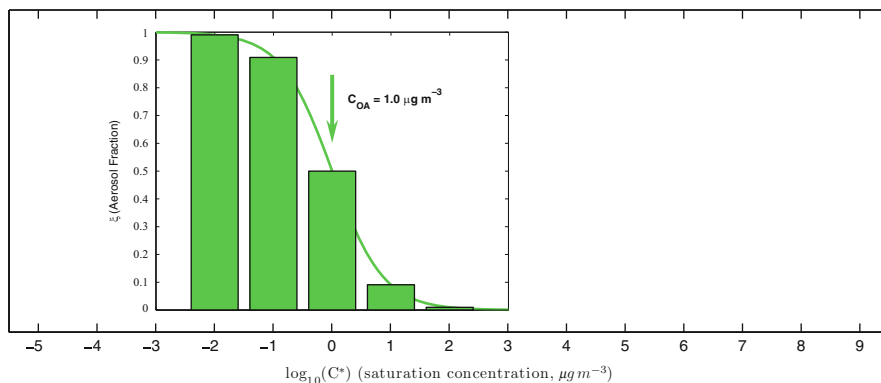
Fig. 1 Partitioning behavior of organics for 1 µg m^{-3} of total organic aerosol (C_{OA}), shown as the fraction in the condensed phase (ξ, height of *bars* and *curve*) vs saturation concentration (C^*)

Volatility Basis Set

Another empirical approach is known as the "Volatility Basis Set" (VBS). Like the two-product model, the VBS is empirical. However, the pseudo-product volatilities are fixed over a wide range, with C^* values typically separated by a single order of magnitude at 300 K [40]. An example is shown in Fig. 1. In a VBS fit the free parameters correspond to the different total concentrations (in any phase) in each volatility "bin" (each pseudo product). Thus, a VBS fit to SOA data with C^* bins at 1, 10, 100, and 1,000 µg m^{-3} has the same number of formal degrees of freedom as a two-product model, but there is a crucial difference. Because the VBS C^* values are fixed, the overall partitioning function (Eq. 1) is only sensitive to the volatility of a given bin when C_{OA} is within about a single order of magnitude of the C^* value for that bin. The VBS parameters are thus relatively robust and independent of each other (there is covariance among adjacent bins, however, and so data can often have many equally good fits where material is divided differently among neighboring bins [56]). VBS parameters can only be fitted to data over slightly more than the range of C_{OA} values in a dataset – the extremes at lower or higher volatility must be constrained by other means, such as an overall carbon balance. With those constraints, a nine-bin VBS is often employed with C^* ranging from 0.01 µg m^{-3} to 10^6 µg m^{-3} [38]. This spans the full range of fully condensed organics, semi-volatile vapors, and "intermediate volatility" species and permits a good carbon mass balance. Though this requires nine species for transport in a model, if all organics form a pseudo-ideal solution the VBS fits from different OA sources can easily be combined to predict overall partitioning for a mixture without the unexpected consequences sometimes emerging from the two-product model.

Non-ideality

A downside of the empirical approaches is they give little insight into non-ideal behavior of complex mixtures, including mixing effects of different organics (their activity coefficients), interaction with water, and interaction with inorganic constituents including salts and elemental carbon. These latter two types of interactions typically involve significant extrapolation away from the conditions of the experiments used to derive the fits. Unfortunately, there are very few direct measurements of activity coefficients for relevant organic molecules over relevant organic mixtures. It seems reasonable to expect seemingly similar OA, such as SOA derived from different precursors, to interact in a more or less ideal fashion, and indeed isotopic labeling experiments have confirmed this [57, 58]. However, mixing of less similar organics, such as relatively non-polar POA and more polar SOA, is less clear. Some experiments using non-polar organic "seeds" show little enhancement in SOA formation over experiments employing inorganic seeds [59], while other experiments directly observing mixing of SOA and POA by tracking the evolution of different size modes using size-resolved mass spectrometry show more nuanced behavior, with rapid mixing of semi-volatile POA into SOA seeds in some cases but not in others [60].

While methods based on explicit surrogate molecules (or complete enumeration of the organic mixture) can rely on calculated activity coefficients, the empirical methods must rely on approximations. In two-product SOA schemes one approach is to assume that generally similar classes of species mix with each other ideally (for example all SOA pseudo-products), but to permit either ideal mixing or complete phase separation of less similar constituents (for example SOA with POA) [23]. More generally, the empirical methods contain very little information about the molecular structure of OA constituents as they are based only on observed gas-particle partitioning and total mass concentrations. This complicates calculations not only of activity coefficients but also of important properties like the organic mass to organic carbon ratio (OM:OC) or the closely related oxygen to carbon ratio (O:C). Of course, composition information can be added based on additional observations, as with the carbon-number–polarity grid described above [61]. However, with the one-dimensional VBS there is an intrinsic problem: compounds with similar volatility can be very different chemically. For example, two compounds with a (sub-cooled liquid) saturation concentration near $10 \ \mu g \ m^{-3}$ are tricosane ($C_{23}H_{48}$) and levoglucosan ($C_6H_{10}O_5$). Each are important in the atmosphere – tricosane is a constituent of lubricating oil [9] while levoglucosan is an important tracer for wood burning because it is a cellulose pyrolysis product [62] – but it is not surprising that lumping both into an identical bin in the 1D-VBS could obscure critical differences in their behavior.

An important issue to consider is the consequence of non-ideality. Interactions that enhance partitioning to the particle phase are important because they increase

aerosol concentrations and also often shield organics from the gas-phase oxidation discussed below. However, interactions that increase volatility will drive compounds into the gas phase where they will likely be oxidized quickly. In many cases the reaction products will return to the condensed phase, though on different particles and in a higher oxidation state. It is thus essential that one considers phase partitioning and aging together, and also that the coupled issues be considered jointly when developing simplified parameterizations for complex chemical transport models.

Two-Dimensional Volatility Space

A two-dimensional version of the VBS addresses the issues just described, including non-ideality and the substantial differences in species contained in a single bin of the 1D-VBS [63, 64]. In addition, the two-dimensional volatility space (2D-VBS) enables more realistic treatment of aging chemistry and important properties such as hygroscopicity. The second dimension is formally the average oxidation state of carbon (OS_C) described in Kroll et al. [65], which is related to the oxygen to carbon ratio (for "normally" bonded molecules, $OS_C = 2$ O:C – H:C). Figure 2a shows the average molecular composition (carbon number, n_C; hydrogen number n_H; oxygen number n_O) in this space and also the approximate O:C for typical ambient aerosol composition [66]. Also shown are the measured saturation concentrations and OS_C for tricosane and levoglucosan. This shows that the approximate formulae given by the contours are not far off from observations, that these seemingly non-volatile species are in fact quite volatile by atmospheric standards, and that in the 2D space these quite different species are well separated even though their volatilities are nearly identical.

The x axis in the 2D-VBS is formally the pure-component saturation concentration C^o rather than the effective saturation concentration C^*, which includes the activity coefficient: $C^* = \gamma C^o$. A simplifying assumption in the 2D-VBS is that the activity coefficient is a function of the average O:C of the OA as well as the properties of the individual organic solute [63]. Figure 2b shows γ as an example for a case where the O:C of the bulk OA is 0.5 (typical of fairly fresh oxidized organic aerosol (OOA) in an urban setting [67]). In this case the contours are for different pseudo species (or bins) in the 2D-VBS. For example, a species with a C^o of 1 μg m^{-3} and an O:C of 0.1 would have $\gamma = 10$ (the last contour shown), meaning $C^* = 10$ μg m^{-3} for that particular mixture. The notable thing in Fig. 2b is that the predicted activity coefficients are mostly very close to 1, with the exception of very reduced material in the paraffin range typically associated with POA emissions. This confirms that most SOA species (with elevated O:C) will tend to form a nearly ideal solution with each other and only the semi-volatile POA species will tend to either phase separate into a distinct condensed phase or else have a *higher* partial pressure and thus partition toward the gas phase.
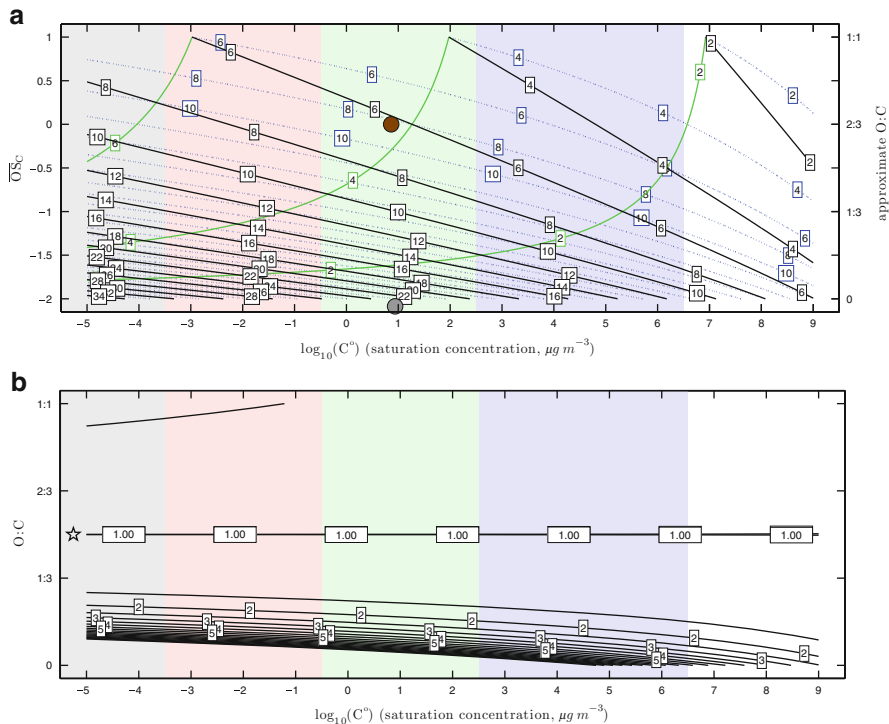
Fig. 2 (**a**) Organic aerosol composition in 2D space defined by pure component saturation concentration (C^o) and average carbon oxidation state (OS_C). *Solid black lines* extending from lower left to upper right are average carbon number (n_C). *Solid green curves* bending from top to lower left are average oxygen number (n_O). *Dashed blue curves* bending from bottom to upper left are average hydrogen number (n_H). Measured saturation concentrations for tricosane ($C_{23}H_{48}$, *gray circle*) and levoglucosan ($C_6H_{10}O_5$, *brown circle*) are shown as well. Both are semi volatile under ambient conditions. (**b**) Activity coefficients of organics in an organic solution with an average O:C = 0.5 (typical of fresh SOA or urban conditions). Contours are spaced by 0.5 and extend to 10.0. Values in the lower left of the space (occupied by compounds typically constituting POA) are much larger than 10.0

Temperature Dependence

The temperature dependence of saturation concentrations can be approximated to first order by an Arrhenius type equation resembling the Clausius Clapeyron equation [40, 68]:

$$C^o(T) = C^o(300) \exp\left[\Delta H_{vap}/R(1/300 - 1/T)\right]. \tag{2}$$

In the VBS formalism the effect of changing temperature is to shift the C^* (or C^o) values of the bins. The bins themselves shift with temperature – one does not

repartition material from one bin to another. This is straightforward [40, 69]. The exact ΔH_{vap} for organic compounds remain a topic of some debate, but for a ΔH_{vap} near 100 kJ mole^{-1}, a temperature change of 20 K results in a one-decade shift in a volatility bin.

2.2 Dynamics of Condensation and Evaporation

The equilibrium thermodynamics described above applies to all systems, but a key question is whether atmospheric systems actually reach that equilibrium. Furthermore, equilibrium phase partitioning says little about what size particles organic compounds end up on. The dynamics of organic condensation and evaporation have recently gained renewed attention for several reasons. First, it is clear that in many environments organic condensation plays a critical role in the growth of freshly nucleated particles up to diameters of 100 nm or so [70–75], where they can influence cloud physics by acting as cloud condensation nuclei. Because the timescale for growth of these ultrafine particles is similar to the production and loss timescales of the condensable vapors, a dynamic treatment is required. Second, there is also growing evidence that many particles containing OA may be in a highly viscous (glassy) state [32–34]. For particle growth, the *net* condensation rate of organics to particles is critical because that controls the growth rate. For glassy particles, diffusion limitations within particles may be rate limiting in condensation and growth, potentially preventing semi-volatile organics from reaching equilibrium on atmospherically relevant timescales [31]. In-particle diffusion limitations could cause apparent mass accommodation coefficients well below unity.

The VBS provides a convenient framework for organic dynamics in addition to equilibrium partitioning because equilibrium is a balance between condensation (the molecular flux from the gas to the particle phase) and evaporation (the molecular flux from the particle phase to the gas). The difference between the vapor concentrations at the particle surface and far away from it serves as a driving force for *net* condensation or evaporation. Because the particle surface is usually assumed to be in equilibrium with the gas phase adjacent to it, evaporation depends explicitly on volatility. Condensation on the other hand depends only on the collision rate of molecules with the surface and so it is first order independent of volatility. The volatility of organic compounds thus affects the aerosol growth dynamics specifically through its influence on the evaporation term in the driving force for mass transport.

It can be shown that the intrinsic growth or evaporation rate associated with a given organic volatility is given by $v_D C_i^*$ where the characteristic velocity v_D is 226 nm h^{-1}/(μg m^{-3}) [75]. This is modified by three important terms – the mass accommodation coefficient, α, the surface-energy (Kelvin) term for particles smaller than 50 nm or so, and the Fuchs term for gas-phase diffusion limitations in the boundary layer around a particle for particles *larger* than 50 nm or so (with Knudsen

numbers $Kn \leq 1$). Barring other limitations, the evaporation rate (in nanometers per hour) for a pure particle with a gas-phase concentration C_i^{vap} held at 0 is thus given by

$$\mathrm{d}d_\mathrm{p}/\mathrm{d}t = F(d_\mathrm{p})K(d_\mathrm{p})C_i^*\alpha_i v_\mathrm{D}. \tag{3}$$

This corresponds to a volume evaporation rate from a spherical particle of

$$\mathrm{d}V/\mathrm{d}t = \tfrac{1}{2}\pi d_\mathrm{p}^2 F(d_\mathrm{p})K(d_\mathrm{p})C_i^*\alpha_i v_\mathrm{D}. \tag{4}$$

Given a volume $V = 1/6\pi d_\mathrm{p}^3$, we can define a timescale for mass transfer via condensation or evaporation from a particle as $\tau_\mathrm{e} = V/(\mathrm{d}V/\mathrm{d}t)$, or

$$\tau_\mathrm{e} = \left(3F(d_\mathrm{p})K(d_\mathrm{p})C_i^*\alpha_i v_\mathrm{D}\right)^{-1}d_\mathrm{p}. \tag{5}$$

This timescale for a given species is independent of the fraction of that species present in an ideal organic mixture, but it is based on the limit of little net diameter change (evaporation of a pure particle will be quicker because the expression must be integrated down to zero volume). The timescale as a function of d_0 is shown in Fig. 3 for unit mass accommodation and pure particles made up of constituents with different C^* values. The central bold curve is for $C^* = 1\ \mu\mathrm{g\ m}^{-3}$. Actual equilibration timescales will differ from this characteristic evaporation timescale; the exact timescale for equilibration of compounds in particles containing organic mixtures will depend on the extent of growth or evaporation required for a mixed particle to reach equilibrium. This in turn depends on the number concentration of particles because that dictates the total mass exchange between condensed and vapor phases, and for low volatility species equilibration timescales are often controlled by the condensational timescale, which can be faster than the evaporation timescale [76, 77]. Regardless, the intrinsic evaporation timescale for $C^* = 1\ \mu\mathrm{g\ m}^{-3}$ organics in 200 nm diameter particles is very nearly 1 h. Timescales for more or less volatile compounds can be found simply by multiplying these values by C^* in $\mu\mathrm{g\ m}^{-3}$, as shown by the parallel curves for different C^* bins. For example, in a typical SOA formation experiment from α-pinene in which 100–1,000 $\mu\mathrm{g\ m}^{-3}$ of SOA is formed, both VBS and two-product fits of product volatilities suggest that much of the SOA consists of species with volatilities also in the 100–1,000 $\mu\mathrm{g\ m}^{-3}$ range. One would thus expect these SOA particles to evaporate substantially in 30 s to 6 min if the gas phase were forced to remain free of vapors.

There are at least three reasons why an evaporation timescale could be *longer* than the intrinsic value shown in Fig. 3. First, the actual mass accommodation coefficient α for the compound could be less than 1 [78, 79]. Mass accommodation is defined as the fraction of vapor collisions with the surface of a particle that wind up adsorbed onto that surface as opposed to more or less immediately rebounding from the surface. There is some debate for light molecules such as water as to whether α must be unity or whether it may be as low as 0.04 [80–84], and the average α for CO_2 from perfluoronated polyether (PFPE) is also approximately 0.5 [85]. Values of
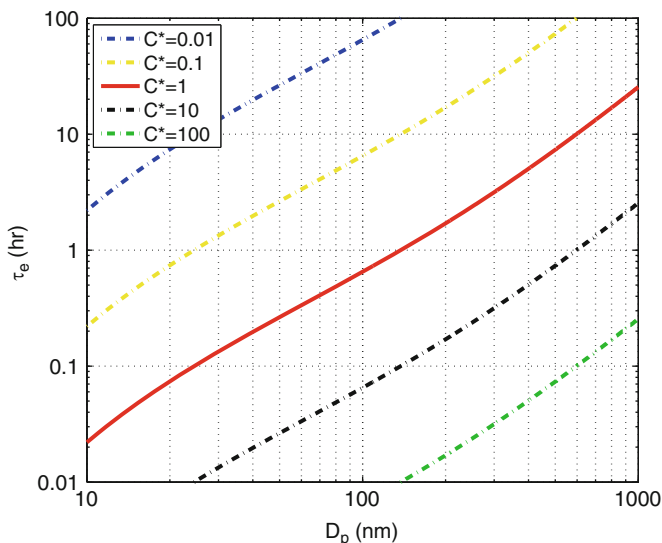
Fig. 3 Characteristic evaporation timescales for organics vs particle diameter for a series of volatilities (C^*) defined by contours. Organics with $C^* = 1$ µg m^{-3} in a 200-nm particle will evaporate in approximately 1 h if mass accommodation is perfect and diffusion within the particle is more rapid than 1 h

$0.1 \leq \alpha \leq 1$ seem plausible and have been reported for pure systems [86]. Lower values seem unlikely. However, even the meaning of α at a molecular level is not firmly established and so non-unit accommodation coefficients must remain under consideration. Regardless of the exact value, at any given time the accommodation and evaporation coefficients for a molecule must be the same, or else the physical process responsible for changing α would instead really be changing the C^* value itself.

The second possibility for slower evaporation is diffusion limitations within the particle itself, or possibly slow annealing of a particle to its equilibrium morphology (as in Ostwald's ripening). In this case the surface composition would not reflect the average composition of the particle. Glassy particles typify this possibility. The timescale for diffusive mixing of a constituent in a spherical particle is $\tau_m = d_p^2/(4\pi^2 \times 3{,}600\,D)$ [87], where D in cm^2 s^{-1} is the diffusion constant of that constituent in the particle, and τ_m is again expressed in h. Just as we use 1 µg m^{-3} as a characteristic volatility, we shall use 200 nm as a characteristic diameter (200 nm^2 is 4×10^{-10} cm^2). Given these constraints, a 1-h or greater mixing timescale in a 200 nm diameter particle requires a diffusion constant (for the diffusing constituent in the mixture) of $D \leq 10^{-14}$ cm^2 s^{-1}. Alternately, it has been suggested that a thin coating of very viscous material on particles may inhibit organic mass transfer of higher volatility molecules to the particle surface, thus slowing or preventing evaporation [31]. Assuming a coating thickness of 10 nm, the diffusion coefficient of the evaporating molecules in this crust would have to be $D \leq 3 \times 10^{-16}$ cm^2 s^{-1}

for the timescale to exceed 1 h. These are very low numbers, and no direct measurements of molecules/mixtures with such low binary diffusivities exist. Koop et al. [34] report that the primary predictor for the glass transition temperature in organics (indicative of $D \leq 10^{-20}\,\mathrm{cm}^2\,\mathrm{s}^{-1}$) is the molecular weight, followed by the degree of oxygenation (i.e., molecular polarity). Compounds with glass transition temperatures of 300 K are tricarboxylic acids with molecular weights of order 200 g/mole. Extension to $D(T)$ for mixtures containing much less polar constituents remains unclear.

A third factor potentially influencing evaporation timescales of organic compounds is the presence of weakly bound oligomeric species or organic salts with dissociation lifetimes greater than the evaporation timescale. Even a weakly bound species, with a binding energy of 100 kJ mole^{-1} and a unimolecular dissociation A factor of 10^{14} s^{-1}, would have a 1-h dissociation timescale at 300 K. Alone among these confounding factors, thermal decomposition can easily lead to an evaporation timescale that is independent of particle size; if the decomposition itself is the rate-limiting step for particle evaporation, the timescale will be fixed by the chemistry and not a mass-transfer limitation.

3 Evidence for Volatility in Atmospheric Aerosol

There is compelling evidence that a significant fraction of OA constituents are semi-volatile, with dynamic gas-particle partitioning under atmospheric conditions. However, the evidence also suggests that volatility is greatest near source regions, where aerosol is "fresh" [69, 88]. This is consistent with the hypothesis that chemical aging generally reduces, or really "resolves" volatility, driving semi-volatile species either toward relatively stable lower volatility products or toward highly volatile, highly oxidized small organic molecules (and ultimately CO_2).

3.1 Volatility of Primary Organic Aerosol

Despite the historical tendency of models to represent POA as a non-volatile mixture, there is longstanding and compelling evidence that POA emissions are substantially semi-volatile. The evidence comes in two major forms. First, both volatility-based chromatography and molecular elucidation of emissions profiles for various sources show clearly that most POA emissions span a wide range of C^* values and that most of those are $\gg 1$ μg m^{-3} [89, 90]. This is often simply a consequence of the properties of the parent materials for the emissions, such as lubricating oil. Second, when the gas-particle equilibrium is perturbed, either via isothermal dilution or via heating, POA particles shrink.

The second characteristic of primary organic emissions is that they tend to be relatively reduced. Using the average carbon oxidation state as a measure [65], most
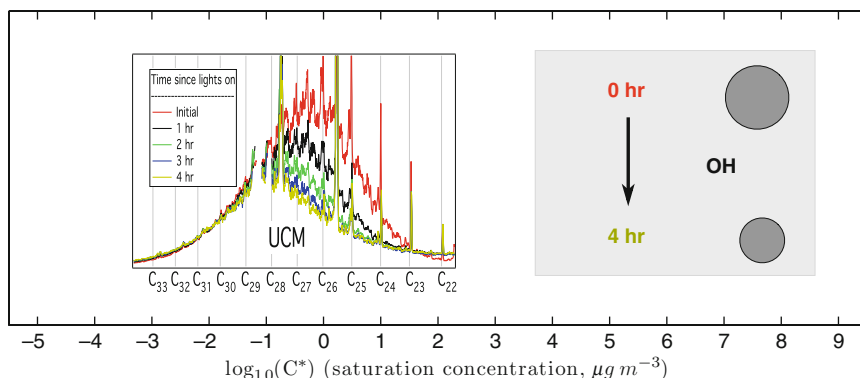
Fig. 4 Oxidation of a motor oil mixture by OH radicals in a smog chamber, followed by thermal desorption gas chromatograms (TAG) taken every hour. Carbon numbers in the chromatogram are registered to typical saturation concentrations. More volatile organics ($n_C < 28$) are removed more rapidly, indicating that gas-phase oxidation dominates the removal

but not all primary organic emissions have an $OS_C \leq -1.5$. This has significant consequences for aging chemistry, but in practical terms it also means that the emissions are relatively nonpolar and thus relatively easy to elute from standard gas-chromatograph columns.

As just one example of volatility separation, in Fig. 4 we show chromatograms of nebulized motor oil particles from an experiment in the CMU smog chamber using a thermal-desorption aerosol gas-chromatography (TAG) system [91], registered in the 1D-VBS. The figure shows two things. First, the red trace shows the initial chromatogram from oil droplets at $C_{OA} \sim 10$ μg m^{-3}. Only hydrocarbons with $n_C \geq 23$ appear in the condensed phase because the more volatile constituents evaporate once the droplets are diluted to low concentrations in the chamber. Second, the experiment involved subsequent exposure to OH radicals, and the series of colored traces show chromatograms of non-polar material for each hour [92, 93]. Clearly, the more volatile fraction of the motor oil decayed much more rapidly than the less volatile fraction. The experiments showed simultaneous buildup of secondary oxidized organics on the particles [93]. This is consistent with gas-phase oxidation of vapors from that volatile fraction causing evaporation to compensate for the gas-phase loss, while heterogeneous oxidation of the less volatile constituents via OH uptake is evidently much slower [92].

Isothermal dilution consistently reveals that POA particles are semi-volatile [90]. Specifically, when POA samples are diluted, the particles shrink. They shrink because the gas-phase dilution lowers the partial pressure of vapors over the particles, and the particles respond to this perturbation by evaporating to raise the partial pressure of those vapors back to equilibrium. Analyses of POA dilution data suggest that a large fraction of the POA mass falls in the 1–1,000 μg m^{-3} range [56, 94].

Evaporation upon heating can complement isothermal dilution. Most POA species are saturated and so are relatively inert and thermally stable; heating is thus unlikely to induce chemistry. Consequently, shrinking on heating in a thermodenuder is unambiguous evidence that the condensed-phase species in a POA particle are semi-volatile. An extra uncertainty associated with thermodenuders is the vaporization enthalpy of the organics [68]; however, as discussed above, a temperature change of 20 K corresponds roughly to an order of magnitude change in C^* (also a change in n_C of 2 corresponds to an order of magnitude change in C^*). Most POA emissions evaporate quite readily in a thermodenuder [56]. For example, lubricating oil such as that shown in Fig. 4 evaporates almost completely when heated by 40 K, and one can see that a shift in the (unreacted) mode from $n_C = 26.5$ to 30.5 should indeed correspond by substantial evaporation.

Several studies of primary particles near sources such as roadways [95] and fires [96] have also established that primary particles tend to shrink as they are isothermally diluted during dispersion downwind of a concentrated source [97, 98].

The bottom line is that emissions from (typically high-temperature) POA sources such as internal combustion engines, wood burning, and food preparation are all characterized by constituents with a broad range of volatilities, a large fraction of which have $C^* > 1$ μg m^{-3} [90]. Consequently, most of these emissions, even those with vapor pressures many orders of magnitude lower than traditional "volatile organic carbon," will be in the gas phase very soon after emission (in seconds to minutes). The subsequent gas-phase chemistry of those vapors is thus one form of aging to consider in organic-aerosol evolution.

3.2 Volatility of Secondary Organic Aerosol

Somewhat ironically given the history of SOA and POA, SOA volatility is a more complicated topic than POA volatility. The principal reason is that SOA species are by definition products of reactions in the atmosphere, and many product compounds are themselves highly reactive. In addition, more oxidized organic species tend to be more polar than their reduced precursors and thus more difficult to sample using separation techniques. Furthermore, the added functionality associated with oxygenation opens up a vast space of potential chemical species, rendering complete speciation of a sample practically impossible [65]. In spite of this, there is every reason to believe that most SOA (especially "fresh" SOA) has a significant amount of semi-volatile mass.

Because of their comparatively large flux to the atmosphere [99], terpenes have long been a major focus of SOA-formation experiments [15]. Significant effort has been expended on speciating SOA, and while the complete mass has not been elucidated, many important product species have been identified [100, 101]. For example, with α-pinene SOA many C_{10} products have been identified, and their C^* values range from roughly 1 to $> 1,000$ μg m^{-3} [46, 49]. Recently,

two-dimensional chromatography has been employed to combine volatility and polarity separation in a manner highly complementary to the 2D-VBS described above. 2D-GC can be mapped onto the 2D-VBS and, for example, a substantial amount of the eluted material from SOA formed via the longifolene + ozone reaction falls in the 0.1–10 μg m^{-3} range, with O:C varying systematically from about 0.25 at the low C^* end to about 0.1 at the high C^* end [102]. Longifolene is a sesquiterpene ($C_{15}H_{24}$), and the observed C^*–O:C range is consistent with the range expected for product molecules with 12–15 carbons seen in Fig. 1a.

Less volatile compounds have been observed from terpene-ozone SOA as well, including C_{20} and larger "oligomers" [103–105] and very low volatility organosulfates [106]. It remains unclear what fraction of the SOA mass is comprised of these less volatile species, but estimates range from 1/3 to 1/2 [105]. It is also not clear whether the majority of oligomers are formed irreversibly or whether they are in equilibrium with monomer species [107]. What is clear is that a substantial fraction of the SOA mass consists of semi-volatile monomeric species, and one thus expects phase partitioning to play a major role in their behavior.

Indeed, absorptive partitioning theory [18] played a critical role in the interpretation of SOA chamber data, making sense of a confusing disarray of mass yield data [17]. Specifically, partitioning theory explains the general tendency for mass yields to increase with increasing total OA concentrations. In Fig. 5 we show mass yield data for the α-pinene + ozone reaction along with a representation of the rising yields with increasing C_{OA}. In this figure C_{OA} (in micrograms per cubic meter) is plotted on the same axis as C^* (also in micrograms per cubic meter). The concentration range over which mass yields rise sharply is the concentration range where the bulk of the products lie – in this case $C^* \geq 1$ μg m^{-3}. An extremely important caveat is that this partitioning analysis is only valid if the overall product distribution (including the condensed and vapor phases) remains constant during a chamber experiment, so that only thermodynamics and not chemical aging governs the amount of material that partitions into the particle phase (in other words, C_{OA} responds to the amount of identical products being produced and not to changes in the product and volatility distribution over the course of a reaction). The very small mass yields at very low C_{OA} pose a challenge to quantitative treatment of the oligomerization reactions described above, as even at fairly low C_{OA} particles in chamber experiments are quite stable, maintaining a constant diameter over many hours [101] and thus showing no clear evidence (no increase of SOA mass) of any slow chemical reactions that might slowly alter the volatility distribution.

To be truly consistent with partitioning theory, particles must also shrink upon dilution, much like POA described above. Different experiments have confirmed that α-pinene + ozone SOA particles do evaporate upon dilution, but not in the minute or so suggested by the volatility distribution in Fig. 5 and the timescales in Fig. 3. Rather, particles relax back to equilibrium after dilution over hours [31, 108], though they do eventually reach the size predicted from equilibrium partitioning theory [108]. This delay is consistent with some phenomenon slowing evaporation by at least a factor of 100. Potential causes for this delay include dissociation of weakly bound oligomers [108] or slowed diffusion in the particles themselves
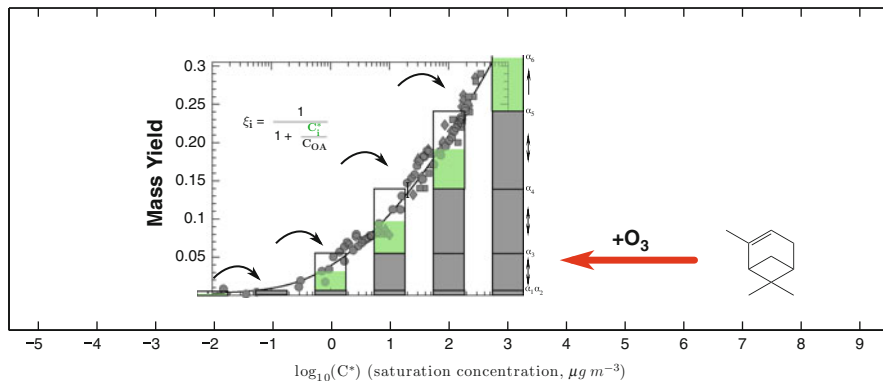
Fig. 5 SOA mass yields from α-pinene ozonolysis vs total SOA mass (C_{OA}). Increasing mass fractions with increasing C_{OA} are consistent with progressive partitioning of more volatile products at higher loadings, as shown

[31, 108]. A recent study [31] reports that size selected α-pinene + ozone SOA particles at $d_p = 160$ and 250 nm showed nearly identical evaporation behavior, whereas the timescales in Fig. 3 are a factor of 2 different. That is consistent with a dissociation timescale being rate limiting as opposed to pure evaporation.

A final element in the evidence supporting a substantially semi-volatile nature for most "fresh" SOA comes from thermodenuders. As with POA, SOA formed in smog chambers evaporates quite readily in thermodenuders [109–113]. Quantitative analysis (inverting thermodenuder data to find a volatility distribution) is difficult because of several confounding factors. These include uncertainties in ΔH^{vap} as well as the mass accommodation coefficient [69, 77]. An extra cause of concern with SOA, unlike POA, is the potential for the SOA to change chemically when it is heated [68]. However, with significant evaporation of chamber-derived "fresh" SOA mass after only 40 K of heating, thermodenuder data are certainly consistent with a substantial fraction of the SOA mass from chamber experiments being semi volatile [110, 114].

Ambient SOA, or at least the highly-oxygenated OOA, generally loses much less mass in thermodenuders [29, 69, 115] than fresh SOA, suggesting that it is much less volatile. Inversions using a VBS framework find a very broad distribution of C^* values for OOA constituents, suggesting (along with the high degree of oxidation) that OOA has undergone substantial oxidative aging in the atmosphere [64, 69].

3.2.1 Do OA Particles Form Mixtures?

In order for mixing thermodynamics to apply, an OA particle must actually be mixed. There are compelling reasons to believe this is so but also some reasons to question whether the mixing is complete. This question really splits into two questions: is the *equilibrium* for OA constituents a uniform mixture and, if so, do

ambient particles relax to that equilibrium more rapidly than they are transported or lost?

There is little doubt that most organic compounds in ambient particles exist in some form of mixture, simply because the particles are composed of an enormous number of different molecules. In the most extreme cases a single constituent can make up as much as 10% of some ambient particles (for example levoglucosan near some fire plumes or certain isoprene oligoesters in very isoprene-rich environments) [116, 117]. However, in most cases the most abundant identified constituent in OA samples comprises less than 1% of the total OA mass. Consequently most organic molecules in most particles are far more likely to be solvated by and interacting with many different molecules with a variety of carbon chain lengths, branching structures, and numbers and types of functional groups. This is one reason why crystallization seems highly unlikely for most particles and consequently why the mixing thermodynamics are developed for amorphous mixtures (thus employing the sub-cooled liquid vapor pressure as the starting point for partial-pressure calculations) [18]. This also provides information on experimental design, especially relating to organic "seeds" for SOA formation that might promote condensation via absorptive partitioning. High fractions of any individual seed species will enhance the probability that a separate (potentially crystalline) "seed phase" will form in an experiment, while more realistic seed mixtures will be less vulnerable to such phase separation.

A second factor favoring mixtures is that most OA constituents arrive in a particle via condensation. The organic condensation rate in the boundary layer under many conditions is roughly 1–10 nm h^{-1} [73]. Near sources there will be (sometimes concurrent) evaporation and condensation of POA species, and both near and far from sources there will be condensation of oxidized secondary molecules as well as uptake of oxidants. Furthermore, in many cases important inorganic species such as sulfuric acid, nitric acid, and ammonia are condensing (and in the latter two cases evaporating) from particles simultaneously. Perhaps most importantly, as relative humidity (RH) varies, the activity of water in a particle will vary as well. Above about 90% RH, more than half of the volume of most particles will be water, and this water will form an extremely high ionic strength aqueous phase incorporating at least some of the more soluble organic molecules (and even the "hydrophobic" residual organic phase may include significant water). Under many circumstances air parcels move vertically through the boundary layer in minutes, and consequently they cycle through a wide RH range (often including saturation if a cloud layer is present) [118].

If the organic mixture does indeed form a single phase at equilibrium, then the conditions for complete equilibration require equal composition in each particle. Actually attaining this equilibrium requires mass exchange, which in turn can occur only through coagulation (which is not really an exchange mechanism) or interparticle mass transfer (condensation–evaporation) [39]. Strict equilibration would require that all species be present in (the organic fraction of) all particles in equal abundances; however, we can also define a "volatility equilibrium" in which particles are neither growing nor shrinking because their "volatility composition"

is equilibrated even though their exact composition is not. Specifically, within the VBS the mass fraction of each VBS bin represented in each particle would be the same, so the fraction of semi-volatiles in each particle would be the same. A trivial example of this is a suspension of single-component particles in which some particles have an isotopic label. The particles would be at all times in volatility equilibrium and there would be no driving force for a net mass change, and yet to reach full equilibrium the isotopic composition of each particle would need to become identical, driven by the entropy of mixing.

The concept of volatility equilibration is important when considering very low volatility constituents in particles. The timescale for equilibration of extremely low volatility molecules via net condensation approaches infinity; the molecules will simply never leave their initial particles. However, the more volatile molecules in a mixture can still attain volatility equilibrium by independently establishing equal activity over all particles long before the less volatile constituents have been able to equilibrate. The overall timescale for this process may be complex as different constituents evolve simultaneously.

Condensation, Aging, and Mixing

Mixing for atmospheric aerosol essentially always involves some form of condensational uptake to particles. A unique characteristic of condensational uptake is that it is proportional to the (modified) surface area of particles and not their volume ("modified" refers to the Fuchs correction for gas-phase diffusion for larger particles with $Kn \lesssim 1$, which reduces the effective surface area for condensation). Because the surface area to volume ratio of particles increases as their diameter decreases, condensation tends to have a larger effect on smaller particles, when measured on a mass (or volume) basis. The concept of "surface limited" vs "volume limited" aging has been used before to diagnose different processes in aerosol evolution [119]. However, condensation also tends to drive mixtures out of equilibrium, as the volume fraction of condensing vapors will grow more rapidly for smaller particles than for larger particles. This can be a very useful diagnostic of mixing effects in particles. As an example of "pure condensation" we shall discuss condensation of SOA from the α-pinene + ozone reaction onto pre-existing ammonium sulfate "seed" particles, and then we shall discuss two other cases with more interesting mixing effects.

The condensation rate of organics to a particle surface is given by Eq. 3, multiplied by the saturation ratio of the organic vapors ($S = C_i(\text{gas})/C_i^*$) [75]. In Fig. 6 we show the theoretical condensation of organic vapors to inert seeds with an initial lognormal mass mode centered at 300 nm and a Gaussian width of 0.2. The vapors condense onto the inert seeds in proportion to the diffusion-modified seed surface area. The figure shows the initial and final total aerosol size distributions (dashed curves) as well as the final mass distribution of condensed organics and inert seeds (labeled "sulfate" because we tend to use ammonium sulfate for seeds). In the final distribution the condensed organics strongly favor the smaller particles.
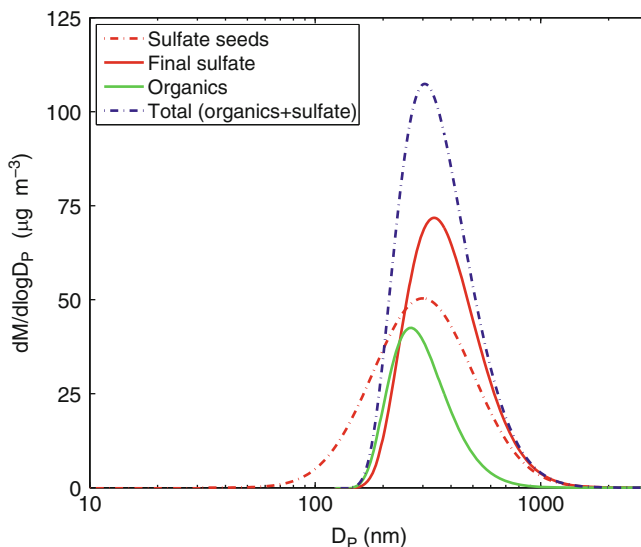
Fig. 6 Calculated condensational growth of organics onto inert (sulfate) seeds, shown as mass distributions vs log of particle diameter. Initial seeds are shown as a *dashed red* Gaussian centered at 300 nm. The final total size distribution is shown as a dashed blue curve. The final sulfate mass distribution is shown as a *solid red curve*, shifted to a 370-nm mode because of organic condensation. The final organic mass distribution is shown as a solid green curve. The organic mass mode after condensation is at 270 nm because condensation (of organics in this case) strongly favors smaller particles with larger surface area to volume and less inhibition from gas-phase diffusion. Because the organics and sulfate do not form a mixture, the final composition (organic:sulfate) is a strong function of particle diameter

This weighting toward smaller sizes of a purely condensational process is characteristic of the interaction between condensing vapors and an inert seed (or of completely non-volatile condensation). It is what drives "condensational narrowing" [120] which is evident in the distorted final distributions in the simulation. In either case the composition of the particles is a strong function of size: in Fig. 6 the 200-nm particles are more than 80% organic, while the 500-nm particles are less than 20% organic; if the particles comprised a single condensed phase they would be far out of equilibrium.

Many SOA formation experiments use inorganic seed particles to encourage condensation onto suspended particles instead of chamber walls [121]. Often the assumption in these experiments is that the inorganic seeds do not influence the SOA mass yields, and mass-yield data confirm this assumption [122]. In Fig. 7 we show size-resolved mass spectra obtained using an aerosol mass spectrometer in particle time of flight (pToF) mode for SOA formed from the toluene + OH reaction and condensed onto dried ammonium sulfate seeds at 15% RH from experiments reported in Hildebrandt et al. [123]. The pToF data show exactly the features expected for condensation onto inert seeds. Very similar data are shown in Prisle et al. [124] for SOA formed from α-pinene + ozone. It is worth noting that
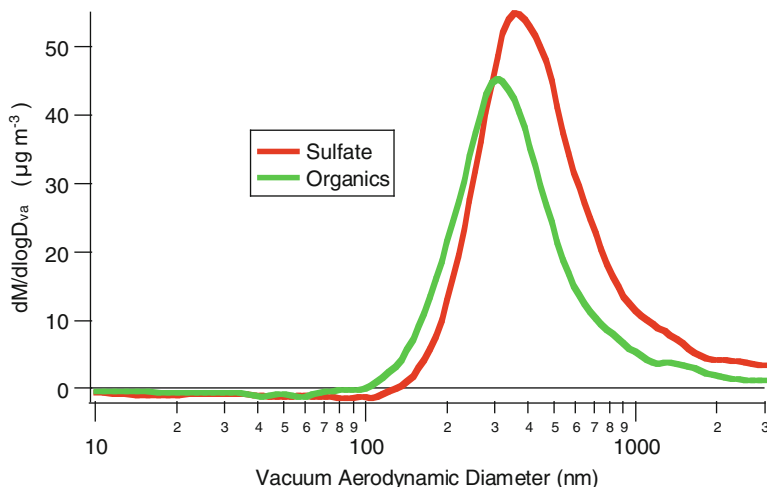
Fig. 7 Measured organic (*green*) and sulfate (*red*) mass distributions from Aerosol Mass Spectrometer particle time of flight (AMS pToF) data. Data are for SOA from toluene oxidation in the presence of ammonium sulfate seeds. Observations closely follow predictions shown in Fig. 6

ambient particles often do *not* show this displacement between organics and sulfate because *both* the organics and sulfate accumulate via condensation, often more or less simultaneously. How particles anneal to a phase-separated morphology with distinct inorganic and organic phases (if indeed this is the equilibrium state [125, 126]) remains unclear.

The situation is very different when organics mix with each other. In Fig. 8 we show AMS pToF data from a mixing experiment first reported by Asa Awuku et al. [60]. In this case POA from a diesel engine was injected into a chamber containing SOA from α-pinene + ozone. As shown in the top panel, the POA initially appeared as a distinct mode with ion fragments characteristic of primary emissions and a modal diameter significantly smaller than the SOA particles. Within 5 min the distinct POA mode vanished and the characteristic ion fragments migrated to the SOA mode, as shown in the lower panel. This clearly indicates that relatively volatile POA evaporated and re-condensed into the SOA, with the lower activity of the POA species in the SOA particles acting as a thermodynamic driving force for the mixing. There were, however, strong indications that the mixing was non-ideal. Both composition and concentration influenced these effects. Specifically, an injection of motor-oil droplets similar to the diesel POA remained stable for hours as a distinct mode while the diesel POA quickly mixed with the SOA seeds. The activity coefficients of the oil vapors were thus significantly greater than 1 in the SOA particles, so at some finite concentration of POA species in the SOA (and vice versa, though the mass spectra did not show this directly) the suspension became stable, with two distinct condensed phases present [60]. Also, the rapid (5 min) mixing of a significant quantity of POA into the SOA particles clearly shows that (in this case at least) diffusion of the POA species into the SOA was not a
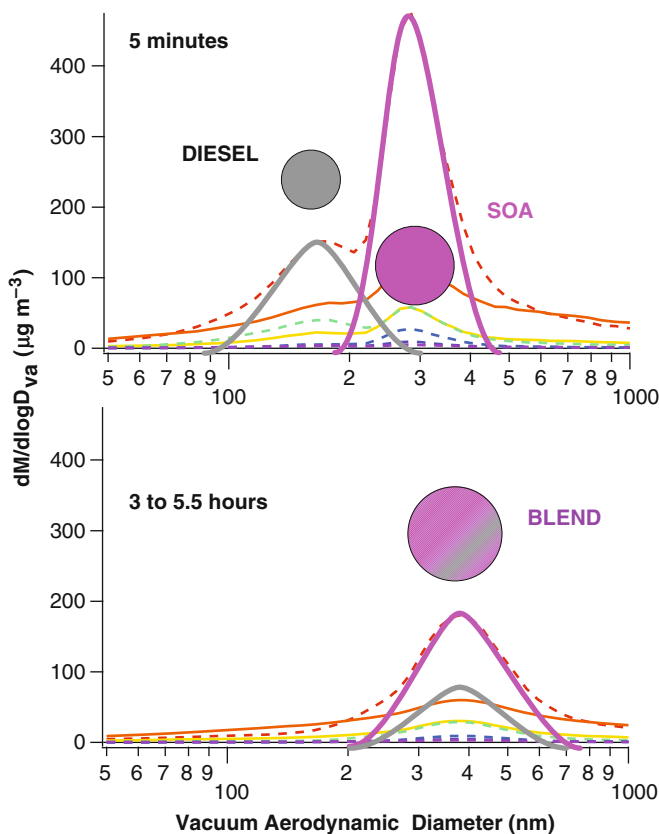
Fig. 8 Measured AMS pToF distributions for diesel POA particles injected into a smog chamber containing SOA from α-pinene ozonolysis. POA particles are evident as a distinct mode at 180 nm for only 5 min (*upper panel*) after which they vanish into the SOA seeds (initially at 300 nm, ultimately at 400 nm, *lower panel*). Both the timing and coincident size distributions of the ultimate particle distribution confirm that mixing of POA into SOA occurred via evaporation of fresh POA and subsequent condensation and full (volume) mixing into the SOA seeds

significant impediment; the lack of complete mixing in some cases likely indicates non-ideality as opposed to delayed equilibration.

A final example involves gas-phase aging chemistry. In Fig. 9 we show two pToF spectra from semi-volatile diesel oxidation experiments described elsewhere [127–129]. In these experiments, diesel emissions were diluted to near ambient levels and then exposed to photolytically generated OH radicals [128]. The pToF data are shown for two key ion fragments, $m/z = 57$ and 44, which are traditionally indicative of reduced ("hydrocarbon like") POA and oxidized SOA [130]. In these experiments the total OA concentrations more than doubled in 5 h due to SOA formation. The figure reveals that the $m/z = 44$ marker characteristic of the SOA remained locked into the mode characteristic of the POA defined by $m/z = 57$, even as the $m/z = 44$ abundance increased due to condensation. Data are shown just
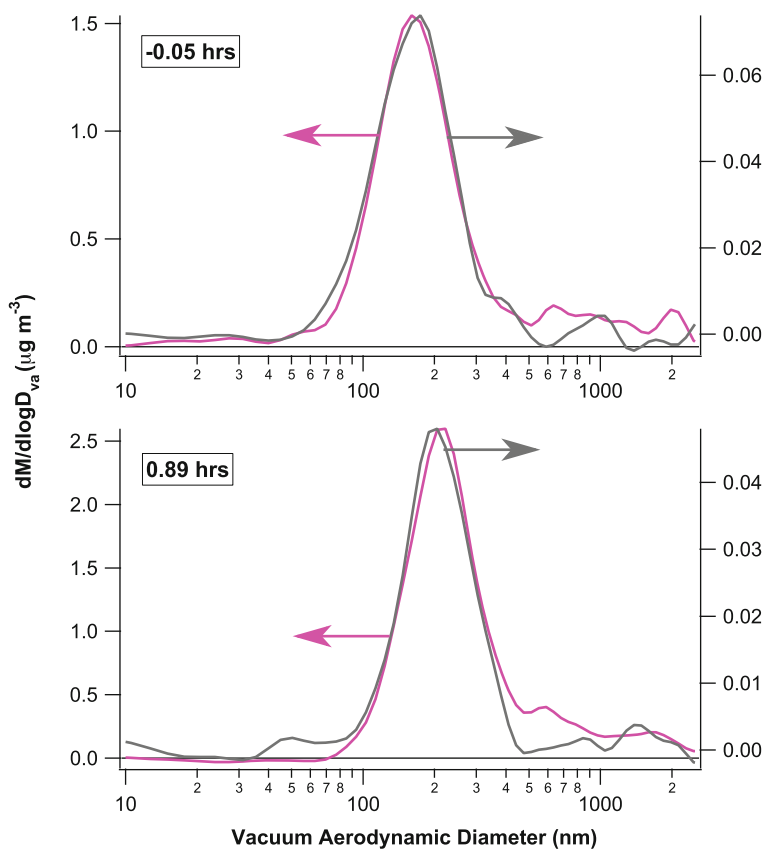
Fig. 9 SOA production on diesel seed particles. SOA formed from photooxidation of diesel vapors shown by increasing mass fraction of $m/z = 44$ (largely CO_2^+, *pink*) fragment, left scale vs $m/z = 57$ (largely $C_4H_9^+$, *gray*) fragment, right scale. The *horizontal arrows* point toward each axis at a constant y value in the two panels to illustrate the extent of condensation by SOA. Concurrent diameter growth shows that condensation and evaporation maintain equal mass fractions of more reduced and more oxidized organic species in all particles, independent of size

before oxidation and after 1 h of photochemistry, but the OOA mode never lagged behind the POA mode in the manner characteristic of condensation to inert seeds shown in Figs. 6 and 7. The evidence is thus strong that the POA and SOA formed a mixture throughout the diesel oxidation experiment.

To maintain the equal mixing shown in Fig. 9, condensation alone is not sufficient; the only way to keep the volume (mass) distributions of species constant during a period of strong condensational growth is via *net* condensation, meaning that some species also evaporate significantly from relatively enriched particles and re-condense on relatively depleted ones. From these data there is no way to tell whether it was the POA or the SOA species (or both) evaporating and recondensing, only that this surely occurred with more or less complete volume mixing on a timescale faster than the growth (faster than 1 h or so). However, if

the mixing experiment shown in Fig. 6 and the calculations shown in Fig. 3 offer any indication, it is likely that the POA vapors were largely responsible for this equilibration.

4 Aging

The previous example brings us to aging. Here "aging" refers to chemical aging – in other words chemical reactions that alter the composition of an organic aerosol. There are at least five modes of aging: gas-phase oxidation of organic vapors, heterogeneous uptake of oxidants, condensed-phase reactions among organics, acid–base reactions involving organics, and aqueous reactions involving organics. As discussed in the introduction, the focus of this work is largely on gas-phase aging.

4.1 Gas-Phase Oxidation

Gas-phase chemistry is a key player in organic-aerosol evolution. We shall discuss organic oxidation chemistry first because this is a homogenous process. There are no circumstances where it will not happen – no diffusion limitations or other inhibiting phenomena. If an organic compound is oxidized in the gas phase and an oxidation product has a sufficiently low C^*, that product will condense to a particle when it collides with it. Thus, when we consider gas-phase oxidation we are interested principally in the volatility distribution of the reaction products as well as their composition. All increases in OA mass due to gas-phase chemistry can be called "secondary organic aerosol" (SOA) because the reaction products are secondary molecules and the aerosol mass increases, so the added mass is secondary mass. These topics have been extensively covered in numerous publications and reviews, and so we shall touch only briefly on key issues here. For historical and practical reasons we shall split our discussion between SOA formed from volatile precursors (sometimes called "traditional" SOA) and SOA formed from less volatile precursors (one class of so-called "non-traditional" SOA). Hydrocarbon oxidation is an inexorable process proceeding from a highly reduced primary compound (often relatively volatile) ultimately to CO_2 (also highly volatile) [65]; however, intermediates in this process can have extremely low vapor pressures.

4.1.1 VOC Secondary Organic Aerosol

SOA from VOCs has a long history [15, 17, 51] and is also discussed elsewhere in this volume. The key finding relevant to a broader aging discussion is that products of gas-phase oxidation reactions can have lower C^* than the precursor. A recent

focus has been to conserve carbon when parameterizing an SOA formation process, i.e., in a VBS formulation

$$\text{VOC} + \text{Ox} \rightarrow \left\{ \alpha_i\, C_i^* \right\},$$
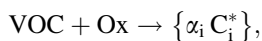
where $\{\alpha_i\}$ is a set of carbon mass yields (i.e., micrograms per cubic meter of OC formed for 1 μg m^{-3} of VOC consumed). The total OA mass can then be obtained with some added information – specifically OM:OC$_i$, the ratio of organic mass to organic carbon within each product bin. This can be estimated from loading-dependent composition (C:H:O) measurements during SOA formation [131] and is directly constrained within a 2D formulation of the VBS that includes composition information as a second dimension [63, 64].

The relevant issue here is that many analyses suggest that much of the SOA mass is semi volatile, as discussed above. In addition, because the SOA mass yields are generally well below 1, it is clear than many other reaction products are lower in volatility than the precursor but too volatile to influence the SOA mass. All of those vapors are in play for subsequent later-generation aging chemistry.

4.1.2 IVOC and SVOC Secondary Organic Aerosol

Intermediate volatility organics (IVOCs) are much less volatile than VOCs but still much more volatile than species that can condense under ambient conditions. Most of the first-generation SOA products shown in the VBS fits in Fig. 10, with $300 < C^* < 3 \times 10^6$ μg m^{-3}, are considered IVOCs. In addition, a substantial fraction of primary emissions from high-temperature combustion, including wood burning, food preparation, internal combustion engines, and turbine engines, consists of IVOCs and SVOC (with $0.3 < C^* < 300$ μg m^{-3}) [90]. We shall discuss direct formation of SOA from IVOC and primary emissions first because the kinetics and initial mechanisms of these reactions have been studied more widely.

SOA from Primary IVOC Emissions

A challenge with the atmospheric chemistry of IVOC is the exponential increase in chemical complexity with increasing carbon number, even for "simple" hydrocarbons containing only carbon and hydrogen [35]. Consequently, studies of SOA formation from IVOCs fall into two categories: study of individual molecules or sequences of molecules as representative model systems and study of undifferentiated "whole" emissions diluted to near ambient conditions to encourage atmospherically relevant partitioning of the primary emissions.

Two broad classes of lower volatility hydrocarbons have been studied extensively: alkanes and polycyclic aromatics. Alkanes have been more systematically treated with regard to their potential for SOA formation, while the chemistry and

phase partitioning of polycyclic aromatics were in many ways the foundation for the ambient partitioning theory described in this chapter because of the significant concerns over PAH health effects.

Alkanes

Alkanes are an excellent model system because they present a homologous sequence in both carbon number (and thus volatility) as well as structure (and thus varying chemical behavior). Alkane SOA formation has been studied systematically by Ziemann and coworkers [132] as well as others. Broadly, the SOA formation potential of *n*-alkanes increases systematically with carbon number [132, 133] as the precursor volatility decreases. Substitution in the form of branching significantly decreases SOA formation at a given carbon number, while cyclization increases SOA formation. In each case the reason is fragmentation of secondary products: branched alkanes are more vulnerable to C–C bond cleavage during oxidation, while cycloalkanes can sustain one C–C bond cleavage event without a decrease in carbon number because of the tethering effect of the cyclic structure [134].

Polycyclic Aromatics

PAHs have been studied for decades because of their high potential for negative health effects [135–137]. Investigators quickly realized that PAH volatility spanned a wide range and thus that important PAH species would be found in both the gas and condensed phases in the atmosphere. Partitioning theory was developed for atmospheric applications in large measure to address these issues. For some time, adsorption to surfaces was considered to be more important than absorption into an organic condensed phase [138]; however, by stages it became evident that the total mass of the condensed phase (TSP) was significant to partitioning [139] and ultimately that absorptive partitioning with the condensed organic phase was often the appropriate framework for partitioning [140]. While that work laid the foundation for the perspective on partitioning described here, consideration of the SOA formation from PAH oxidation is much more recent. Like the alkanes, PAH oxidation has been studied as a potentially important model for SOA formation from IVOCs [141].

Evaporated Primary Emissions

Real primary emissions consist of a complex mixture including linear and branched alkanes, mono aromatics, substituted aromatics (alkyl benzenes), and PAHs, among many other compounds [7, 142]. The most direct evidence that SOA formation is important for typical atmospheric IVOC mixtures thus comes from experiments on vapors from these very mixtures [127, 143–148].
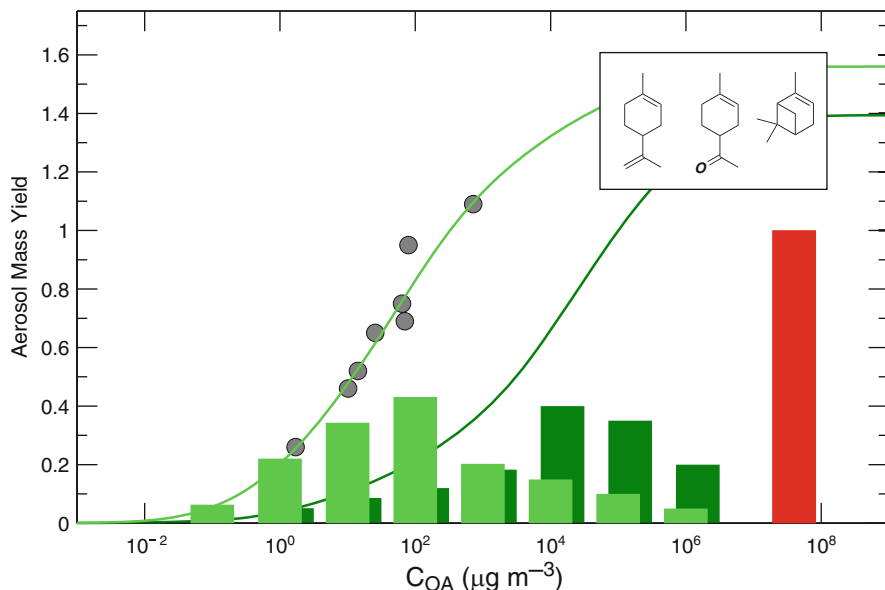
Fig. 10 SOA product volatility distributions for α-pinene and limonaketone in *dark green* and mass yields vs C_{OA} as *dark green curve*. Precursors with similar volatility, structure, and chemistry have similar yields. Product volatility distribution and yields for D-limonene ozonolysis are shown as *light green bars* and a *light green curve* (and *gray* data points). Oxidation of the additional exocyclic double bond in limonene results in substantially less volatile SOA products and correspondingly higher SOA yields

4.1.3 Aging of VOC SOA

All of the first-generation vapors from VOC SOA will certainly undergo further gas-phase oxidation, which will in turn influence the phase partitioning thermodynamics of the OA mixture, i.e., gas-phase aging of SOA.

Multiple Ozonolysis Generations

Several forms of aging of SOA vapors have been observed. One clear form is oxidation of multiply unsaturated alkenes. Many terpenes have multiple unsaturations, and in some cases different double bonds have very different rate constants for reaction with ozone. Examples include terpinolene, myrcene, limonene, α-humulene, and β-caryophyllene [149, 150]. In these systems, ozone will react with one double bond in the terpene and produce some SOA. However, after the precursor is completely removed, SOA levels can continue to rise as the first-generation semi-volatile products continue to react with ozone to produce less volatile second-generation products [149].

Limonene is a revealing example. It is similar to α-pinene in possessing a methyl-substituted endocyclic double bond in a six-member ring, but in addition it has an exocyclic terminal unsaturation. Figure 10 shows SOA mass-yield data and

a corresponding VBS product distribution (in light green) for the limonene + ozone reaction under low-NO_x conditions [150]. The inset shows structures for limonene, limona ketone, and α-pinene. The darker green histogram and yield curve is valid for α-pinene and limona ketone, which generate almost identical SOA mass distributions after ozonolysis [38]. Initial ozonation of limonene also produces SOA much like α-pinene and limona ketone, but subsequent ozonation of the exocyclic double bond in the first-generation products strongly favors the ketone-oxide over the ketone moiety shown in limona ketone and consequently forms substantially less volatile second-generation products [150–152]. As Fig. 10 shows, the resulting product distribution is two to three orders of magnitude less volatile than typical first-generation terpene ozonolysis products, which is consistent with additional peroxide and carboxylic acid functionality [153] greatly offsetting the loss of one carbon from the terminal methylene.

An interesting wrinkle in the limonene story is that the second ozonolysis reaction can be heterogeneous. The fresh SOA produced when ozone reacts with the endocyclic double bond is unsaturated [153], but under low-NO_x conditions it reacts much more rapidly than is plausible based on gas-phase kinetics, but at a rate consistent with a heterogeneous ozone uptake coefficient of roughly 10^{-3} [150]. Under high-NO_x conditions the SOA (which contains organic nitrate functionality) has a much lower heterogeneous reactivity to ozone and consequently species remain in the gas phase that oxidize at a rate consistent with the ozonolysis of terminal double bonds, forming second-generation SOA more slowly, long after the limonene itself has been completely oxidized [150].

Multi-generation OH Oxidation

Oxidation by OH radicals (or photooxidation in general) is much more difficult to deconvolve than ozonolysis because there is seldom the clear separation in timescales that can appear in the ozonolysis aging just discussed. However, later-generation oxidation by OH is likely to be much more important in the atmosphere because it is ubiquitous. OH will react with essentially all organic molecules, though the kinetics and mechanisms of the highly substituted species typical of first-generation and later-generation oxidation products remain highly uncertain. Nonetheless, there is no doubt that these reactions will occur, and little doubt that they will be quite rapid, in most cases oxidizing semi-volatile vapors within hours [64].

Multiple-generation oxidation has been studied theoretically via mechanism generators that apply structure activity relations for rate constants and product distributions [49]. Several specific tracers of later-generation oxidation have been proposed. One is a C_8 triacid formed via gas-phase oxidation of *cis*-pinonic acid, which is itself a first-generation oxidation product of α-pinene [154]. The triacid is produced rapidly when gas-phase *cis*-pinonic acid is exposed to OH radicals, but not when the pinonic acid is partitioned into SOA at low temperatures [155]. For bulk SOA characteristics, Chhabra et al. [156] have shown that SOA formation

from oxidized precursors results in SOA whose mass spectrum is higher in the
f_{44}–f_{43} "triangle" space recently proposed as a diagnostic for ambient OA
processing [157].

In the recent multiple chamber chemical aerosol aging study (MUCHACHAS),
first-generation SOA was produced from α-pinene + ozone and then exposed to
OH radicals in a subsequent, separate step [112, 113, 155, 158–160]. The OH
exposure caused a substantial jump in SOA mass concentrations [112, 113, 158]
and significant changes in SOA volatility and hygroscopicity [112, 113, 159]. This
controlled experiment strongly confirmed that long-term gas-phase aging by OH
radicals can substantially alter OA properties.

There is thus compelling evidence that gas-phase OH oxidation will age OA by
oxidizing semi-volatile vapors as well as slightly more volatile IVOC intermediate
products. This will occur throughout the atmosphere with a rate constant estimated
to be of order 2×10^{-11} cm^3 molec^{-1} s^{-1}, giving a lifetime for typical OH
concentrations of order 8 h [92, 158]. Other aging mechanisms can be scaled by
this ubiquitous value to assess their relative importance.

4.2 Heterogeneous Aging

A large body of work addresses aging of organic particulate matter via heteroge-
neous uptake of oxidants, especially OH and ozone. Just as partitioning theory
progressed from a focus on adsorptive to absorptive behavior, heterogeneous
uptake has been viewed in terms of uptake of oxidants controlled by Langmuir-
Hinshelwood type adsorptive isotherms [79, 161], but diffusion of oxidants into a
bulk aerosol has also been considered in various contexts [162]. Heterogeneous
formulations can differ depending on whether the principal focus is the loss of an
oxidant upon uptake [87] or the loss of condensed-phase constituents due to oxidant
uptake [163–166]. The "Pöschl Rudich Ammann" framework was initially
presented with a principal focus on gas–surface interactions for multiphase pro-
cesses, but has recently been extended to resolve diffusion into a spherically
symmetric bulk as well [87]. The objective here is not to review even a small
portion of the literature on heterogeneous oxidant uptake but to focus on the
interplay between heterogeneous oxidation and organic phase partitioning.

Heterogeneous oxidation by OH is intrinsically slower than homogeneous
gas-phase oxidation of organic vapors, since most molecules in a given particle
are shielded from gas-phase radicals colliding with the surface. A rate constant
for the gas-phase reaction of OH radicals with large organic species of
2×10^{-11} cm^3 molec^{-1} s^{-1} is at least ten times larger than that of gas-phase OH
with an organic species within a submicron particle [92]. The rate at which a
molecule will undergo oxidation in each phase is a function not only of these rate
constants but also by its abundance (as measured by mole fraction) in each phase.
This is illustrated in Fig. 11 which shows the effective oxidation rate constant
in each phase as a function of volatility as well as the total rate constant including
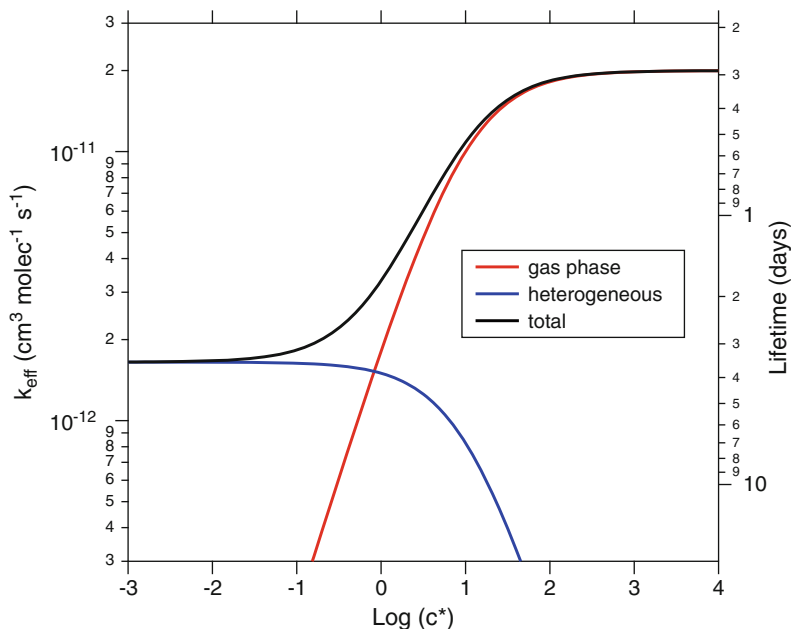
Fig. 11 Effective OH oxidation rate constants for organics in gas phase (*red curve*) and condensed phase (*blue curve*) for a gas-phase OH rate constant of 2×10^{-11} cm^3 molec^{-1} s^{-1} and a heterogeneous OH uptake coefficient of 1, for 200 nm diameter particles and 10 µg m^{-3} total organic aerosol. Results are given as equivalent gas-phase values, modified by the fraction of organics in each phase and diffusion limitations of gas-phase OH to condensed-phase organics. Oxidation lifetimes (in days) are given on left-hand *y* axis, for 2×10^6 OH cm^{-3}

oxidation in either phase. Rates were calculated assuming a gas-phase rate constant of 2×10^{-11} cm^3 molec^{-1} s^{-1}, reactive uptake coefficient (γ) of 1, particle diameter of 200 nm, and organic aerosol loading (C_{OA}) of 10 µg m^{-3}. The figure shows that gas-phase oxidation will almost always dominate over heterogeneous oxidation unless the molecule is very low in volatility (C^* of 0.1 µg m^{-3} or lower). Molecules almost wholly in the condensed phase of course can only be oxidized there. It is important to note that the heterogeneous timescale of 3–4 days is still shorter than the characteristic atmospheric residence time of submicron particles of 1 week or more [167]. Consequently, heterogeneous oxidation is still clearly an important process for organic compounds contained within aerosol particles.

In addition to providing insight into the kinetics of multiphase aging, studies of heterogeneous oxidation also serve as indirect probes of the mixing effects discussed earlier. Measuring the rate and extent of degradation of individual aerosol components provides information not only on molecular-level reactivity but also on mixing within the particle. This is because the reactive-diffusive length of OH in organic particles is of order 1 nm [168], and so heterogeneous OH reactions will be

confined to the particle surface. For example, in a study of the multigenerational heterogeneous oxidation of squalane ($C_{30}H_{62}$), squalane degradation followed a simple pseudo-first-order kinetics (exponential decay) over multiple oxidation lifetimes, with concentrations eventually falling to zero [169]. Similarly, the first and second generation products reacted away at the same rates. This indicates that, at any given time, a sufficient amount of reactant (squalane and early-generation products) is present at or near the surface of a (pump oil) particle to react with OH; mixing within the particle is thus very fast on the timescale of the experiment (37 s). A similar conclusion can be drawn for heterogeneous oxidation of α-pinene SOA by OH. Experiments with very high SOA concentrations (which favors the condensed phase and thus heterogeneous oxidation) and very high OH exposure in 37 s found almost complete conversion of fresh SOA into highly aged material. The aged aerosol strongly resembled ambient low-volatility oxidized organic aerosol (LV-OOA) while maintaining almost no correlation with the original fresh SOA mass spectrum [30]. This would not be possible unless essentially all of the organic species within the particles were able to diffuse to the particle surface (or even evaporate) in 30 s or less. On the other hand, in similar experiments on the heterogeneous oxidation of levoglucosan ($C_6H_{10}O_5$) and erythritol ($C_4H_{10}O_4$), the reactants were not totally lost after an initial rapid decay, consistent with the formation of viscous materials with mixing timescales of at least several minutes. This serves as an illustration that generalizations about diffusion limitations within organic particles may be very difficult to draw, as the specific particle composition (including organics, inorganics, and water) as well as temperature may alter constituent diffusivities by many orders of magnitude.

Heterogeneous oxidation experiments also allow for the investigation of the possibility that organic condensation may "coat" existing particles, isolating the core of the particle from the surrounding gas. Such a coating implies a lack of mixing between the condensing vapor (the coating material) and the particle core, but this can be a dangerous assumption if the two are miscible. One example of this is shown in Fig. 12, which is a relative kinetics plot of particle-phase cholestane loss compared to gas-phase oxidation of meta-xylene by OH radicals [143]. For the reasons discussed above, it is reasonable to regard heterogeneous loss of condensed-phase organics as a fairly precise surface probe. Figure 12 shows two things. First, coating of POA particles containing cholestane by a nominally quite thick layer of α-pinene SOA did nothing to slow down heterogeneous cholestane loss, suggesting that the SOA formed a uniform mixture with the POA. That is consistent with the mixing experiments described above [60]. Second, cholestane loss slowed significantly at high RH (~75%), suggesting that an aqueous surface layer formed, excluding nonpolar compounds such as cholestane. This is consistent with recent findings that two distinct condensed phases form for wet OA particles as long as the O:C of the organics is below approximately 0.7 [125, 126].
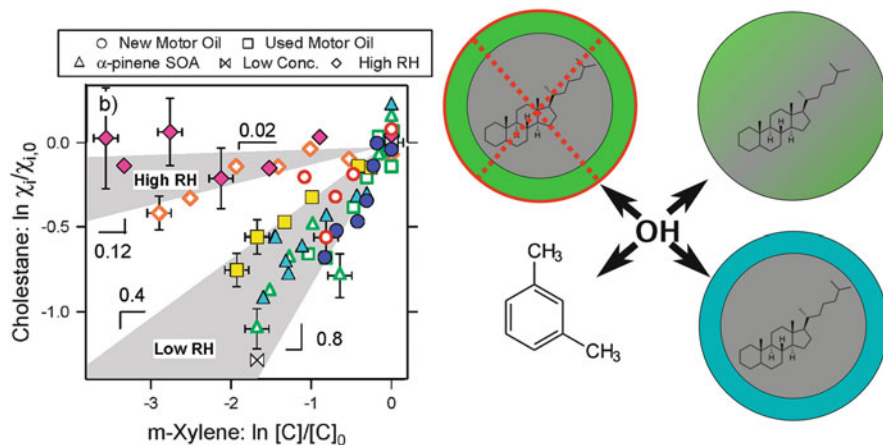
Fig. 12 Relative oxidation rates by OH radicals of condensed-phase cholestane vs gas-phase *m*-xylene in different organic-aerosol matrices, all of which include a high fraction of motor oil. Cholestane oxidation is independent of OA concentration or the presence of a substantial SOA "coating" consisting of up to half of the total particle mass. However, high relative humidity slows cholestane oxidation by an order of magnitude. This suggests that a thin film of water on oil can significantly retard cholestane oxidation, perhaps by excluding the cholestane from the particle surface; the SOA, on the other hand, does not coat the particle surface but rather mixes with the oil and thus does not impede cholestane oxidation

4.3 Aqueous-Phase Aging

In recent years there has been intense interest in the formation and evolution of atmospheric particulate matter within the aqueous phase [170]. Such processes occur by dissolution of organics into a water droplet (deliquesced particle or cloud droplet) followed by oxidation by a dissolved oxidant (most likely OH). Studies of these pathways have been reviewed in detail very recently [118, 171] and so will not be discussed here; instead, as in the previous section, the focus here is on the relationship between partitioning and aging chemistry.

The relative importance of the gas and the aqueous phases as media for the oxidation of organic species depends critically on the fraction of the species present in each phase. This in turn is a function both of the compound's intrinsic tendency to partition between each (as described by its effective Henry's Law Constant, H^*) and the concentration of liquid water present [118]. Thus partitioning into the aqueous phase is governed by the same general considerations as partitioning into the organic phase (which is governed by saturation vapor pressure and organic aerosol loading). In fact, the Henry's Law solubility of a compound is really just a measure of the volatility of that compound over water. As with purely organic mixtures, Raoult's law will apply for ideal solutions, but the activity can be strongly modified by some activity coefficient related to the interaction of that species with water. Accordingly, it is useful to express the Henry's Law solubility as volatility
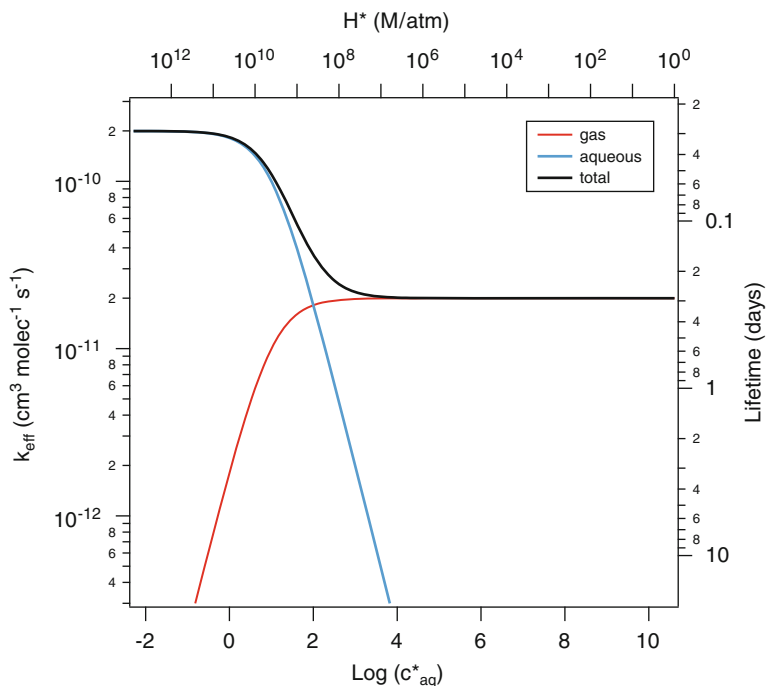
Fig. 13 Effective OH oxidation rate constants for organics in gas phase (*red curve*) and aqueous phase (*cyan curve*) for a gas-phase rate constant of 2×10^{-11} cm^3 molec^{-1} s^{-1} and an effective aqueous-phase OH rate constant of 2×10^{-10} cm^3 molec^{-1} s^{-1}. The principal abscissa is the effective saturation concentration with respect to dissolution in 10 μg m^{-3} of liquid water. Oxidation lifetimes (in days) are given on the left-hand *y* axis, for 2×10^6 OH cm^{-3} in the gas phase

(micrograms per cubic meter), for comparison with the liquid water content (just as C^* can be compared to C_{OA}). Following Ervens et al. [172], this volatility over water is called C_{aq}^*, and is equal to $(R\,T\,H^*/\rho_w)^{-1}$, where H^* is the effective Henry's Law constant (M atm^{-1}), T is temperature (K), R is the gas constant (0.08206 L atm K^{-1} mol^{-1}), and ρ_w is the density of water (10^{12} μg m^{-3}).

Figure 13 shows the effective rate constants for gas-phase and aqueous-phase oxidation as a function of C_{aq}^* (and H^*), assuming a liquid water content (C_w) of 10 μg m^{-3} (a typical ambient value for deliquesced aerosol). This is directly analogous to Fig. 11, which shows the rates of heterogeneous vs gas-phase oxidation as a function of C^*. As in Fig. 11, the gas-phase OH rate constant is set at 2×10^{-11} cm^3 molec^{-1} s^{-1}. The effective aqueous-phase OH rate constant is chosen to be ten times higher at 2×10^{-10} cm^3 molec^{-1} s^{-1}), reflecting the possibility that aqueous OH concentrations may be higher than in the gas phase [173]. (The actual aqueous-phase rate constants can be quite variable, but are

generally similar to those in the gas phase [173].) Even with this higher rate, aqueous-phase oxidation will dominate only when the molecule of interest is exceedingly water soluble ($H^* > 7 \times 10^8$ M atm^{-1}) due to the small amount of liquid water available. Most atmospheric species, even those that are considered to be highly water-soluble (such as glyoxal, glycolaldehyde, and diacids), have H^* well below this threshold [174], and thus will not partition sufficiently into the aerosol aqueous phase to undergo significant aqueous-phase aging under these conditions.

There are several important caveats to this analysis, however. First, OH concentrations in the aqueous phase are highly uncertain, since there are no measurements of [OH] in deliquesced particles or cloud droplets. If aqueous OH concentrations are still higher than indicated in Fig. 13 (as suggested by some models [173]), the threshold for aqueous-phase oxidation would move to higher values of C_{aq}^* (lower values of H^*); on the other hand, if aqueous OH concentrations are lower (as suggested by other models [170]), even lower values of C_{aq}^* (higher values of H^*) would be needed for aqueous oxidation to dominate. This highlights the need for an improved understanding of oxidant concentrations in the atmospheric aqueous phase. Unless there is substantial radical recycling (OH regeneration) in the aqueous phase, aqueous oxidation by OH will be subject to the same diffusion limitations on heterogeneous oxidation.

A second caveat involves the effect of liquid water content C_w; the value used (10 µg m^{-3}) is reasonable for ambient fine particulate matter but would be orders of magnitude higher for cloud water (with C_w as high as 1 g m^{-3}). Under such conditions, partitioning into the aqueous phase will happen for much more volatile species (H^* of 7×10^4 M atm^{-1} or higher), including the water-soluble species mentioned above. Third, this analysis assumes that Henry's Law accurately describes partitioning between the gas and aqueous phase, independent of aqueous-phase concentrations. In reality, the high concentrations in the aerosol aqueous phase are likely to introduce substantial deviations from ideality; these substantial activity coefficients could have a dramatic (and uncertain) effect on partitioning. Finally, under some conditions, particles may include multiple phases [125, 175], so that partitioning between at least three phases (gas, organic, aqueous) must be considered. In such cases the simple two-phase picture in Fig. 13 (or Fig. 11) is insufficient to describe the aging chemistry of the entire system, as the relative values of C^*, C_{aq}^*, C_{OA}, and C_W must be considered when predicting the equilibrium phase of the organic species.

In spite of all these uncertainties, the description of aqueous oxidation in terms of simple partitioning (Fig. 13) clearly shows that only molecules with very large Henry's Law solubilities can undergo significant oxidation in the aqueous phase. This includes highly water-soluble species such as glyoxal, at least when aqueous [OH] and/or liquid water content is high, but categorically excludes all hydrocarbons as well as most monofunctional organic species that have more

than one carbon [174]. It also points to the need to run laboratory studies of aqueous oxidative processing under atmospherically relevant partitioning conditions, with liquid water contents in the range of 10 μg m^{-3} (for deliquesced particles) to 1 g m^{-3} (for cloud water). To date, most (though not all [176, 177]) laboratory studies of aqueous oxidation have been carried out in bulk aqueous solution, with liquid water contents that are far higher than this, on the order of 10^6 g m^{-3} (the density of liquid water). These studies are unlikely to be representative of the gas-droplet partitioning conditions typical of the atmosphere, and thus may not accurately reflect atmospheric aging.

As with heterogeneous oxidation, aqueous-phase oxidation may play an important role in aging water-soluble organics already present in particles, and it can also play a unique role for a small but important set of highly water soluble, low carbon-number organic vapors [172].

5   Conclusions

Phase partitioning and aging chemistry are inexorably linked when considering the chemical evolution of organic aerosol, both because the phase defines the aerosol and because absolute rate of aging depends strongly on the phase holding an organic compound. A key observation in ambient organic aerosol is that the aerosol becomes highly oxidized very rapidly [30, 178, 179]. Heterogeneous oxidation mechanisms appear to be incapable of oxidizing OA with sufficient speed, while gas-phase oxidation can do so. However, heterogeneous processes still compete favorably with the residence time of OA in the atmosphere and thus certainly play an important atmospheric role. In addition, processes that might simply retard mass transfer between the particle and gas phases appear unable to provide sufficiently rapid oxidation.

Overall, the coupling among these multiphase processes, including chemistry in all phases and the equilibria and dynamics of mass transfer among the phases, needs to be described in detail before we can resolve with certainty the relative role of each process under atmospheric conditions. The timescales for all three processes discussed here – gas-phase, heterogeneous, and aqueous-phase oxidation – are competitive with the residence time of particles in the atmosphere. Gas-phase oxidation will win out for most organic vapors because it is homogeneous and fast, but condensed-phase processes may have a vital role in the full maturation of organic aerosol over longer timescales during long-range transport.

References

1. Hildemann LM, Mazurek MA, Cass GR, Simoneit BRT (1991) Quantitative characterization of urban sources of organic aerosol by high-resolution gas-chromatography. Environ Sci Technol 25(7):1311–1325
2. Schauer JJ, Cass GR (2000) Source apportionment of wintertime gas-phase and particle-phase air pollutants using organic compounds as tracers. Environ Sci Technol 34 (9):1821–1832
3. Mazurek MA, Cass GR, Simoneit BRT (1991) Biological input to visibility-reducing aerosol-particles in the remote arid southwestern United States. Environ Sci Technol 25(4):684–694
4. Rogge WF, Hildemann LM, Mazurek MA, Cass GR, Simoneit BRT (1998) Sources of fine organic aerosol. 9. Pine, oak and synthetic log combustion in residential fireplaces. Environ Sci Technol 32(1):13–22
5. Robinson AL, Subramanian R, Donahue NM, Bernardo-Bricker A, Rogge WF (2006) Source apportionment of molecular markers and organic aerosol. 2. Biomass smoke. Environ Sci Technol 40:7811–7819
6. Rogge WF, Hildemann LM, Mazurek MA, Cass GR, Simoneit BRT (1993) Sources of fine organic aerosol. 2. Noncatalyst and catalyst-equipped automobiles and heavy-duty diesel trucks. Environ Sci Technol 27(4):636–651
7. Schauer JJ, Rogge WF, Hildemann LM, Mazurek MA, Cass GR, Simoneit BRT (1996) Source apportionment of airborne particulate matter using organic compounds as tracers. Atmos Environ 30(22):3837–3855
8. Subramanian R, Donahue NM, Bernardo-Bricker A, Rogge WF, Robinson AL (2006) Contribution of motor vehicle emissions to organic carbon and fine particle mass in Pittsburgh. Pennsylvania: effects of varying source profiles and seasonal trends in ambient marker concentrations. Atmos Environ 40:8002–8019
9. Schauer JJ, Kleeman MJ, Cass GR, Simoneit BRT (1999) Measurement of emissions from air pollution sources. 2. C-1 through C-30 organic compounds from medium duty diesel trucks. Environ Sci Technol 33(10):1578–1587
10. Rogge WF, Hildemann LM, Mazurek MA, Cass GR, Simonelt BRT (1991) Sources of fine organic aerosol. 1. Charbroilers and meat cooking operations. Environ Sci Technol 25 (6):1112–1125
11. Nolte CG, Schauer JJ, Cass GR, Simoneit BRT (1999) Highly polar organic compounds present in meat smoke. Environ Sci Technol 33(19):3313–3316
12. Schauer JJ, Fraser MP, Cass GR, Simoneit BRT (2002) Source reconciliation of atmospheric gas-phase and particle-phase pollutants during a severe photochemical smog episode. Environ Sci Technol 36(17):3806–3814
13. Robinson AL, Subramanian R, Donahue NM, Bernardo-Bricker A, Rogge WF (2006) Source apportionment of molecular markers and organic aerosol. 3. Food cooking emissions. Environ Sci Technol 40:7820–7827
14. Rogge WF, Hildemann LM, Mazurek MA, Cass GR (1994) Sources of fine organic aerosol. 6. Cigarette-smoke in the urban atmosphere. Environ Sci Technol 28(7):1375–1388
15. Paulson SE, Pandis SN, Baltensperger U, Seinfeld JH, Flagan RC, Palen EJ, Allen DT, Schaffner C, Giger W, Portmann A (1990) Characterization of photochemical aerosols from biogenic hydrocarbons. J Aerosol Sci 21:S245–S248
16. Kamens R, Jang MS, Hu JX, Coe D, Strommen M (1996) Equilibrium and atmospheric semi-volatiles. Abstr Pap Am Chem Soc 211, 121-ANYL
17. Odum JR, Hoffmann T, Bowman F, Collins D, Flagan RC, Seinfeld JH (1996) Gas/particle partitioning and secondary organic aerosol yields. Environ Sci Technol 30(8):2580–2585
18. Pankow JF (1994) An absorption-model of gas-particle partitioning of organic-compounds in the atmosphere. Atmos Environ 28(2):185–188

19. Liousse C, Penner JE, Chuang C, Walton JJ, Eddleman H, Cachier H (1996) A global three-dimensional model study of carbonaceous aerosols. J Geophys Res Atmos 101 (D14):19411–19432
20. Lurmann FW, Wexler AS, Pandis SN, Musarra S, Kumar N, Seinfeld JH (1997) Modelling urban and regional aerosols. 2. Application to California's south coast air basin. Atmos Environ 31:2695–2715
21. Griffin RJ, Cocker DR, Seinfeld JH, Dabdub D (1999) Estimate of global atmospheric organic aerosol from oxidation of biogenic hydrocarbons. Geophys Res Lett 26 (17):2721–2724
22. Pun BK, Griffin RJ, Seigneur C, Seinfeld JH (2002) Secondary organic aerosol - 2. Thermodynamic model for gas/particle partitioning of molecular constituents. J Geophys Res Atmos 107(D17):D4333. doi:10.1029/2001jd000542
23. Koo BY, Ansari AS, Pandis SN (2003) Integrated approaches to modeling the organic and inorganic atmospheric aerosol components. Atmos Environ 37:4757–4768
24. Spracklen DV, Carslaw KS, Kulmala M, Kerminen VM, Sihto SL, Riipinen I, Merikanto J, Mann GW, Chipperfield MP, Wiedensohler A, Birmili W, Lihavainen H (2008) Contribution of particle formation to global cloud condensation nuclei concentrations. Geophys Res Lett 35(6):L06808. doi:10.1029/2007gl033038
25. Heald CL, Ridley DA, Kreidenweis SM, Drury EE (2010) Satellite observations cap the atmospheric organic aerosol budget. Geophys Res Lett 37:L24808. doi:10.1029/2010gl045095
26. Novakov T, Penner JE (1993) Large contribution of organic aerosols to cloud-condensation-nuclei concentrations. Nature 365(6449):823–826
27. Cruz CN, Pandis SN (1997) A study of the ability of pure secondary organic aerosol to act as cloud condensation nuclei. Atmos Environ 31:2205–2214
28. Huff Hartz KE, Tischuk JE, Chan MN, Chan CK, Donahue NM, Pandis SN (2006) Cloud condensation nuclei activation of limited solubility organic aerosol. Atmos Environ 40:605–617
29. Huffman JA, Docherty KS, Aiken AC, Cubison MJ, Ulbrich IM, DeCarlo PF, Sueper D, Jayne JT, Worsnop DR, Zieann PJ, Jimenez JL (2009) Chemically-resolved aerosol volatility measurements from two megacity field studies. Atmos Chem Phys 9:7161–7182
30. Jimenez JL, Canagaratna MR, Donahue NM, Prevot ASH, Zhang Q, Kroll JH, DeCarlo PF, Allan JD, Coe H, Ng NL, Aiken AC, Docherty KS, Ulbrich IM, Grieshop AP, Robinson AL, Duplissy J, Smith JD, Wilson KR, Lanz VA, Hueglin C, Sun YL, Tian J, Laaksonen A, Raatikainen T, Rautiainen J, Vaattovaara P, Ehn M, Kulmala M, Tomlinson JM, Collins DR, Cubison MJ, Dunlea EJ, Huffman JA, Onasch TB, Alfarra MR, Williams PI, Bower K, Kondo Y, Schneider J, Drewnick F, Borrmann S, Weimer S, Demerjian K, Salcedo D, Cottrell L, Griffin R, Takami A, Miyoshi T, Hatakeyama S, Shimono A, Sun JY, Zhang YM, Dzepina K, Kimmel JR, Sueper D, Jayne JT, Herndon SC, Trimborn AM, Williams LR, Wood EC, Middlebrook AM, Kolb CE, Baltensperger U, Worsnop DR (2009) Evolution of organic aerosols in the atmosphere. Science 326(5959):1525–1529. doi:10.1126/science.1180353
31. Vaden TD, Imre D, Beranek J, Shrivastava M, Zelenyuk A (2011) Evaporation kinetics and phase of laboratory and ambient secondary organic aerosol. Proc Natl Acad Sci USA 108 (6):2190–2195
32. Zobrist B, Marcolli C, Pedernera DA, Koop T (2008) Do atmospheric aerosols form glasses? Atmos Chem Phys 8(17):5221–5244
33. Virtanen A, Joutsensaari J, Koop T, Kannosto J, Yli-Pirila P, Leskinen J, Makela JM, Holopainen JK, Poschl U, Kulmala M, Worsnop DR, Laaksonen A (2010) An amorphous solid state of biogenic secondary organic aerosol particles. Nature 467(7317):824–827
34. Koop T, Bookhold J, Shiraiwa M, Poschl U (2011) Glass transition and phase state of organic compounds: dependency on molecular properties and implications for secondary organic aerosols in the atmosphere. Phys Chem Chem Phys 13(43):19238–19255

35. Goldstein AH, Galbally IE (2007) Known and unexplored organic constituents in the Earth's atmosphere. Environ Sci Technol 41(5):1514–1521
36. Hallquist M, Wenger JC, Baltensperger U, Rudich Y, Simpson D, Claeys M, Dommen J, Donahue NM, George C, Goldstein AH, Hamilton JF, Herrmann H, Hoffmann T, Iinuma Y, Jang M, Jenkin ME, Jimenez JL, Kiendler-Scharr A, Maenhaut W, McFiggans G, Mentel TF, Monod A, Prevot ASH, Seinfeld JH, Surratt JD, Szmigielski R, Wildt J (2009) The formation, properties and impact of secondary organic aerosol: current and emerging issues. Atmos Chem Phys 9(14):5155–5236
37. Spracklen DV, Jimenez JL, Carslaw KS, Worsnop DR, Evans MJ, Mann GW, Zhang Q, Canagaratna MR, Allan J, Coe H, McFiggans G, Rap A, Forster P (2011) Aerosol mass spectrometer constraint on the global secondary organic aerosol budget. Atmos Chem Phys 11(23):12109–12136. doi:10.5194/acp-11-12109-2011
38. Donahue NM, Robinson AL, Pandis SN (2009) Atmospheric organic particulate matter: from smoke to secondary organic aerosol. Atmos Environ 43(1):94–106. doi:10.1016/j. atmosenv.2008.09.055
39. Marcolli C, Luo BP, Peter T, Wienhold FG (2004) Internal mixing of the organic aerosol by gas phase diffusion of semivolatile organic compounds. Atmos Chem Phys 4:2593–2599
40. Donahue NM, Robinson AL, Stanier CO, Pandis SN (2006) Coupled partitioning, dilution, and chemical aging of semivolatile organics. Environ Sci Technol 40:2635–2643
41. Aumont B, Szopa S, Madronich S (2005) Modelling the evolution of organic carbon during its gas-phase tropospheric oxidation: development of an explicit model based on a self generating approach. Atmos Chem Phys 5:2497–2517
42. Fredenslund A, Jones RL, Prausnitz JM (1975) Group-contribution estimation of activity-coefficients in nonideal liquid-mixtures. Aiche J 21(6):1086–1099
43. Clegg SL, Seinfeld JH, Brimblecombe P (2001) Thermodynamic modelling of aqueous aerosols containing electrolytes and dissolved organic compounds. J Aerosol Sci 32(6): 713–738
44. Nannoolal Y, Rarey J, Ramjugernath D (2008) Estimation of pure component properties - Part 3. Estimation of the vapor pressure of non-electrolyte organic compounds via group contributions and group interactions. Fluid Phase Equilib 269(1–2):117–133
45. Zuend A, Marcolli C, Booth AM, Lienhard DM, Soonsin V, Krieger UK, Topping DO, McFiggans G, Peter T, Seinfeld JH (2011) New and extended parameterization of the thermodynamic model AIOMFAC: calculation of activity coefficients for organic–inorganic mixtures containing carboxyl, hydroxyl, carbonyl, ether, ester, alkenyl, alkyl, and aromatic functional groups. Atmos Chem Phys 11(17):9155–9206
46. Chen Q, Liu YJ, Donahue NM, Shilling JE, Martin ST (2011) Particle-phase chemistry of secondary organic material: modeled compared to measured O:C and H:C elemental ratios provide constraints. Environ Sci Technol 45(11):4763–4770
47. Xia AG, Michelangeli DV, Makar PA (2008) Box model studies of the secondary organic aerosol formation under different HC/NO(x) conditions using the subset of the Master Chemical Mechanism for alpha-pinene oxidation. J Geophys Res Atmos 113:D10
48. Capouet M, Mueller JF, Ceulemans K, Compernolle S, Vereecken L, Peeters J (2008) Modeling aerosol formation in alpha-pinene photo-oxidation experiments. J Geophys Res Atmos 113(D2):D02308
49. Valorso R, Aumont B, Camredon M, Raventos-Duran T, Mouchel-Vallon C, Ng NL, Seinfeld JH, Lee-Taylor J, Madronich S (2011) Explicit modelling of SOA formation from alpha-pinene photooxidation: sensitivity to vapour pressure estimation. Atmos Chem Phys 11(14):6895–6910
50. Pun BK, Wu SY, Seigneur C, Seinfeld JH, Griffin RJ, Pandis SN (2003) Uncertainties in modeling secondary organic aerosols: three-dimensional modeling studies in Nashville/ Western Tennessee. Environ Sci Technol 37:3647–3661
51. Kroll JH, Seinfeld JH (2008) Chemistry of secondary organic aerosol: formation and evolution of low-volatility organics in the atmosphere. Atmos Environ 42(16):3593–3624

52. Kroll JH, Ng NL, Murphy SM, Flagan RC, Seinfeld JH (2006) Secondary organic aerosol formation from isoprene photooxidation. Environ Sci Technol 40(6):1869–1877. doi:Doi 10.1021/Es0524301

53. Griffin RJ, Cocker DR, Flagan RC, Seinfeld JH (1999) Organic aerosol formation from the oxidation of biogenic hydrocarbons. J Geophys Res Atmos 104(D3):3555–3567

54. Presto AA, Huff Hartz KE, Donahue NM (2005) Secondary organic aerosol production from terpene ozonolysis. 2. Effect of NOx concentration. Environ Sci Technol 39:7046–7054

55. Barsanti KC, Smith JN, Pankow JF (2011) Application of the np plus mP modeling approach for simulating secondary organic particulate matter formation from alpha-pinene oxidation. Atmos Environ 45(37):6812–6819

56. Grieshop AP, Miracolo MA, Donahue NM, Robinson AL (2009) Constraining the volatility distribution and gas-particle partitioning of combustion aerosols using isothermal dilution and thermodenuder measurements. Environ Sci Technol 43(13):4750–4756. doi:10.1021/es8032378

57. Dommen J, Hellen H, Saurer M, Jaeggi M, Siegwolf R, Metzger A, Duplissy J, Fierz M, Baltensperger U (2009) Determination of the aerosol yield of isoprene in the presence of an organic seed with carbon isotope analysis. Environ Sci Technol 43(17):6697–6702

58. Hildebrandt L, Henry KM, Kroll JH, Worsnop DR, Pandis SN, Donahue NM (2011) Evaluating the mixing of organic aerosol components using high-resolution aerosol mass spectrometry. Environ Sci Technol 45(15):6329–6335

59. Song C, Zaveri RA, Alexander ML, Thornton JA, Madronich S, Ortega JV, Zelenyuk A, Yu X-Y, Laskin A, Maughan DA (2007) Effect of hydrophobic primary organic aerosols on secondary organic aerosol formation from ozonolysis of alpha-pinene. Geophys Res Lett 34 (20):L20803

60. Asa-Awuku A, Miracolo MA, Kroll JH, Robinson AL, Donahue NM (2009) Mixing and phase partitioning of primary and secondary organic aerosols. Geophys Res Lett 36:L15827. doi:10.1029/2009gl039301

61. Pankow JF, Barsanti KC (2009) The carbon number-polarity grid: a means to manage the complexity of the mix of organic compounds when modeling atmospheric organic particulate matter. Atmos Environ 43(17):2829–2835

62. Simoneit BRT, Schauer JJ, Nolte CG, Oros DR, Elias VO, Fraser MP, Rogge WF, Cass GR (1999) Levoglucosan, a tracer for cellulose in biomass burning and atmospheric particles. Atmos Environ 33(2):173–182

63. Donahue NM, Epstein SA, Pandis SN, Robinson AL (2011) A two-dimensional volatility basis set: 1. organic-aerosol mixing thermodynamics. Atmos Chem Phys 11(7):3303–3318

64. Donahue NM, Kroll JH, Pandis SN, Robinson AL (2012) A two-dimensional volatility basis set – part 2: diagnostics of organic-aerosol evolution. Atmos Chem Phys 12:615–634. doi:10.5194/acp-12-615-2012

65. Kroll JH, Donahue NM, Jimenez JL, Kessler SH, Canagaratna MR, Wilson KR, Altieri KE, Mazzoleni LR, Wozniak AS, Bluhm H, Mysak ER, Smith JD, Kolb CE, Worsnop DR (2011) Carbon oxidation state as a metric for describing the chemistry of atmospheric organic aerosol. Nat Chem 3(2):133–139. doi:10.1038/nchem.948

66. Heald CL, Kroll JH, Jimenez JL, Docherty KS, DeCarlo PF, Aiken AC, Chen Q, Martin ST, Farmer DK, Artaxo P (2010) A simplified description of the evolution of organic aerosol composition in the atmosphere. Geophys Res Lett 37:L08803. doi:10.1029/2010gl042737

67. Aiken AC, Decarlo PF, Kroll JH, Worsnop DR, Huffman JA, Docherty KS, Ulbrich IM, Mohr C, Kimmel JR, Sueper D, Sun Y, Zhang Q, Trimborn A, Northway M, Ziemann PJ, Canagaratna MR, Onasch TB, Alfarra MR, Prevot ASH, Dommen J, Duplissy J, Metzger A, Baltensperger U, Jimenez JL (2008) O/C and OM/OC ratios of primary, secondary, and ambient organic aerosols with high-resolution time-of-flight aerosol mass spectrometry. Environ Sci Technol 42(12):4478–4485

68. Epstein SA, Riipinen I, Donahue NM (2010) A semiempirical correlation between enthalpy of vaporization and saturation concentration for organic aerosol. Environ Sci Technol 44 (2):743–748. doi:10.1021/es902497z

69. Cappa CD, Jimenez JL (2010) Quantitative estimates of the volatility of ambient organic aerosol. Atmos Chem Phys 10(12):5409–5424

70. Kulmala M, Toivonen A, Makela JM, Laaksonen A (1998) Analysis of the growth of nucleation mode particles observed in boreal forest. Tellus B Chem Phys Meteorol 50 (5):449–462

71. Anttila T, Kerminen VM, Kulmala M, Laaksonen A, O'Dowd CD (2004) Modelling the formation of organic particles in the atmosphere. Atmos Chem Phys 4:1071–1083

72. Riipinen I, Manninen HE, Yli-Juuti T, Boy M, Sipila M, Ehn M, Junninen H, Petaja T, Kulmala M (2009) Applying the condensation particle counter battery (CPCB) to study the water-affinity of freshly-formed 2–9 nm particles in boreal forest. Atmos Chem Phys 9 (10):3317–3330

73. Riipinen I, Pierce JR, Yli-Juuti T, Nieminen T, Hakkinen S, Ehn M, Junninen H, Lehtipalo K, Petaja T, Slowik J, Chang R, Shantz NC, Abbatt J, Leaitch WR, Kerminen VM, Worsnop DR, Pandis SN, Donahue NM, Kulmala M (2011) Organic condensation: a vital link connecting aerosol formation to cloud condensation nuclei (CCN) concentrations. Atmos Chem Phys 11 (8):3865–3878. doi:10.5194/acp-11-3865-2011

74. Pierce JR, Riipinen I, Kulmala M, Ehn M, Petaja T, Junninen H, Worsnop DR, Donahue NM (2011) Quantification of the volatility of secondary organic compounds in ultrafine particles during nucleation events. Atmos Chem Phys 11(17):9019–9036

75. Donahue NM, Trump ER, Pierce JR, Riipinen I (2011) Theoretical constraints on pure vapor-pressure driven condensation of organics to ultrafine particles. Geophys Res Lett 38:L16801

76. Wexler AS, Lurmann FW, Seinfeld JH (1994) Modeling urban and regional aerosols. 1. Model development. Atmos Environ 28(3):531–546

77. Riipinen I, Pierce JR, Donahue NM, Pandis SN (2010) Equilibration time scales of organic aerosol inside thermodenuders: evaporation kinetics versus thermodynamics. Atmos Environ 44(5):597–607. doi:10.1016/j.atmosenv.2009.11.022

78. Worsnop DR, Zahniser MS, Kolb CE, Gardner JA, Watson LR, Vandoren JM, Jayne JT, Davidovits P (1989) Temperature-dependence of mass accommodation of So2 and H2o2 on aqueous surfaces. J Phys Chem 93(3):1159–1172

79. Ammann M, Pöschl U, Rudich Y (2003) Effects of reversible adsorption and Langmuir-Hinshelwood surface reactions on gas uptake by atmospheric particles. Phys Chem Chem Phys 5(2):351–356

80. Davidovits P, Worsnop DR, Jayne JT, Kolb CE, Winkler P, Vrtala A, Wagner PE, Kulmala M, Lehtinen KEJ, Vesala T, Mozurkewich M (2004) Mass accommodation coefficient of water vapor on liquid water. Geophys Res Lett 31(22):L22111. doi:10.1029/2004gl020835

81. Smith JD, Cappa CD, Drisdell WS, Cohen RC, Saykally RJ (2006) Raman thermometry measurements of free evaporation from liquid water droplets. J Am Chem Soc 128 (39):12892–12898

82. Laaksonen A, Vesala T, Kulmala M, Winkler PM, Wagner PE (2005) Commentary on cloud modelling and the mass accommodation coefficient of water. Atmos Chem Phys 5:461–464

83. Winkler PM, Vrtala A, Wagner PE, Kulmala M, Lehtinen KEJ, Vesala T (2004) Mass and thermal accommodation during gas–liquid condensation of water. Phys Rev Lett 93(7): 075701

84. Kolb CE, Cox RA, Abbatt JPD, Ammann M, Davis EJ, Donaldson DJ, Garrett BC, George C, Griffiths PT, Hanson DR, Kulmala M, McFiggans G, Poschl U, Riipinen I, Rossi MJ, Rudich Y, Wagner PE, Winkler PM, Worsnop DR, O' Dowd CD (2010) An overview of current issues in the uptake of atmospheric trace gases by aerosols and clouds. Atmos Chem Phys 10(21):10561–10605

85. Nogueira JJ, Vazquez SA, Mazyar OA, Hase WL, Perkins BG, Nesbitt DJ, Martinez-Nunez E (2009) Dynamics of CO(2) scattering off a perfluorinated self-assembled monolayer. Influence of the incident collision energy, mass effects, and use of different surface models. J Phys Chem A 113(16):3850–3865

86. Saleh R, Khlystov A, Shihadeh A (2012) Determination of evaporation coefficients of ambient and laboratory-generated semivolatile organic aerosols from phase equilibration kinetics in a thermodenuder. Aerosol Sci Technol 46(1):22–30

87. Shiraiwa M, Ammann M, Koop T, Poschl U (2011) Gas uptake and chemical aging of semisolid organic aerosol particles. Proc Natl Acad Sci USA 108(27):11003–11008

88. Lanz VA, Alfarra MR, Baltensperger U, Buchmann B, Hueglin C, Szidat S, Wehrli MN, Wacker L, Weimer S, Caseiro A, Puxbaum H, Prevot ASH (2008) Source attribution of submicron organic aerosols during wintertime inversions by advanced factor analysis of aerosol mass spectra. Environ Sci Technol 42(1):214–220

89. Fraser MP, Cass GR, Simoneit BRT, Rasmussen RA (1997) Air quality model evaluation data for organics .4. C-2-C-36 non-aromatic hydrocarbons. Environ Sci Technol 31(8):2356–2367

90. Robinson AL, Grieshop AP, Donahue NM, Hunt SW (2010) Updating the conceptual model for fine particle mass emissions from combustion systems. J Air Waste Manag Assoc 60 (10):1204–1222. doi:10.3155/1047-3289.60.10.1204

91. Williams BJ, Goldstein AH, Kreisberg NM, Hering SV (2006) An in-situ instrument for speciated organic composition of atmospheric aerosols: thermal desorption aerosol GC/MS-FID (TAG). Aerosol Sci Technol 40(8):627–638. doi:Doi 10.1080/02786820600754631

92. Lambe AT, Miracolo MA, Hennigan CJ, Robinson AL, Donahue NM (2009) Effective rate constants and uptake coefficients for the reactions of organic molecular markers (n-alkanes, hopanes, and steranes) in motor oil and diesel primary organic aerosols with hydroxyl radicals. Environ Sci Technol 43(23):8794–8800. doi:10.1021/es901745h

93. Miracolo MA, Presto AA, Lambe AT, Hennigan CJ, Donahue NM, Kroll JH, Worsnop DR, Robinson AL (2010) Photo-oxidation of low-volatility organics found in motor vehicle emissions: production and chemical evolution of organic aerosol mass. Environ Sci Technol 44(5):1638–1643. doi:10.1021/es902635c

94. Shrivastava MK, Lipsky EM, Stanier CO, Robinson AL (2006) Modeling semivolatile organic aerosol mass emissions from combustion systems. Environ Sci Technol 40:2671–2677

95. Fraser MP, Cass GR, Simoneit BRT (1998) Gas-phase and particle-phase organic compounds emitted from motor vehicle traffic in a Los Angeles roadway tunnel. Environ Sci Technol 32 (14):2051–2060

96. Yokelson RJ, Crounse JD, DeCarlo PF, Karl T, Urbanski S, Atlas E, Campos T, Shinozuka Y, Kapustin V, Clarke AD, Weinheimer A, Knapp DJ, Montzka DD, Holloway J, Weibring P, Flocke F, Zheng W, Toohey D, Wennberg PO, Wiedinmyer C, Mauldin L, Fried A, Richter D, Walega J, Jimenez JL, Adachi K, Buseck PR, Hall SR, Shetter R (2009) Emissions from biomass burning in the Yucatan. Atmos Chem Phys 9(15):5785–5812

97. Zhang KM, Wexler AS (2004) Evolution of particle number distribution near roadways - part I: analysis of aerosol dynamics and its implications for engine emission measurement. Atmos Environ 38(38):6643–6653

98. Zhang Y, Liu P, Liu XH, Jacobson MZ, McMurry PH, Yu FQ, Yu SC, Schere KL (2010) A comparative study of nucleation parameterizations: 2. Three-dimensional model application and evaluation. J Geophys Res Atmos 115:D20213

99. Guenther A, Hewitt CN, Erickson D, Fall R, Geron C, Graedel T, Harley P, Klinger L, Lerdau M, McKay WA, Pierce T, Scholes B, Steinbrecher R, Tallamraju R, Taylor J, Zimmerman P (1995) A global-model of natural volatile organic-compound emissions. J Geophys Res Atmos 100(D5):8873–8892. doi:10.1029/94jd02950

100. Jaoui M, Kamens RM (2001) Mass balance of gaseous and particulate products analysis from alpha-pinene/NOx/air in the presence of natural sunlight. J Geophys Res Atmos 106 (D12):12541–12558

101. Presto AA, Huff Hartz KE, Donahue NM (2005) Secondary organic aerosol production from terpene ozonolysis. 1. Effect of UV radiation. Environ Sci Technol 39:7036–7045

102. Isaacman G, Worton DR, Kreisberg NM, Hennigan CJ, Teng AP, Hering SV, Robinson AL, Donahue NM, Goldstein AH (2011) Understanding evolution of product composition and volatility distribution through in-situ GC x GC analysis: a case study of longifolene ozonolysis. Atmos Chem Phys 11(11):5335–5346

103. Tolocka MP, Jang M, Ginter JM, Cox FJ, Kamens RM, Johnston MV (2004) Formation of oligomers in secondary organic aerosol. Environ Sci Technol 38(5):1428–1434. doi:Doi 10.1021/Es035030r

104. Baltensperger U, Kalberer M, Dommen J, Paulsen D, Alfarra MR, Coe H, Fisseha R, Gascho A, Gysel M, Nyeki S, Sax M, Steinbacher M, Prevot ASH, Sjogren S, Weingartner E, Zenobi R (2005) Secondary organic aerosols from anthropogenic and biogenic precursors. Faraday Discuss 130:265–278. doi:Doi 10.1039/B417367h

105. Hall WA, Johnston MV (2011) Oligomer content of alpha-pinene secondary organic aerosol. Aerosol Sci Technol 45(1):37–45

106. Surratt JD, Kroll JH, Kleindienst TE, Edney EO, Claeys M, Sorooshian A, Ng NL, Offenberg JH, Lewandowski M, Jaoui M, Flagan RC, Seinfeld JH (2007) Evidence for organosulfates in secondary organic aerosol. Environ Sci Technol 41(2):517–527

107. Kroll JH, Seinfeld JH (2005) Representation of secondary organic aerosol laboratory chamber data for the interpretation of mechanisms of particle growth. Environ Sci Technol 39(11):4159–4165. doi:Doi 10.1021/Es048292h

108. Grieshop AP, Donahue NM, Robinson AL (2007) Is the gas-particle partitioning in alpha-pinene secondary organic aerosol reversible? Geophys Res Lett 34(14):L14810. doi:10.1029/2007gl029987

109. An WJ, Pathak RK, Lee BH, Pandis SN (2007) Aerosol volatility measurement using an improved thermodenuder: application to secondary organic aerosol. J Aerosol Sci 38(3):305–314. doi:10.1016/j.jaerosci.2006.12.002

110. Huffman JA, Ziemann PJ, Jayne JT, Worsnop DR, Jimenez JL (2008) Development and characterization of a fast-stepping/scanning thermodenuder for chemically-resolved aerosol volatility measurements. Aerosol Sci Technol 42(5):395–407

111. Lee BH, Pierce JR, Engelhart GJ, Pandis SN (2011) Volatility of secondary organic aerosol from the ozonolysis of monoterpenes. Atmos Environ 45(14):2443–2452. doi:10.1016/j.atmosenv.2011.02.004

112. Tritscher T, Dommen J, DeCarlo PF, Gysel M, Barmet PB, Praplan AP, Weingartner E, Prévôt ASH, Riipinen I, Donahue NM, Baltensperger U (2011) Volatility and hygroscopicity of aging secondary organic aerosol in a smog chamber. Atmos Chem Phys 11(22):11477–11496. doi:10.5194/acp-11-11477-2011

113. Salo K, Hallquist M, Jonsson AM, Saathoff H, Naumann KH, Spindler C, Tillmann R, Fuchs H, Bohn B, Rubach F, Mentel TF, Muller L, Reinnig M, Hoffmann T, Donahue NM (2011) Volatility of secondary organic aerosol during OH radical induced ageing. Atmos Chem Phys 11(21):11055–11067

114. Kostenidou E, Lee BH, Engelhart GJ, Pierce JR, Pandis SN (2009) Mass spectra deconvolution of low, medium, and high volatility biogenic secondary organic aerosol. Environ Sci Technol 43(13):4884–4889. doi:10.1021/es803676g

115. Lee BH, Kostenidou E, Hildebrandt L, Riipinen I, Engelhart GJ, Mohr C, DeCarlo PF, Mihalopoulos N, Prevot ASH, Baltensperger U, Pandis SN (2010) Measurement of the ambient organic aerosol volatility distribution: application during the Finokalia Aerosol Measurement Experiment (FAME-2008). Atmos Chem Phys 10(24):12149–12160. doi:10.5194/acp-10-12149-2010

116. Simoneit BRT (2002) Biomass burning - a review of organic tracers for smoke from incomplete combustion. Appl Geochem 17(3):129–162

117. Chan MN, Surratt JD, Claeys M, Edgerton ES, Tanner RL, Shaw SL, Zheng M, Knipping EM, Eddingsaas NC, Wennberg PO, Seinfeld JH (2010) Characterization and quantification of isoprene-derived epoxydiols in ambient aerosol in the southeastern United States. Environ Sci Technol 44(12):4590–4596

118. Ervens B, Turpin BJ, Weber RJ (2011) Secondary organic aerosol formation in cloud droplets and aqueous particles (aqSOA): a review of laboratory, field and model studies. Atmos Chem Phys 11(21):11069–11102

119. Maria SF, Russell LM, Gilles MK, Myneni SCB (2004) Organic aerosol growth mechanisms and their climate-forcing implications. Science 306(5703):1921–1924

120. Seinfeld JH, Pandis SN (2006) Atmospheric chemistry and physics, 2nd edn. Wiley, Hoboken

121. Kroll JH, Chan AWH, Ng NL, Flagan RC, Seinfeld JH (2007) Reactions of semivolatile organics and their effects on secondary organic aerosol formation. Environ Sci Technol 41 (10):3545–3550

122. Pathak R, Donahue NM, Pandis SN (2008) Ozonolysis of beta-pinene: temperature dependence of secondary organic aerosol mass fraction. Environ Sci Technol 42(14):5081–5086. doi:10.1021/es070721z

123. Hildebrandt L, Donahue NM, Pandis SN (2009) High formation of secondary organic aerosol from the photo-oxidation of toluene. Atmos Chem Phys 9(9):2973–2986

124. Prisle NL, Engelhart GJ, Bilde M, Donahue NM (2010) Humidity influence on gas-particle phase partitioning of alpha-pinene + O(3) secondary organic aerosol. Geophys Res Lett 37:5. doi:10.1029/2009gl041402

125. Bertram AK, Martin ST, Hanna SJ, Smith ML, Bodsworth A, Chen Q, Kuwata M, Liu A, You Y, Zorn SR (2011) Predicting the relative humidities of liquid-liquid phase separation, efflorescence, and deliquescence of mixed particles of ammonium sulfate, organic material, and water using the organic-to-sulfate mass ratio of the particle and the oxygen-to-carbon elemental ratio of the organic component. Atmos Chem Phys 11(21):10995–11006

126. Zuend A, Marcolli C, Peter T, Seinfeld JH (2010) Computation of liquid-liquid equilibria and phase stabilities: implications for RH-dependent gas/particle partitioning of organic–inorganic aerosols. Atmos Chem Phys 10(16):7795–7820

127. Robinson AL, Donahue NM, Shrivastava MK, Weitkamp EA, Sage AM, Grieshop AP, Lane TE, Pierce JR, Pandis SN (2007) Rethinking organic aerosols: semivolatile emissions and photochemical aging. Science 315(5816):1259–1262

128. Weitkamp EA, Sage AM, Pierce JR, Donahue NM, Robinson AL (2007) Organic aerosol formation from photochemical oxidation of diesel exhaust in a smog chamber. Environ Sci Technol 41(20):6969–6975

129. Sage AM, Weitkamp EA, Robinson AL, Donahue NM (2008) Evolving mass spectra of the oxidized component of organic aerosol: results from aerosol mass spectrometer analyses of aged diesel emissions. Atmos Chem Phys 8(5):1139–1152

130. Zhang Q, Alfarra MR, Worsnop DR, Allan JD, Coe H, Canagaratna MR, Jimenez JL (2005) Deconvolution and quantification of hydrocarbon-like and oxygenated organic aerosols based on aerosol mass spectrometry. Environ Sci Technol 39(13):4938–4952

131. Shilling JE, Chen Q, King SM, Rosenoern T, Kroll JH, Worsnop DR, DeCarlo PF, Aiken AC, Sueper D, Jimenez JL, Martin ST (2009) Loading-dependent elemental composition of alpha-pinene SOA particles. Atmos Chem Phys 9(3):771–782

132. Lim YB, Ziemann PJ (2005) Products and mechanism of secondary organic aerosol formation from reactions of n-alkanes with OH radicals in the presence of NOx. Environ Sci Technol 39(23):9229–9236

133. Presto AA, Miracolo MA, Donahue NM, Robinson AL (2010) Secondary organic aerosol formation from high-NO(x) photo-oxidation of low volatility precursors: n-alkanes. Environ Sci Technol 44(6):2029–2034. doi:10.1021/es903712r

134. Lim YB, Ziemann PJ (2009) Effects of molecular structure on aerosol yields from OH radical-initiated reactions of linear, branched, and cyclic alkanes in the presence of NOx. Environ Sci Technol 43(7):2328–2334

135. Pitts JN, Vancauwenberghe KA, Grosjean D, Schmid JP, Fitz DR, Belser WL, Knudson GB, Hynds PM (1978) Atmospheric reactions of polycyclic aromatic-hydrocarbons - facile formation of mutagenic nitro-derivatives. Science 202(4367):515–519

136. Kamens RM, Fulcher JN, Zhishi G (1986) Effects of temperature on wood soot pah decay in atmospheres with sunlight and low Nox. Atmos Environ 20(8):1579–1587
137. Pankow JF, Isabelle LM, Buchholz DA, Luo WT, Reeves BD (1994) Gas-particle partitioning of polycyclic aromatic-hydrocarbons and alkanes to environmental tobacco-smoke. Environ Sci Technol 28(2):363
138. Pankow JF (1987) Review and comparative-analysis of the theories on partitioning between the gas and aerosol particulate phases in the atmosphere. Atmos Environ 21(11): 2275–2283
139. Pankow JF (1991) Common gamma-intercept and single compound regressions of gas particle partitioning data vs 1/T. Atmos Environ Part A General Topics 25(10):2229–2239
140. Pankow JF (1994) An absorption-model of the gas aerosol partitioning involved in the formation of secondary organic aerosol. Atmos Environ 28(2):189–193
141. Chan AWH, Kautzman KE, Chhabra PS, Surratt JD, Chan MN, Crounse JD, Kurten A, Wennberg PO, Flagan RC, Seinfeld JH (2009) Secondary organic aerosol formation from photooxidation of naphthalene and alkylnaphthalenes: implications for oxidation of interme-diate volatility organic compounds (IVOCs). Atmos Chem Phys 9(9):3049–3060
142. Rogge WF, Hildemann LM, Mazurek MA, Cass GR, Simoneit BRT (1996) Mathematical modeling of atmospheric fine particle-associated primary organic compound concentrations. J Geophys Res Atmos 101(D14):19379–19394
143. Weitkamp EA, Lambe AT, Donahue NM, Robinson AL (2008) Laboratory measurements of the heterogeneous oxidation of condensed-phase organic molecular makers for motor vehicle exhaust. Environ Sci Technol 42(21):7950–7956. doi:10.1021/es800745x
144. Chirico R, DeCarlo PF, Heringa MF, Tritscher T, Richter R, Prevot ASH, Dommen J, Weingartner E, Wehrle G, Gysel M, Laborde M, Baltensperger U (2010) Impact of aftertreatment devices on primary emissions and secondary organic aerosol formation poten-tial from in-use diesel vehicles: results from smog chamber experiments. Atmos Chem Phys 10(23):11545–11563
145. Grieshop AP, Donahue NM, Robinson AL (2009) Laboratory investigation of photochemical oxidation of organic aerosol from wood fires 2: analysis of aerosol mass spectrometer data. Atmos Chem Phys 9(6):2227–2240
146. Heringa MF, DeCarlo PF, Chirico R, Tritscher T, Dommen J, Weingartner E, Richter R, Wehrle G, Prevot ASH, Baltensperger U (2011) Investigations of primary and secondary particulate matter of different wood combustion appliances with a high-resolution time-of-flight aerosol mass spectrometer. Atmos Chem Phys 11(12):5945–5957
147. Miracolo MA, Hennigan CJ, Ranjan M, Nguyen NT, Gordon TD, Lipsky EM, Presto AA, Donahue NM, Robinson AL (2011) Secondary aerosol formation from photochemical aging of aircraft exhaust in a smog chamber. Atmos Chem Phys 11(9):4135–4147
148. Hennigan CJ, Sullivan AP, Collett JL, Robinson AL (2010) Levoglucosan stability in biomass burning particles exposed to hydroxyl radicals. Geophys Res Lett 37:L09806. doi:10.1029/2010gl043088
149. Ng NL, Kroll JH, Keywood MD, Bahreini R, Varutbangkul V, Flagan RC, Seinfeld JH, Lee A, Goldstein AH (2006) Contribution of first- versus second-generation products to secondary organic aerosols formed in the oxidation of biogenic hydrocarbons. Environ Sci Technol 40(7):2283–2297
150. Zhang JY, Hartz KEH, Pandis SN, Donahue NM (2006) Secondary organic aerosol formation from limonene ozonolysis: homogeneous and heterogeneous influences as a function of NOx. J Phys Chem A 110(38):11053–11063
151. Leungsakul S, Jaoui M, Kamens RM (2005) Kinetic mechanism for predicting secondary organic aerosol formation from the reaction of d-limonene with ozone. Environ Sci Technol 39(24):9583–9594
152. Donahue NM, Tischuk JE, Marquis BJ, Huff Hartz KE (2007) Secondary organic aerosol from limona ketone: insights into terpene ozonolysis via synthesis of key intermediates. Phys Chem Chem Phys 9(23):2991–2998

153. Maksymiuk CS, Gayahtri C, Gil RR, Donahue NM (2009) Secondary organic aerosol formation from multiphase oxidation of limonene by ozone: mechanistic constraints via two-dimensional heteronuclear NMR spectroscopy. Phys Chem Chem Phys 11(36): 7810–7818. doi:10.1039/b820005j

154. Claeys M, Szmigielski R, Kourtchev I, Van der Veken P, Vermeylen R, Maenhaut W, Jaoui M, Kleindienst TE, Lewandowski M, Offenberg JH, Edney EO (2007) Hydroxydicarboxylic acids: markers for secondary organic aerosol from the photooxidation of alpha-pinene. Environ Sci Technol 41(5):1628–1634

155. Mueller L, Reinnig MC, Naumann KH, Saathoff H, Mentel TF, Donahue NM, Hoffmann T (2012) Formation of 3-methyl-1,2,3-butanetricarboxylic acid via gas phase oxidation of pinonic acid - a mass spectrometric study of SOA aging. Atmos Chem Phys 12:1483–1496. doi:10.5194/acp-12-1483-2012

156. Chhabra PS, Ng NL, Canagaratna MR, Corrigan AL, Russell LM, Worsnop DR, Flagan RC, Seinfeld JH (2011) Elemental composition and oxidation of chamber organic aerosol. Atmos Chem Phys 11(17):8827–8845

157. Ng NL, Canagaratna MR, Zhang Q, Jimenez JL, Tian J, Ulbrich IM, Kroll JH, Docherty KS, Chhabra PS, Bahreini R, Murphy SM, Seinfeld JH, Hildebrandt L, Donahue NM, DeCarlo PF, Lanz VA, Prevot ASH, Dinar E, Rudich Y, Worsnop DR (2010) Organic aerosol components observed in northern hemispheric datasets from aerosol mass spectrometry. Atmos Chem Phys 10(10):4625–4641. doi:10.5194/acp-10-4625-2010

158. Donahue NM, Henry KM, Mentel TF, Scharr AK, Spindler C, Bohn B, Brauers T, Dorn HP, Fuchs H, Tillmann R, Wahner A, Saathoff H, Naumann KH, Möhler O, Leisner T, Müller L, Reinnig M-C, Hoffmann T, Salow K, Hallquist M, Frosch M, Bilde M, Tritscher T, Barmet P, Praplan AP, DeCarlo PF, Dommen J, Prévôt ASH, Baltensperger U (2012) Aging of biogenic secondary organic aerosol via gas-phase OH radical reactions. Proc Natl Acad Sci 109(34): 13503–13508. doi:10.1073/pnas.1115186109

159. Frosch M, Bilde M, DeCarlo PF, Juranyi Z, Tritscher T, Dommen J, Donahue NM, Gysel M, Weingartner E, Baltensperger U (2011) Relating cloud condensation nuclei activity and oxidation level of alpha-pinene secondary organic aerosols. J Geophys Res Atmos 116: D22212

160. Barmet P, Dommen J, DeCarlo PF, Tritscher T, Praplan AP, Platt SM, Prévôt ASH, Donahue NM, Baltensperger U (2012) OH clock determination by proton transfer reaction mass spectrometry at an environmental chamber. Atmos Meas Tech 5:7471–7498. doi:10.5194/amt-5-647-2012

161. Rudich Y, Donahue NM, Mentel TF (2007) Aging of organic aerosol: bridging the gap between laboratory and field studies. Annu Rev Phys Chem 58:321–352

162. Massoli P, Lambe AT, Ahern AT, Williams LR, Ehn M, Mikkila J, Canagaratna MR, Brune WH, Onasch TB, Jayne JT, Petaja T, Kulmala M, Laaksonen A, Kolb CE, Davidovits P, Worsnop DR (2011) Relationship between aerosol oxidation level and hygroscopic properties of laboratory generated secondary organic aerosol (SOA) particles (vol 37, L24801, 2010). Geophys Res Lett 38:L03805. doi:10.1029/2011gl046687

163. Hearn JD, Lovett AJ, Smith GD (2005) Ozonolysis of oleic acid particles: evidence for a surface reaction and secondary reactions involving Criegee intermediates. Phys Chem Chem Phys 7(3):501–511

164. Sage AM, Weitkamp EA, Robinson AL, Donahue NM (2009) Reactivity of oleic acid in organic particles: changes in oxidant uptake and reaction stoichiometry with particle oxidation. Phys Chem Chem Phys 11(36):7951–7962. doi:10.1039/b904285g

165. Donahue NM, Robinson AL, Hartz KEH, Sage AM, Weitkamp EA (2005) Competitive oxidation in atmospheric aerosols: the case for relative kinetics. Geophys Res Lett 32:L16805

166. Huff Hartz KE, Weitkamp EA, Sage AM, Donahue NM, Robinson AL (2007) Laboratory measurements of the oxidation kinetics of organic aerosol mixtures using a relative rate constants approach. J Geophys Res Atmos 112:D04204

167. Wagstrom KM, Pandis SN (2009) Determination of the age distribution of primary and secondary aerosol species using a chemical transport model. J Geophys Res Atmos 114: D14303. doi:10.1029/2009jd011784

168. Worsnop DR, Morris JW, Shi Q, Davidovits P, Kolb CE (2002) A chemical kinetic model for reactive transformations of aerosol particles. Geophys Res Lett 29(20):1996

169. Smith JD, Kroll JH, Cappa CD, Che DL, Liu CL, Ahmed M, Leone SR, Worsnop DR, Wilson KR (2009) The heterogeneous reaction of hydroxyl radicals with sub-micron squalane particles: a model system for understanding the oxidative aging of ambient aerosols. Atmos Chem Phys 9(9):3209–3222

170. Lim HJ, Carlton AG, Turpin BJ (2005) Isoprene forms secondary organic aerosol through cloud processing: model simulations. Environ Sci Technol 39(12):4441–4446

171. Lim YB, Tan Y, Perri MJ, Seitzinger SP, Turpin BJ (2010) Aqueous chemistry and its role in secondary organic aerosol (SOA) formation. Atmos Chem Phys 10(21):10521–10539

172. Ervens B, Volkamer R (2010) Glyoxal processing by aerosol multiphase chemistry: towards a kinetic modeling framework of secondary organic aerosol formation in aqueous particles. Atmos Chem Phys 10(17):8219–8244

173. Herrmann H, Hoffmann D, Schaefer T, Brauer P, Tilgner A (2010) Tropospheric aqueous-phase free-radical chemistry: radical sources, spectra. Reaction kinetics and prediction tools. Chemphyschem 11(18):3796–3822

174. Sander R (1999) Compilation of Henry's law constants for inorganic and organic species of potential importance in environmental chemistry. http://www.rolf-sander.net/henry/henry.pdf

175. Griffin RJ, Nguyen K, Dabdub D, Seinfeld JH (2003) A coupled hydrophobic-hydrophilic model for predicting secondary organic aerosol formation. J Atmos Chem 44(2):171–190

176. Volkamer R, Ziemann PJ, Molina MJ (2009) Secondary organic aerosol formation from acetylene (C(2)H(2)): seed effect on SOA yields due to organic photochemistry in the aerosol aqueous phase. Atmos Chem Phys 9(6):1907–1928

177. Galloway MM, Huisman AJ, Yee LD, Chan AWH, Loza CL, Seinfeld JH, Keutsch FN (2011) Yields of oxidized volatile organic compounds during the OH radical initiated oxidation of isoprene, methyl vinyl ketone, and methacrolein under high-NO(x) conditions. Atmos Chem Phys 11(21):10779–10790

178. DeCarlo PF, Dunlea EJ, Kimmel JR, Aiken AC, Sueper D, Crounse J, Wennberg PO, Emmons L, Shinozuka Y, Clarke A, Zhou J, Tomlinson J, Collins DR, Knapp D, Weinheimer AJ, Montzka DD, Campos T, Jimenez JL (2008) Fast airborne aerosol size and chemistry measurements above Mexico City and central Mexico during the MILAGRO campaign. Atmos Chem Phys 8(14):4027–4048

179. Hildebrandt L, Kostenidou E, Mihalopoulos N, Worsnop DR, Donahue NM, Pandis SN (2010) Formation of highly oxygenated organic aerosol in the atmosphere: insights from the Finokalia aerosol measurement experiments. Geophys Res Lett 37:L23801. doi:10.1029/2010gl045193

Bio-Organic Materials in the Atmosphere and Snow: Measurement and Characterization

P.A. Ariya, G. Kos, R. Mortazavi, E.D. Hudson, V. Kanthasamy, N. Eltouny, J. Sun, and C. Wilde

Abstract Bio-organic chemicals are ubiquitous in the Earth's atmosphere and at air-snow interfaces, as well as in aerosols and in clouds. It has been known for centuries that airborne biological matter plays various roles in the transmission of disease in humans and in ecosystems. The implication of chemical compounds of biological origins in cloud condensation and in ice nucleation processes has also been studied during the last few decades, and implications have been suggested in the reduction of visibility, in the influence on oxidative potential of the atmosphere and transformation of compounds in the atmosphere, in the formation of haze, change of snow-ice albedo, in agricultural processes, and bio-hazards and bio-terrorism. In this review we critically examine existing observation data on bio-organic compounds in the atmosphere and in snow. We also review both conventional and cutting-edge analytical techniques and methods for measurement and characterisation of bio-organic compounds and specifically for microbial communities, in the atmosphere and snow. We also explore the link between biological compounds and nucleation processes. Due to increased interest in decreasing emissions of carbon-containing compounds, we also briefly review (in an Appendix) methods and techniques that are currently deployed for bio-organic remediation.

Keywords Bio-organic materials · Atmosphere · Snow · Measurement · Methods

P.A. Ariya (✉), G. Kos, R. Mortazavi, E.D. Hudson, V. Kanthasamy, N. Eltouny, J. Sun, and C. Wilde
Departments of Chemistry, Atmospheric and Oceanic Sciences, McGill University, 801 Sherbrooke St. W., Montreal, QC, Canada
e-mail: parisa.ariya@mcgill.ca

Contents

1 Introduction

Airborne condensed bio-organic materials are called bioaerosols. These include biological particles of living beings (or dead bodies) such as viruses, bacteria, fungi and algae, as well as remnants of biological activities such as macromolecules and (semi)volatile organic compounds. They can be emitted directly to the atmosphere (primary source) or formed through (photo)chemical reactions of primary bioaerosols (secondary source) in the atmosphere or at environmental interfaces. Selected chemical reactions of gas-phase volatile organic compounds (VOC) lead to the formation of less volatile compounds, which can form new aerosols or be taken up by existing atmospheric particles. The importance of organic compounds such as cloud condensation and ice forming nuclei has now been recognised. Moreover, the importance of bio-organic matter such as green algae and bacteria in snow and ice colour is known to affect the ice/snow reflectivity or albedo. There is an increasing body of evidence pointing to the importance of the impact of bio-organic matter, over the tropical and sub-tropical forests, on the chemistry and physics of the atmosphere [1, 2], and even in studies of biological weapons [3, 4]. In recent years, many reports have indicated an association between the presence of bioaerosols (indoor or outdoor) and several respiratory, cardiovascular and health disorders (e.g. cancer) [3, 4]. These processes and interactions are summarised and illustrated in Fig. 1.

The role of bio-organic matter at atmospheric interfaces has also been studied. In this review we focus on snow. The chemical composition of the snow pack has received increased attention in recent years, focusing first on inorganic and selected organic species, e.g. organic acids and PAH [5]. It has been shown that the snow pack acts as source and sink of chemical species and that it has the ability to transform compounds through photochemical and biological processes (metabolisation) [6–9]. As a consequence, the chemical profile and concentrations
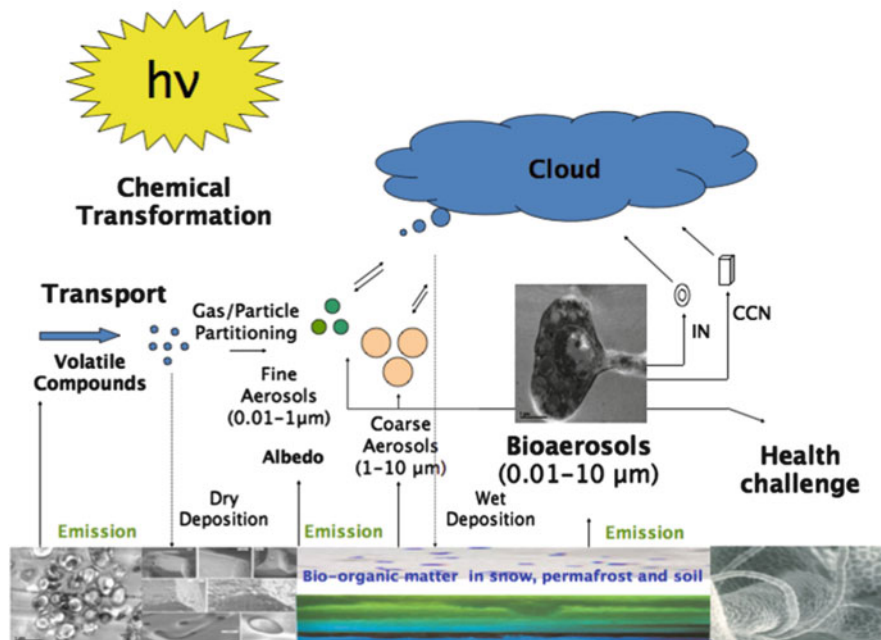
Fig. 1 Simplified schematic of the role of bioaerosols in atmospheric processes

of atmospheric species are dynamically changed. The chemical processes involved may be very different from atmospheric reactions; as a result, the compounds released into, or removed from, the troposphere by these processes may be very different from those resulting from atmospheric processes alone [5, 10–12].

The foremost reason for these differences is the complex and variable structure of the snow pack, which acts as a reaction medium for snow chemical reactions [13]. Gaseous (interstitial air), liquid (water) and solid (ice) phases are present at different ratios. The availability of reaction surfaces and media is typically very large, and is exemplified by fine structure ice crystals, which change over time as the snow pack consolidates and ages. The snow pack density, which regulates the penetration depth of solar radiation and wind pumping, also changes over time. These influence photochemistry and the supply of reactants deposited into the snowpack and volatilisation of products [14]. The snowpack therefore potentially plays a significant role in the availability and transformation of organic and inorganic compounds in the boundary layer of the atmosphere. Given that large parts of both hemispheres are covered with snow for at least parts of the year [15, 16], it will profoundly influence not only the planetary albedo but also the processing of atmospheric chemical species. Snow pack physical properties related to snow photochemistry have been previously investigated and summarized [17].

Organic species present in the snow pack have not, however, been fully explored. Some were suggested to have direct biological origins, while others result

from photochemical processes involving dissolved organic compounds [18, 19]. The chemistry of volatile organic species (VOC), such as the light aldehydes that directly affect atmospheric photochemistry through the production of HO$_x$ radicals, is quite well studied [20]. A large variety of other VOC and semi-volatile VOC (SVOC) species with different chemical functionalities have been shown to occur, but their chemical change in the snow pack remains largely unexplored [21].

SVOCs are higher aldehydes (e.g. nonanal), aromatics (e.g. toluene, acetophenone) and compounds with six or more carbon atoms that have relatively long atmospheric lifetimes compared to very volatile species such as formaldehyde. SVOCs have biological and anthropogenic origins. The differentiation between VOC and SVOC is not standardised and as a consequence the terms are always used in conjunction with the compounds to be discussed. The United States Environmental Protection Agency (USEPA) [22], citing the World Health Organisation (WHO), defined very VOC as having a boiling point of <0 to 50–100°C, VOC as boiling between 50–100 and 240–260°C and semi-volatile organic compounds as boiling between 240–260 and 380–400°C. This definition encompasses a wide range of species with different properties, and reflects the need for detailed explanations in the scientific literature.

SVOCs, e.g. toluene [23], are nevertheless photochemically active species. Furthermore, and relevant for snow pack chemistry, a number of species, e.g. dicarboxylic acids [10], can serve as nutrients for bacteria and fungi. Substituted aromatic species are the subject of significant research regarding degradation by micro-organisms for bioremediation purposes [24]. It can be speculated as to whether volatile photochemical and microbiological degradation products can be re-emitted into the atmosphere, or whether this kind of degradation permanently removes organic species from the atmospheric carbon pool.

Preliminary laboratory studies suggest that irradiation with the solar energy spectrum results in changes to the chemical composition of melted snow [13], providing further motivation to study the decomposition of organic species in the snow pack. However, the analysis of the chemical composition of snow is complex and challenging. The photochemical and biochemical availability would depend on whether the compound is principally found in the ice, liquid or interstitial air phases, and on suitable conditions for penetration of UV radiation and microbiological growth [25].

Since there are several excellent review papers on ice nucleation by biological particles [26, 27], cloud nucleation processes involving bio-materials, aerosol analysis and microbiology of bio-particles, we intend here (1) to provide a summary of the existing measurements of bio-organic materials in the atmosphere and snow and (2) to review critically the atmospheric analytical techniques for measurement and characterization of bio-organic matter in the gas-phase, aerosol and ice matrices in atmosphere and atmosphere-snow interfaces. We will explore their advantages and disadvantages, and will provide suggestions for progress in this field.

2   Measurement and Characterization of Bio-Organic Material

The assessment of the role of biogenic and bioavailable compounds in the environment is a multi-faceted process that starts with the determination of concentrations of individual compounds or compound groups in one or multiple environmental matrices (e.g. air, soil, water). As a next step, it would then be possible to assess their role, transformation, sources and sinks. A number of analytical methods with different degrees of sensitivity and specificity have been reported and the following section focuses on the compounds listed in Table 1 and selected matrices that have received increased attention by researchers in recent years such as the snowpack, where a large number of species (up to 50%) remain unidentified [28]. It is noteworthy that several techniques described in this chapter can be used in a complementary manner. Furthermore, a subsection deals with the determination of biological species themselves, i.e. bacteria and fungi. While organic species might be of either anthropogenic or biogenic origin, or both, the method of environmental analysis is the same and typically non-discriminatory. Source attribution is carried out by including additional information (e.g. emission inventories) or experiments (e.g. bacterial degradation of organics under similar, but controlled conditions and isotope measurements).

2.1   Methods for and Concentrations of Biogenic and Bioavailable Organic Compounds in Snow and in Air

For the determination of volatile organic species in snow or the snow/air interface, sampling procedures play a key role in determining how representative and interpretable the analysis results are [29]. Since most of these compounds are present at low concentrations (mixing ratios of low ppb to high ppt range), sample pre-concentration is generally employed prior to analysis. Typically, gas-phase samples are collected by drawing air through Teflon™ tubes into preconditioned stainless-steel canisters for later analysis or into a pre-concentration set-up for in situ analysis [30]. Firn air, which is interstitial air from multi-year aged and compressed snow, was previously sampled using a stainless steel probe. It consists of a stainless steel cylinder through which a Teflon™ sampling line is inserted. A Teflon™ stainless tube and then the probe were carefully inserted so as not to disturb the snowpack. The temperature was monitored with a thermocouple mounted on the tip of the probe [19, 31]. Interstitial air sampling was also tested by Albert et al. [32] using a Teflon™ snow probe that was inserted into a hole drilled into the snow pack and pumping sample air into the laboratory for the

Table 1 Characteristics of biogenic and biological organic constituents of the atmosphere

Compound class or particle type	Typical concentration(s) (continental/marine, remote/rural/urban)	Principal biogenic sources	Atmospheric residence time
Hydrocarbons			
Methane	1.7 ppmv [184]	Bacterial anaerobic respiration	10 years [31]
Aliphatic	Pptv–ppbv Continental: 3–50 ppbv total alkanes) [185]	Terrestrial plants [185], marine phytoplankton [186, 187]	Minutes–weeks [185]
Aldehydes and ketones	10–20 ppbv or more total (urban) [188] 10^{-2} pptv–10^{0} ppbv (remote marine) [189–193]	Terrestrial plants [194], marine plankton [195–198]	0.07–28 days (calculated from [20])
Alcohols	Typically 10^{1}–10^{2} ppbv (urban) [199]; methanol: background >3 ppbv (marine), 6 ppbv (rural) [200]	Terrestrial plants [201, 202]	Methanol: 10 days [203]; ethanol: 3.5 days [204]
Carboxylic acids	C_1–C_4 in mountain cloud water: 2.27 mg L^{-1} [205] Total aerosol dicarboxylic acids: 7–605 ng m^{-3} (average 85 ng m^{-3}) (remote marine) [70]	Vegetation [206, 207], soil bacteria [208]	Photo-oxidation: <25 days [49] Wet/dry deposition: h^{-1} week [209]
Amines	<1–14 nmol N m^{-3} [84]	Marine algae and bacteria, vegetation [211]	Hours [211][b]
Peptides/proteins	Protein-containing particles: <10 cm^{-3} [210]		

Class	Concentration	Sources	Lifetime/notes
Halocarbons	Methyl chloride: 540 pptv [212] Chloroform: 16 pptv [212] Other chlorocarbons at lower concentrations [212] 1 ppbv Cl total [213] Bromocarbons: ≤10 pptv each (20 pptv Br total) [214]	Marine algae [215–219] Forest and grassland soils [220–222], forest fungi [223]	<2 years[a] [213]
Sulphur compounds	Dimethyl sulphide (DMS): 50–100 pptv (clean marine, Atlantic) [224] Methanethiol: <5 pptv (remote continental/ marine) [225]	Marine bacteria/phytoplankton [224, 226], vegetation [227]	DMS typically <1 day [225]
Lipids	Remote marine: 10^{-1}–10^{1} ng m^{-3} for each lipid class [228] 68–4,300 ng m^{-3} total lipid (-petroleum residue) [229]	Sea surface, terrestrial plants [229]	
Carbohydrates	Forest: 10–180 ng m^{-3} total aerosol sugars [230]	Marine organic carbon (POC, DOC) [231], vegetation, fungal spores [230, 232]	

(continued)

Table 1 (continued)

Compound class or particle type	Typical concentration(s) (continental/ marine, remote/rural/urban)	Principal biogenic sources	Atmospheric residence time
	Open ocean: <0.4 μg m^{-3} in aerosols [231] Cellulose: 0.374 μg m^{-3} (urban) [25]		
Bacteria	1 × 10^4 m^{-3} (marine), 1.1 × 10^5 m^{-3} (cropland), 6.5 × 10^5 m^{-3} (urban) [233]	(Biogenic)	Days [234]
Viruses	3 × 10^4 m^{-3}, 60 ng m^{-3} [234]	(Biogenic)	<1 day [234, 235]
Fungi (spores)	~1 μg m^{-3} (global) [236] 3,000 m^{-3} [237] 357–2,900 m^{-3} [238] <3,200 m^{-3} [239] <8,761 m^{-3} (rural) [240]	(Biogenic)	0.03–10 days, depending on particle size and emission altitude (modelled) [241]

Ppmv parts per million volume, *ppbv* parts per billion volume, *pptv* parts per trillion volume

[a]While many chlorocarbons present in the atmosphere have lifetimes exceeding 2 years, those from natural sources all have lifetimes shorter than 2 years [212]; bromo- and iodocarbons typically have much shorter lifetimes [214, 215]

[b]Half-lives against OH oxidation

determination of ozone. The authors critically evaluated the approach of continuous sampling causing advection from different depths of atmospheric air. Sampling of discrete volumes from each layer would be preferable. Other interstitial air sampling methods included direct sampling for flow injection analysis and the use of stainless steel probes [33–35]. Pumps have also been used for the transfer of firn air into glass and stainless-steel flasks employing transfer lines made of nylon and Dekabon, a polyethylene–aluminium composite [36, 37]. Although not for analysis of organics, a snow sampling tower fitted with inlets at several depth levels was employed for interstitial air sampling [38, 39]. Sampling of filtered air was achieved using sampling lines employing pumps at a rate of 1.2 mL min^{-1} for 12 min at each depth level, followed by 48 min equilibration time in order to minimise artificial air flow. (Interstitial) air sampling for analysis for VOC and SVOC employing proton transfer mass spectrometry (PTR-MS) required comparatively high flows of 3–100 standard litres per minute (slpm), the former for interstitial air, the latter for air sampled by two inlets, suggesting artificial air flows for the former (especially given the relatively shallow burial depth of 15 cm in the snow pack [40]). The air sampling procedures described are quite generic and suitable for gaseous or very small particulate species (i.e. passing a 1-μm filter), provided that interaction with tubing or pumps causing loss of species by adhesion or reaction is avoided. Further sample treatment such as adsorption [41], chemical reaction (e.g. by derivatization) [42] or specific detection methods, e.g. PTR-MS [40], determine which species can be investigated.

A similar principle (generic sampling, then specificity achieved by preparation and analysis) applies to snow sampling. In the majority of recent studies, grab sampling of solid surface snow or pit sampling of defined strata was carried out (e.g. [43, 44]). Clean aluminium and stainless steel tools were usually employed, although the pre-cleaning procedure was not always specified in detail [45]. Core samplers were also employed and resolution by strata may or may not have been provided [46]. The concentration of a wide variety of organic compounds in the snow was determined using melted snow samples collected in glass jars or glass vials with Teflon-lined lids [31, 47–51]. Specialised samplers for organic species have been developed to overcome losses usually observed during grab sampling and melting before analysis, though these devices are not widely used. These samplers are gas tight and enable separation of the ice from liquid melt water. All three phases can then be probed separately [29]. Herbert et al. [52] provided a tabular summary of tools and containers used for snow sampling in previous studies. While grab sampling is popular, convenient and easy to use, care has to be taken when interpreting the data. While representativeness for the liquid water and ice phase is maintained as a sum parameter, species present in interstitial air are not properly accounted for. Sampling snow into a dedicated container will also shift the different phase equilibria of the species under investigation, making this approach error-prone and subject to positive and negative artefacts. In general, however, any of the described set-ups for inorganic trace gases could be envisioned

for the determination of organics, provided the sampled air can be transferred to a suitable system for analysis or containers such as electropolished canisters or by direct transfer to an analysis system.

2.1.1 Determination of Organics

Low molecular weight organic compounds play an important role in the chemistry of the polar troposphere by influencing its oxidative capacity [35]. Observations, monitoring enrichment and losses in firn air or interstitial air compared to tropo-sphere concentrations require simultaneous measurements in all matrices [35]. For example, formaldehyde is the most investigated low molecular weight carbonyl compound in the polar regions and its concentrations in firn air, ambient air and melted snow samples have been widely reported in the literature. Formaldehyde was mostly analysed by flow injection analysis (FIA) with a fluorescence detector, e.g. [53]. Gas phase formaldehyde was scrubbed into a liquid phase, derivatised using a suitable agent and then analysed with a fluorescence detector in a flow system set-up [19, 31, 51, 54–59]. Chromatography was also often used for separation prior to analysis. For example, gas-phase formaldehyde was first extracted into water through a Nafion™ membrane diffusion scrubber, wet effluent diffusion denuder or coil scrubber and then reacted with 1,3-cyclohexanedione or 2,4-pentanedione and ammonium acetate for derivatisation. The fluorescent prod-uct (emission at 465 nm) was then analysed [31, 60]. Interference from atmospheric hydrogen peroxide was noted for this reaction since it also reacts with cyclohex-anedione to form a competing fluorescent product and hydrogen peroxide-free water was used as a scrubber [56]. However, it was shown that this interference is insignificant in most cases compared to the measurement uncertainty at low formaldehyde/hydrogen peroxide ratios [31]. Similarly gas-phase acetaldehyde and acetone were analysed by derivatising with DaNSyl-Acetamido-Oxy-Amine (DNSAOA), separated using HPLC and quantified with a fluorescence detector [47, 49]. Acetaldehyde and acetone in firn air and ambient air were also measured using a gas chromatography/ion-trap mass spectrometry (GC-ITMS) in which they were detected as their CH_3CO^+ ion fragment (43 amu) [61]. GC-MS-FID with pre-concentration using stainless steel tubes filled with adsorbents such as Carbotrap™ and Carbosieve™ was also employed for the detection of other low molecular weight compounds such as methanol, ethanol, propanal, butanal and methyl ethyl ketone in interstitial air [33]. GC-FID was common instrumentation used for the analysis of lightweight alkanes and alkenes such as propane, ethane, ethene and ethyne [33]. Compounds such as methyl bromide and methyl iodide are measured with a combination of GC-MS with FID and ECD detectors [30]. Swanson et al. [44] demonstrated the selective use of analytical methodologies for optimised sensitivity by determining C_2–C_6 hydrocarbons employing GC-FID, C_1–C_2 halocarbons and C_1–C_5 alkyl nitrates by GC-MS.

Similar to their analysis in air, light aldehydes and ketones in the melted snow samples were chemically modified using a derivatising agent in order to bring their molecular mass and detection sensitivity into the optimal detector range, separated chromatographically, and then analysed using a suitable detector [57, 62]. Bhatia et al. have analyzed the dissolved organic carbon species in snow and ice in samples from the Greenland ice sheet via electro-spray ionization (ESI) coupled to a Fourier transform ion cyclotron resonance mass spectrometer (ESI FTICR-MS). Source attribution is carried out (with dissolved organic compound species originating from soot, but also a number of biological sources such as lignins, protein and lipids [63]. Dissolved organic matter was also characterised using ^{1}H NMR spectroscopy. Results highlighted the importance of microbial sources for organic species in Antarctic glacier ice [64].

In the case of carboxylic acids, analytical procedures are quite different due to their ionic character. Ion chromatography is the method of choice for more volatile carboxylic acids and data are regularly included with inorganic analysis of major ions such as phosphate and sulphate [65, 66]. Formic, acetic and propionic acids are most commonly reported. Recent studies have only been carried out in air. Concentrations in snow were most recently reported by Kippenberger and co-workers [67], who used a liquid chromatography method with time of flight mass spectrometric detection on snow samples from the Fee glacier in Switzerland (at altitudes from 3,056 to 3,580 m asl). The authors also provided older comparison data from remote and urban sites [68–70].

The determination of amines in the atmosphere is rarely carried out. In the recent past only a small number of reports have been published [71–73]. Akyüz [71] provided amine concentrations in Zonguklak province, Turkey. Example concentration ranges are given in Table 2. Finessi et al. [73] determined amines as part of the evaluation of the biogenic secondary aerosol fraction in boreal forest samples employing Aerosol Mass Spectrometry (AMS). The current state-of-the-art of AMS was summarised by Pratt et al. in a two-part review [74, 75], discussing off-line and on-line mass spectrometric analysis of aerosols. On-line AMS provides fast, real time characterisation of the atmosphere's aerosol load, typically implemented with a particle sizer in order to obtain the aerosol size distribution [76–80]. Samples are collected at ambient pressure and transferred into the vacuum via a series of electronic focusing lenses. Ionization is available via hard (electron impact) and soft (chemical ionization) techniques to generate mass spectra with different degrees of fragmentation, which are subsequently detected through quadrupole or time of flight (TOF) mass filters [81]. The former provides a robust set-up with unit mass resolution and a maximum m/z limit of 700, suitable for smaller species. The latter has a high mass range and better resolution that is well suited for large molecules. A special case is chemical ionization using H^+ ions from water molecules (i.e. proton transfer reactions) leading to very little fragmentation. Recent proton transfer reaction mass spectrometric (PTR-MS) results determining organic species in snow and air were reported by Gao et al. [40]. Off-line

Table 2 Summary of analytical methodology for the determination of VOC in snow. Concentrations as given by the authors for the original publication

Compound	Concentrations	Methodology	Location/campaign	Type	Reference
Formaldehyde	300–1,500 ppt	FIA-FLD	Alert 1999	Gas phase (1 m above snow pack)	[31]
	50–200 ppt	FIA-FLD			[55]
	200–600 ppt	FIA-FLD			[54]
	100–370 ppt (dark period) 35–360 ppt (after full sunrise)	FIA-FLD (LOD 20 ppt)	Alert 2000	Ambient	[19]
	120 ppt	FIA-FLD (LOD 30 ppt)	Alert 2000	Ambient	[55]
	0.40 ppb max (winter) 0.10–0.70 ppb (summer)	FIA-FLD	Neumayer, Antarctica	Ambient	[58]
	27–184 pptv	FIA-FLD (LOD < 40 ppt)	Amundsen–Scott, Antarctica	Ambient	[51]
	12.2–22.1 ppbw	FIA-FLD (LOD 0.19 ppbw)	Amundsen–Scott, Antarctica	Frost	[51]
	425–1,238 pptv	FIA-FLD (LOD <40 ppt)	Amundsen–Scott, Antarctica	Fir air	[51]
	0.3–6 ppbw 1.4–5 ppbw 0.2 ppbw 3.5 ppbw	FIA-FLD	Amundsen–Scott, Antarctica Siple Dome Antarctica Dome C, Antarctica Summit, Greenland	Snow	[62]
	50–200 pptv	FIA-FLD (LOD < 0.05 ppbv)	Antarctica	Ambient	[59]
	78–372 ppt (dark period) 52–690 ppt (sunlit period)	FIA-FLD	Arctic	Ambient	[35]

	Concentration	Method	Location	Phase	Ref.
	12.5 ppbw (diamond dust, winter) 8 ppbw (surface snow, winter) 4.7 ppbw (wind packed, winter) 1.2 ppbw (depth hoar, winter) 6.5 ppbw (diamond dust, spring) 7 ppbw (crusted snow, spring) 6.5 ppbw (loose snow, spring) 6.2 ppbw (semi-hard snow, spring) 3.5 ppbw (wind packed, spring) 0.2 ppbw (depth hoar, spring)	DNSAOA derivatisation with FLD after HPLC separation (LOD < 0.3 ppbw)	Alert 2000	Snow	[57]
	200 pptv (winter) 150 pptv (spring)	FIA-FLD	Alert 2000	Gas phase	[57]
Acetaldehyde	0.11–2.57 ppbw	DNSAOA derivatisation with FLD after HPLC separation (LOD 0.05 ppbw)	Near Fairbanks, AK	Snowpack	[47]
	2.5 ppbw (fresh surface snow, February) 1.3–2.6 ppbw (aged layers, February) 5–10 ppbw (fresh surface snow, April) 0.7–3 ppbw (aged layers, April)	DNSAOA derivatisation with FLD after HPLC separation (LOD 0.1–0.3 ppbw)	Alert, NU	Snow	[57]
	75 pptv (February) 230 pptv (April)	DNSAOA derivatisation with FLD after HPLC separation (LOD 0.1–0.3 ppbw)	Alert, NU	Ambient	[49]

(continued)

Table 2 (continued)

Compound	Concentrations	Methodology	Location/campaign	Type	Reference
	275–100 ppt (April) 75–100 ppt (April) approx. 30 ppt	GC–ITMS (LOD 40 ppt)	Alert, NU	Interstitial air Ambient air	[61]
	42–452 pptv (dark) 68–552 pptv (transition) 26–459 pptv (24 h light)	GC–MS–FID	Alert, NU	Ambient air	[33]
Acetone	1.5–3 ppbw	DNSAOA derivatisation with FLD after HPLC separation (LOD 0.1–0.3 ppbw)	Alert, NU	Snow	[49]
	About 575–375 ppt (April) About 175 ppt (February) Approx. 400 ppt (April) Approx. 200 ppt (February)	GC–ITMS (LOD 130 ppt)	Alert, NU	Interstitial air Ambient air	[61]
	18–776 pptv (dark) 265–945 pptv (transition) 183–1,470 pptv (24h light)	GC–MS–FID with pre-concentration system (Carbotrap C, Carbosieve SIII)	Alert 2000	Ambient	[33]
Ethane	1,403 ppbv (dark, March) 1,596 ppbv (>18 h sunlight, March) 1,068 ppbv (May)	GC–FID with pre-concentration system	Alert, NU Alert Ice Camp 2000	Ambient air	[242]
	1,373 ppbv (dark, March) 1,669 ppbv (>18 h sunlight, March) 957 ppbv (May)	GC–FID with pre-concentration system	Alert, NU	Snow pack interstitial air Ice Camp	[242]

Propane	736 ppbv (dark, March) 589 ppbv (>18 h sunlight, March)	GC–FID with pre-concentration system	Alert, NU	Ambient air	[242]
	831 ppbv (dark, March) 580 ppbv (>18 h sunlight, March)	GC–FID with pre-concentration system	Alert, NU	Snow pack interstitial air	[242]
n-Butane	298 ppbv (dark, March) 189 ppbv (>18 h sunlight, March)	GC–FID with pre-concentration system	Alert, NU	Snowpack interstitial air	[242]
	266 ppbv (dark, March) 190 ppbv (>18 h sunlight, March)	GC–FID with pre-concentration system	Alert, NU	Ambient air	[242]
2-Methyl-propane	179 ppbv (dark, March) 100 ppbv (>18 h sunlight, March)	GC–FID with pre-concentration system	Alert, NU	Snowpack interstitial air	[242]
	149 ppbv (dark, March) 112 ppbv (>18 h sunlight, March)	GC–FID with pre-concentration system	Alert, NU	Ambient air	[242]
Ethyne	74 ppbv (dark, March) 109 ppbv (>18 h sunlight, March)	GC–FID with pre-concentration system	Alert, NU	Snowpack interstitial air	[242]
	75 ppbv (dark, March) 109 ppbv (>18 h sunlight, March)	GC–FID with pre-concentration system	Alert, NU	Ambient air	[242]
Ethene	42 ppbv (dark, March) 36 ppbv (>18 h sunlight, March)	GC–FID with pre-concentration system	Alert, NU	Snow interstitial air	[242]

(continued)

Table 2 (continued)

Compound	Concentrations	Methodology	Location/campaign	Type	Reference
Ethene	10–100 ppt		Alert, NU	Gas phase	[66]
	8.7 pptv		Summit, Greenland	Gas phase	[243]
	163 pptv		Summit, Greenland	Firn air	[243]
	44 ppbv (dark, March)	GC–FID with pre-concentration system	Alert, NU	Ambient air	[242]
	37 ppbv (>18 h sunlight, March)				
CH_3Br	LOD–0.1 pptv	GC–MS–FID–ECD	South Pole	Ambient and firn air	[30]
	9.4 pptv (ambient, 1m above)		Summit, Greenland		
	21.2 pptv (firn air)				
Methanol	41–424 pptv (dark)	GC–MS–FID	Alert, NU	Ambient air	[33]
	42–571 pptv (transition)				
	34–594 pptv (24 h light)				
Ethanol	19–464 pptv (dark)	GC–MS–FID	Alert, NU	Ambient air	[33]
	LOD–282 pptv (transition)				
	LOD–236 pptv (24 h light)				
Propanal	LOD–31 pptv (dark)	GC–MS–FID	Alert, NU	Ambient air	[33]
	6–28 pptv (transition)				
	LOD–56 pptv (24 h light)				
Butanal	LOD–54 pptv (24 h light)	GC–MS–FID	Alert, NU	Ambient air	[33]
Methyl-ethyl-ketone	LOD–116 pptv (dark)	GC–MS–FID	Alert, NU	Ambient air	[33]
	LOD–194 pptv (transition)				
	LOD–442 pptv (24 h light)				
CH_3I	0.33 pptv	GC–MS–FID–ECD		Surface air	[243]
CH_3I	3.39 pptv	GC–MS–FID–ECD		Firn air	[66]
Formic acid	LOD–8 ppbv	Ion chromatography	Seoul, South Korea	Urban air	[65]
Formic acid	16–77 ng m^{-3}	Ion chromatography	Sao Paulo, Brazil	Urban, forest and biomass burning areas	[66]
Acetic acid	LOD–6 ppbv	Ion chromatography	Seoul, South Korea	Urban air	[65]

Acetic acid	6–40 ng m^{-3}	Ion chromatography	Sao Paulo, Brazil	Urban, forest and biomass burning areas	[66]
Propionic acid	3–9 ppbv	Ion chromatography	Seoul, South Korea	Urban air	[65]
Oxalic acid	114–285 ng m^{-3}	Ion chromatography	Sao Paulo, Brazil	Urban, forest and biomass burning areas	[66]
Fumaric acid	11–96 ng m^{-3}	Ion chromatography	Sao Paulo, Brazil	Urban, forest and biomass burning areas	[66]
Succinic acid	39–103 ng m^{-3}	Ion chromatography	Sao Paulo, Brazil	Urban, forest and biomass burning areas	[66]
Glutaric acid	LOD-31 ng m^{-3}	Ion chromatography	Sao Paulo, Brazil	Urban, forest and biomass burning areas	[66]
Glutaric acid	0.6–7 nmol L^{-1}	SPE–TOF–MS	Fee glacier, Switzerland	Snow	[67]
Adipic acid	0.6–6.1 nmol L^{-1}	SPE–TOF–MS	Fee glacier, Switzerland	Snow	[67]
Pimelic acid	0.2–2.6 nmol L^{-1}	SPE–TOF–MS	Fee glacier, Switzerland	Snow	[67]
Suberic acid	0.4–5.9 nmol L^{-1}	SPE–TOF–MS	Fee glacier, Switzerland	Snow	[67]
Azelaic acid	3.9–4.9 nmol L^{-1}	SPE–TOF–MS	Fee glacier, Switzerland	Snow	[13]
Sebacic acid	0.1–1.2 nmol L^{-1}	SPE–TOF–MS	Fee glacier, Switzerland	Snow	[67]
Undecanedioic acid	LOD-0.3 nmol L^{-1}	SPE–TOF–MS	Fee glacier, Switzerland	Snow	[67]
Dodecanedioic acid	LOD-0.2 nmol L^{-1}	SPE–TOF–MS	Fee glacier, Switzerland	Snow	[67]
Phthalic acid	0.4–6.0 nmol L^{-1}	SPE–TOF–MS	Fee glacier, Switzerland	Snow	[67]
Monoacids (see individual species in reference)	0.02–2.44 mg L^{-1} snowmelt	GC–MS	Alert, NU; Summit, Greenland	Snow	[244]

Table 2 (continued)

Compound	Concentrations	Methodology	Location/campaign	Type	Reference
Diacids (see individual species in reference)	0.02–0.24 mg L^{-1} snowmelt	GC–MS	Alert, NU; Summit, Greenland	Snow	[244]
Methylamine	2.33–7.13 mg m^{-3}	Conventional extraction, GC–MS	Zonguklak, Turkey	Air, aerosols	[19]
	2.33–7.13 mg m^{-3}	Conventional extraction, GC–MS	Zonguklak, Turkey	Air, aerosols	[70]

FIA-FLD flow injection analysis with fluorescence detection, *GC* gas chromatography, *MS* mass spectrometry (quadrupole mass filter), *ECD* electron capture detector, *FID* flame ionisation detector, *LOD* limit of detection, *HPLC* high performance liquid chromatography, *ITMS* ion trap mass spectrometry

instrumentation, while assembled from similar instrument components (EI, CI, quadrupole or TOF mass filters) requires separate sample collection such as filters and several preparation steps often including derivatization. Methods are prone to artefact formation, but provide sensitive compound identification and quantification for a wide range of organic species, which is not always achievable using on-line instrumentation (see Gao et al. [40]). Other soft ionization techniques that are quite widely used for the determination of polycyclic aromatic hydrocarbons are electrospray ionization (ESI) [82] and atmospheric pressure chemical ionization (APCI), e.g. [83].

Other nitrogen-containing species such as peptides and proteins were not directly determined in the atmosphere, but typically as part of a general biological characterisation of atmospheric samples, methods of which are covered in Sect. 2.3. Older reports listed the concentration range of aliphatic amines from <0.0002 to 2.7 μmol N L^{-1} as compiled by Cornell et al. [84]. Lipids and carbohydrates, together with other species of direct biological origin, were typically determined as part of the characterisation of micro-organisms in air and snow and will be covered in Sect. 2.3.

For sulphur-containing species such as methanethiol, which are mainly related to anthropogenic activities (livestock, animal waste and composting), determination has recently been carried out using mass spectrometry (GC-MS [85] and PTR-MS [86]). Measurements of background atmospheric concentrations or data not directly measured at the source do not exist. The determination of dimethylsulphide together with other reduced sulphur compounds in air was reviewed by Pandey and Kim [87], including ion chromatography, electrochemical methods (e.g. voltammetry) and gas chromatographic methods, including GC-MS.

A summary of sampling locations, species' identities and concentrations is given in Tables 2 and 3. Additional concentration data for SVOC species were published by Kos and Ariya [21].

2.1.2 SVOC Measurement and Characterisation

Gas chromatography, coupled with flame-ionisation, electron capture (for halogenated species) and mass spectrometric detectors, is the most popular tool for determination of SVOCs in melted snow samples [44]. A prerequisite is the efficient separation of the analytes from the aqueous matrix, which can be accomplished using filtration onto quartz fibre filters and solid phase extraction [88]. Solid phase micro-extraction, which utilises equilibrium-based adsorption of analytes onto a polymer fibre bundle, has also been proposed and tested in laboratory studies [13, 89]. Both methods allow for an efficient transfer into the injection port of a gas chromatograph without water contamination. Directly coupled inlet sampler with GC-FID instrumentation has also been used [90]. The air sample was pre-concentrated using adsorbents (Carbotrap B, Carbosieve), followed by heating and collection on a cryofocuser (a fused silica capillary tube packed with

Table 3 Summary of analytical methodology for the determination of SVOC in snow

Compound	Concentrations with sample information	Methodology	Location/campaign	Type	Reference
Ethylbenzene	$1.0–1.1\ \mu g\ L^{-1}$	GC/MS	Valdez, AK	Snow	[45]
	$0.13–2.7\ \mu g\ L^{-1}$	GC/MS	Dubendorf, Switzerland	Snow	[245]
	$0.04–0.06\ \mu g\ m^{-3}$ (air) $172–285\ ng\ L^{-1}$ (snow)	GC/FID	Jungfraujoch, Switzerland	Snow and air	[90]
m-/p-Xylene	$3.0–3.3\ \mu g\ L^{-1}$	GC/MS	Valdez, AK	Snow	[45]
	$0.17–7.4\ \mu g\ L^{-1}$	GC/MS	Dubendorf, Switzerland	Snow	[245]
	$0.04–0.06\ \mu g\ m^{-3}$ (air) $104–169\ ng\ L^{-1}$ (snow)	GC/FID	Jungfraujoch, Switzerland	Snow and air	[90]
o-Xylene	$0.4–1.1\ \mu g\ L^{-1}$	GC/MS	Valdez, AK	Snow	[45]
	$0.067–1.5\ \mu g\ L^{-1}$	GC/MS	Dubendorf, Switzerland	Snow	[245]
	$0.05–0.07\ \mu g\ m^{-3}$ (air) $166–238\ ng\ L^{-1}$ (snow)	GC/FID	Jungfraujoch, Switzerland	Snow and air	[90]
1,3,5-Trimethylbenzene	$0.4–0.8\ \mu g\ L^{-1}$	GC/MS	Valdez, AK	Snow	[45]
	$0.15–0.23\ \mu g\ m^{-3}$ (air) $42–68\ ng\ L^{-1}$ (snow)	GC/FID	Jungfraujoch, Switzerland	Snow and air	[90]
1,2,4-Trimethylbenzene	$0.4–1.3\ \mu g\ L^{-1}$	GC/MS	Valdez, AK	Snow	[45]
	$0.027–1.3\ \mu g\ L^{-1}$	GC/MS	Dubendorf, Switzerland	Snow	[245]
	$0.04–0.06\ \mu g\ m^{-3}$ (air) $203–477\ ng\ L^{-1}$ (snow)	GC/FID	Jungfraujoch, Switzerland	Snow and air	[90]
p-Hydroxybenzaldehyde	$0.07–0.69\ mg\ L^{-1}$	GC/MS	Alert, NU; Summit, Greenland	Snow	[244]
p-Hydroxyacetophenone	$0.02–0.16\ mg\ L^{-1}$	GC/MS	Alert, NU; Summit, Greenland	Snow	[244]
Benzene	$0.33–0.37\ \mu g\ m^{-3}$ (air) $69\ ng\ L^{-1}$ (snow)	GC/FID	Jungfraujoch, Switzerland	Snow and air	[90]
Toluene	$0.15–0.19\ \mu g\ m^{-3}$ (air) $397–558\ ng\ L^{-1}$ (snow)	GC/FID	Jungfraujoch, Switzerland	Snow and air	[90]

Concentrations as given by the authors for the original publication

GC gas chromatography, *MS* mass spectrometry (quadrupole mass filter)

Carbopack and Envicarb X) before transfer to the GC by heating. A similar approach for batch samples (electro polished SUMMA canisters) was employed by trapping analytes at liquid nitrogen temperatures before introduction into a GC-FID by Hudson and Ariya [91]. Both adsorption methods allowed for the determination of VOC and SVOC.

Halogenated species were quantified using electron capture detection after gas chromatographic separation to ensure best analyte sensitivity. For organic species, gas chromatography coupled to a mass spectrometric detector (GC-MS) is by far the most popular for laboratory-based measurements, but difficult to deploy in the field [13, 88, 89]. The latter would be preferable to avoid potential changes in the sample during storage and transport, which take up to several days for remote regions, leading to inevitable warming of the samples. Blas et al. [92] provided an extensive summary of atmospheric concentrations detected in snow samples and the authors briefly mentioned the techniques employed for the determination of inorganic and organic species. A summary of sampling locations, species identities and concentrations is given in Table 2.

2.2 Sampling and Analysis of Bioaerosols

Biological airborne particles are collected by using two different methodologies that can be classified as passive and active sampling. The efficacy of a bioaerosol sampler is determined by its extraction efficiency, collection efficiency, and its effect on the biological activity of the captured microorganisms. The existence of a wide range of biological particles in air and sampling methods has effectively inhibited the establishment of standardised protocols. In general an ideal sampling technique fulfils two criteria: (1) capturing all bioaerosols and (2) preserving the original state of viability. During air sampling, various factors such as aerosol concentration and composition, inlet orientation, aerosol charge, particle desiccation and shear forces, wind speed, particle breakup and sampling flow rate changes may affect viability, cultivability and the number of microbes collected [93].

Bioaerosols can be analysed by two different means: (1) by total number of cultivable species on the agar plate or (2) by total number in the air, including those that are not cultivable such as airborne toxins or pollen grains. The latter is used mainly for viable bacterial cells, endospores and some fungal spores. However, classical methods for determining the number of viable bacteria rely on the ability of cells to grow on solid medium. The number of detected colonies is not truly representative of the total population of microorganisms collected in air sampling. This is due to the fact that many of the microorganisms are not cultivable under laboratory setting conditions [94], or because they have lost their ability to form colonies during the sampling process [95]. To overcome this limitation, different techniques have been used to detect their physiological viability [96], metabolic activity and nucleic acid analysis [50, 97, 98] and to numerate microorganisms using flow cytometry or fluorescent staining [99–101]. Over the years, different air

sampling techniques have evolved that can be generally categorised as: (1) sedimentation and inertial samplers, (2) filtration, (3) optical counters/analysers and (4) electrical mobility techniques. For each technique the first reference given provides a schematic of the discussed technique. All samplers discussed in Sects. 2.2.1–2.2.8, have the capability to sample both aerosols and bioaerosols. Discrimination takes place at the analysis stage by cultivation or, e.g. mass spectral analysis of specific biological markers.

2.2.1   Sedimentation and Inertial Samplers

Sedimentation or settling plates are the most primitive method for sampling airborne microorganisms. A Petri dish containing a non-selective agar is exposed directly to air for a given period of time and bioaerosols will eventually settle by gravity. Plates are incubated at specific temperatures to permit the growth of colonies. Results are obtained via colony forming units (CFU) or particles per minute. It is a passive, non-volumetric method and imprecise due to over-representing larger particles because of their rapid settling rate. The limitation of this technique is the detection of only viable biological particles and those with a specific size range, which are able to sediment. Thus, the results cannot be quantitatively analysed. Furthermore, it can take from many hours to days for the growth of microbes, since agar plates are prone to non-airborne contamination, and overgrowth occurs in highly polluted areas, which makes it difficult to analyse. The advantage is that the method is simple and inexpensive.

In active monitoring, air sampling instruments bring a specific volume of air into a collection vessel. The main methods that are used for sampling and quantification of viable airborne microorganisms are impaction on solid surface, filtration, centrifugation, cyclones, electrostatic precipitation, and the impingement in liquids (Table 4).

2.2.2   Impactors

The collection media in impactor samplers are solid or adhesive media. The impactor is basically a jet (pump or fan) that draws air into a sampling device, which then directs the air stream at the collection plate containing agar medium [102]. On impact with the collection surface, the direction of the air diverges from that of the suspended particles, which accumulate and stick to the surface of the agar plate. Impaction results in low sampling stresses during collection, and sample manipulation are not required. The impaction methods give higher particle recovery than other methods. The number of colonies grown in agar media gives an estimation of the number of microorganisms in the air. Impaction sample collector plates tolerate high flow rates, are sterile and are easy to use. There are two different impaction types: slit samplers (e.g. Casella slit sampler) and sieve samplers

Table 4 Methods for the collection, detection and quantification of airborne microorganisms

Methodology	Advantages	Disadvantages
Culture	(1) Detection in real time (2) Simple device (3) Inexpensive	(1) Time consuming (2) Labour intensive (3) Detects only culturable microorganism (4) Detects only specific size range able to sediment (5) Fast-growing microorganisms may overgrow slower ones (6) Takes days for growth (7) Underestimates the number of microorganism (8) Agar plates are prone to non-airborne contamination (9) Overgrowth of microorganism in high polluted area
Impactors	(1) Simultaneous analysis of size and composition (2) Preserve the original state of sample (3) Surface control for impacted particles (4) Possibility of separation of particles into numerous size classifications (5) High particle recovery (6) Allow time-sedimentation particle measurement	(1) Not a true representation of total microbial communities (2) Operationally complex (3) Interpretation of data is often complex (4) High costs (5) Not capable of collecting small particles (<0.5) (6) Dehydration of media; thus: poor bacterial growth, reduction of viable count of stress sensitive microorganisms
Impingers	(1) Separation by size (2) Quantitative analysis (3) Preservation of original state of sample (4) Collection of various sizes of microorganisms (5) Rapid and direct analysis of sample by different methods	(1) Glass sample containers are not disposable (2) Preparation of sample container is long (3) Susceptibility to retention rate of the microorganism (4) Preservation of original state of sample is proportional to sampling time
Centrifugal sampler	(1) Battery operated (2) Small (hand size)	(1) Sampling accuracy affected by vortexing (higher counts, false higher efficiency rating) (2) Counts should be done manually (use of strip) (3) Flow rate only quantifiable theoretically (4) Questionable accuracy of the collected sample (5) Limitation on collection of small particles onto the collection surface
Cyclones	(1) Allows for spatially variable samples (2) Elimination of sample transfer loss	

(continued)

Table 4 (continued)

Methodology	Advantages	Disadvantages
Filter	(1) Low cost (2) Simple to operate (3) Availability of various pore size for selecting particle sample	(1) Possible dehydration and chemical transformation of the sample (2) Limited choice of filter types
Optical Counter	(1) Sensitive and easy to use	(1) Unable to distinguish types of particles (number only) (2) Labour-intensive (if manual optical counting)
Optical particle counter	(1) Analyzing particle size from 0.25 to 20 μm	(1) Calibration and performance is influenced by particles with very different refractive indices (and shape factors) (2) Requirement of periodical calibration and recalibration
Laser Diffractometry	(1) Broad measurement range for a given optical configuration (0.1 μm to several mm) (2) Excellent reproducibility between measurements of the same aerosol (3) No calibration required	(1) Particles are assumed to be spherical (2) Bias due to high concentration or absence of the finest particles in the distribution
Phase Doppler Particle Analysis Systems	(1) Non-intrusive optical method (2) Measure the size or speed of spherical particles (liquid and solid)	
Intensity Deconvolution System	(1) Absolute particle concentration, particle size distribution, and average particle speed (2) Capable of resolving a size range of 0.2–200 μm up to a concentration of 10^7 particles/cm^3	(1) Any random particle trajectory does not give uniform beam intensity (2) Very expensive
LIDAR	(1) Continuous monitoring (2) Accurate and fast	(1) Impossible in rainy or misty conditions and certain atmospheric conditions (2) Cannot distinguish background aerosol particles (diesel, smoke, pollen) from potential bioagent plumes (3) Distinguish clouds having similar distributions in aerosol size but of different material compositions
Biosensors	(1) Highly sensitive (2) Selective biological recognition (3) Speed of response (typically less than 1 min) (4) Inexpensive and easy to use	(1) Lacks robustness (2) Available only for limited number of organisms

(e.g. Andersen multistage sieve sampler). Viable biological aerosols have recently been determined by Raisi et al. using an Andersen type impactor [103].

Slit Samplers

Slit samplers are usually cylindrical and a known volume of air is drawn by vacuum through a slit opening [104]. The air flow moves across a solid surface with abrupt changes in direction and accelerated air is directed toward the surface of a Petri dish containing agar media. Wetted wall cyclone samplers suitable for bioaerosols are also available [105]. The plate containing the Petri dish rotates at a known rate, which varies. Microorganisms with a higher mass are impacted on the agar surface and the rest of the air flows around the plate and exits the air sampler. Slit samplers are used to determine the concentration of microorganisms as a function of time. The direct growth of microorganisms from Petri dishes allows the establishment of the time of settlement for each particle.

This technique has several deficiencies. First, slit samplers do not separate and differentiate the size of airborne particles. Second, between the vacuum action and the rotating plate, the medium often dehydrates which can lead to poor bacterial growth and reduction in the viable count of stress-sensitive microorganisms. Third, the collected air sample is not a true representation of the air quality since about 10% of total particles are not deposited on the impaction medium. Lastly, only large particles with sufficient inertia will deviate from the streamlines and impact onto the agar surface. Small particles (<0.5 μm) miss the agar surface and are ejected back into the atmosphere.

Sieve Samplers

Sieve samplers are operated by drawing air through a large number of small evenly placed holes drilled in a metal plate (sieve), e.g. used by Wang et al. in a setup for road dust sampling [106]. The suspended particles deviate from the air flow by inertia and impact on an agar surface located a few millimetres below the perforated plate. In multistage (e.g. Andersen) sieve samplers, particles are separated by size through multistage acceleration and each perforated plate is held above an agar plate with successive plates with smaller holes. This arrangement causes increased particle velocity as air flows through the apparatus. At a constant flow, larger particles impact on the first stage, whereas smaller particles impact on the last impaction stage. Like slit samplers, no diluting or plating is required and results are expressed as particles per unit volume. The major advantage of this sampler is that it provides data on particle size. Limitations associated with sieve impactors are: (1) significant inhibition of the growth of microorganisms by drying the nutrient agar during long periods of sampling and low humidity, (2) expensive and cumbersome and (3) lack of full capability of collecting very small particles, particularly colloidal-type structures.

2.2.3   Impingers

In impingers, the collection medium is liquid. In all-glass impingers (AGIs), airborne particles are accelerated by a narrow orifice that is placed at a distance from the bottom of the flask. A suction pump directs air through a curved narrow suction glass inlet tube. A pressure drop in the flask forces the air to enter horizontally through the inlet, which then curves to a vertical position. The air is forced downward and impacted onto a liquid medium at the bottom of the flask and can be used for sampling aerosols with diameters as small as the nanometre size range [107].

Any suspended particles in air are impinged into the collection liquid as a result of the sudden change in direction of the air after encountering the surface of liquid medium. The air flow rate is determined by the diameter of the inlet tube. By using the air flow rate, sample volume can be calculated, allowing for the quantitative assessment of results. Bioaerosols were also separated by size using multiple liquid impingers [108, 109]. For instance, in a design of impinger models, BioSampler™, three tangential sonic nozzles force air toward the base of the flask, which contains a liquid medium. The swirling motion of the collection medium provides less harsh conditions compared to the old models (e.g. AGI [110]). The liquid medium protects bioaerosols from dehydration and preserves their original state. The liquid medium can later be analysed by culturing, filtering or molecular biology techniques. Sampling time is an important factor in optimizing the original state of bioaerosols in liquid impinger as deagglomeration and re-aerosolization of microorganisms can occur [111, 112]. Moreover, the microbial stress and the agitation motion may impact the viable count of microorganisms over time.

A suitable collecting medium must preserve the viability of the microorganism while inhibiting its multiplication during the longer duration of sampling. The advantage of this method is that it collects various sizes of microorganisms, and the liquid medium containing the air sample can be analysed rapidly and directly by different methods such as PCR. However, since the glass containers are not disposable and must be sterile before each use, preparation time is long. Moreover, the long duration of sample collection causes evaporation of the collected liquid as well as cooling of the sample, thus affecting the retention rate of microorganisms.

2.2.4   Centrifugal Samplers

In centrifugal samplers, aerosols are spun in a circular path at high velocity toward the inner wall of the drum that is lined with a plastic strip supporting a thin layer of agar medium. The major advantage of these devices is that they are battery operated and are small enough to be held in the hand [110]. This device has several limitations. First, the vortex affects sampling accuracy by showing higher counts not representative of the actual value in the atmosphere. Second, due to the use of the strip, the counts should be done manually. Third, the sampler exhausts the air

stream from the same opening used to create the vortex, which causes disruption of the surrounding atmosphere. Thus, the flow rate can only be quantified theoretically, and the volumetric accuracy of the collected sample is in question. Lastly, these devices fail to produce enough centrifugal force to propel small particles onto the collection surface.

2.2.5 Cyclones

The principle separation of particles from a gas stream in a cyclone is by creating a vortex that uses both gravitational and centrifugal forces. See Kim et al. for a schematic in a combination instrument with an impinger [113]. The cyclone sampler works by taking in air at an angle to the wall of the micro-centrifuge tube, thus creating centrifugal force and pushing the denser particles into the walls of the tube so that they eventually settle at the bottom of the tube. From the top of the cyclone body, polluted air enters the inlet at high velocity and is moved along the inner wall. Inertial forces push the particles outward. Larger particles cannot follow the spinning path and impact on the cyclone wall. Meanwhile, gravity pulls the spinning particulates down along the cyclone body where they are collected at the bottom. It allows for spatially variable samples, and eliminates transfer losses during analysis because the particle collection occurs in the micro-centrifuge tubes with 90% for particles in the 1 μm range.

2.2.6 Filtration

Filters are widely used for aerosol sampling because of their low cost and simplicity of operation. For example, see Moosmüller et al. for a filter setup for spectroscopic characterisation of aerosols [114]. Filters with different pore sizes are able to trap bioaerosols selectively. The efficiency of a filter is governed by the following five basic mechanisms: (1) interception, (2) inertial impaction, (3) diffusion, (4) gravitational settling and (5) electrostatic attraction. Filters are made commercially in different compositions (e.g. cellulose, polycarbonate and polytetrafluoroethylene), pore size and thickness.

The air filtration apparatus consists of cellulose fibre, sodium alginate, glass fibre, a gelatine membrane filter (GMF; pore size 3 μm) or synthetic membrane filters (pore size 0.45 or 0.22 μm) mounted in an appropriate holder and connected to a vacuum source through a flow rate controller. For analysis, the filter containing microbes can be analysed directly using microscopic examination. The whole fibre filter or a section of it may further be agitated in a suitable liquid until the particles are uniformly dispersed. Aliquots of the suspension are then assayed by appropriate microbiological and molecular techniques. Membrane filters can either be treated similarly to fibre filters or placed directly on an agar surface and incubated. Bioaerosols collected on filters are exposed to desiccation, which might reduce the viability of cells using culture analysis. Specific filters are able to trap ultra-fine

particles. For instance, High-Efficiency Particulate Air (HEPA) filter traps 99.97% of airborne particles with an aerodynamic diameter of 0.3 μm and larger. The Ultra-Low Penetration Air (ULPA) filter traps even more, 99.99% of particles 0.12 μm and larger and HyperHEPA filters are certified to filter down to 0.003 μm with a guaranteed minimum efficiency of over 99.5%.

2.2.7   Optical Counters/Analysers

Aerosols can be analysed using techniques that are based on the interactions between particles and light. The examination of a scattered beam of light by a detector after hitting a particle is the basis for many optical instruments. For example, the number of scattered light pulses is a measure of particle number. Furthermore, the intensity and spatial scattering pattern can also be used for determination of particle size and particle shape, respectively. Optical methods are sensitive and easy to use. These methods are classified into four categories: (1) optical particle counter, (2) laser diffractometer, (3) phase Doppler system and (4) intensity deconvolution system.

Optical Particle Counter

The optical particle counter (OPS) uses the principle of light scattering from airborne particles to determine particle size distribution [26]. It is a real time instrument that is typically used to measure particles above 0.05 μm in diameter. Many well established techniques are available for counting air particles. However, the calibration of any two air particle counters with the same reproducibility while taking the same air sample has created many challenges.

OPSs are capable of characterizing particle size within the range 0.25–20 μm. They are compact laser-based devices which use a 90° scattering angle in combination with a high-intensity white light source. Their high sensitivity allows for the use in low and high aerosol concentration (1×10^7 cm^{-3}) in clean room or industrial filter testing [26]. The size of particles are determined by using a calibration curve based on the refractive index of a broad range of monodisperse size classes of aerosol particles in the super-micrometre size range. The coverage of the laser by dust, and measuring of various particles with very different refractive indices (and shape factors), affect its calibration and performance. Thus, periodical calibration and recalibration of such devices is often required.

Laser Diffractometer

Laser diffractometry (LD) determines particle size (either solid particles or liquid droplets) indirectly from the interpretation of the pattern of light scattering intensity falling on the detector of the instrument [115]. Only the diffraction component of

scattered light (not reflection, refraction and polarization) is used for analysis in laser diffractometers. Laser diffraction measurements are based on particle ensembles rather than on single particles. A suitable optical model is necessary to convert this information accurately into a particle size distribution [116, 117]. There are two theoretical optical models to convert light energy diffraction patterns into size distributions: Fraunhofer and Lorenz–Mie theories. According to the Lorenz–Mie theory, the calculation is based on the comparison of the complex refractive index of the particle with the supporting medium to account for light deflection and absorption components. The Fraunhofer theory assumes that all particles are much larger than the laser wavelength and considers only near/forward scattering. The measurements are only accurate for particles >25 µm in diameter [115]. Comparing these two theories, the Mie theory gives a better analysis for small particles in the micrometre size range since the Fraunhofer theory simulates non-existing fine particle fractions [118].

Phase Doppler Particle Analysis Systems

The phase Doppler method, a non-intrusive optical method, is based upon the principles of light scattering interferometry to measure the size or speed of spherical particles (typically liquid sprays, but also some bubbles and solid spheres) [119]. Measurements are made repeatedly at a small, optical probe volume defined by the intersection of two laser beams. As a particle passes through the probe volume, it scatters light from the beams into a multi-detector receiving probe, strategically located at an off-axis collection angle. The phase shift between the Doppler burst signals from different detectors is proportional to the size of the spherical particles.

The velocity of the drops/particles is also determined by the scattered light which forms an interference fringe pattern. The scattered interference pattern produced by the moving particle is proportional to the drop velocity. The fringe spacing can be calculated from the optical set-up. The fringe spacing divided by the time to transit one fringe, gives the velocity of the particle passing through the probe volume.

Intensity Deconvolution System

An intensity deconvolution system measures the absolute light intensity scattered from a focused laser beam on an optically defined volume, and a deconvolution algorithm is used to determine the variation of particle size [120]. After the collection of a large number of scattered light signals, the absolute particle concentration, particle size distribution and average particle speed are determined by using an intensity deconvolution algorithm. This technique is capable of resolving a size range of 0.2–200 µm up to a concentration of 107 particles/cm^3, but is very expensive.

2.2.8   Electrical Mobility Techniques

Electrical methods use the physical properties of charged particles, especially the mobility in an electric field.

Electrical Aerosol Analyser

The electrical aerosol analyser (EAA) consists of three main components: an aerosol charger, a mobility analyser, and an electrometer current sensor [121]. The aerosol charger is based on diffusion charging from a positive corona discharge. Under well-controlled conditions, each particle size is charged with a certain number of charges. The charged particle flows into the annular shell of the mobility analyser. In fact it operates as an electrostatic precipitator and accumulates those particles with a high electrical mobility. The specific electrical mobility of each particle can be used to compute the size distribution (to within about 10 nm) of the aerosol sample [122]. EAA can be used for both solid and volatile particles. Furthermore, it is rapid and is able to do repetitive in situ measurements [123].

Differential Mobility Analyser

A differential mobility analyser (DMA) works on the same principle as the EAA, with some operational differences. In a DMA, an electrostatic classifier is used instead of a mobility analyser and aerosol particles can be sorted by size from 0.01 to 0.9 μm while suspended in air [124].

DMA applies an electric charge to the particles. Small particles with single positive charges are sorted while other uncharged particles will be discarded. After entering the DMA, the migration of charged particles is controlled by an electric field. The rate of migration is determined by electrical mobility of the particles, which is dependent on both the size and the electrical charge. To determine the size distribution of particles, DMA scans over the segment of particles' mobilities by varying the applied field. The measured number concentrations in each segment are then converted to a size distribution by using the distribution of charges produced by the charger and the known relation between mobility and size.

Light Detection and Ranging

Light Detection and Ranging (LIDAR or LADAR) is an optical remote sensing technology that can measure the distance to – or other properties of – a target by illuminating the target with light, often using pulses from a laser. It uses ultraviolet (UV) light to excite natural substances such as amino acids, coenzymes and fluorophores to fluoresce [125]. The most common UV laser wavelengths are

266 and 355 nm. A grating spectrometer combined with an intensified charge-coupled device (iCCD) camera collects the emitted fluorescence from microorganisms and the fluorescence spectra are identified as their laser-induced fluorescence (LIF) spectral signatures [126]. Simard et al. have employed LIDAR effectively for detection of bacterial clouds at long distances; a schematic of their system is also illustrated [127, 128].

2.2.9 Biosensors

Biosensors detect pathogens by using analytical, biochemical and/or genetic recognition methods. The main analytical methods used are mass spectrometry (MS) [53], modern infra-red [129, 130] and Raman spectroscopy [130, 131].

Biosensors are categorised into four main groups: optical, mass, electrochemical and thermal sensors [132–134]. Recently, a novel method – triangulation identification for the genetic evaluation of risks (TIGER) – has been developed which is able to identify bioaerosols or pathogens at strain level without prior knowledge of the pathogen's nucleic acid sequence [135]. This technique incorporates the polymerase chain reaction (PCR) to amplify DNA and high-performance electrospray mass spectrometry time-of-flight (TOF) instrument to drive base compositions of PCR products. In this method, certain selected DNA regions of the microorganism are amplified by using multiple pairs of primers that target conserved regions such as ribosomal sequences and conserved elements from essential protein-coding genes. The resulting amplicons are purified for electrospray using a mass spectrometer. The mass spectrometer detects the amplicons. A list of all detected masses based on spectral signals, and their conversion to base composition (adenosines, guanosines, cytidines and thymidines) is prepared and compared with a database of calculated base compositions that is derived from the sequences of known organisms to determine the identities of any microorganism, down to strain level.

2.2.10 Other Sampling and Detection Methods

Swabbing

Airborne microorganisms can also be detected by simple methods of swabbing the surfaces of air purifier filters (Table 4) [136, 137].

Total VOC

Markers of moulds, such as ergosterol, beta-glucans or VOC of microbial origin (MVOC) that are emitted during different developmental stages of fungi are used as an indication of fungal growth or degradation. A Radiello™ type passive diffusion tube is able to collect the VOC. Then the VOC can be analysed using a combination

of three techniques: gas chromatography (GC) to separate the VOC, a flame ionization detector (FID) to detect different compounds (best for detecting hydrocarbons and other easily flammable components) and mass spectrometry (MS) to identify the different compounds (based on measuring the mass-to-charge ratio of charged particles) [138].

Cytometry Analysis

In solid-phase cytometry (SPC), microorganisms are analysed by a combination of both epifluorescence microscopy and flow cytometry [139]. Air is impacted on a water-soluble polymer film present in a standard Petri dish (polyvinyl alcohol plate). After filtration, viable cells are labeled. The filter is scanned by a laser in a solid-phase cytometer. Using different software, fluorescent particles are distinguished from microorganisms.

Total luminescence spectroscopy (TLS) is the simultaneous measurement of excitation, emission and intensity wavelengths of compound fluorophores [140–142]. This technique is mainly used for large cell numbers in aqueous suspensions. In TLS the distinct fluorescence data that is generated from a three-dimensional matrix or excitation-emission matrix (EEM) of a specific microorganism is used for identification. Compared to two-dimensional emission spectra, this technique is highly sensitive and selective [143].

Before recent advances in molecular biology, identification of microorganisms was based on similarities and differences observed in their phenotypic characteristics which relied on availability of pure culture, subsequent growth characteristics and biochemical profiling. The limitations of monitoring and identification of microorganisms imposed by microscopy and cultural methods are overcome by molecular biology techniques [144]. Molecular approaches using full length sequencing of 16S ribosomal gene in bacteria have provided a powerful identification tool. In this method, DNA is extracted and its 16S rDNA sequence is analysed by PCR. The microorganism is identified by matching its DNA sequence to known sequences in GenBank. Quantitative PCR (qPCR) provides both quantitative and qualitative analysis [145, 146]. An important limitation of the DNA-based technologies is its inability to distinguish between live and dead microorganisms.

The sequence of prokaryote 16S rDNA is unique and highly conserved [147] among various bacteria. Moreover, 16S rDNA gene can be easily and rapidly sequenced for accurate identification of bacteria, and phylogenetic relationships which have facilitated the discovery of novel bacterial species [148–150]. The earliest in-depth analyses of microbial communities with high phylogenetic resolution power were carried out using Sanger sequencing [151–155]. Phylogenetic oligonucleotide microarrays, and next-generation sequencing (NGS) including pyrosequencing (introduced by 454 Life Sciences, Inc.) as well as other platforms such as Solexa (Illumina, Inc.) and SOLid (ABI, Inc.) are the recent advances in DNA sequencing techniques. Compared to the Sanger method, the DNA microarray

offers simultaneous detection of thousands of genes on a single glass slide or silicon surface [156]. Furthermore, the new high throughput 454 GS-FLX Titanium pyrosequencing (released to market in 2005) is a superior method compared to the Sanger method in terms of its capacity of sequencing per run, time, cost per sequenced nucleotide [157] and its no a priori sequence information. It is based on sequencing-by-synthesis and the pyrosequencing is performed within a complex reaction that includes enzymes (ATP sulphurylase and luciferase) and substrates (adenosine 5′ phosphosulphate and luciferin).

The first step of the 454 techniques is the generation of a DNA library (single stranded DNA or PCR amplicons) containing flanking adaptor sequences, which are used to immobilise the DNA library fragments to capture streptavidin beads. Then emulsion PCR is performed for the DNA amplification step. By using the correct stoichiometric amount of the DNA library, each adaptor-modified DNA library is independently confined in a droplet of oil and water containing PCR reagents, and beads. This ensures the amplification of one DNA fragment per bead. The next step after amplification is the breakage of emulsions and enrichment of beads with streptavidin-coated magnetic beads for selective purification of beads containing the biotin-labeled amplified product. The isolated DNA bound to beads are annealed with a sequencing primer and are distributed into a fibre-optic PicoTiter™ plate containing 1.6 million picoliter wells that are surrounded by enzyme beads for pyrosequencing. The diameter of each well is designed to allow only one bead per well. Nucleotides are allowed to flow one at a time over the plate and template-dependent incorporation releases pyrophosphate, which is converted to light through an enzymatic process.

The steps involved in pyro-sequencing can be summarised as the release of pyrophosphate (PPi) during the DNA polymerase reaction, the quantitative conversion of pyrophosphate to ATP by sulphurylase and ATP-dependent conversion of luciferin to oxyluciferin by luciferase. Light pulses are emitted with the production of oxyluciferin, which is directly proportional to the incorporation of one or more nucleosides. The amount of light produced by luciferase is detected by a light-sensitive device such as a luminometer or a CCD (charge-coupled device) camera. The flowgrams are analysed and a nucleotide sequence is determined for each read using specific software.

2.3   Role of Biogenic Aerosols in Nucleation Processes

Aerosols, including those of biogenic origin, have important impacts on atmospheric radiation, both directly, and indirectly through the nucleation of atmospheric water. The impact of biogenic aerosols on radiation through direct and indirect effects depends on their physical and chemical properties. Table 5 shows the main chemical and physical properties of aerosols that influence their interaction with radiation, and with other atmospheric compounds, resulting in the formation of secondary particles, as well as their influence on cloud formation. Chemical

Table 5 Chemical and physical properties of aerosols, which affect their nucleating properties

Property	Definition	Theoretical model, description and/ or experimental determination	Impact
Morphology/ size/shape	Arrangement of phases within a particle [246]	Scattering phase function is size [170] and shape dependent [207] Mixing state can be inferred from particle mobility size and mass changes [247] or imaged using electron microscopy Recent studies report physical as well as chemical identification of phases by combining X-ray microanalysis and Raman microspectrometry [248], AFM with Raman [249], SEM with energy dispersive X-ray (EDS) [250], scanning tunnelling X-ray microscopy with near edge X-ray absorption fine structure (stxm-nexafs) [251], TEM with EDS [252], as well as laser single particle laser time of flight ablation spectrometer (SPLAT II) [253]	Light scattering [207] Contact angle and radii of curvature [246] Uptake of other components [254] Diffusion within particle e.g. solid or semi solid organic component can slow down uptake and diffusion, which limits reactions to surface and affects the lifetime of the particle [255]
Surface tension		Calculated from Young's equation (Kwok and Neumann form): [256] $\gamma_{sv} = (\gamma_{lv}(\cos\theta + 1)^2)/4$ γ_{sv}: solid surface tension γ_{lv}: surface tension of water at ambient T $(=72.7 \text{ mJ m}^{-2})$ θ: contact angle	Affects super saturation % required for droplet activation, e.g. organics can cause decrease in surface tension resulting in lower super saturation and enhanced CCN [172]

| Contact angle | Angle between nucleus and substrate | For heterogeneous nucleation on ice $\cos\theta = (\sigma_{LN} - \sigma_{IN})/\sigma_{LI}$ where σ are interfacial tensions between liquid, L, nucleus, N, and ice, I | Affects water uptake [162] on aerosol and IN ability |
| | $K_{p,i}$ Equilibrium partitioning coefficient | $K_{p,i} = (F_i/M)/A_i = f_{om}RT/(MW_{om}10^6\xi_i P_{L,i}^0)$ F_i: mass concentration of "i" in aerosol phase ($\mu g\ m^{-3}$ of air)·A_i: mass concentration of "i" in gas phase ($\mu g\ m^{-3}$ of air) M: concentration of particulate material ($\mu g\ m^{-3}$ of air)·f_{om}: mass fraction of the largely organic material portion of the particulate matter into which partitioning is occurring R: universal gas constant (m^3 atm K^{-1} mol^{-1}), T: temperature, MW_{om}: average molecular weight of particulate matter phase into which partition is occurring (g mol^{-1}), ξ_i: activity coefficient of compound "i", $P_{L,i}^0$: vapour pressure of compound "i" [257] | Affects chemical composition and subsequent reactions resulting in SOA |

Table 5 (continued)

Property	Definition	Theoretical model, description and/or experimental determination	Impact
Hygroscopicity	Ability to uptake water and grow to form droplets	Secondary Organic Aerosol (SOA) yield: $M \Sigma (\alpha_i . K_{p,i}/1 + M K_{p,i})$ Assuming T, P, n_s are constant with change in particle diameter, D_p: For a dilute solution where volume occupied by solute is negligible $\ln (P_w(D_p)/P^o_{flat}) = (4M_w \sigma_w/RT\rho_w D_p) - (6n_s M_w/\pi\rho_w D_p^3)$	Impact on CCN activity Dependence on surface tension
Heterogeneous ice nucleation	Formation of ice crystals in the presence of an insoluble nucleus	$J_{heterogeneous} = (kT/h)\exp((-\Delta F_{diff}(T)/kT) \times n_s \exp(-\Delta G_{het}(T)/kT)$ where n_s is the number density of water molecules at the nucleus/water interface	Dependence on contact angle $\Delta G_{het}(T) = \Delta G_{hom}(T)f(\theta)$

Fig. 2 The simulation with Phillips' Scheme in the condensation and immersion freezing modes. (**a**) Spatial and temporal evolution of the primary ice nucleation rate ($L^{-1} s^{-1}$) (*shaded area*) and the ice splinter production rate ($L^{-1} s^{-1}$) (*solid lines*). (**b**) Spatial and temporal evolution of ice particles (L^{-1}) (*shaded area*) and bacteria-containing ice particles (L^{-1}) (*solid lines*). Courtesy of Sun et al. (Personal Communication, 2013)
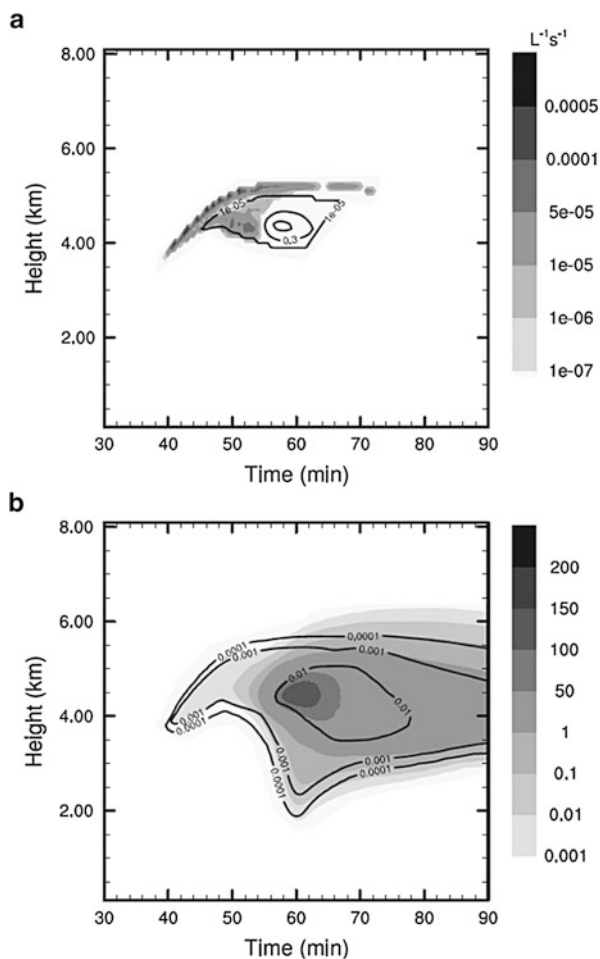
composition is affected by partitioning, e.g. increased hydrophilicity [158], which influences hygroscopicity and CCN ability. Chemical composition influences subsequent aging reactions, which were found to depend on chemical structure [159] and oxidation states [160, 161]. Physical state such as size, shape and morphology is also affected by partitioning, e.g. restructuring of aggregated particles (e.g. soot) [162]. Physical state directly affects the interaction of the aerosol with light and the ability to act as surfaces for heterogeneous ice nucleation. Depicted in Figs. 2 and 3, are some examples of atmospheric modelling runs that attempt to address the importance of bioaerosols in the atmosphere.

Fig. 3 Spatial and temporal evolution of the primary ice nucleation rate $(L^{-1} s^{-1})$ (*shaded area*) and the ice splinter production rate $(L^{-1} s^{-1})$ (*solid lines*) for the simulation with Chen's scheme in the immersion freezing mode. (**a**) Spatial and temporal evolution of the primary ice nucleation rate $(L^{-1} s^{-1})$ (*shaded area*) and the ice splinter production rate $(L^{-1} s^{-1})$ (*solid lines*). (**b**) Spatial and temporal evolution of ice particles (L^{-1}) (*shaded area*) and bacteria-containing ice particles (L^{-1}) (*solid lines*). Courtesy of Sun et al. (Personal Communication, 2013)
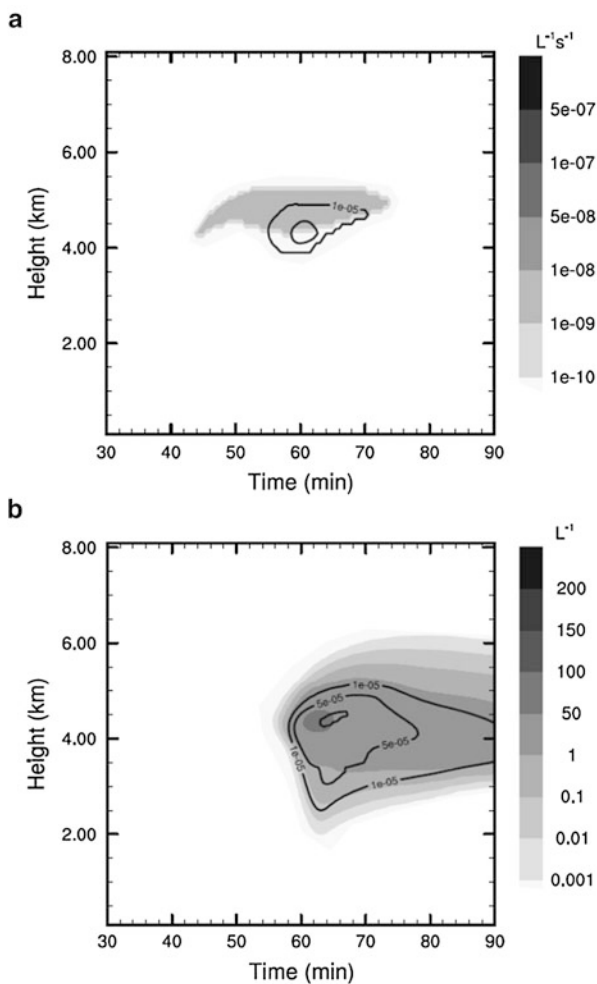
3 Future Outlook

Herein we attempted to review conventional and current state-of-the-art techniques and methods involving bio-organic matter, as well as to provide a summary of existing measurement methods for bio-organic compounds. We have explored advantages and disadvantages, and the limits and uncertainties of the measured data. To obtain complementary information on physical and chemical characterization of bio-organic matter, there is an increasing tendency to deploy several techniques and methods. There is currently no "perfect" technique to address most chemical and physical characteristics that atmospheric scientists might be interested in. However, there has been significant progress during the last couple of decades, namely in optical spectroscopy, mass spectrometry and genomics, which can assist scientists to address more fundamental questions about nucleation,

surface interactions, volatilisation, gas-to-particle conditioning, new aerosol formation and so forth. Our abilities are negligible when it concerns studies of surface processes that are relevant to environmental conditions. Understanding aerosol–ice–snow interfaces still cannot be achieved at molecular levels. Non-destructive, preferably (ultra)fast-resolved real-time instruments capable of studying physical and chemical properties as well as exploring biological characteristics of bio-organic matters will provide better means for next-generation research. However, we are not there yet!

Appendix

A Brief Review of Mitigation of Atmospheric Bio-organic Compounds

Bioaerosols are not released as a result of human activity to the same extent as other pollutants. However, significant anthropogenic sources include waste treatment, agriculture, food production, paper and wood production and horticulture, as well as municipal composting [163, 164]. Development and deployment of bioaerosol mitigation technologies is very limited due to the lack of regulations governing acceptable bioaerosol emission rates and ambient concentrations [60]. The Republic of Korea has set a maximum allowable total bacterial bioaerosol concentration of 800 CFU m^{-3} for indoor environments [165]. Licensed "green waste" composting sites in England and Wales are subject to guidelines limiting total fungi and bacteria concentrations to below 1,000 CFU m^{-3}, and Gram-negative bacteria below 300 CFU m^{-3} at 250 m from the site boundary [163]. However, neither the US Environmental Protection Agency (EPA) nor the World Health Organization (WHO) has established bioaerosol concentration standards [165] (incineration or biofiltration), but also include UV radiation and ion emission [164, 166, 167]. In industrial settings, the measures in place to control dust and odour emissions will generally remove bioaerosols as well, but some reports indicate that these do not always control the emission of certain pathogens [168]. The above-mentioned pollution control technologies and other techniques can also be applied to treat indoor air. Increased ventilation rates and the use of high-efficiency particulate air (HEPA) filters are popular approaches, but both greatly increase the power requirements of heating, ventilation and air conditioning (HVAC) systems. Methods such as thermal degradation or ESP could be more energy efficient, but work needs to be done to determine the best way to implement these technologies into HVAC systems [60, 169].

VOCs are one class of compounds that can be emitted from biogenic or anthropogenic sources. Among anthropogenic activities, the transport and industrial sectors and biomass burning are responsible for most of the global anthropogenic VOCs emissions. Their detrimental impact on the atmosphere is multifaceted, as they are readily oxidised by OH radical and through a series of reactions allowing the formation of tropospheric ozone, a main component of photochemical smog plaguing the air quality of many urban cities and causing increased premature deaths [170]. Exposure to benzene, an aromatic compound, has been directly linked to leukaemia [171]. Consequently, a variety of control technologies to prevent the release of VOC by degradation or recovery have been developed. Detailed accounts of existing and emerging techniques have been reviewed [172, 173].

Destruction techniques aim at oxidizing the parent VOC into CO_2 and H_2O. High removal efficiencies are obtained by common techniques like thermal and catalytic oxidation, which can achieve more than 95% removal of VOCs [173]. Destruction can also be achieved by radical formation, using photo-catalysts like TiO_2, for example. However, thermal processes have a high energy demand due to the high temperature required for oxidation. In addition, both thermal- and photocatalytic-based oxidation involve the formation of toxic by-products and can reduce a catalyst's lifetime due to poisoning [174–176]. Recovery techniques involve two steps. First a transfer of the pollutants from the air stream to another medium and second the recovery of the pollutants. In adsorption-based techniques the pollutant is separated from the polluted stream by binding chemically or physically to the adsorbent upon exposure. The pollutant is then collected during the regeneration of the saturated adsorbent; details on various regeneration methods are reported in the literature [177–179]. So far the two leading materials in adsorption have been activated carbon for its high surface area and zeolites for their thermal stability and size selective properties. New materials, however, are being developed to overcome some of the challenges that face activated carbon and zeolites such as humidity sensitivity, flammability during regeneration and cost [172]. In the context of VOC remediation, mesoporous transition metal oxides, ordered mesoporous silica (OMS) and carbon nanotubes (CNT) can overcome some of the challenges faced by the traditional adsorbents [172, 180]. However, the complexity and inherent formation of wastes during the large-scale synthesis of these new materials, particularly OMS and CNT, is a subject of environmental concern for large scale production [180–182]. Recovery by absorption is based on transferring the gaseous pollutants to a liquid. The system is limited to highly soluble gases [173]. Investigations on phthalates as absorbents for VOCS have recently been reported [183]. Recovery by membranes is based on separation due to a concentration gradient, pressure differential and electrochemical potential [173]. Separation by membranes is selective, which can limit its efficiency since VOCs are made up of a mixture of gases. Improving membranes involves developing materials that can separate a range of organic compounds [173]. VOCs can also be separated by condensation techniques where the VOCs are cooled to low temperatures. The various remediation techniques for VOCs are summarised in Table 6.

Table 6 Industrial pollution control for large stationary point-source emissions of carbonaceous aerosols, including those applicable to bioaerosols

Control process or equipment	Mechanism	Advantages	Disadvantages
Cyclone	Particles pushed to wall of device by centrifugal force where they agglomerate and fall to collection device below	High efficiency models can achieve ~99% capture of larger particles (>10 μm) [258] Withstand high temperature and pressure Low cost and space requirement Can handle high particulate concentrations	Generally low efficiency when removing small particles (20–40% capture of 2.5 μm particles) [259]
Electrostatic precipitator (ESP)	Particles charged by electric field then collected on grounded plate	High capture efficiency (>99.5% on average); though more effective for larger particles than those in sub-μm range [260] Low operating cost Can treat large gas flows with little pressure drop	High capital cost and space requirement Inability to treat particles of high electrical resistivity
Fabric filter	Flue gas flows through porous filter media on which particulates are collected, forming a cake	Very high capture efficiency (99.6–99.95%; even for particles in sub-μm range [260] Capture of particles with low and high electrical resistivity	High maintenance cost and space requirement Large pressure drop across device Low operating temperature (maximum 290°C for typical materials) [261]
Scrubber	Water droplets injected into flue gas; particles adhere to droplets which are then separated from the gas (typically by cyclones)	Can achieve capture efficiencies of >99% [262] Low capital cost Can capture much smaller particles (sub-micrometre) than cyclone alone Useful for removal of hygroscopic or sticky particles and gas streams with high moisture contents	Pumping cost can be significant, particularly for large flows Requires subsequent separation of particles from water

Simultaneous Mitigation of Multiple Air Pollutants

While mitigation options for VOCs and bioaerosols were considered separately here, the implementation of some pollution mitigation options to target one pollutant may have an effect on the amount of another pollutant released. In many cases, the implementation of some mitigation options will reduce the emission rates of several pollutants. However, some process modifications and material substitutions lead to trade-offs, limiting the production of one pollutant while increasing that of another. For example, operating a combustion process at a higher temperature with excess oxygen will generally improve combustion efficiency, reducing the amount of carbonaceous aerosols and VOCs produced, but will increase the quantity of NO_x produced.

Future Anthropogenic Emission Projections

A wide variety of different pollution control approaches exist and in many cases emissions of pollutants such as VOCs and bioaerosols from anthropogenic sources can be effectively reduced to zero. Pollution control technologies are constantly being refined and adapted to more and more emission sources that release some of the above-mentioned pollutants.

References

1. Whitehead JD, Gallagher MW, Dorsey JR, Robinson N, Gabey AM, Coe H, McFiggans G, Flynn MJ, Ryder J, Nemitz E, Davies F (2010) Aerosol fluxes and dynamics within and above a tropical rainforest in South–East Asia. Atmos Chem Phys 10:9369
2. Artaxo P, Martins JV, Yamasoe MA, Procopio AS, Pauliquevis TM, Andreae MO, Guyon P, Gatti LV, Leal AMC (2002) Physical and chemical properties of aerosols in the wet and dry seasons in Rondonia, Amazonia. J Geophys Res Atmos 107:49–14
3. Karol MH (1991) Allergic reactions to indoor air pollutants. Environ Health Perspect 95:45
4. Welch LS (1991) Severity of health effects associated with building-related illness. Environ Health Perspect 95:67
5. Dibb JE, Jaffrezo JL (1997) Air-snow exchange investigations at summit, Greenland: an overview. J Geophys Res Oceans 102:26795
6. Amoroso A, Domine F, Esposito G, Morin S, Savarino J, Nardino M, Montagnoli M, Bonneville JM, Clement JC, Ianiello A, Beine HJ (2010) Microorganisms in dry polar snow are involved in the exchanges of reactive nitrogen species with the atmosphere. Environ Sci Technol 44:714
7. Ariya PA, Hopper JF, Harris GW (1999) C2–C7 hydrocarbon concentrations in arctic snowpack interstitial air: potential presence of active Br within the snowpack. J Atmos Chem 34:55
8. Beine H, Colussi AJ, Amoroso A, Esposito G, Montagnoli M, Hoffmann MR (2008) HONO emissions from snow surfaces. Environ Res Lett 3:045005
9. Klan P, Del FD, Ansorgova A, Klanova J, Holoubek I (2001) Photodegradation of halobenzenes in water ice. Environ Sci Pollut R 8:195

10. Cote V, Kos G, Mortazavi R, Ariya PA (2008) Microbial and "de novo" transformation of dicarboxylic acids by three airborne fungi. Sci Total Environ 390:530
11. Daly GL, Wania F (2005) Organic contaminants in mountains. Environ Sci Technol 39:385
12. Domine F, Shepson PB (2002) Air-snow interactions and atmospheric chemistry. Science 297:1506
13. Ariya PA, Domine F, Kos G, Amyot M, Cote V, Vali H, Lauzier T, Kuhs WF, Techmer K, Heinrichs T, Mortazavi R (2011) Snow – a photobiochemical exchange platform for volatile and semi-volatile organic compounds with the atmosphere. Environ Chem 8:62
14. Seok B, Helmig D, Williams MW, Liptzin D, Chowanski K, Hueber J (2009) An automated system for continuous measurements of trace gas fluxes through snow: an evaluation of the gas diffusion method at a subalpine forest site, Niwot Ridge, Colorado. Biogeochemistry 95:95
15. Xu L (2013) Satellite-based applications on climate change. Springer, Dordrecht
16. Brutel-Vuilmet C, Ménégoz M, Krinner G (2013) An analysis of present and future seasonal Northern Hemisphere land snow cover simulated by CMIP5 coupled climate models. Cryosphere 7(1):67–80
17. Domine F, Albert M, Huthwelker T, Jacobi HW, Kokhanovsky AA, Lehning M, Picard G, Simpson WR (2008) Snow physics as relevant to snow photochemistry. Atmos Chem Phys 8:171
18. McNeill VF, Grannas AM, Abbatt JPD, Ammann M, Ariya P, Bartels-Rausch T, Domine F, Donaldson DJ, Guzman MI, Heger D, Kahan TF, Klan P, Masclin S, Toubin C, Voisin D (2012) Organics in environmental ices: sources, chemistry, and impacts. Atmos Chem Phys 12:9653
19. Sumner AL, Shepson PB, Grannas AM, Bottenheim JW, Anlauf KG, Worthy D, Schroeder WH, Steffen A, Domine F, Perrier S, Houdier S (2002) Atmospheric chemistry of formaldehyde in the Arctic troposphere at Polar Sunrise, and the influence of the snowpack. Atmos Environ 36:2553
20. Atkinson R (2000) Atmospheric chemistry of VOCs and NOx. Atmos Environ 34:2063
21. Kos G, Ariya PA (2010) Volatile organic compounds in snow in the Quebec–Windsor Corridor. J Geophys Res Atmos 115:D01302
22. USEPA (2011) Volatile organic compounds (VOCs): technical overview. USEPA, Washington, DC
23. Chan LY, Chu KW, Zou SC, Chan CY, Wang XM, Barletta B, Blake DR, Guo H, Tsai WY (2006) Characteristics of nonmethane hydrocarbons (NMHCs) in industrial, industrial-urban, and industrial-suburban atmospheres of the Pearl River Delta (PRD) region of south China. J Geophys Res Atmos 111:D11304
24. Pons B, Fernandez-Torroba MA, Ortiz G, Tena MT (2003) Monitoring and evolution of the pollution by volatile organic compounds (VOCs) in the groundwaters of the Najerilla River Basin (Spain). Int J Environ Anal Chem 83:495
25. Puxbaum H, Tenze-Kunit M (2003) Size distribution and seasonal variation of atmospheric cellulose. Atmos Environ 37:3693
26. Sachweh B, Umhauer H, Ebert F, Büttner H, Friehmelt R (1998) In situ optical particle counter with improved coincidence error correction for number concentrations up to 10E7 particles cm-3. J Aerosol Sci 29:1075
27. Morris CE, Georgakopoulos DG, Sands DC (2004) Ice nucleation active bacteria and their potential role in precipitation. J Phys IV 121:87
28. Beine H, Anastasio C, Domine F, Douglas T, Barret M, France J, King M, Hall S, Ullmann K (2012) Soluble chromophores in marine snow, seawater, sea ice and frost flowers near Barrow, Alaska. J Geophys Res 117:D00R15
29. Herbert BMJ, Halsall CJ, Fitzpatrick L, Villa S, Jones KC, Thomas GO (2004) Use and validation of novel snow samplers for hydrophobic, semi-volatile organic compounds (SVOCs). Chemosphere 56:227

30. Swanson AL, Blake NJ, Blake DR, Sherwood RF, Dibb JE, Lefer BL, Atlas E (2007) Are methyl halides produced on all ice surfaces? Observations from snow-laden field sites. Atmos Environ 41:5162

31. Dassau TM, Sumner AL, Koeniger SL, Shepson PB, Yang J, Honrath RE, Cullen NJ, Steffen K, Jacobi HW, Frey M, Bales RC (2002) Investigation of the role of the snowpack on atmospheric formaldehyde chemistry at summit, Greenland. J Geophys Res Atmos 107:9–14

32. Albert MR, Grannas AM, Bottenheim J, Shepson PB, Perron FE (2002) Processes and properties of snow-air transfer in the high Arctic with application to interstitial ozone at Alert, Canada. Atmos Environ 36:2779

33. Boudries H, Bottenheim JW, Guimbaud C, Grannas AM, Shepson PB, Houdier S, Perrier S, Domine F (2002) Distribution and trends of oxygenated hydrocarbons in the high Arctic derived from measurements in the atmospheric boundary layer and interstitial snow air during the alert 2000 field campaign. Atmos Environ 36:2573

34. Jacobi HW, Bales RC, Honrath RE, Peterson MC, Dibb JE, Swanson AL, Albert MR (2004) Reactive trace gases measured in the interstitial air of surface snow at summit, Greenland. Atmos Environ 38:1687

35. Sumner AL, Shepson PB (1999) Snowpack production of formaldehyde and its effect on the Arctic troposphere. Nature 398:230

36. Battle MO, Severinghaus JP, Sofen ED, Plotkin D, Orsi AJ, Aydin M, Montzka SA, Sowers T, Tans PP (2011) Controls on the movement and composition of firn air at the West Antarctic Ice Sheet Divide. Atmos Chem Phys 11:11007

37. Butler JH, Battle M, Bender ML, Montzka SA, Clarke AD, Saltzman ES, Sucher CM, Severinghaus JP, Elkins JW (1999) A record of atmospheric halocarbons during the twentieth century from polar firn air. Nature 399:749

38. Bocquet F, Helmig D, Oltmans SJ (2007) Ozone in interstitial air of the mid-latitude, seasonal snowpack at Niwot Ridge, Colorado. Arct Antarct Alp Res 39:375

39. Helmig D, Seok B, Williams MW, Hueber J, Sanford R (2009) Fluxes and chemistry of nitrogen oxides in the Niwot Ridge, Colorado, snowpack. Biogeochemistry 95:115

40. Gao SS, Sjostedt SJ, Sharma S, Hall SR, Ullmann K, Abbatt JPD (2012) PTR-MS observations of photo-enhanced VOC release from Arctic and midlatitude snow. J Geophys Res 117:1–10

41. Avino P, Cinelli G, Notardonato I, Russo MV (2011) Evaluation of different adsorbents for large-volume pre-concentration for analyzing atmospheric persistent organic pollutants at trace levels. Anal Bioanal Chem 400:3561

42. Hudson ED, Okuda K, Ariya PA (2007) Determination of acetone in seawater using derivatization solid-phase microextraction. Anal Bioanal Chem 388:1275

43. Jaffrezo JL, Clain MP, Masclet P (1994) Polycyclec aromatic hydrocarbons in the Polar ice of Greenland: geochemical use of these atmospheric tracers. Atmos Environ 28:1139

44. Swanson AL, Lefer BL, Stroud V, Atlas E (2005) Trace gas emissions through a winter snowpack in the subalpine ecosystem at Niwot Ridge, Colorado. Geophys Res Lett 32, L03805

45. Bower JP, Hood E, Hoferkamp LA (2008) Major solutes, metals, and alkylated aromatic compounds in high-latitude maritime snowpacks near the Trans-Alaska pipeline terminal, Valdez, Alaska. Environ Res Lett 3:045010

46. Gabrieli J, Decet F, Luchetta A, Valt M, Pastore P, Barbante C (2010) Occurrence of PAH in the seasonal snowpack of the Eastern Italian Alps. Environ Pollut 158:3130

47. Domine F, Houdier S, Taillandier A-S, Simpson WR (2010) Acetaldehyde in the Alaskan subarctic snowpack. Atmos Chem Phys 10:919

48. Houdier S, Perrier S, Defrancq E, Legrand M (2000) A new fluorescent probe for sensitive detection of carbonyl compounds: sensitivity improvement and application to environmental water samples. Anal Chim Acta 412:221

49. Houdier S, Perrier S, Dominé F, Cabanes A, Legagneux L, Grannas AM, Guimbaud C, Shepson PB, Boudries H, Bottenheim JW (2002) Acetaldehyde and acetone in the Arctic snowpack during the alert 2000 campaign. Snowpack composition, incorporation processes and atmospheric impact. Atmos Environ 36:2609

50. Sheridan GEC, Masters CI, Shallcross JA, Mackey BM (1998) Detection of mRNA by reverse transcription PCR as an indicator of viability in *Escherichia coli* cells. Appl Environ Microbiol 64:1313

51. Hutterli MA, McConnell JR, Chen G, Bales RC, Davis DD, Lenschow DH (2004) Formaldehyde and hydrogen peroxide in air, snow and interstitial air at South Pole. Atmos Environ 38:5439

52. Herbert BMJ, Halsall CJ, Jones KC, Kallenborn R (2006) Field investigation into the diffusion of semi-volatile organic compounds into fresh and aged snow. Atmos Environ 40:1385

53. Van Baar BLM (2002) Realtime sizing and detection of biological aerosol particles by a matrix-assisted laser desorbtion/ionisation time-of-flight mass spectrometry. In: Materials of the second international symposium on detection technologies, Arlington, VA

54. Hutterli MA, Rothlisberger R, Bales RC (1999) Atmosphere-to-snow-to-firn transfer studies of HCHO at Summit, Greenland. Geophys Res Lett 26:1691

55. Jacobi HW, Frey MM, Hutterli MA, Bales RC, Schrems O, Cullen NJ, Steffen K, Koehler C (2002) Measurements of hydrogen peroxide and formaldehyde exchange between the atmosphere and surface snow at Summit, Greenland. Atmos Environ 36:2619

56. Frey MM, Stewart RW, McConnell JR, Bales RC (2005) Atmospheric hydroperoxides in West Antarctica: links to stratospheric ozone and atmospheric oxidation capacity. J Geophys Res Atmos 110:D23301

57. Perrier S, Houdier S, Domine F, Cabanes A, Legagneux L, Sumner AL, Shepson PB (2002) Formaldehyde in Arctic snow. Incorporation into ice particles and evolution in the snowpack. Atmos Environ 36:2695

58. Riedel K, Weller R, Schrems O (1999) Variability of formaldehyde in the Antarctic troposphere. Phys Chem Chem Phys 1:5523

59. Salmon RA, Bauguitte SJ, Bloss W, Hutterli MA, Jones AE, Read K, Wolff EW (2008) Measurement and interpretation of gas phase formaldehyde concentrations obtained during the CHABLIS campaign in coastal Antarctica. Atmos Chem Phys 8:4085

60. Peccia J, Milton DK, Reponen T, Hill J (2008) A role for environmental engineering and science in preventing bioaerosol-related disease. Environ Sci Technol 42:4631

61. Guimbaud C, Grannas AM, Shepson PB, Fuentes JD, Boudries H, Bottenheim JW, Dominé F, Houdier S, Perrier S, Biesenthal TB, Splawn BG (2002) Snowpack processing of acetaldehyde and acetone in the Arctic atmospheric boundary layer. Atmos Environ 36:2743

62. Hutterli MA, Bales RC, McConnell JR, Stewart RW (2002) HCHO in Antarctic snow: preservation in ice cores and air-snow exchange. Geophys Res Lett 29

63. Bhatia MP, Das SB, Longnecker K, Charette MA, Kujawinski EB (2010) Molecular characterization of dissolved organic matter associated with the Greenland ice sheet. Geochim Cosmochim Acta 74:3768–3784

64. Pautler BG, Simpson AJ, Simpson MJ, Tseng L-H, Spraul M, Dubnick A, Sharp MJ, Fitzsimons SJ (2011) Detection and structural identification of dissolved organic matter in Antarctic glacial ice at natural abundance by SPR-W5-WATERGATE 1H NMR spectroscopy. Environ Sci Technol 45:4710

65. Lee B, Hwangbo Y, Lee DS (2009) Determination of low molecular weight monocarboxylic acid gases in the atmosphere by parallel plate diffusion scrubber-ion chromatography. J Chromatogr Sci 47:516

66. Vasconcellos PC, Souza DZ, Sanchez-Ccoyllo O, Bustillos JOV, Lee H, Santos FC, Nascimento KH, Araújo MP, Saarnio K, Teinilä K, Hillamo R (2010) Determination of anthropogenic and biogenic compounds on atmospheric aerosol collected in urban, biomass burning and forest areas in São Paulo, Brazil. Sci Total Environ 408:5836

67. Kippenberger M, Winterhalter R, Moortgat GK (2008) Determination of higher carboxylic acids in snow samples using solid-phase extraction and LC/MS-TOF. Anal Bioanal Chem 392:1459
68. Kawamura K, Watanabe T (2004) Determination of stable carbon isotopic compositions of low molecular weight dicarboxylic acids and ketocarboxylic acids in atmospheric aerosol and snow samples. Anal Chem 76:5762
69. Narukawa M, Kawamura K, Li SM, Bottenheim JW (2002) Dicarboxylic acids in the Arctic aerosols and snowpacks collected during alert 2000. Atmos Environ 36:2491
70. Sempere R, Kawamura K (1994) Comparative distributions of dicarboxylic-acids and related polar compounds in snow rain and aerosols from urban atmosphere. Atmos Environ 28:449
71. Akyüz M (2008) Simultaneous determination of aliphatic and aromatic amines in ambient air and airborne particulate matters by gas chromatography-mass spectrometry. Atmos Environ 42:3809
72. Chang I-H, Lee C-G, Lee DS (2003) Development of an automated method for simultaneous determination of low molecular weight aliphatic amines and ammonia in ambient air by diffusion scrubber coupled to ion chromatography. Anal Chem 75:6141
73. Finessi E, Decesari S, Paglione M, Giulianelli L, Carbone C, Gilardoni S, Fuzzi S, Saarikoski S, Raatikainen T, Hillamo R (2012) Determination of the biogenic secondary organic aerosol fraction in the boreal forest by NMR spectroscopy. Atmos Chem Phys 12:941
74. Pratt KA, Prather KA (2012) Mass spectrometry of atmospheric aerosols – recent developments and applications. Part I: off-line mass spectrometry techniques. Mass Spectrom Rev 31:1
75. Pratt KA, Prather KA (2012) Mass spectrometry of atmospheric aerosols – recent developments and applications. Part II: on-line mass spectrometry techniques. Mass Spectrom Rev 31:17
76. Drewnick F, Schneider J, Hings SS, Hock N, Noone K, Targino A, Weimer S, Borrmann S (2007) Measurement of ambient, interstitial, and residual aerosol particles on a mountaintop site in central Sweden using an aerosol mass spectrometer and a CVI. J Atmos Chem 56:1
77. Canagaratna MR, Jayne JT, Jimenez JL, Allan JD, Alfarra MR, Zhang Q, Onasch TB, Drewnick F, Coe H, Middlebrook A, Delia A, Williams LR, Trimborn AM, Northway MJ, DeCarlo PF, Kolb CE, Davidovits P, Worsnop DR (2007) Chemical and microphysical characterization of ambient aerosols with the aerodyne aerosol mass spectrometer. Mass Spectrom Rev 26:185
78. Jimenez JL, Jayne JT, Shi Q, Kolb CE, Worsnop DR, Yourshaw I, Seinfeld JH, Flagan RC, Zhang XF, Smith KA, Morris JW, Davidovits P (2003) Ambient aerosol sampling using the aerodyne aerosol mass spectrometer. J Geophys Res Atmos 108:1–13
79. DeCarlo PF, Kimmel JR, Trimborn A, Northway MJ, Jayne JT, Aiken AC, Gonin M, Fuhrer K, Horvath T, Docherty KS, Worsnop DR, Jimenez JL (2006) Field-deployable, high-resolution, time-of-flight aerosol mass spectrometer. Anal Chem 78:8281
80. Jayne JT, Leard DC, Zhang XF, Davidovits P, Smith KA, Kolb CE, Worsnop DR (2000) Development of an aerosol mass spectrometer for size and composition analysis of submicron particles. Aerosol Sci Technol 33:49
81. Hearn JD, Smith GD (2004) A chemical ionization mass spectrometry method for the online analysis of organic aerosols. Anal Chem 76:2820
82. Grosse S, Letzel T (2007) Liquid chromatography/atmospheric pressure ionization mass spectrometry with post-column liquid mixing for the efficient determination of partially oxidized polycyclic aromatic hydrocarbons. J Chromatogr A 1139:75
83. Lintelmann J, Fischer K, Matuschek G (2006) Determination of oxygenated polycyclic aromatic hydrocarbons in particulate matter using high-performance liquid chromatography-tandem mass spectrometry. J Chromatogr A 1133:241
84. Cornell SE, Jickells TD, Cape JN, Rowland AP, Duce RA (2003) Organic nitrogen deposition on land and coastal environments: a review of methods and data. Atmos Environ 37:2173

85. Andersen KB, Hansen MJ, Feilberg A (2012) Minimisation of artefact formation of dimethyl disulphide during sampling and analysis of methanethiol in air using solid sorbent materials. J Chromatogr A 1245:24

86. Feilberg A, Liu DZ, Adamsen APS, Hansen MJ, Jonassen KEN (2010) Odorant emissions from intensive pig production measured by online proton-transfer-reaction mass spectrometry. Environ Sci Technol 44:5894

87. Pandey SK, Kim KH (2009) A review of methods for the determination of reduced sulfur compounds (RSCs) in air. Environ Sci Technol 43:3020

88. Arellano L, Fernandez P, Tatosova J, Stuchlik E, Grimalt JO (2011) Long-range transported atmospheric pollutants in snowpacks accumulated at different altitudes in the Tatra Mountains (Slovakia). Environ Sci Technol 45:9268

89. Kos G, Ariya PA (2006) Determination of a wide range of volatile and semivolatile organic compounds in snow by use of solid-phase micro-extraction (SPME). Anal Bioanal Chem 385:57

90. Starokozhev E, Fries E, Cycura A, Puttmann W (2009) Distribution of VOCs between air and snow at the Jungfraujoch high alpine research station, Switzerland, during CLACE 5 (winter 2006). Atmos Chem Phys 9:3197

91. Hudson ED, Ariya PA (2007) Measurements of non-methane hydrocarbons, DOC in surface ocean waters and aerosols over the Nordic seas during polarstern cruise ARK-XX/1 (2004). Chemosphere 69:1474

92. Blas M, Cichala-Kamrowska K, Sobik M, Polkowska Z, Namiesnik J (2010) Conditions controlling atmospheric pollutant deposition via snowpack. Environ Rev 18:87

93. Macher JM, Willeke K (1992) Performance criteria for bioaerosol samplers. J Aerosol Sci 23 (Suppl 1):647

94. Ward DM, Weller R, Bateson MM (1990) 16S ribosomal-RNA sequences reveal numerous uncultured microorganisms in a natural community. Nature 345:63

95. Blackburn CD, McCarthy JD (2000) Modifications to methods for the enumeration and detection of injured *Escherichia coli* O157: H7 in foods. Int J Food Microbiol 55:285

96. Kogure K, Simidu U, Taga N (1979) A tentative direct microscopic method for counting living marine bacteria. Can J Microbiol 25:415

97. del Mar Lleo M, Pierobon S, Tafi MC, Signoretto C, Canepari P (2000) mRNA detection by reverse transcription-PCR for monitoring viability over time in an *Enterococcus faecalis* viable but nonculturable population maintained in a laboratory microcosm. Appl Environ Microbiol 66:4564

98. McCarty SC, Atlas RM (1993) Effect of amplicon size on PCR detection of bacteria exposed to chlorine. PCR Methods Appl 3:181

99. Nebe-von Caron G, Stephens P, Badley RA (1998) Assessment of bacterial viability status by flow cytometry and single cell sorting. J Appl Microbiol 84:988

100. Diaper JP, Edwards C (1994) Survival of Staphylococcus aureus in lakewater monitored by flow cytometry. Microbiology 140:35

101. Turner K, Porter J, Pickup R, Edwards C (2000) Changes in viability and macromolecular content of long-term batch cultures of *Salmonella typhimurium* measured by flow cytometry. J Appl Microbiol 89:90

102. Vincent JH, Ramachandran G, Kerr SM (2001) Particle size and chemical species fingerprinting of aerosols in primary nickel production industry workplaces. J Environ Monit 3:565

103. Raisi L, Aleksandropoulou V, Lazaridis M, Katsivela E (2013) Size distribution of viable, cultivable, airborne microbes and their relationship to particulate matter concentrations and meteorological conditions in a Mediterranean site. Aerobiologia 29(2):233–248

104. Grinshpun SA, Adhikari A, Cho S-H, Kim K-Y, Lee T, Reponen T (2007) A small change in the design of a slit bioaerosol impactor significantly improves its collection characteristics. J Environ Monit 9:855

105. Bergman W, Lochner JS, Sawyer S, Milanovich F, Mariella R Jr (2005) High air flow, low pressure drop, bio-aerosol collector using a multi-slit virtual impactor. J Aerosol Sci 36:619

106. Wang C-F, Chang C-Y, Tsai S-F, Chiang H-L (2005) Characteristics of road dust from different sampling sites in northern Taiwan. J Air Waste Manag Assoc 55:1236
107. Wei Z, Rosario RC, Montoya LD (2010) Collection efficiency of a midget impinger for nanoparticles in the range of 3–100 nm. Atmos Environ 44:872
108. Donaldson AI, Wardley RC, Martin S, Ferris NP (1983) Experimental Aujeszky's disease in pigs: excretion, survival and transmission of the virus. Vet Rec 113:490
109. Donaldson AI, Gibson CF, Oliver R, Hamblin C, Kitching RP (1987) Infection of cattle by airborne foot-and-mouth disease virus: minimal doses with O1 and SAT 2 strains. Res Vet Sci 43:339
110. Willeke K, Lin X, Grinshpun SA (1998) Improved aerosol collection by combined impaction and centrifugal motion. Aerosol Sci Technol 28:439
111. Juozaitis A, Willeke K, Grinshpun SA, Donnelly J (1994) Impaction onto a glass slide or agar versus impingement into a liquid for the collection and recovery of airborne microorganisms. Appl Environ Microbiol 60:861
112. Willeke K, Grinshpun SA, Ulevicius V, Terzieva S, Donnelly J, Stewart S, Juozaitis A (1995) Microbial stress, bounce and re-aerosolization in bioaerosol samplers. J Aerosol Sci 26 (Suppl 1):S883
113. Kim DS, Lim KS, Xiang RB, Lee KW (2002) Design and performance evaluation of an aerosol separator. J Aerosol Sci 33:1405
114. Moosmüller H, Chakrabarty RK, Arnott WP (2009) Aerosol light absorption and its measurement: a review. J Quant Spectrosc Radiat Transf 110:844
115. Mitchell JP, Nagel MW, Nichols S, Nerbrink O (2006) Laser diffractometry as a technique for the rapid assessment of aerosol particle size from inhalers. J Aerosol Med Deposition Clearance Effects Lung 19:409
116. Swithenbank J, Beer JM, Taylor DS, Abbot D, McCreath GC (1977) A laser diagnostic technique for the measurement of droplet and particle size distribution. Progress Astronautics Aeronautics 53:421
117. Organization IS, (1999) Particle size analysis – laser diffraction methods: part 1: general principles. International Standards Organization (ISO)
118. Merkus HG, Marijnissen JCM, Jansma HL, Scarlett B (1994) Droplet size distribution measurements for medical nebulizers by the forward light scattering technique ("laser diffraction"). J Aerosol Sci 25(Suppl 1):319
119. Schaub SA, Alexander DR, Barton JP (1994) Theoretical analysis of the effects of particle trajectory and structural resonances on the performance of a phase-Doppler particle analyzer. Appl Opt 33:473
120. Holve DJ, Annen KD (1984) Optical particle counting, sizing, and velocimetry using intensity deconvolution. Opt Eng 23:235591
121. Liu BY, Pui DY (1975) On the performance of the electrical aerosol analyzer. J Aerosol Sci 6:249
122. Whitby KT, Husar RB, Liu BYH (1972) The aerosol size distribution of Los Angeles smog. J Colloid Interface Sci 39:177
123. Yeh HC, Cheng YS, Kanapilly GM (1981) Electrical aerosol analyzer: data reduction for high altitude or reduced pressure. Atmos Environ 15(1967):713
124. Song DK, Moon Lee H, Chang H, Soo Kim S, Shimada M, Okuyama K (2006) Performance evaluation of long differential mobility analyzer (LDMA) in measurements of nanoparticles. J Aerosol Sci 37:598
125. Werkhaven JA, Reinisch L, Sorrell M, Tribble J, Ossoff RH (1994) Noninvasive optical diagnosis of bacteria causing otitis media. Laryngoscope 104:264
126. Buteau S, Simard JR, Lahaie P, Roy G, Mathieu P, Dery B, Ho J, McFee J (2008) In: Kim YJ, Platt U (eds) Advanced environmental monitoring Springer, New York, pp 203–216
127. Simard JR, Roy G, Mathieu P, Larochelle V, McFee J, Ho J (2004) Standoff sensing of bioaerosols using intensified range-gated spectral analysis of laser-induced fluorescence. IEEE Trans Geosci Remote Sens 42:865

128. Weikamp C (2005) Lidar: range-resolved optical remote sensing of the atmosphere. Springer, New York

129. Schuster KC, Mertens F, Gapes JR (1999) FTIR spectroscopy applied to bacterial cells as a novel method for monitoring complex biotechnological processes. Vibrat Spectrosc 19:467

130. Petrich W (2001) Mid-infrared and Raman spectroscopy for medical diagnostics. Appl Spectrosc Rev 36:181

131. Scully MO, Kattawar GW, Lucht RP, Opatrny T, Pilloff H, Rebane A, Sokolov AV, Zubairy MS (2002) FAST CARS: engineering a laser spectroscopic technique for rapid identification of bacterial spores. Proc Natl Acad Sci USA 99:10994

132. Gopel W (1991) Chemical sensing, molecular electronics and nanotechnology – interface technologies down to the molecular scale. Sens Actuators B Chem 4:7

133. Gopel W, Heiduschka P (1995) Interface analysis in biosensor design. Biosens Bioelectron 10:853

134. Sethi RS (1994) Transducer aspects of biosensors (Reprinted from Gec J Res 9:81, 1991). Biosens Bioelectron 9:243

135. Hofstadler SA, Sampath R, Blyn LB, Eshoo MW, Hall TA, Jiang Y, Drader JJ, Hannis JC, Sannes-Lowery KA, Cummins LL, Libby B, Walcott DJ, Schink A, Massire C, Ranken R, Gutierrez J, Manalili S, Ivy C, Melton R, Levene H, Barrett-Wilt G, Li F, Zapp V, White N, Samant V, McNeil JA, Knize D, Robbins D, Rudnick K, Desai A, Moradi E, Ecker DJ (2005) TIGER: the universal biosensor. Int J Mass Spectrom 242:23

136. Lewandowski R, Kozlowska K, Szpakowska M, Stepinska M, Trafny EA (2010) Use of a foam spatula for sampling surfaces after bioaerosol deposition. Appl Environ Microbiol 76:688

137. Albrecht M, Gauthier R, Leaper D (2009) Forced-air warming: a source of airborne contamination in the operating room? Orthop Rev (Pavia) 1:e28

138. Moularat S, Robine E, Ramalho O, Oturan MA (2008) Detection of fungal development in closed spaces through the determination of specific chemical targets. Chemosphere 72:224

139. Lisle JT, Hamilton MA, Willse AR, McFeters GA (2004) Comparison of fluorescence microscopy and solid-phase cytometry methods for counting bacteria in water. Appl Environ Microbiol 70:5343

140. Sharma A, Schulman S (1999) Introduction to fluorescence spectroscopy. Wiley, New York

141. Anderson JE, Webb SR, Fischer RL, Kester KM, Brown BL (2001) Baseline and in vivo total photoluminescence of endospore material using the parasitoid wasp C-congregata. Appl Spectrosc 55:684

142. Lakowicz JR (1999) Principles of fluorescence spectroscopy. Kluwer Academic, New York

143. Bronk BV, Reinisch L (1993) Variability of steady state bacterial fluorescence with respect to growth conditions. Appl Spectrosc 47:436

144. McCartney HA, West JS (2007) In: Dijksterhuis J, Samson RA (eds) Food mycology – a multifaceted approach to fungi and food. CRC, Boca Raton, pp 65–81

145. Williams RH, Ward E, McCartney HA (2001) Methods for integrated air sampling and DNA analysis for detection of airborne fungal spores. Appl Environ Microbiol 67:2453

146. Calderon C, Ward E, Freeman J, McCartney A (2002) Detection of airborne fungal spores sampled by rotating-arm and Hirst-type spore traps using polymerase chain reaction assays. J Aerosol Sci 33:283

147. Fox GE, Stackebrandt E, Hespell RB, Gibson J, Maniloff J, Dyer TA, Wolfe RS, Balch WE, Tanner RS, Magrum LJ, Zablen LB, Blakemore R, Gupta R, Bonen L, Lewis BJ, Stahl DA, Luehrsen KR, Chen KN, Woese CR (1980) The phylogeny of prokaryotes. Science 209:457

148. Edwards RA, Rodriguez-Brito B, Wegley L, Haynes M, Breitbart M, Peterson DM, Saar MO, Alexander S, Alexander EC, Rohwer F (2006) Using pyrosequencing to shed light on deep mine microbial ecology. BMC Genomics 7:1–13

149. Angly FE, Felts B, Breitbart M, Salamon P, Edwards RA, Carlson C, Chan AM, Haynes M, Kelley S, Liu H, Mahaffy JM, Mueller JE, Nulton J, Olson R, Parsons R, Rayhawk S, Suttle CA, Rohwer F (2006) The marine viromes of four oceanic regions. PLoS Biol 4:2121

150. Brown MV, Philip GK, Bunge JA, Smith MC, Bissett A, Lauro FM, Fuhrman JA, Donachie SP (2009) Microbial community structure in the North Pacific ocean. ISME J 3:1374
151. Eckburg PB, Bik EM, Bernstein CN, Purdom E, Dethlefsen L, Sargent M, Gill SR, Nelson KE, Relman DA (2005) Diversity of the human intestinal microbial flora. Science 308:1635
152. Ley RE, Turnbaugh PJ, Klein S, Gordon JI (2006) Microbial ecology – human gut microbes associated with obesity. Nature 444:1022
153. Turnbaugh PJ, Ley RE, Mahowald MA, Magrini V, Mardis ER, Gordon JI (2006) An obesity-associated gut microbiome with increased capacity for energy harvest. Nature 444:1027
154. Zhou X, Bent SJ, Schneider MG, Davis CC, Islam MR, Forney LJ (2004) Characterization of vaginal microbial communities in adult healthy women using cultivation-independent methods. Microbiol SGM 150:2565
155. Shendure J, Ji HL (2008) Next-generation DNA sequencing. Nat Biotechnol 26:1135
156. Gentry TJ, Wickham GS, Schadt CW, He Z, Zhou J (2006) Microarray applications in microbial ecology research. Microb Ecol 52:159
157. Hugenholtz P, Tyson GW (2008) Microbiology – metagenomics. Nature 455:481
158. Xue HX, Khalizov AF, Wang L, Zheng J, Zhang RY (2009) Effects of coating of dicarboxylic acids on the mass–mobility relationship of soot particles. Environ Sci Technol 43:2787
159. Isaacman G, Chan AWH, Nah T, Worton DR, Ruehl CR, Wilson KR, Goldstein A (2012) Heterogeneous OH oxidation of motor oil particles causes selective depletion of branched and less cyclic hydrocarbons. Environ Sci Technol 46(19):10632–10640
160. Kroll JH, Smith JD, Che DL, Kessler SH, Worsnop DR, Wilson KR (2009) Measurement of fragmentation and functionalization pathways in the heterogeneous oxidation of oxidized organic aerosol. Phys Chem Chem Phys 11:8005
161. Lambe AT, Onasch TB, Croasdale DR, Wright JP, Martin AT, Franklin JP, Massoli P, Kroll JH, Canagaratna MR, Brune WH, Worsnop DR, Davidovits P (2012) Transitions from functionalization to fragmentation reactions of laboratory secondary organic aerosol (SOA) generated from the OH oxidation of alkane precursors. Environ Sci Technol 46:5430
162. Miljevic B, Surawski NC, Bostrom T, Ristovski ZD (2012) Restructuring of carbonaceous particles upon exposure to organic and water vapours. J Aerosol Sci 47:48
163. Pankhurst LJ, Akeel U, Hewson C, Maduka I, Pham P, Saragossi J, Taylor J, Lai KM (2011) Understanding and mitigating the challenge of bioaerosol emissions from urban community composting. Atmos Environ 45:85
164. Kummer V, Thiel WR (2008) Bioaerosols – sources and control measures. Int J Hyg Environ Health 211:299
165. Lee BU, Hong IG, Lee DH, Chong E-S, Jung JH, Lee JH, Kim HJ, Lee I-S (2012) Bacterial bioaerosol concentrations in public restroom environments. Aerosol Air Quality Res 12:251
166. Li C-S, Wen Y-M (2003) Control effectiveness of electrostatic precipitation on airborne microorganisms. Aerosol Sci Technol 37:933
167. Lin C-Y, Li C-S (2002) Control effectiveness of ultraviolet germicidal irradiation on bioaerosols. Aerosol Sci Technol 36:474
168. Millner PD (2009) Bioaerosols associated with animal production operations. Bioresour Technol 100:5379
169. Jung JH, Lee JE, Kim SS (2009) Thermal effects on bacterial bioaerosols in continuous air flow. Sci Total Environ 407:4723
170. Seinfeld JH, Pandis SN (2006) Atmospheric chemistry and physics: from air pollution to climate change. Wiley, Hoboken
171. Kacew S, Lemaire I (2000) Recent developments in benzene risk assessment. J Toxicol Environ Health A 61:485
172. Parmar GR, Rao NN (2009) Emerging control technologies for volatile organic compounds. Crit Rev Environ Sci Technol 39:41
173. Khan FI, Aloke A (2000) Removal of volatile organic compounds from polluted air. J Loss Prev Process Ind 13:527

174. Kohno H, Tamura M, Shibuya A, Honda S, Berezin AA, Chang JS, Yamamoto T (1998) Destruction of volatile organic compounds used in a semiconductor industry by a capillary tube discharge reactor. IEEE Trans Ind Appl 34:953

175. Environment Australia (1999) Incineration and dioxins: review of formation processes. Consultancy report prepared by Environmental and Safety Services for Environment Australia. Commonwealth Department of the Environment and Heritage, Canberra

176. Heck RM, Farrauto RJ, Gulati ST (2002) Catalytic air pollution control: commercial technology. Wiley-Interscience, New York

177. Mycock JC, McKenna JD, Theodore L (1995) Handbook of air pollution control engineering and technology. CRC, Boca Raton

178. Sheintuch M, Matatov-Meytal YI (1999) Comparison of catalytic processes with other regeneration methods of activated carbon. Catalysis Today 53:73

179. Bandosz TJ (2006) Activated carbon surfaces in environmental remediation. Elsevier, Amsterdam

180. Jaroniec M (2006) In: Loureiro J, Kartel M (eds) Combined and hybrid adsorbents. Springer, Netherlands, pp 23–36

181. Plata DL, Hart AJ, Reddy CM, Gschwend PM (2009) Early evaluation of potential environmental impacts of carbon nanotube synthesis by chemical vapor deposition. Environ Sci Technol 43:8367

182. Yang RT (2003) Adsorbents: fundamentals and applications. Wiley-Interscience, Hoboken

183. Bourgois D, Vanderschuren J, Thomas D (2008) Determination of liquid diffusivities of VOC (paraffins and aromatic hydrocarbons) in phthalates. Chem Eng Process Process Intensif 47:1363

184. Hobbs PV (2000) Introduction to atmospheric chemistry. Cambridge University Press, Cambridge

185. Warneck P (2000) Chemistry of the natural atmosphere. Academic, San Diego

186. Broadgate WJ, Liss PS, Penkett SA (1997) Seasonal emissions of isoprene and other reactive hydrocarbon gases from the ocean. Geophys Res Lett 24:2675

187. Yassaa N, Peeken I, Zollner E, Bluhm K, Arnold S, Spracklen D, Williams J (2008) Evidence for marine production of monoterpenes. Environ Chem 5:391

188. Grosjean E, Grosjean D, Fraser MP, Cass GR (1996) Air quality model evaluation data for organics. 2. C-1-C-14 carbonyls in Los Angeles air. Environ Sci Technol 30:2687

189. Marandino CA, De Bruyn WJ, Miller SD, Prather MJ, Saltzman ES (2005) Oceanic uptake and the global atmospheric acetone budget. Geophys Res Lett 32:1–4

190. Shepson PB, Sirju AP, Hopper JF, Barrie LA, Young V, Niki H, Dryfhout H (1996) Sources and sinks of carbonyl compounds in the Arctic Ocean boundary layer: polar ice floe experiment. J Geophys Res Atmos 101:21081

191. Singh H, Chen Y, Staudt A, Jacob D, Blake D, Heikes B, Snow J (2001) Evidence from the Pacific troposphere for large global sources of oxygenated organic compounds. Nature 410:1078

192. Singh H, Chen Y, Tabazadeh A, Fukui Y, Bey I, Yantosca R, Jacob D, Arnold F, Wohlfrom K, Atlas E, Flocke F, Blake D, Blake N, Heikes B, Snow J, Talbot R, Gregory G, Sachse G, Vay S, Kondo Y (2000) Distribution and fate of selected oxygenated organic species in the troposphere and lower stratosphere over the Atlantic. J Geophys Res Atmos 105:3795

193. Williams J, Holzinger R, Gros V, Xu X, Atlas E, Wallace DWR (2004) Measurements of organic species in air and seawater from the tropical Atlantic. Geophys Res Lett 31:3795–3805

194. Kirstine W, Galbally I, Ye YR, Hooper M (1998) Emissions of volatile organic compounds (primarily oxygenated species) from pasture. J Geophys Res Atmos 103:10605

195. Nemecek-Marshall M, Wojciechowski C, Kuzma J, Silver GM, Fall R (1995) Marine *Vibrio* species produce the volatile organic compound acetone. Appl Environ Microbiol 61:44

196. Nemecek-Marshall M, Wojciechowski C, Wagner WP, Fall R (1999) Acetone formation in the vibrio family: a new pathway for bacterial leucine catabolism. J Bacteriol 181:7493

197. Nuccio J, Seaton PJ, Kieber RJ (1995) Biological production of formaldehyde in the marine environment. Limnol Oceanogr 40:521

198. Wichard T, Poulet SA, Pohnert G (2005) Determination and quantification of α, β, γ, δ-unsaturated aldehydes as pentafluorobenzyl-oxime derivates in diatom cultures and natural phytoplankton populations: application in marine field studies. J Chromatogr B 814:155

199. Nguyen HTH, Takenaka N, Bandow H, Maeda Y, de Oliva ST, Botelho MMF, Tavares TM (2001) Atmospheric alcohols and aldehydes concentrations measured in Osaka, Japan and in Sao Paulo, Brazil. Atmos Environ 35:3075

200. Millet DB, Jacob DJ, Custer TG, de Gouw JA, Goldstein AH, Karl T, Singh HB, Sive BC, Talbot RW, Warneke C, Williams J (2008) New constraints on terrestrial and oceanic sources of atmospheric methanol. Atmos Chem Phys 8:6887

201. Kesselmeier J, Kuhn U, Rottenberger S, Biesenthal T, Wolf A, Schebeske G, Andreae MO, Ciccioli P, Brancaleoni E, Frattoni M, Oliva ST, Botelho ML, Silva CMA, Tavares TM (2002) Concentrations and species composition of atmospheric volatile organic compounds (VOCs) as observed during the wet and dry season in Rondonia (Amazonia). J Geophys Res Atmos 107:20–13

202. Kesselmeier J, Staudt M (1999) Biogenic volatile organic compounds (VOC): an overview on emission, physiology and ecology. J Atmos Chem 33:23

203. Jacob DJ, Field BD, Li QB, Blake DR, de Gouw J, Warneke C, Hansel A, Wisthaler A, Singh HB, Guenther A (2005) Global budget of methanol: constraints from atmospheric observations. J Geophys Res Atmos 110:1–17

204. Singh HB, Salas LJ, Chatfield RB, Czech E, Fried A, Walega J, Evans MJ, Field BD, Jacob DJ, Blake D, Heikes B, Talbot R, Sachse G, Crawford JH, Avery MA, Sandholm S, Fuelberg H (2004) Analysis of the atmospheric distribution, sources, and sinks of oxygenated volatile organic chemicals based on measurements over the Pacific during TRACE-P. J Geophys Res Atmos 109:1–20

205. Löflund M, Kasper-Giebl A, Schuster B, Giebl H, Hitzenberger R, Puxbaum H (2002) Formic, acetic, oxalic, malonic and succinic acid concentrations and their contribution to organic carbon in cloud water. Atmos Environ 36:1553

206. Kesselmeier J (2001) Exchange of short-chain oxygenated volatile organic compounds (VOCs) between plants and the atmosphere: a compilation of field and laboratory studies. J Atmos Chem 39:219

207. Formenti P, Schütz L, Balkanski Y, Desboeufs K, Ebert M, Kandler K, Petzold A, Scheuvens D, Weinbruch S, Zhang D (2011) Recent progress in understanding physical and chemical properties of African and Asian mineral dust. Atmos Chem Phys 11:8231

208. Sanhueza E, Andreae MO (1991) Emission of formic and acetic-acids from tropical savanna soils. Geophys Res Lett 18:1707

209. Chebbi A, Carlier P (1996) Carboxylic acids in the troposphere, occurrence, sources, and sinks: a review. Atmos Environ 30:4233

210. Jaenicke R (2005) Abundance of cellular material and proteins in the atmosphere. Science 308:73

211. Ge X, Wexler AS, Clegg SL (2011) Atmospheric amines – part I. A review. Atmos Environ 45:524

212. Khalil MAK, Moore RM, Harper DB, Lobert JM, Erickson DJ, Koropalov V, Sturges WT, Keene WC (1999) Natural emissions of chlorine-containing gases: reactive chlorine emissions inventory. J Geophys Res Atmos 104:8333

213. Khalil MAK (1999) In: Fabian P, Singh ON (eds) The handbook of environmental chemistry. Springer, Berlin, pp 45–78

214. Quack B, Wallace DWR (2003) Air-sea flux of bromoform: controls, rates, and implications. Global Biogeochem Cycles 17:1–27

215. Moore RM (2003) In: Gribble GW (ed) The handbook of environmental chemistry. Springer, Berlin, pp 85–101
216. Murphy CD, Moore RM, White RL (2000) An isotopic labeling method for determining production of volatile organohalogens by marine microalgae. Limnol Oceanogr 45:1868
217. Scarratt MG, Moore RM (1996) Production of methyl chloride and methyl bromide in laboratory cultures of marine phytoplankton. Marine Chem 54:263
218. Scarratt MG, Moore RM (1998) Production of methyl bromide and methyl chloride in laboratory cultures of marine phytoplankton II. Marine Chem 59:311
219. Scarratt MG, Moore RM (1999) Production of chlorinated hydrocarbons and methyl iodide by the red microalga *Porphyridium purpureum*. Limnol Oceanogr 44:703
220. Leri AC, Satish CC (2010) Organochlorine turnover in forest ecosystems: the missing link in the terrestrial chlorine cycle. Global Biogeochem Cycles 24:1–8
221. Rai V, Victor DG, Thurber MC (2010) Carbon capture and storage at scale: lessons from the growth of analogous energy technologies. Energy Policy 38:4089
222. Rhew RC, Abel T (2007) Measuring simultaneous production and consumption fluxes of methyl chloride and methyl bromide in annual temperate grasslands. Environ Sci Technol 41:7837
223. Moore RM, Gut A, Andreae MO (2005) A pilot study of methyl chloride emissions from tropical woodrot fungi. Chemosphere 58:221
224. Hewitt CN, Davison B (1997) Field measurements of dimethyl sulphide and its oxidation products in the atmosphere. Philos Trans R Soc Lond B Biol Sci 352:183
225. Barnes I (2003) In: James RH (ed) Encyclopedia of atmospheric sciences. Academic, Oxford, pp 2429–2438
226. Davison B, Hewitt CN (1994) Elucidation of the tropospheric reactions of biogenic sulfur species from a field measurement campaign in NW Scotland. Chemosphere 28:543
227. Pham M, Muller JF, Brasseur GP, Granier C, Megie G (1995) A three-dimensional study of the tropospheric sulfur cycle. J Geophys Res Atmos 100:26061
228. Kawamura K, Ishimura Y, Yamazaki K (2003) Four years' observations of terrestrial lipid class compounds in marine aerosols from the western North Pacific. Global Biogeochem Cycles 17:3–19
229. Simoneit BRT, Cardoso JN, Robinson N (1991) An assessment of terrestrial higher molecular-weight lipid compounds in aerosol particulate matter over the south-Atlantic from about 30–70°S. Chemosphere 23:447
230. Medeiros PM, Conte MH, Weber JC, Simoneit BRT (2006) Sugars as source indicators of biogenic organic carbon in aerosols collected above the Howland Experimental Forest, Maine. Atmos Environ 40:1694
231. Russell LM, Hawkins LN, Frossard AA, Quinn PK, Bates TS (2010) Carbohydrate-like composition of submicron atmospheric particles and their production from ocean bubble bursting. Proc Natl Acad Sci USA 107:6652
232. Jia Y, Bhat S, Fraser MP (2010) Characterization of saccharides and other organic compounds in fine particles and the use of saccharides to track primary biologically derived carbon sources. Atmos Environ 44:724
233. Burrows SM, Elbert W, Lawrence MG, Pöschl U (2009) Bacteria in the global atmosphere – part 1: review and synthesis of literature data for different ecosystems. Atmos Chem Phys 9:9263
234. Despres VR, Huffman JA, Burrows SM, Hoose C, Safatov AS, Buryak G, Frohlich-Nowoisky J, Elbert W, Andreae MO, Poschl U, Jaenicke R (2012) Primary biological aerosol particles in the atmosphere: a review. Tellus Ser B Chem Phys Meteorol 64:1–58
235. McDevitt JJ, Milton DK, Rudnick SN, First MW (2008) Inactivation of poxviruses by upper-room UVC light in a simulated hospital room environment. PLoS One 3:e3186
236. Elbert W, Taylor PE, Andreae MO, Pöschl U (2007) Contribution of fungi to primary biogenic aerosols in the atmosphere: wet and dry discharged spores, carbohydrates, and inorganic ions. Atmos Chem Phys 7:4569

237. Cheng JYW, Chan CK, Lee CT, Lau APS (2009) Carbon content of common airborne fungal species and fungal contribution to aerosol organic carbon in a subtropical city. Atmos Environ 43:2781
238. Lang-Yona N, Dannemiller K, Yamamoto N, Burshtein N, Peccia J, Yarden O, Rudich Y (2012) Annual distribution of allergenic fungal spores in atmospheric particulate matter in the Eastern Mediterranean; a comparative study between ergosterol and quantitative PCR analysis. Atmos Chem Phys 12:2681
239. Sousa SIV, Martins FG, Pereira MC, Alvim-Ferraz MCM, Ribeiro H, Oliveira M, Abreu I (2008) Influence of atmospheric ozone, PM10 and meteorological factors on the concentration of airborne pollen and fungal spores. Atmos Environ 42:7452
240. Oliveira M, Ribeiro H, Delgado J, Abreu I (2009) The effects of meteorological factors on airborne fungal spore concentration in two areas differing in urbanisation level. Int J Biometeorol 53:61
241. Wilkinson DM, Koumoutsaris S, Mitchell EAD, Bey I (2012) Modelling the effect of size on the aerial dispersal of microorganisms. J Biogeogr 39:89
242. Bottenheim JW, Boudries H, Brickell PC, Atlas E (2002) Alkenes in the Arctic boundary layer at Alert, Nunavut, Canada. Atmos Environ 36:2585
243. Swanson AL, Blake NJ, Dibb JE, Albert MR, Blake DR, Rowland FS (2002) Photochemically induced production of CH_3Br, CH_3I, C_2H_5I, ethene, and propene within surface snow at Summit, Greenland. Atmos Environ 36:2671
244. Grannas AM, Shepson PB, Filley TR (2004) Photochemistry and nature of organic matter in Arctic and Antarctic snow. Global Biogeochem Cycles 18:GB1006
245. Czuczwa J, Leuenberger C, Giger W (1988) Seasonal and temporal changes of organic compounds in rain and snow. Atmos Environ 22:907
246. Krieger UK, Marcolli C, Reid JP (2012) Exploring the complexity of aerosol particle properties and processes using single particle techniques. Chem Soc Rev 41:6631–6662
247. Zhang R, Khalizov AF, Pagels J, Zhang D, Xue H, McMurry PH (2008) Variability in morphology, hygroscopicity, and optical properties of soot aerosols during atmospheric processing. Proc Natl Acad Sci USA 105:10291
248. Sobanska S, Hwang H, Choël M, Jung H-J, Eom H-J, Kim H, Barbillat J, Ro C-U (2012) Investigation of the chemical mixing state of individual Asian dust particles by the combined use of electron probe X-ray microanalysis and Raman microspectrometry. Anal Chem 84:3145
249. Freedman MA, Baustian KJ, Wise ME, Tolbert MA (2010) Characterizing the morphology of organic aerosols at ambient temperature and pressure†. Anal Chem 82:7965
250. Bladt H, Schmid J, Kireeva ED, Popovicheva OB, Perseantseva NM, Timofeev MA, Heister K, Uihlein J, Ivleva NP, Niessner R (2012) Impact of Fe content in laboratory-produced soot aerosol on its composition, structure, and thermo-chemical properties. Aerosol Sci Technol 46:1337
251. Bahadur R, Russell LM, Prather K (2010) Composition and morphology of individual combustion, biomass burning, and secondary organic particle types obtained using urban and coastal ATOFMS and STXM-NEXAFS measurements. Aerosol Sci Technol 44:551
252. Bzdek BR, Pennington MR, Johnston MV (2012) Single particle chemical analysis of ambient ultrafine aerosol: a review. J Aerosol Sci 52:109
253. Masciangioli T, Alper J (2012) Challenges in characterizing small particles: exploring particles from the nano- to microscales. National Academies, Washington
254. Han C, Liu Y, Ma J, He H (2012) Effect of soot microstructure on its ozonization reactivity. J Chem Phys 137:1–9
255. Koop T, Bookhold J, Shiraiwab M, Poschl U (2011) Glass transition and phase state of organic compounds: dependency on molecular properties and implications for secondary organic aerosols in the atmosphere. Phys Chem Chem Phys 13:19238
256. Han C, Liu Y, Liu C, Ma J, He H (2012) Influence of combustion conditions on hydrophilic properties and microstructure of flame soot. J Phys Chem A 116:4129

257. Perraud V, Bruns EA, Ezell MJ, Johnson SN, Yu Y, Alexander ML, Zelenyuk A, Imre D, Chang WL, Dabdub D, Pankow JF, Finlayson-Pitts BJ (2012) Nonequilibrium atmospheric secondary organic aerosol formation and growth. Proceedings of the National Academy of Sciences 109:2836

258. Cooper CDAFC (1994) Air pollution control: a design approach. Waveland, Prospect Heights

259. Endres E, Dueck J, Neesse T (2012) Hydrocyclone classification of particles in the micron range. Miner Eng 31:42

260. Nguyen H, Morrison AL, Nelson PF (2008) Analysis of pollution control costs in coal based electricity generation

261. Shanthakumar S, Singh DN, Phadke RC (2008) Flue gas conditioning for reducing suspended particulate matter from thermal power stations. Progress Energy Combust Sci 34:685

262. Mussatti DC (2002) EPA air pollution control cost manual. Air Quality Strategies and Standards Division of the Office of Air Quality Planning and Standards, U.S. Environmental Protection Agency, Research Triangle Park, NC 27711

Surface-Active Organics in Atmospheric Aerosols

V. Faye McNeill, Neha Sareen, and Allison N. Schwier

Abstract Surface-active organic material is a key component of atmospheric aerosols. The presence of surfactants can influence aerosol heterogeneous chemistry, cloud formation, and ice nucleation. We review the current state of the science on the sources, properties, and impacts of surfactants in atmospheric aerosols.

Keywords Aerosol · Cloud condensation nuclei · Surface tension · Surfactant

Contents

V.F. McNeill (✉), N. Sareen, and A.N. Schwier
Department of Chemical Engineering, Columbia University, New York, NY 10027, USA
e-mail: vfm2013@columbia.edu

List of Abbreviations and Symbols Used

AMS	Aerodyne aerosol mass spectrometer
ARG	Abdul-Razzak and Ghan
CCN	Cloud condensation nucleus/nuclei
CCNc	Thermal gradient static cloud diffusion chamber
CDN	Cloud droplet nuclei
CFSTGC	Continuous-flow streamwise thermal gradient chamber
CMC	Critical micelle concentration
DOM	Dissolved organic matter
ESP	Equilibrium spreading pressure
FTIR	Fourier transform infrared spectroscopy
HTDMA	Humidified tandem differential mobility analyzer
HULIS	Humic-like substances
IHSS	International Humic Substances Society
IN	Ice nucleus/nuclei
KTA	Köhler theory analysis
LC/ESI MS-MS	Liquid chromatography/electrospray ionization tandem mass spectrometry
MVK	Methylvinylketone
OA	Organic aerosol
OC	Organic carbon
SD CCNC	Static diffusion CCN counter
SDS	Sodium dodecyl sulfate
S–L	Szyszkowski–Langmuir
SFRA	Suwannee River fulvic acid
SOA	Secondary organic aerosol
TEM	Transmission electron microscopy
TOC	Total organic carbon
TOF-SIMS	Time of flight secondary ionization mass spectrometry
UV	Ultraviolet
VOC	Volatile organic compound
WSOC	Water-soluble organic compound
a	Parameter, Szyszkowski–Langmuir equation
a_i	Activity of species i
b	Parameter, Szyszkowski–Langmuir equation
C	Molality of organic carbon
χ_i	Molality fraction of compound i, Szyszkowski–Langmuir equation
d	Diameter
d_c	Critical diameter
γ	Reactive uptake coefficient
κ	Hygroscopicity parameter
M	Molarity

m	Mass, Köhler equation
M_i	Molecular weight of species i
ν	Number of ions
ϕ	Osmotic coefficient
R	Universal gas constant
r	Radius
ρ	Density
S	Saturation ratio
S_c	Critical supersaturation
σ	Surface tension
T	Temperature
V	Volume

1 Introduction

Atmospheric particulate matter impacts Earth's climate both directly, by scattering and absorbing solar radiation, and indirectly by influencing cloud formation and properties [1]. Internal mixtures of inorganic and organic material are common in tropospheric aerosols, with organic matter typically comprising 10–90% of fine aerosol mass [2, 3]. While hundreds of organic species found in atmospheric particles have been identified, the majority of organic aerosol mass often remains unspeciated. Organic aerosol material (OA) can affect the heterogeneous reactivity of aerosol particles, their ability to act as cloud condensation nuclei (CCN) or ice nuclei (IN), and their optical properties.

One special class of organic material commonly found in atmospheric aerosols are *surface-active* species, also known as surfactants, including organic acids and diacids, proteins, and humic-like substances (HULIS). The distinguishing characteristic of surface-active molecules is that they are comprised of both hydrophilic and hydrophobic moieties. In aqueous solutions they will tend to form structures that allow the hydrophobic groups to avoid contact with water while the hydrophilic groups remain in solution. To this end, surface-active molecules may partition to the gas–liquid interface, where they form a film with the hydrophobic groups protruding into the gas phase. Surface-active organic molecules may form a surface layer on aqueous atmospheric aerosols, in what has been referred to as an "inverted micelle" configuration (Fig. 1) [4, 5]. Other arrangements are also possible, including micelles (aggregates with the hydrophilic head groups in solution), lenses, oil or lamellar phases, and crystals, and these may exist in equilibrium with each other and/or a surface monolayer [6–11]. Furthermore, liquid–liquid phase separations are possible for mixed inorganic–organic systems under atmospherically relevant conditions [12], and at low temperatures glasses may form [13, 14]. An organic film at the gas–aerosol interface will lower the aerosol surface tension and may act as a barrier to mass transport between the gas and aqueous phases. In this chapter we discuss the
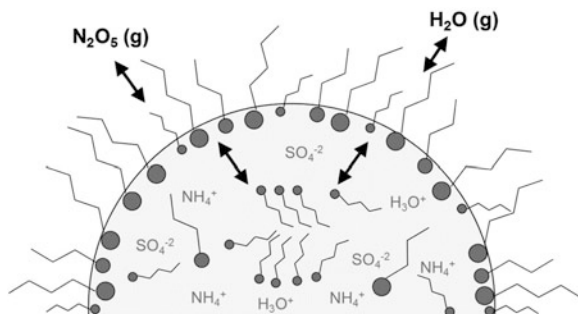
Fig. 1 Schematic of surface-active organic material in a deliquesced aerosol particle. Surface organics can potentially inhibit the uptake of gas-phase species to the particle, enhance ice nucleation, and depress particle surface tension, with important implications for aerosol heterogeneous chemistry and cloud formation

implications of those physical phenomena for aerosol heterogeneous chemistry and cloud droplet formation.

Despite their potential significance, the existence of organic surface films on ambient aqueous aerosols has not been confirmed *directly* to date due to a lack of appropriate analytical techniques. However, abundant indirect evidence for these films exists. Surfactants were first extracted from marine (sea salt) aerosol by Blanchard almost 50 years ago by collecting the aerosol onto fine platinum wire and observing the spreading of an organic film from the wire into a film of partially oxidized motor oil [15]. Atmospheric aerosols have been collected and observed ex situ to consist of organic coatings surrounding crystalline inorganic cores [9, 16–22]. Soft X-ray spectromicroscopy and time-of-flight secondary ion mass spectrometry (TOF-SIMS) have revealed organic coatings on marine and continental aerosol particles [17–23]. For all these studies particles were dried before analysis. It is well known that salts tend to expel impurities to the surface as they crystallize [24], so the possibility exists that the observed core-shell morphology could have been an artifact of the sampling and drying processes. Additional indirect evidence of surface films on atmospheric aerosols has been obtained via measurements of surface tension depression in aqueous extracts of collected aerosol particles [25–31] as well as in fogwater [27, 28, 32] and rainwater [33]. However, the dilution of aerosol chemical components inherent in these techniques makes it difficult to infer conclusively a surface film on the in situ aerosol from observations of surface tension depression in the sample. Other morphologies have also been observed for mixed organic/inorganic particles, such as primarily organic particles with inorganic inclusions [9] and gel-like mixtures [7, 8].

We currently lack sufficient data on the phase behavior and surface-bulk partitioning of most naturally occurring organic surfactants under conditions typical of aqueous aerosols to predict accurately the formation of organic surface films in ambient aerosols. The pH of atmospheric aerosols can range from 0 to 8, a range that includes the pKa of most naturally occurring organic acids [34, 35]. Most

experimental work has been performed at pH > 3, and few studies deal with the transition from ionized to unionized state. In addition, at typical atmospheric relative humidity, aerosols generally become supersaturated with salt. It is not possible to perform routine measurements in bulk solutions at those salt concentrations; as a result, most studies in the literature have focused only on surface tension behavior in water or dilute salt solutions. Phase behavior, especially for fatty acids, is highly temperature dependent, and little data are available for temperatures lower than ambient, which would be particularly relevant for surfactants in clouds. Finally, for many systems only surface tension has been studied and other important parameters including phase, equilibrium spreading pressures, and critical micelle concentrations are not known. Some recent studies have highlighted the dynamic nature of the organic surface layer using techniques including aerosol optical tweezers coupled with nonlinear Raman spectroscopy [36], sum frequency generation [37, 38], and neutron reflection [39].

Surface-active organics and organic surface films likely influence aerosol chemistry and physics in a number of ways. Organic coatings have been shown to influence ice nucleation in aerosols. By reducing the droplet surface tension, surface films can reduce the critical supersaturation required for cloud droplet activation, but they may also present a barrier to gas–aerosol mass transport that can retard water uptake. This resistance to the transfer of gas phase species to and from the particle bulk can also affect its heterogeneous chemistry. Consequences include impacts on atmospheric composition (due to changes in aerosol heterogeneous chemistry) and climate (via cloud formation and freezing). In this chapter we review the current understanding of the sources, properties, and impacts of surface-active organics in atmospheric aerosols.

2   Sources

Many *primary* sources of surface-active organic aerosol material exist, including biomass burning [9, 22, 25, 40–42], leaf abrasion and other primary biological sources [43–48], emissions from vehicles and other fossil fuel combustion [22, 43, 49–59], and cooking emissions [60–67]. Marine aerosols may obtain a surfactant component (including long-chain fatty acids) via a bubble-bursting mechanism due to the organic-rich surface layer that is present on seawater during periods of high biological activity [15, 68–76]. Fatty acids have been shown to be prevalent in marine aerosol sampled over the North Atlantic [26, 77] and North Pacific [75, 78, 79], with maximum concentrations occurring during periods of high biological productivity. Tervahattu and coworkers used TOF-SIMS to identify the main component of the organic layer on dried marine aerosols as palmitic acid [20, 21].

Gas-to-particle conversion is an important *secondary* source of aerosol surfactants. Inorganic aerosols may acquire an organic component via in situ interactions with volatile organic compounds (VOCs), a family of processes

known as secondary organic aerosol (SOA) formation. Two major pathways for SOA formation have been identified:

- *"Traditional" (condensational) SOA formation*: gas-phase oxidation of VOCs in the atmosphere can lead to the formation of less-volatile products, which may then condense onto existing aerosol particles, increasing their organic content [80, 81].
- *Condensed-phase SOA formation*: water-soluble VOCs may dissolve into the aqueous phase of cloud droplets or wet aerosols. Subsequent aqueous-phase reactions (e.g., oxidation and/or oligomerization) can lead to the formation of low-volatility secondary organic material [82–87]. In particular, the dicarbonyl VOCs glyoxal and methylglyoxal have been studied as potential precursors for this SOA formation pathway. Recently, aqueous-phase reactions of isoprene-derived epoxydiols have also been shown to be efficient pathways to SOA formation in the aerosol aqueous phase [88–91].

SOA material formed by either pathway may be surface-active. For example, organic acids including *cis*-pinonic acid, which is formed via the oxidation of the biogenic VOC α-pinene, are "traditional" SOA products which have been shown to be surface-active [92–96]. Alkene ozonolysis has also been shown to yield water-soluble surface-active organic compounds [97].

Condensed-phase chemistry is another possible source of aerosol surfactants. The oxidation of aerosol organic material yields functionalized products which may be surface-active [98]. Oxidative processing of water-soluble species in cloud or aerosol water may result in the formation of surface-active organic acids such as malonic and malic acids [99, 100]. Surface-active HULIS or organosulfate species may also form in situ in aerosol or cloud water [84, 85, 101–104].

3   Impact on Aerosol Heterogeneous Chemistry

It has long been known that the presence of a long-chain fatty acid layer at the air–water interface inhibits the evaporation of a macroscopic water film [105–107]. In recent years it has been shown that organic surface films can significantly influence reactive gas uptake to laboratory-generated aerosols as well [108–117]. Film thickness in these studies ranged from less than a monolayer (single molecule layer) [112, 113] to macroscopic [108, 111]. The composition of the organic films in these laboratory aerosols had varying degrees of complexity, from single-component monolayers [112, 113, 115, 118–120] to mixtures of SOA species [108, 110, 111] to humic acid [109].

Not all organic surface monolayers block gas–aerosol mass transport to the same degree; the barrier action of the surfactant monolayer tends to increase with increasing organic chain length and packing density [115, 116, 119, 121–127]. Fatty acids with 16 or more carbon atoms form close-packed, incompressible films due to the attractive forces between the neighboring hydrophobic tails [107, 128].

Short-chained surfactants (and those with irregular, bent, or branched chains) are known to form less tightly packed films and provide a lower barrier to water evaporation than longer-chained surfactants [105, 107]. For these films, which are sometimes referred to as "compressible" or "expanded," the degree of packing of the surfactant will change with increasing surface coverage, resulting in a nonlinear relationship between the number of surfactant molecules on the surface and the degree of inhibition of gas-to-aerosol mass transfer [113].

For single-chain surfactants like fatty acids the head group also influences how closely the surfactant molecules can pack at the surface [129]. Surfactants typically present in atmospheric aerosols can have carboxylic acid, alcohol, aldehyde, ketone, ester, or amine head groups [5, 18, 19, 21, 75]. Studies of uptake or water evaporation through two-component mixed films show that the barrier action is generally intermediate between that of the two pure components [107, 114, 119, 127, 130]. Additionally, barrier action depends on the identity of the penetrating gas-phase molecule. For example, monolayers of oleic acid ($C_{18}H_{34}O_2$), which has a double bond that prevents close packing, have been observed to inhibit efficiently the uptake of N_2O_5, but not HNO_3, from the gas phase [112, 115].

In the following sections we review laboratory, field, and modeling studies of the influence of surfactant films on aerosol heterogeneous chemistry.

3.1 Laboratory Studies

Early studies of the influence of interfacial organic films on gas uptake to aqueous films and aerosols were reviewed previously by Donaldson and Vaida [131]. Donaldson and Valsaraj also recently reviewed the adsorption of VOCs at the air–aqueous interface and their reaction with atmospheric oxidants [132]. For an overview of techniques and principles of laboratory studies of aerosol heterogeneous chemistry the reader is referred to the recent review article of Kolb et al. [133].

Gilman and Vaida studied acetic acid (CH_3COOH) uptake to an aqueous film through long-chain alcohol monolayers, and surface layers of the alkane nonacosane [130]. They showed that straight-chain alcohols which form close-packed monolayers were more effective at inhibiting CH_3COOH uptake than bent-chain species, and the monolayer resistance increased with increasing chain length. Clifford et al. showed that submonolayer coverage of 1-octanol inhibited the rate of nitric acid and ammonia uptake to aqueous films [134]. They saw little effect from butanol films and uncompressed stearic acid films.

Nathanson and coworkers performed a series of molecular beam scattering studies of reactive gas uptake to supercooled (213 K) deuterated sulfuric acid films coated with short chain monolayers [135]. They found that a butanol coating did not inhibit proton exchange by HCl and HBr, and in fact suggest that the hydrophilic head groups of the butanol may provide additional sites for interaction with the adsorbate [126]. They also investigated evaporation of HCl and HBr

Fig. 2 Summary of N$_2$O$_5$ uptake suppression for coated particles and films. The ratio of the reactive uptake coefficient, γ$_{N2O5}$, with and without an organic surface coating, as a function of aerosol organic mass fraction (*top panel*) and fractional surface coverage (*bottom panel*)
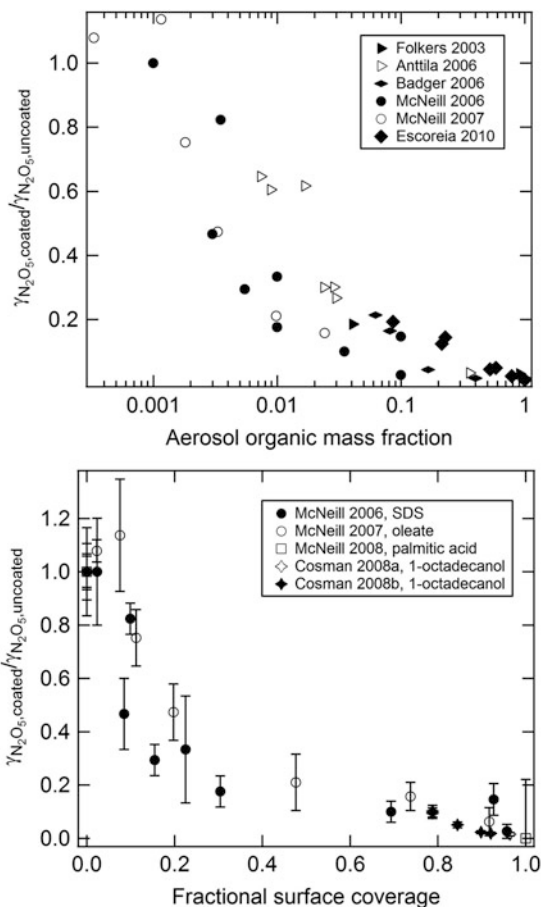
through hexanol films [124]. Enhanced HCl-DCl proton exchange was observed at low organic surface coverage, and inhibition was observed at higher coverage when the film was expected to be more tightly packed. Similar observations were made for pentanoic acid films [136].

Many laboratory and modeling studies of the impact of organic surface films on aerosol heterogeneous chemistry have focused on N$_2$O$_5$ uptake. This process is an important sink of NO$_x$, and therefore has a significant impact on tropospheric photochemistry [137, 138], influencing surface-level O$_3$ concentrations by up to 35% [139]. The results of several laboratory studies are summarized in Fig. 2, which shows the impact of organic surface films on the measured reactive uptake coefficient for N$_2$O$_5$ (γ$_{N2O5}$).

Badger et al. investigated the effect of humic acid – a high molecular weight, water-soluble, compressible surfactant – on N$_2$O$_5$ uptake to ammonium sulfate aerosols and found that the reactive uptake decreased with increasing humic acid mass fraction [109]. Nathanson and coworkers observed that butanol and hexanol

films inhibit N_2O_5 uptake to supercooled (216 K) deuterated sulfuric acid films [127]. Thornton and Abbatt found that the presence of hexanoic acid decreased the N_2O_5 reactive uptake coefficient on artificial seawater aerosol by a factor of 3–4 at room temperature and 70% relative humidity [116]. Malonic acid, a short-chain, water-soluble dicarboxylic acid that is known to depress surface tension in bulk solutions [93, 96, 140–143] did not present a barrier to N_2O_5 uptake [117]. McNeill et al. later showed that even small, submonolayer amounts of sodium dodecyl sulfate (SDS) or sodium oleate can decrease the reactive uptake of N_2O_5 to aqueous aerosols by up to a factor of 10 [112, 113]. Bertram and coworkers studied N_2O_5 uptake to sulfuric acid films at 273 K and found that uptake was inhibited by monolayers of stearic acid, 1-hexadecanol, or 1-octadecanol, but not the branched-chain fatty acid phytanic acid [119, 120]. Due to its smaller head group and thus closer packing, 1-octadecanol showed greater uptake resistance than stearic acid, its fatty acid analog. When even a small fraction of phytanic acid was introduced to the 1-octadecanol monolayers, the uptake resistance was greatly reduced [118]. Ammann and coworkers found that expanded monolayers, such as those formed by short-chain fatty acids or bent molecules like oleic acid, did not efficiently inhibit the uptake of HNO_3 by sea salt aerosols [115], unlike what was observed previously for N_2O_5 [112, 113, 116]. They also observed that monolayers of stearic acid, the saturated straight-chain analog to oleic acid which makes compressed films, did inhibit HNO_3 uptake.

Halogen activation is another important class of aerosol heterogeneous reactions, primarily involving sea salt aerosols [144]. Besides inhibiting gas-aerosol mass transfer, organics at the gas–aerosol interface could have an additional impact on surface-specific heterogeneous halide chemistry by repelling anionic reactants from the near-surface region with their hydrophilic head groups [145]. McNeill et al. found that, although the reactive uptake coefficient for N_2O_5 reacting with NaCl and laboratory-generated seawater aerosols was significantly suppressed by submonolayer surfactant coatings; the yield of $ClNO_2$ per molecule of N_2O_5 taken up was not affected [113]. Clifford and Donaldson investigated the uptake of O_3 by NaBr solutions and found that 1-octanol films promoted halogen activation by enhancing the surface concentration of O_3 [146]. Rouvière and Ammann studied O_3 uptake to aqueous potassium iodide aerosol with fatty acid coatings [114]. They observed that the reactive uptake coefficient decreased for long straight-chain surfactants, and the barrier action of mixed component films was intermediate between that of the individual pure component films.

Another type of organic material that has been investigated for its influence on the heterogeneous chemistry of aerosols is SOA. While the SOA coatings used in these experiments are often macroscopic, many SOA species are surface-active, and at low organic loadings thin layers may form. Folkers et al. showed that a multilayer α-pinene SOA coating (≥ 15 nm) reduced N_2O_5 uptake significantly [111]. Anttila extended this study to lower organic loadings and other precursors (myrcene, sabinene, and limonene), and established a modeling framework to describe N_2O_5 uptake to aerosols with multilayer organic coatings [108]. Escoreia et al. studied the impact of α-pinene coatings on N_2O_5 uptake to ammonium

bisulfate aerosols, and found a factor of 10 reduction in the uptake coefficient with the smallest amount of SOA material present (9 wt% organic), with smaller additional reductions as aerosol organic content increased [110].

3.2 Field Studies

While ample evidence from the laboratory suggests that surfactant films significantly influence aerosol heterogeneous chemistry, no direct evidence of this effect for ambient aerosols exists at this time. In part this is due to the challenges of characterizing aerosol morphology in situ.

Studies of aerosol heterogeneous chemistry in the field have generally consisted of simultaneous measurements of expected gas phase reactants and products as well as aerosol properties, followed by data analysis using models to infer reactive uptake coefficients. For example, during the New England Air Quality Study, Brown et al. found high N_2O_5 reactive uptake in regions with high aerosol sulfate:organic ratio as measured by an Aerodyne Aerosol Mass Spectrometer, and low N_2O_5 uptake when the sulfate:organic ratio was low [147]. While this is consistent with organic material inhibiting N_2O_5 uptake, no information is available as to whether the organic material was surface-active, or the morphology or phase state of the particles.

Bertram and Thornton recently introduced a method for performing direct aerosol flow tube uptake studies on ambient aerosol particles [148, 149]. They are able to correlate observed N_2O_5 reactive uptake coefficients with simultaneous measurements of aerosol composition using other techniques. When the flow tube technique of Bertram and Thornton is coupled with a technique capable of detecting the presence of surface-active organics in the aerosol, potential exists for the influence of these organics on N_2O_5 uptake by ambient aerosol to be inferred.

3.3 Modeling

Parameterizations of the effects of organic surface films on aerosol heterogeneous chemistry are not included in most large-scale prognostic atmospheric chemistry models at this time. This is mostly due to uncertainty in predictions of film formation as a function of aerosol chemical composition, and the additional complexity this phenomenon adds to models. Evans and Jacob recommended a low reactive uptake coefficient for N_2O_5 on aerosols classified as "organic," and their parameterization was implemented into the GEOS-CHEM model [138]. Bertram and Thornton provided a more detailed parameterization of the impact of organic material on N_2O_5 uptake to aerosols [150]. They focused on the influence of organic material on aerosol liquid water content, and the effect of surface films was not treated.

Anttila and coworkers developed a parameterization for N_2O_5 uptake to aerosols with SOA coatings ranging from ~3 to 150 nm in thickness based on laboratory studies [108]. Riemer et al. extended this parameterization to study the impact of coatings originating from α-pinene and limonene on summertime N_2O_5 chemistry in Europe [151]. They found a significant impact of aerosol organic coatings on nighttime mixing ratios of N_2O_5, NO_3, aerosol nitrate, and VOCs for conditions where N_2O_5 and SOA coexist, with (NO_3 + $2N_2O_5$) increasing 15–90% depending on initial particle nitrate content.

In the most detailed modeling treatment to date, Smoydzin and von Glasow investigated the impact of organic surface films on sea salt aerosol heterogeneous chemistry [152]. Starting with various initial concentrations of organic material in the aerosols, they assumed that all aerosol organics partitioned to the gas–aerosol interface, and that a full monolayer was necessary to reduce the uptake of gas phase species. They also considered the oxidation of the surfactants by gas-phase species. Despite significant uncertainties in their treatment of the surfactant surface layer, they found that gas-phase concentrations of halogen species in the marine boundary layer could decrease if organic coatings on marine aerosols block the uptake of gas-phase species involved in halogen activation or the diffusion of halogen-containing product gases out of the aqueous phase.

4 Impact on Ice Nucleation

In the absence of ice nuclei, pure water droplets in the atmosphere supercool to ~-35 °C due to kinetic limitations on homogeneous nucleation [153]. Ice nuclei, for example aerosol particles included in or which come in contact with supercooled water droplets, can induce freezing closer to the melting point of ice. Organic surface films, such as those formed by partitioning of surfactant to the gas–droplet interface, have also been suggested to serve as a nucleus for ice in aqueous droplets.

Lahav, Leiserowitz, and coworkers performed a series of laboratory studies demonstrating the ability of a surface monolayer of long-chain aliphatic alcohols and/or fatty acids to nucleate ice in supercooled water droplets [154–157]. They found that the presence of a monolayer enhanced ice nucleation inside the droplets by acting as a template for the formation of hexagonal ice. Pure component films and those composed of longer-chain surfactants were more effective ice templates, probably due to their tendency to form compressed, well-ordered surface films [154, 155, 157]. Majewski et al. [156] observed that the tilt angle of a long-chain alcohol monolayer changed as temperature decreased until freezing occurred, then the structure of the monolayer was preserved upon freezing and even after the temperature was elevated and the ice melted [156]. Their results suggest that freezing is preceded by the formation of critical ice nuclei consisting of approximately 50 water molecules each. Inspired by this work, Seeley and Seidler performed a theoretical study of nucleation in drops with monolayer coatings of

long-chain aliphatic alcohols. Their results suggest that nucleation in these systems is a two-dimensional process, and hence should scale with droplet surface area rather than volume [158]. This is supported by the experimental observations of Cantrell and coworkers. They studied the freezing of water [159] and electrolyte solutions [160] catalyzed by long-chain alcohols using attenuated total reflection (ATR) Fourier transform infrared spectroscopy (FTIR). They observed change in the structure of the alcohol monolayer coupled with change in the hydrogen bonding network of the water as temperature decreased to the point of freezing. This led them to conclude that freezing occurs via the formation of ordered water clusters adjacent to the organic film, with order extending further into the bulk with decreasing temperature. They suggested that the ability of the organic monolayer to adapt to the strain at the ice–nucleus interface created by freezing was part of what made it a particularly good nucleus.

Zobrist and coworkers showed that nucleation rates in water droplets coated with nonadecanol have a weaker dependence on temperature than the homogeneous nucleation rates for uncoated droplets [161]. They were able to reproduce the observed behavior using classical nucleation theory with a parameterized change in contact angle with temperature. They later performed freezing experiments on particles of various compositions, including aqueous droplets with monolayer coatings of nonadecanol. They showed that water activity is a convenient basis for parameterizing the freezing temperatures for heterogeneous nucleation, regardless of the chemical composition of the freezing solution [162].

Recently, Knopf and Forrester studied the freezing of aqueous NaCl droplets coated with monolayers of 1-nonadecanol or 1-nonadecanoic acid [163]. They found that 1-nonadecanol coatings, which result in a compressed film, led to a freezing temperature ~25 K higher than homogeneous nucleation in uncoated droplets. 1-Nonadecanoic acid coatings also promoted freezing, but not as effectively as 1-nonadecanol. Based on their measurements of the equilibrium spreading pressure and Langmuir isotherms, they found that 1-nonadecanoic acid monolayers exist in an expanded state but form compressed films at high (20 wt%) NaCl concentrations; the freezing enhancement was observed only at high NaCl concentrations and low water activities. This apparent requirement of a compressed film for ice nucleation is consistent with the findings of Lahav, Leiserowitz, and coworkers [154, 155, 157]. Knopf and Forrester also found similar trends in the contact angle as a function of temperature as Zobrist et al. [161], providing further support to the notion that the monolayer is restructured with decreasing temperature [161]. Finally they presented a parameterization of freezing rates as well as freezing temperatures for heterogeneous ice nucleation as a function of water activity.

5 Impact on Cloud Droplet Formation

Cloud droplets are formed in the atmosphere when water vapor condenses onto aerosol particles. The influence of aerosols largely determines the number distribution, chemical composition, and reflectivity of cloud droplets, thereby also affecting
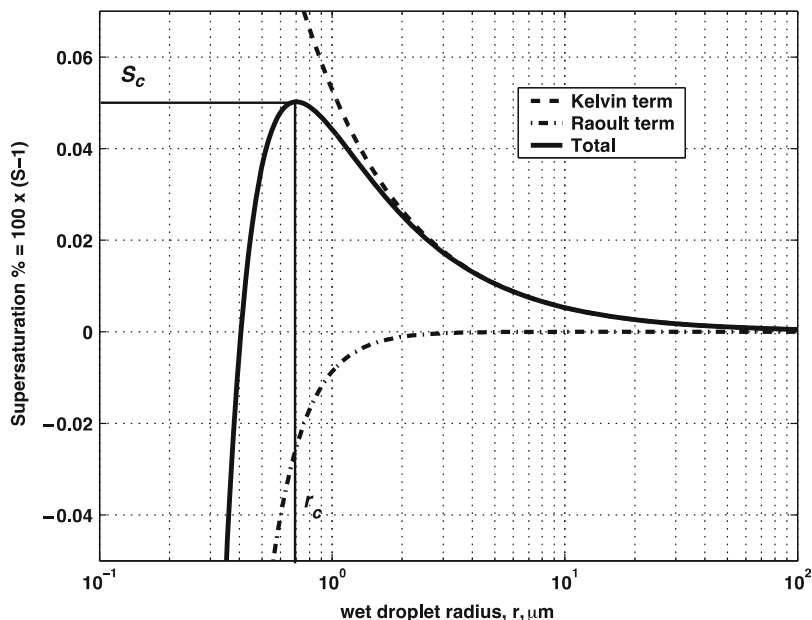
Fig. 3 Köhler curve, showing the contributions of the Kelvin and Raoult terms. Reproduced with permission from [299]

cloud albedo [122]. Numerous experimental [122, 141, 164–169] and field studies [32, 170] have shown that the presence of surfactants in aerosols can impact the ability of an aerosol to nucleate and grow into cloud droplets, also known as CCN activity. In this section, we give brief overviews of the theoretical description of aerosol CCN activity and the effect of organics on surface tension, and expand on the impacts of surface-active organics on CCN activity and cloud droplet growth kinetics.

5.1 Köhler Theory and κ-Köhler Theory

Köhler theory describes cloud droplet activation and growth from soluble particles as an equilibrium process [171]. The Köhler equation takes into account two competing effects: the Raoult or solute, effect which tends to decrease the equilibrium vapor pressure of water over the growing droplet, and the Kelvin, or curvature effect, which serves to increase the equilibrium vapor pressure. The Köhler curve (Fig. 3) for a growing droplet describes the equilibrium saturation ratio of water as a function of droplet size and several parameters inherent to the aerosol particle [171, 172]:

$$\ln\left(\frac{p_{\mathrm{w}}(D_{\mathrm{p}})}{p^{o}}\right) = \frac{A}{D_{\mathrm{p}}} - \frac{B}{D_{\mathrm{p}}^{3}} \tag{1}$$

with

$$A = \frac{4M_{\mathrm{w}}\sigma_{\mathrm{w}}}{RT\rho_{\mathrm{w}}} \quad \text{and} \quad B = \frac{6n_{\mathrm{s}}M_{\mathrm{w}}}{\pi\rho_{\mathrm{w}}} \tag{1a}$$

where $p_{\mathrm{w}}(D_{\mathrm{p}})$ is the water vapor pressure over the droplet of diameter D_{p}, p^{o} is the water vapor pressure over a flat surface at the same temperature, M_{w} is the molecular weight of water, σ_{w} is the droplet surface tension; ρ_{w} is the water density, R is the universal gas constant, T is temperature, and n_{s} is the moles of solute.

The maximization of (1) with respect to particle size defines the critical saturation ratio (S_{c}) and the corresponding critical droplet diameter (d_{c}). According to the assumptions of Köhler theory, when the ambient water saturation ratios exceed S_{c} (or when particle size exceeds d_{c}), the particles spontaneously activate and grow to form cloud droplets. In real systems, droplet growth may be inhibited by various kinetic limitations, which will be discussed in Sect. 5.5 [173, 174]. It should also be noted that Köhler theory is strictly not applicable for systems containing volatile solutes. A one-dimensonal cloud model using the three-component Köhler theory has been developed by Kulmala and coworkers to study the effects of acid vapors on CCN activity [175]. Their simulations show that including the effect of nitric acid vapors alters the cloud activation potential of particles as compared to traditional Köhler theory. This work has been further extended by reformulating Köhler theory to include the effect of soluble gases and slightly soluble aerosol matter [176]. Recently, Topping and McFiggans developed a method to study the volatility effect of more than one organic component. They observed that the saturation ratio of water vapor needed for droplet activation decreases significantly when co-condensation of multiple organics is taken into account [177].

Padró et al. developed a method called Köhler theory analysis (KTA) which uses Köhler theory coupled with measurements of surface tension, chemical composition, and CCN activity to infer molar volume and solubility [178]. This is a powerful tool for the characterization of the cloud droplet formation potential of ambient particles containing water-soluble organic compounds (WSOC).

Equation (1) is very effective in modeling the CCN activity of water-soluble inorganic compounds, but it does not describe particles with lower hygroscopicity (especially organic or mixed organic–inorganic particles) so successfully. In order to do so, extensions of Köhler theory have been used, which require knowledge of various properties of the aerosol components such as molecular weight, dry particle density, dissociable ions, and water activity coefficients [93, 176, 179]. In a simpler approach, an extension of Köhler theory, known as κ-Köhler theory, was developed by Petters and Kreidenweis [180]. This theory uses a single parameter, κ, the hygroscopicity parameter, which is defined as

$$\frac{1}{a_{w}} = 1 + \kappa \frac{V_{s}}{V_{w}} \tag{2}$$

where a_{w} is the activity of water in solution, V_{s} is the volume of the dry particulate matter, and V_{w} is the volume of water. Essentially, for any compound, κ is a constant parameter that describes its aerosol water uptake characteristics and CCN activity. κ values between 0.5 and 1.4 are indicative of highly-CCN-active salts, those between 0.01 and 0.5 indicate slightly to very hygroscopic organic species, and 0 indicates non-hygroscopic components. Based on experiments conducted with the surfactant fulvic acid, it seems that this approach may be appropriate for mixed particles that contain surface-active material, but further verifications are needed [180].

Additionally, models have been developed and molecular dynamic simulations performed in order to understand the effects of surfactants on water droplets and CCN activity; more details can be found in Sect. 5.4.

5.2 Observations of Surface Tension Depression

The presence of an organic film at the gas–liquid interface of an aerosol can depress the surface tension, possibly affecting the aerosol's ability to nucleate cloud droplets. Observations of depressed surface tension in collected aerosol particles, fogwater, rainwater, or laboratory aerosol mimics are also an indirect indicator of surface film formation. Surface tension is easily studied for bulk samples in the laboratory setting by various dynamic and static methods, such as a Wilhelmy plate, de Nouy tensiometry, oscillating bubble tensiometry, axisymmetric drop analysis, pendant drop tensiometry, and ring down tensiometry. Dynamic surface tension measurements occur as surfactant molecules undergo surface-bulk partitioning in solution as the mixture approaches an equilibrium state, whereas static measurements occur at equilibrium. The surface tension of aerosol particles can only be inferred indirectly through observations of CCN activation coupled with Köhler theory, or by measuring the surface tension of water extract of collected aerosols.

The International Critical Tables [181] are often used as a reference for surface tension data for both isolated inorganic and organic systems, but mixed systems are not well-represented. Multiple semi-empirical models have been developed to describe the surface tension behavior of (mixed) electrolyte solutions, over a range of temperatures [182–185]. For a review of quantitative structure–property relationship studies of surfactants, we refer the reader to Hu et al. [186].

The presence of salt alone in an aqueous solution is known to increase surface tension. However, a net decrease in surface tension with respect to that of water is commonly observed in mixed inorganic/organic aqueous solutions containing surfactants. In mixed inorganic/organic solutions, especially at high ionic concentrations, the solubility of the organic component may decrease, in a

phenomenon known as "salting out" [187]. This may result in enhanced organic film formation at the gas–solution interface [188]; [257] and further surface tension depression, possibly offsetting the surface-tension increase due to the inorganic component.

The Szyszkowski–Langmuir (S–L) equation is often used to empirically describe measured surface tension data:

$$\sigma = \sigma_0(T) - aT \ln(1 + bC) \tag{3}$$

where σ and σ_0 are the surface tension of the solution with and without the presence of an organic, respectively, T is temperature (K), C is the molality of the organic carbon (mol carbon (kg water)$^{-1}$), and a and b are fit parameters [189]. Henning and coworkers developed the following linearly additive model for systems containing a complex mixture of non-reacting organics:

$$\sigma = \sigma_0(T) - \sum_i \chi_i a_i T \ln(1 + b_i C) \tag{4}$$

where i is the ith organic compound, and χ_i is the molality fraction of compound i out of the total soluble carbon concentration in solution ($\chi_i = C_i\, C^{-1}$) [166]. Some mixed organic and inorganic/organic systems have been modeled using (4) and similar models [85, 95, 102, 166, 190–192], but none have captured the behavior of reactive systems well.

In the following discussion we focus on studies of organic compounds and systems directly relevant to atmospheric aerosols.

5.2.1   Ambient Fog/Cloud/Aerosol Measurements and HULIS

Measurements of surface tension depression in aqueous extracts of collected aerosol particles [25–31], fogwater [27, 28, 32], and rainwater [33] have in general shown decreasing surface tension with increasing organic concentration, with increased surface tension depression in samples collected in more polluted regions. The results of several studies are summarized in Fig. 4.

Barger and Garrett collected airborne particulate matter on ships in both the Mediterranean Sea (during July 1973) and the Pacific Ocean near the Galapagos Islands (during February 1974) [194]. Film pressure-vs-area isotherms were calculated and the surface tension was measured using a Wilhelmy plate. There was evidence of surface-active organics, including C_9–C_{18} fatty acids, and polar compounds, but surface-active species were not the majority of the detected organic compounds. Assuming certain fog properties (fog droplet diameter, concentration, and organic distribution), they calculated that there was enough organic material to coat a particle the size of the nuclei of typical fog droplets (0.08–0.8 μm diameter); however, there was not enough organic material present to coat fully formed fog droplets.
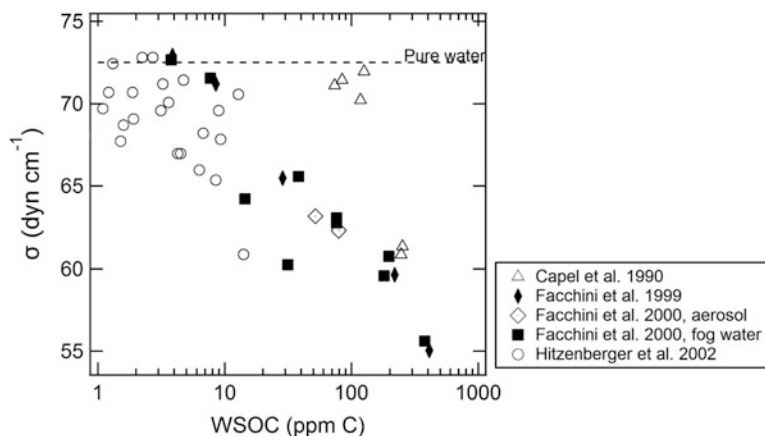
Fig. 4 Summary of surface tension data for ambient samples. Adapted from Facchini et al. [28] and Hitzenberger et al. [193]

The surface tension of rainwater, melted snow, and atmospheric particles was sampled 1979–1981 in Frankfurt/Main by Seidl and Hänel [195]. They found that concentrations of both soluble and insoluble organic material were too small (normalized to 2×10^{-6} and 2.5×10^{-7} mol L^{-1}, respectively) to affect both water uptake and loss, but that there was slight surface tension depression. They suggested that in areas with higher urban pollution, these effects might be enhanced.

Capel et al. collected urban area fog water in Dübendorf, Switzerland (near Zurich) over a period of 6 nights in November–December 1986–1987 [196]. The samples (tested at 20 °C) showed increasing surface tension depression with increasing organic concentration. Most of the organic material remained unspeciated; however, alkanes, biphenyls, alkylbenzenes, formate, and acetate were detected.

Hitzenberger et al. collected 26 cloud water samples at Rax mountain in central Europe in March 2000 [193]. Surface tension measurements, using ring tensiometry at ambient temperature, showed an average surface tension of 95.2% ($\pm 3.7\%$) of the surface tension of water, with a range from 83.8% to 100.5%. The minimum surface tension lowered S_c by 25%, which could affect cloud droplet number and size; the average surface tension value lowered S_c by 7%. They calculated, using the known liquid water content and assuming a cloud number concentration, that the amount of organic carbon in the samples could not form a full monolayer on all cloud droplets but could form a monolayer just before cloud droplet activation.

Moore et al. measured the surface tension of oceanic dissolved organic matter (DOM) from Atlantic Ocean samples off the coast of Georgia, USA [197]. Using pendant drop tensiometry at 24 °C they saw clear surface tension depression from surface-active organics, which followed the Szyszkowski–Langmuir equation, $\sigma = \sigma_o - 2.952T \ln (1 + 2 \times 10^{-6}C)$, where C is in units mg L^{-1}. Surface tension as inferred using KTA also showed excellent agreement with the direct measurements.

HULIS are a common component of aerosol organic matter and are characterized as high molecular weight, highly functionalized, surface-active, light absorbing organic materials which resemble humic or fulvic acids in their properties [198]. Aerosol HULIS can originate from biomass burning [31] or be formed in situ via oligomerization reactions [84]. Table 1 summarizes surface tension measurements performed on ambient and laboratory samples including natural humic and fulvic acids. Measurements of the surface tension of aqueous solutions of humic and fulvic acids originating from terrestrial or aquatic sources indicate that surface tension depression depends on concentration, pH, temperature, and the presence of metal ions [199–201, 205, 206]. Surface tension decreases with increasing temperature, but the dependence on pH is complex. The formation of micelles likely influences surface tension under some conditions, especially when metal ions are present [201]. Aumann et al. observed that "salting out" by NaCl and $(NH_4)_2SO_4$ did not significantly affect the surface tension of humic and fulvic acids in water [204]. Surface tension has also been shown to have a synergistic effect when humic acids are mixed with surfactants like SDS [207].

Facchini and coworkers collected fog water in the Po Valley, Italy (a heavily polluted site) and measured up to 30% surface tension depression compared to that of water at droplet activation concentrations [32]. The S–L equation was fit to the data, giving $\sigma = 72.8 - 0.0187T \ln (1 + 629.14C)$. The samples were determined to be 80% salt and 20% organic, containing a complex mixture of acidic oxygenated compounds. The depressed surface tension lowered the cloud droplet concentration by up to 20%, and changed the mean particle size by -6%. In a separate study they collected aerosol and fog water samples from the S. Pietro Capofiume field station in the Po Valley, with some additional cloud water samples collected at the Puy de Dôme and in Tenerife [28]. Significant surface tension depression (10–20%) was seen in the wet aerosol and fog droplets, positively correlated with the organic concentration. After fractionating the Po Valley fog samples into three organic classes and measuring the surface tension of each (at 20 °C), the overall surface tension depression was attributed mainly to polycarboxylic acids, analogous to humic substances. In addition, dynamic surface tension measurements showed that the majority of the organic material present was water soluble. The dynamic surface tension of fulvic acid and water was later measured at ambient temperature by Decesari and coworkers [27]. In comparisons of ambient cloud water and aerosol from Brazil during the burning season, from Mexico City, Los Angeles, the Po Valley, Italy, and Korea, the data showed that ambient samples have dynamic surface tensions and elasticity properties highly similar to fulvic acid, a water-soluble surfactant. This implied that a majority of the organics that form organic films on aerosols are WSOC. In the spring and autumn of 2002, Cavalli and coworkers collected ambient marine aerosols from Mace Head Atmospheric Research Station [26]. The surface tension of both fine and coarse aerosol particles was measured, showing a decrease with increasing organic content, following $\sigma = 72 - 0.17T \ln (1 + 11.86C)$. WSOC speciation identified some of the organic compounds as dicarboxylic acids, possible humic substances, and other surface-active species.

Table 1 Summary of surface tension measurements for humic and fulvic acids

Organic compound	Type	Concentration	Minimum σ (mN m^{-1})	pH	Ref.
Humic acid	Canadian soil	3% w/v	51.8	7	[199]
	O Horizon	145 mg C/L	63.9	7	[200]
		50 mg C/L	59	2.7	
	A Horizon	60 mg C/L	67	7	
		50 mg C/L	64	2.76	
	SR[a]	150 mg C/L	71	7	
		50 mg C/L	66.7	2.8	
	IHSS soil[a]	150 mg C/L	70.4	7	
		50 mg C/L	66	2.8	
	Leonardite	500 mg/L	59.4	4	[201]
	SR[a]	500 mg/L	61	3.7	
	Latahco silt loam	500 mg/L	63.6	2.5	
	Leonardite blend	500 mg/L	64.3	6	
	Acros organics	5 mg/mL	59		[95]
	Aerosol from K-puszta, Hungary	1.6 g/L	41.6	2	[29]
		1.35 g/L in 2 M AS[a]	37.5	2	
	Urban aerosol from Budapest	1.023 mg/mL	50		[30]
		102 mg/L	55	12	
	Wood burning HULIS	1 mg/mL	40.4		[31]
	Sigma Aldrich	0.5 wt%	57.5	9.7	[202]
	Sigma Aldrich	1 g/L	63.4		[203]
	IHSS soil[a]	1 g/L	64.0		
	Lignohumate	1 g/L	68.4		
	Synthesized (lab)	1 g/L	52.2		
	Daugava River	1 g/L	69.9		
	Olaine bog peat	1 g/L	62.4		
	Livani bog peat	1 g/L	55.1		
	Kemeri bog peat	1 g/L	63.5		
	Sewer sludge	1 g/L	52.1		
	sulfopropyl derivatized	1 g/L	61.0		
	Trimethylammonio derivatized	1 g/L	55.3		
	Sulfoalkyl derivatized	1 g/L	54.0		
	Hydroxyl derivatized	1 g/L	49.6		
	Sigma Aldrich	10.7 g/L	52.5		[204]
	Fluka	10.7 g/L	65.9		
Fulvic acid	Canadian soil	3% w/v	47.4	1.8–3.2	[199]
	SR[a]	500 mg/L	65	2.8–3.5	[201]
	Waskish peat	10.7 g/L	44.4		[204]
	SR[a]	10.7 g/L	44.8		[204]
	Nordic reference IHSS in AS (50:50 mass mixture)[a]	1 wt%	61		[205]

All measurements were performed in aqueous solution ($\sigma_0 = 72$ mN m^{-1}) unless otherwise noted

[a]*IHSS* International Humic Substances Society, *SR* Suwannee River, *AS* (NH$_4$)$_2$SO$_4$

Ambient aerosols containing HULIS, collected at K-puszta on the Great Hungarian Plain near Budapest (from September 1999 to August 2000), were compared to laboratory measurements by Kiss et al. [29]. The aerosol samples were acidified to pH 2 before measurement at 25 °C. The laboratory humic and fulvic acid samples, from both natural sources and Suwannee River standards, were at alkaline pH levels. Aerosol samples with the highest organic concentration (1 g L^{-1}) depressed surface tension by 25–42% from that of water. A seasonal trend was also apparent, with minimum surface tensions in the summer, increasing in the spring, fall, and then winter. The elemental composition over all seasons was similar, leading to the idea that any surface tension variability throughout the seasons must be due to different types of functional groups, aromaticity, etc. The addition of 2 M $(NH_4)_2SO_4$ to the ambient samples depressed the surface tension further. Laboratory experiments of natural humic material showed similar trends to the aerosol data, but showed less efficient surface tension depression. A marked difference was also visible between aquatic and terrestrial sources.

Salma and coworkers collected ambient humic substances in $PM_{2.5}$ from Budapest, Hungary from April to May 2002, and measured OC, WSOC, TOC, and surface tension at 20 °C [30]. The surface tension for the most concentrated solution (~1 g L^{-1}) was depressed by 30% from that of water, whereas the more dilute solutions (~44 mg L^{-1}) showed an 18% decrease. The maximum organic concentration approximately corresponded to the amount of organic material at the critical activation size. The time scale necessary to reach the minimum surface tension for both solutions was different, attributable to the different amphiphilic properties of the functional groups of the HULIS in solution. They also performed experiments with varying pH and saw similar behavior to Yates et al. [201]; the surface tension initially decreased with decreasing pH, but increased again at the lowest pH values tested due to low organic surface activity. Ambient HULIS were collected from both fresh and slightly aged wood burning smoke particles and ambient urban aerosols and compared to Suwannee River fulvic acid by Taraniuk and coworkers [31]. The surface tension was found to decrease as a function of time as the sample approached equilibrium, and to decrease with increasing organic concentration (measurements were performed at 24 °C).

Asa-Awuku et al. collected biomass burning particulate matter from prescribed burnings in Georgia in April 2004 [25]. The surface tension of the aqueous extracts was measured as a function of carbon concentration at 25 °C. At a WSOC concentration of 850 mg C L^{-1}, the surface tension of the sample was 59 mN m^{-1}, an 18% reduction from the surface tension of water. Fractionating the sample and taking surface tension measurements, the majority of the surface tension depression was found to be from the presence of hydrophobic organics. $(NH_4)_2SO_4$ and NaCl were also added to the aqueous extract to determine the effect of electrolytes on surface tension; these salts further depressed the surface tension of the sample by up to 20%, probably due to "salting out" [187].

More recently, Klavins and Purmalis studied the specific effect of humic substances on surface tension and found that industrially produced humic materials did not strongly impact surface tension, whereas substances isolated from nature

Table 2 Summary of surface tension measurements for saccharides

Organic compound	Concentration (g L^{-1})	Minimum σ (mN m^{-1})	Ref.
Levoglucosan	<5	–	[95]
	<215	69.5	[204]
D-glucose	<595[a]	76.3	
D-galactose	<450[a]	74.2	
D-maltose	<534[a]	69.9	
Sucrose	<705[a]	75.8	

All measurements were performed in aqueous solution ($\sigma_0 = 72$ mN m^{-1})
[a]Experiments performed up to solubility limit

had a much larger effect [203]. Humic acids were isolated in Latvia from soil, peat, and water and compared to commercial humic acid (Sigma Aldrich), reference International Humic Substances Society (IHSS) humic acid (Pahokee, USA), and derivatized humic acid (lab synthesized). Surface tension measurements were performed in triplicate using a tensiometer at 22 °C. They found that different natural humic acids (100 mg/L) had surface tension values between 50 and 69 mN m^{-1}, while commercial humic acid was 63 mN m^{-1}.

5.2.2 Saccharides

Saccharides are common components in atmospheric aerosols associated with biomass burning [41, 42]. Their impact on aerosol surface tension is thought to be small. The results of existing laboratory studies are summarized in Table 2. Tuckermann and Cammenga measured the surface tension of levoglucosan (with increasing concentrations up to 5 g L^{-1}) in water using a Wilhelmy plate at 20 °C, and saw no apparent decrease in surface tension [95]. Aumann and coworkers measured the surface tension of aqueous solutions containing varying concentrations of levoglucosan, glucose, galactose, maltose, and sucrose using a thermostated tensiometer at 25 °C [204]. Levoglucosan and maltose were the only two that decreased the surface tension with increasing concentration, though the overall effect was nearly negligible. Glucose, galactose, and sucrose *increased* the surface tension of water, similar to inorganic salts. Aumann et al. measured levoglucosan at concentrations up to 40× higher than those of Tuckermann and Cammenga, which could explain the discrepancies between the two studies.

5.2.3 Carboxylic Acids (≤10 Carbons)

Significant progress has been made in the parameterization of surface tension depression by water-soluble dicarboxylic acids in solution, including in the presence of salts and multiple water soluble organic species. In general it is observed that surface tension depression for these species increases with increasing carbon chain length and concentration. The results of several laboratory studies are summarized in Table 3.

Table 3 Summary of surface tension measurements for carboxylic acids ($\leq$10 carbons)

Organic compound	Concentration	Minimum σ (mN m^{-1})	Fitted equation	Ref.
3-Hydroxybutanoic acid	5.5 mg/mL	67.5		[95]
3-Hydroxybenzoic acid	5 mg/mL	70.4		
Malonic acid	3.2 M	59.8		[93]
	Solubility limit	62.2		[142]
	40 wt%	64	$71.5 - 0.381c + 0.00503c^2$	[96]
	2.02 M	61.5		[141]
Maleic acid	Solubility limit	59.5		[142]
	40 wt%	61	$71.3 - 58.9 \exp(-5.08c^{-0.292})$	[96]
Malic acid	Solubility limit	66.8		[142]
	40 wt%	68	$72.04 - 285 \exp(-7.086c^{-0.143})$	[96]
Glutaric acid	2.4 M	51.8		[93]
	Solubility limit	51.8	$10^{-3}(72 - 0.0222T \log (1 + 189.61x))$	[208]
	40 wt%	58	$70.4 - 112 \exp(-4.17c^{-0.176})$	[96]
	2.8 M	54		[204]
Succinic acid	0.45 M	67		[93]
	Solubility limit	67.5	$10^{-3}(72 - 0.0127T \log (1 + 175.28x))$	[208]
	Solubility limit	66.7		[142]
	1 wt%	70		[96]
	0.15 M	69.2		[141]
	0.6 M	66.4		[204]
in NaCl, $x = 0.06$	$x = 0.0075$	70.7		[209]
in AS (50:50 mass)	20 wt%	66		[205]
Oxalic acid	0.65 M	71.3		[93]
	Solubility limit	70.1		[142]
	5 wt%	71		[96]
	0.93 M	70.4		[204]
in AS (50:50 mass)	5 wt%	72		[205]
Adipic acid	0.15 M	64.8		[93]
	1 wt%	68	$67.2/(1 + (-0.0675 \exp (-2.39c)))$	[96]
	0.12 M	64.9		[141]
	0.12 M	65.5		[204]
	Solubility limit	64.6		[210]
in AS (50:50 mass)	1 wt%	69		[205]
Phthalic acid	0.04 M	70.6		[93]
	0.04 M	68.9		[204]

(continued)

Table 3 (continued)

Organic compound	Concentration	Minimum σ (mN m^{-1})	Fitted equation	Ref.
Azelaic acid	5 mg/mL	45.7		[95]
	0.01 M	61.1		[204]
Trimesic acid	0.01 M	71.3		[204]
Citric acid	40 wt%	65	$70.1 - 0.339c + 0.00497c^2$	[96]
in AS (50:50 mass)	20 wt%	66		[205]
cis-Pinonic acid	0.04 M	58.3		[93]
in 2 M NaCl	0.006 M	55.4		
	Solubility limit	53.9		[142]
	5.2 mg/mL	57.8		[95]
in 5.4 M NaCl	1 g/L	60.5		[94]
	0.5 wt%	58	$70.9 - 48.4c + 43.6c^2$	[96]
in AS (50:50 mass)	2 wt%	56		[205]

All measurements were performed in aqueous solution ($\sigma_0 = 72$ mN m^{-1}) except as noted

Shulman and coworkers measured the surface tensions of malonic, glutaric, succinic, oxalic, adipic, phthalic, and cis-pinonic acids in water and 0.5–2 M $(NH_4)_2SO_4$ at room temperature [93]. Surface tension depression was visible with increasing organic concentration and carbon number for all species except for phthalic and oxalic acid, which had no surface tension effect. The concentration of salt used did not affect the surface tension of any organic material except for cis-pinonic acid, which showed increased surface tension depression as salt concentration increased, possibly due to "salting out" [187]. Vanhanen et al. studied succinic acid in NaCl solutions from 283 to 303 K, and found enhanced surface tension depression as soon as succinic acid was added [209].

Dash and Mohanty measured the surface tension of oxalic, malonic, succinic, adipic, and glutaric acid in aqueous solutions between 288 and 318 K [140]. Surface tension depression was apparent in all of the solutions, and increased further if the concentration of the organic and temperature increased. In addition, calculated ΔG^0, ΔH^0, and ΔS^0 values suggested that the organic was absorbed in the surface region as a disordered organic layer.

Tuckermann and Cammenga measured the surface tension of azelaic, 3-hydroxybutanoic, cis-pinonic, 3-hydroxybenzoic, and humic acids in water at 20 °C [95]. 3-Hydroxybenzoic acid showed negligible surface tension depression, while the other compounds were more surface active. Azelaic acid reduced surface tension up to 14 mN m^{-1} at a concentration of 1 mg mL^{-1}.

Oxalic, malonic, succinic, maleic, malic, and cis-pinonic acids were studied by Hyvärinen and coworkers in water up to each compound's solubility limit and with varying temperature (10–30 °C) [142]. Surface tension depression was visible as the carbon chain length and concentration increased, with the greatest depression for cis-pinonic acid. Riipinen performed similar studies on adipic acid in water up to the solubility limit and with varying temperature (278–313 K), and saw the same

trend as Hyvärinen [210]. Tuckermann later used a thermostated tensiometer at 20 °C to measure the surface tension of varying concentrations of *cis*-pinonic acid in varying amounts of NaCl (~0.01–5 M) [94]. At low organic concentrations the surface tension trended upwards, due to the dominance of the inorganic species. At higher organic concentrations the surface tension decreased as the organic material was forced towards the surface of the droplet by "salting out," consistent with the observations of Shulman et al.

Varga et al. measured surface tension at room temperature of aqueous solutions of oxalic, malonic, succinic, glutaric, adipic, maleic, malic, citric, and *cis*-pinonic acid [96]. Surface tension decreased with increasing hydrophobic chain length. *cis*-Pinonic acid was found to decrease the surface tension effectively over a wider range of concentrations than the other organics.

The surface tension was measured for malonic, succinic, and adipic acids and polyols (C_3–C_6) (all ranging between 0 and 2 M) in 0–1 M $(NH_4)_2SO_4$ and/or NaCl by Ekström and coworkers [141]. Linear polyols were found to have negligible surface tension depression. 2-Methyltetrol had a very small effect (σ_{sol} (0.1 M) ~ 70 mN m^{-1}) in water. The organic acids decreased surface tension more efficiently in water (adipic acid, σ_{sol} (0.1 M) ~ 66 mN m^{-1}). Complete Köhler curves (assuming a dry particle diameter of 60 nm) were developed for each organic species studied.

Aumann et al. measured the surface tension of oxalic, succinic, glutaric, adipic, azelaic, phthalic, and trimesic acids up to their solubility points in water using a thermostated tensiometer at 25 °C [204]. The surface activity for the dicarboxylic acids showed an increase with carbon chain length. Phthalic acid was also found to be surface active, but trimesic acid (only slightly soluble) had negligible surface tension depression.

Frosch and coworkers studied the surface tension of binary solutions of adipic, citric, oxalic, succinic, and *cis*-pinonic acids in either ammonium sulfate or sodium chloride aqueous solutions using tensiometry at room temperature [205]. They observed no surface tension depression in solutions containing oxalic acid, and *cis*-pinonic acid had the highest surface activity among the compounds studied.

5.2.4   Long Chain Fatty Acids ($\geq$12 Carbons)

Fatty acid film formation and the associated surface tension depression has been studied extensively for idealized systems (i.e., pure water subphases) by the colloid science community, starting with the work of Langmuir nearly a century ago [211, 212]. Since it is known that fatty acid phase behavior depends strongly on factors such as pH, the presence of salts, and mixed organic content [6, 213, 214], it is not possible to extrapolate measurements performed in pure water or very dilute systems to the relevant aerosol conditions. Here we focus on studies which move towards more atmospherically relevant systems. The results of several studies are summarized in Table 4.

Table 4 Summary of surface tension measurements for long chain fatty acids (≥ 12 carbons)

Organic	Concentration[a]	Minimum σ (mN m^{-1})	Ref.
Stearic acid	Saturated	57 (bubble surface tension)	[215]
Sodium stearate	Saturated	35	[216]
	4.2 mM in 3.1 M AS	55	
Oleic acid	0.3 mM in 2.5 M NaCl	25.1	[10]
Sodium oleate	Saturated	26	[216]
	0.02 M in 3.1 M AS	38	
Sodium laurate	0.01 M	25.7	[204]
Sodium myristate	0.004 M	24.7	

All measurements were performed in aqueous solution ($\sigma_0 = 72$ mN m^{-1}) except as noted

[a]AS = $(NH_4)_2SO_4$

Aumann and coworkers studied the dynamics of organic film formation by stearic acid on various subphases, including electrolytes, acids, and humic acid solutions [202]. By adding droplets of stearic acid to an aqueous solution of humic acid, they determined that the stearic acid crystallized on top of the humic acid surface film without affecting the underlying film in any way. Organic films only formed on the electrolyte solutions (25 wt% NaCl or $(NH_4)_2SO_4$) in an atmospherically relevant time frame. In a separate study, they measured the surface tension of sodium laurate and sodium myristate up to their solubility limit in water with a thermostated tensiometer at 25 °C. These species were observed to be highly surface active, especially compared to smaller organic compounds.

Reid and coworkers studied the morphology of aqueous oleic acid/NaCl aerosols using Raman spectroscopy [10]. It appeared that, rather than spreading to form a uniform surface film, the oleic acid formed a lens on the NaCl droplet. They also measured the surface tension of bulk aqueous oleic acid/NaCl mixtures using the Wilhelmy plate method. The minimum surface tension in these mixtures was 25.1 mN m^{-1}, at a concentration of 0.3 mM oleic acid/2.5 M NaCl.

Schwier et al. [216] studied solutions of oleic and stearic acid individually at varying pH, varying $(NH_4)_2SO_4$ concentration, and varying organic concentration with a pendant drop tensiometer at 25 °C. Both oleic and stearic acids showed increasing surface tension depression with increasing organic concentration and decreasing $(NH_4)_2SO_4$ concentration. At all pH values tested (pH 1–8), significant surface tension depression was seen in water, NaCl, and $(NH_4)_2SO_4$. In water, the surface tension for both organics decreased between pH 3 and 6 due to the ionization range of the organics. The surface tension depression by these organics in saturated salt solutions was approximately constant with pH, showing that the maximum organic concentration had partitioned to the gas–liquid interface due to "salting out".

Bertram and coworkers investigated organic monolayer coatings on 60 wt% aqueous sulfuric acid at 273 K [118, 119]. Studying single-component systems of 1-octadecanol, 1-hexdecanol, stearic acid. and phytanic acid, and a two-component system (1-octadecanol and phytanic acid), they calculated the surface pressure, collapse pressure, and molecular surface area of the organic film (summarized in Table 5), in order to determine how film properties, such as packing efficiency,

Table 5 Equilibrium surface pressure (ESP) and surface area for long chain fatty acids and alcohols

Organic compound	Sub-phase	ESP (mN m^{-1})[a]	Surface area at collapse pressure (Å^2 molec^{-1})	Ref.
1-Octadecanol	60 wt% sulfuric acid		19	[118]
Phytanic acid	60 wt% sulfuric acid		44.5	
1-Octadecanol + phytanic acid	60 wt% sulfuric acid		21.3–47.2 (varies with composition)	
1-Hexdecanol	60 wt% sulfuric acid		19	[119]
Stearic acid	60 wt% sulfuric acid		19	
1-Nonadecanol	Water	24.6 ± 1.0		[163]
	5 wt% NaCl	30.3 ± 1.3		
	10 wt% NaCl	31.3 ± 1.9		
	20 wt% NaCl	35.21 ± 0.2		
1-Nonadecanoic acid	Water	12.2 ± 0.7		
	5 wt% NaCl	23.9 ± 0.9		
	10 wt% NaCl	24.2 ± 0.8		
	20 wt% NaCl	29.7 ± 1.5		

[a]Uncertainty with ESP represents 1σ

affected N_2O_5 uptake. They also found that the two-component organic monolayer was immiscible and could be described as "...patches of phytanic acid distributed within a monolayer of 1-octadecanol (or vice versa)." Knopf and Forrester studied 1-nonadecanol and 1-nonadecanoic acid (1–1.6 mg/mL) monolayer coatings with water and aqueous NaCl solutions (5, 10, 15, and 20 wt%) at 20 or 25 °C, determined the equilibrium spreading pressure, and showed that by altering the sub-phase (adding increasing amounts of NaCl), the packing efficiency of the organic monolayer changes from the expanded to the condensed state [163].

5.2.5 Complex Organic Mixtures

While most available surface tension data are for individual organic species in isolation, ambient aerosols are generally complex mixtures of many organic species. Here we highlight recent studies of surface tension depression in complex organic mixtures (summarized in Table 6).

Tuckermann and Cammenga performed surface tension studies on complex mixtures of water-soluble organics at 20 °C [95]. Mixture WSOC1 was prepared with levoglucosan and humic, *cis*-pinonic, azelaic, 3-hydroxybutanoic, and 3-hydroxybenzoic acids. Mixture WSOC2 contained the same organics in different amounts with the absence of *cis*-pinonic acid. They also used a linearly additive model to describe the contributions of each species to the observed surface tension depression; the predictions by the linearly additive models showed good agreement with the experimental surface tension results, but neither sample showed as much surface tension depression as ambient aerosol measurements taken by Facchini

Table 6 Surface tension summary of complex mixtures

| Organic compound | Conc. | Minimum σ (mN m^{-1}) | Szyszkowski fit parameters $\sigma = \sigma_o - aT \ln(1 + bC)$ | | Ref. |
			a (mN m^{-1} K^{-1})	b (kg mol^{-1})	
WSOC1 (42% humic acid, 17% pinonic acid, 14% azelaic acid, 15% 3-hydroxybutanoic acid, 9% levoglucosan, 3% 3-hydroxybenzoic acid)	10 mg/mL	57.5			[95]
WSOC2 (50% humic acid, 17% azelaic acid, 11% levoglucosan, 18% 3-hydroxybutanoic acid, 4% 3-hydroxybenzoic acid)	10 mg/mL	59.9			
MIXPO (35% NH$_4$NO$_3$, 35% (NH$_4$)$_2$SO$_4$), 12% fulvic acid, 12% succinic acid, 6% levoglucosan)	1.7 mol C/ kg H$_2$O	48.5	0.0316	7.692	[218]
MIXBIO (30% (NH$_4$)$_2$SO$_4$, 18% levoglucosan, 27% succinic acid, 25% fulvic acid)	5.3 mol C/ kg H$_2$O	44	0.0175	50.000	
MIXSEA (50% (NH$_4$)$_2$SO$_4$, 30% NaCl, 10% succinic acid, 10% fulvic acid)	1.2 mol C/ kg H$_2$O	48	0.0437	5.0429	
MIXORG (40% fulvic acid, 20% levoglucosan, 40% succinic acid)	3.5 mol C/ kg H$_2$O	48	0.0206	16.004	

All measurements were performed in aqueous solution ($\sigma_0 = 72$ mN m^{-1})

et al. [32] over the same concentration range (0.01–0.1 mg C/mL). This suggested that possible synergistic effects occur among the complex mixture of surface-active species in ambient aerosols.

Adipic (aa) and succinic (sa) acid surface tension in 2 wt% aqueous NaCl solutions was studied by Henning et al. [166]. Three different mixtures (in mass%) of the organics and salt were tested between 273 and 306 K: 93%aa/5%sa, 80% aa/18%sa, and 5%aa/93%sa. The concentrations of organics were chosen to correspond to those at the moment of droplet activation for dry particles with $d = 50$, 100 nm (mixtures 1 and 2), and $d = 40$, 50, and 100 nm (mixture 3). All mixtures showed a linear dependence of surface tension on temperature, and pure adipic acid was found to cause more surface tension depression than pure succinic acid. Surface tension depression in this non-reactive system was described very well by a linearly additive model based on the S–L equation.

Svenningsson et al. studied mixtures representative of ambient atmospheric aerosols by using varying weight percentages of levoglucosan, succinic, and fulvic acids, and (NH$_4$)$_2$SO$_4$, NaCl, and NH$_4$NO$_3$ [218]. The surface tension was measured as a function of carbon concentration using bubble tensiometry. Four different

mixtures were studied, representative of biomass burning aerosol, marine aerosol, polluted continental aerosol, and a purely organic aerosol. The minimum surface tension of all the mixtures was approximately the same (44–48 mN m^{-1}). The S_c was measured using a CCN counter, and compared to the value calculated using the experimental surface tension and Köhler theory; these values were found to be in close agreement (within 0.05%), but the model tended to overestimate the S_c.

Topping and coworkers also focused on multiple organics (including levoglucosan and oxalic, pinonic, glutaric, succinic, fulvic, malonic, maleic, malic, adipic, and citric acids) in mixed systems with inorganics ((NH$_4$)$_2$SO$_4$, NaCl, and NH$_4$NO$_3$) to determine whether predictive models could accurately describe experimental surface tension [143]. Axisymmetric drop analysis was used to measure the surface tension, and the data were compared to multiple predictive surface tension models (based on individual parameters of the organic compounds (volume weighted fraction, surface tension, type of organic, etc.) and solution thermodynamics (including activity coefficients and surface-bulk partitioning)). The best model, the LiLu model, described mixtures of up to four organics well [185]; however no model performed well in recreating the experimental surface tension magnitude if salt was present in the solution.

Booth and coworkers also studied the surface tension of binary systems (dicarboxylic acids (oxalic, malonic, succinic, glutaric, and adipic acids) and ammonium sulfate) both experimentally (at 21 °C) and using modeling to determine whether additive or thermodynamic surface tension models agreed better with experimental data [190]. Following the methodology of Topping et al. [143] they found that the LiLu model best predicted binary systems.

5.2.6   Secondary Surfactants: Small Carbonyl-Containing Compounds

Carbonyl-containing VOCs such as glyoxal, methylglyoxal, formaldehyde, and acetaldehyde are water-soluble and may be taken up into aerosol or cloud water following Henry's law. Once in the aqueous aerosol phase, these species spontaneously oligomerize to form SOA, including hemiacetals and aldol condensation products [84–86, 102]. In the presence of (NH$_4$)$_2$SO$_4$, organosulfates and nitrogen containing products may also form. These organics may also react with oxidants in the aqueous phase to form surface-active organic acids [99, 100]. The results of recent surface tension studies of these systems are summarized in Table 7.

Formaldehyde, CH$_2$O, and acetaldehyde, C$_2$H$_4$O, are two highly volatile carbonyl compounds, yet evidence from as early as the 1980s suggests that these organics can exist in the particulate phase in significant quantities [219]. McNeill and coworkers used pendant drop tensiometry (at 25 °C) to study the surface tension of mixtures of formaldehyde (0.015–0.21 M) and acetaldehyde (0.018–0.54 M) individually in H$_2$O and in 3.1 M (NH$_4$)$_2$SO$_4$ [102]. The formaldehyde–(NH$_4$)$_2$SO$_4$ mixture showed a 9% reduction in surface tension after 24 h of reaction (minimum surface tension 71.4 dyn cm^{-1}), but none in water, due to the hydrophilic nature of hydrated formaldehyde and its oligomer products. Acetaldehyde and its reaction products depressed surface tension 20.6% and 10% in (NH$_4$)$_2$SO$_4$ and water, respectively.

Table 7 Summary of surface tension measurements for reactive mixtures containing small carbonyl-containing compounds

Organic compound	Conc. (M)	Solution (aqueous unless noted)[a]	Minimum σ (mN m^{-1})	Szyszkowski fit parameters $\sigma = \sigma_o - aT \ln(1 + bC)$			Ref.
				σ_o (mN m^{-1})	a (mN m^{-1} K^{-1})	b (kg H$_2$O (mol C)$^{-1}$)	
Acetaldehyde	0.018–0.54		65	72	0.004 + 0.001	492 + 689	[102]
		3.1 M AS	62	78.5	0.026 + 0.005	8.93 + 3.61	
Formaldehyde	0.015–0.21		–	72	–	–	
		3.1 M AS	71.4	78.5	0.012 + 0.004	50 + 45	[84]
Methylglyoxal	0–2		52	72	0.025 + 0.004	2.53 + 1.08	
		5.1 M NaCl	43	80	0.02 + 0.001	84.2 + 28	
		3.1 M AS	41	78.5	0.019 + 0.001	140 + 34	
Methylglyoxal + glyoxal	0–2		60	72	0.02 + 0.003	2 + 1	[85]
		3.1 M AS	45	78.5	0.02 + 0.001	83 + 13	
Formaldehyde + methylglyoxal	0.5	3.1 M AS	48	78.5	–	–	[102]
Acetaldehyde + methylglyoxal	0.05, 0.5	3.1 M AS	60.5, 48	78.5	–	–	
Formaldehyde, acetaldehyde, methylglyoxal	0.05 (varying ratios)	3.1 M AS	59	78.5	–	–	

Fit factors (a and b) are shown with their corresponding standard deviation

[a] AS = (NH$_4$)$_2$SO$_4$

The McNeill group also studied the surface tension of glyoxal (0–1.62 M) and methylglyoxal (0–2 M) in H_2O and at high salt concentrations (5.1 M NaCl and 3.1 M $(NH_4)_2SO_4$) at 25 °C [84, 86]. The glyoxal mixtures showed no surface tension depression. Methylglyoxal showed surface tension depression in all solutions tested, with an observed minimum surface tension of 41 dyn cm^{-1} in $(NH_4)_2SO_4$. Although glyoxal and methylglyoxal undergo similar self-oligomerization chemistry, glyoxal and its reaction products are highly hydrophilic, whereas the methyl group lends some hydrophobic surface-active character to the methylglyoxal reaction mixture.

Since these compounds are likely to coexist in the ambient atmosphere, surface tension depression in mixtures of methylglyoxal and glyoxal (total organic concentration 0–2 M) in H_2O and 3.1 M $(NH_4)_2SO_4$ was also studied using the same technique [85]. The surface tension trend was described well by the additive Henning model (4) [166] because glyoxal is not surface active, so its contribution to overall surface tension was zero. The same was not observed to be true for binary mixtures of formaldehyde/ methylglyoxal and acetaldehyde/methylglyoxal or tertiary mixtures of those three compounds in 3.1 M $(NH_4)_2SO_4$ [102]. Unlike the glyoxal/methylglyoxal mixtures, the surface tensions of the binary and tertiary mixtures were lower than those predicted by the additive Henning model, suggesting a synergistic effect between the reactive species. However, methylglyoxal did dominate the surface tension depression: the surface tensions of the mixtures were similar if the methylglyoxal concentration was the same, regardless of the identity of the other organic(s).

5.2.7 Secondary Surfactants: Organosulfates

Nozière and coworkers studied organosulfate formation in aqueous aerosol mimics in mixtures of 11 mM isoprene, 0.1–0.5 M methyl vinyl ketone (MVK), 0.1–0.5 M methacrolein, or 0.15 mM α-pinene in either 3.7 M $(NH_4)_2SO_4$ or 1 M Na_2SO_4 [103]. After these solutions were exposed to UV light (280–320 nm), organosulfate products were formed via a sulfate radical pathway, and were detected within 3 h using liquid chromatography/electrospray ionization tandem mass spectrometry (LC/ESI-MSMS). While the organic/sulfate solutions showed no surface tension depression prior to irradiation, the organosulfate products detected after irradiation reduced surface tension by 25–35%. The surface-active organosulfate products were confirmed to be oligomers.

5.3 Observations of Surfactant Effects on CCN Activity

Experimental laboratory and field studies show that, depending on the surfactant type and ambient conditions, surfactants may or may not play a role in affecting the CCN activity.

A field study was conducted in March–April 1992 on El Yunque peak in Puerto Rico, a site that is influenced by both marine air masses and anthropogenic emissions, to determine the relative contributions of sulfate and organic aerosols

to CCN concentrations. It was found that in regions with significant anthropogenic pollutants, organic aerosols may affect the CCN fractions to levels similar to sulfate aerosols [220]. Rivera-Carpio et al. also showed that organic aerosols can dominate CCN concentrations at a marine site like Point Reyes, California [221]. Lab studies done by the same group have provided additional evidence of the role of organics in CCN activity; experiments showed that the CCN activity of biomass smoke particles can be attributed to the water-soluble organics present in these particles [222]. Field measurements at Chebogue Point, Nova Scotia in August–September 1993 have also suggested that oxalate may play a role in CCN activation [170].

In the study previously mentioned in Sect. 5.2.1, Asa-Awuku et al. not only measured surface tension but also characterized the CCN activity of WSOC collected from biomass burning aerosol in a prescribed burning event in Georgia in April 2004 [25]. They found that the presence of inorganics, like ammonium sulfate, in the hydrophobic fraction further depressed surface tension and a synergistic effect between the salts and organics acts to enhance considerably CCN activity. Mochida et al. investigated the relationship between CCN activity and hygroscopicity for urban aerosols in Tokyo and they stressed the importance of knowing the surface tension properties of organics in order to explain accurately the measurements [223]. A CCN closure study conducted on measurements over Houston, Texas as part of the 2006 GoMACCS campaign also suggested that knowledge of surfactant properties of the aerosols are needed to reduce the uncertainties in closure studies [224].

Various studies have determined that the aerosol hygroscopicity and CCN activity of pure oleic acid increases upon oxidation [225, 226]. Recently, to study a more atmospherically relevant system, the CCN activity of sodium salt aerosols (NaCl, Na_2SO_4) internally mixed with oleic acid (OA) was quantified [227]. These multicomponent aerosols showed depressed CCN activity upon oxidation with O_3. The behavior after oxidation was consistent with the disappearance of the organic surface film, supported by KTA. κ-Köhler calculations showed a small decrease in hygroscopicity after oxidation. The important implication of this finding is that oxidative aging may not always enhance the hygroscopicity of internally mixed inorganic–organic aerosols. This trend has also been observed in some smog chamber studies. VanReken et al. [228] measured the CCN activity of biogenic SOAs formed from the ozonolysis of five different compounds (four monoterpenes and one terpenoid alcohol). They observed that each type of SOA becomes less hygroscopic with aging, which may be attributed to the progressive oligomerization of the SOA. In another chamber study, the hygroscopicity of sesquiterpene SOA also decreases with time, which can, like the previous study, be explained by the formation of higher-molecular-weight oligomers [229].

HULIS can also impact aerosol CCN properties and cloud microphysics [3, 228]. The presence of HULIS in aerosols can lower aerosol surface tension (see Sect. 5.2.1 and Table 1). HULIS diffusion to the surface of forming droplets is faster than the rate of droplet growth, which has important implications for their effect on cloud microphysical properties [31]. Dinar et al. studied the CCN activity of HULIS extracted from fresh, aged, and pollution particles collected at the

Weizmann Institute, Rehovot, Israel and compared them to an aquatic source, Suwannee River Fulvic Acid (SRFA) [230]. They found that if the molecular weight and surface tension of the HULIS are known, then Köhler theory can predict the activation diameters. In a follow-up study they measured the hygroscopic growth of these ambient HULIS samples and found them to be more hygroscopic than SRFA fractions [231]. Wex et al. also measured the hygroscopic growth and critical supersaturations of HULIS samples extracted from filters collected in downtown Budapest, Hungary, and then used simple Köhler theory to model these parameters [232]. Their measured and modeled supersaturation values agreed when the effect of HULIS on the surface tension of the droplets was taken into account. In another study, the hygroscopic properties of HULIS extracted from aerosol samples collected at two different sites – a rural site in Hungary and a biomass burning site in Rondônia – were studied using an HTDMA and a CCNC. The Hungarian HULIS samples showed a significant lowering of surface tension (between 34% and 31%) compared to pure water. When the entire water soluble aerosol sample, which includes both the organic and the inorganic components, is studied, the surface tension decrease is not as large, ranging from 2% to 13% [233].

The effect of water-soluble dicarboxylic acid films on aerosol CCN activity has been characterized [93, 94, 143, 166, 178, 209, 210]. Here we will discuss some of the laboratory experiments that look into these effects. Figure 5 and Table 8 show comparisons of the experimental and theoretical activation diameters for some of these organics. Classical Köhler theory or modified forms that account for solubility and surface tension were used to calculate the theoretical activation diameters. Most of the organics mentioned here exhibit surface tension depression; for details please refer to Sect. 5.2.3 and Table 3. Cruz and Pandis [122, 165] initially investigated the ability of pure organics like glutaric acid and adipic acid to act as CCN and then expanded these results to study ammonium sulfate particles coated with glutaric acid. For the pure organic studies, both acids were able to act as CCN at the supersaturations studied (0.3% and 1.0%), with cloud nucleating properties similar to those of ammonium sulfate and sodium chloride [165]. For the mixed studies they concluded that a glutaric acid coating on ammonium sulfate increases the CCN activity of the inorganic core and this behavior could be predicted using Köhler theory [122].

Raymond and Pandis in two separate studies experimentally determined the CCN activities of various single-component organic particles [169] and internally mixed, multicomponent particles [168] such as glutaric acid, adipic acid, pinonic acid, glutamic acid, leucine, cholesterol, pinic acid, norpinic acid, hexadecane, hexadecanol, myristic acid, palmitic acid, and stearic acid with sodium chloride and ammonium sulfate in the latter study. Their results are summarized in Table 8 and Fig. 5.

In agreement with previous studies, Pradeep Kumar et al. showed that particles composed of highly soluble smaller acids like oxalic, malonic, and glutaric acids activate as predicted by Köhler theory, whereas particles containing long-chain fatty acids such as stearic and oleic acids, which are essentially insoluble in water, do not activate for particle diameters up to 140 nm and supersaturations of 0.6 and
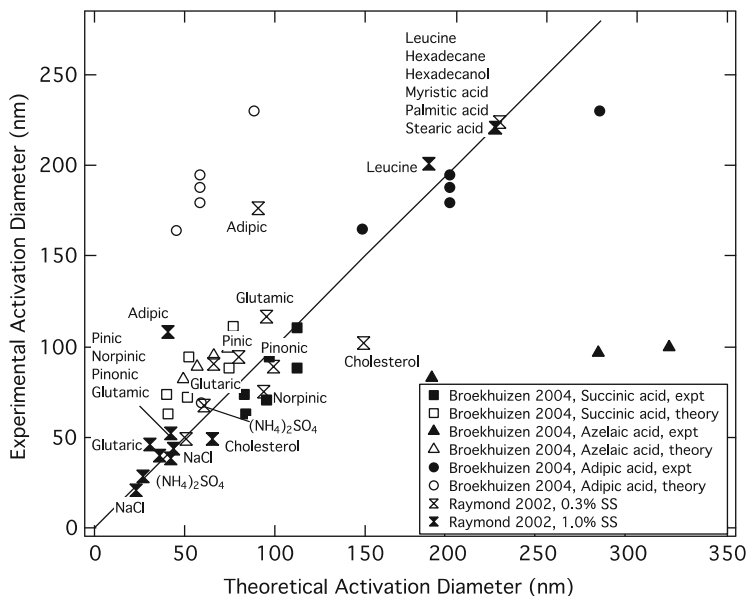
Fig. 5 Experimental results of Broekhuizen et al. [225] and Raymond and Pandis [169] compared to those predicted by Köhler theory. For Broekhuizen et al. [225] each point represents an experiment conducted at a fixed supersaturation between 0.33% and 0.89%. The *solid symbols* represent experimental results compared to the "full" Köhler theory for the crystalline organic and the *open symbols* represent those compared to traditional Köhler theory assuming full solubility. The different species studied by Raymond and Pandis [169] are listed on the graph. In this case, the *open symbols* represent a supersaturation of 0.3% and the *solid symbols* represent a supersaturation of 1.0%. In this case, for the theoretical diameters, Kohler theory assuming complete solubility is used for species which are wetted by water and assuming limited solubility theory for those species which make a finite, nonzero contact angle with water

below [235]. Prenni et al. used a humidified tandem differential mobility analyzer (HTDMA) to investigate the hygroscopic behavior (below saturation) of organic compounds like oxalic, malonic, succinic, glutaric, and adipic acids [167]. Their data suggest that under most humidity conditions, adipic and succinic acids are not likely to exhibit hygroscopic growth. At high humidities, oxalic, malonic, and glutaric acids showed similar water uptake behavior to inorganic particles. Hori et al. explored the CCN activation of water-soluble organics such as ammonium oxalate and malonic, succinic, glutaric, adipic, malic, and phthalic acids [236]. Amongst all of these, ammonium oxalate showed the highest activation capability, comparable to that of ammonium sulfate. The presence of trace levels of a surface-active species such as azelaic acid and nonanoic acid can dramatically enhance the activation of adipic acid, a moderately soluble organic [225]. C3–C6 polyols and 2-methyltetrols, though highly water-soluble, are less CCN efficient than organic acids [141]. Henning et al. stressed the importance of particle phase for cloud droplet activation for aerosols containing organics and inorganics [166].

Table 8 Theoretical and activation diameters for various surfactants

Organic compound[a]	Supersaturation (%)	Theoretical activation diameter (nm)	Experimental activation diameter (nm)	Ref.
Glutaric acid	0.3	98	111	[165]
	1.0	44	60	
Adipic acid	0.3	103	115	
	1.0	46	52	
	0.4	80	148	[164]
	0.5	69	116	
	0.8	51	No data	
Succinic acid	0.4	71	82	
	0.5	64	64	
	0.8	45	41	
Glucose	0.4	83	74	
	0.5	71	57	
	0.8	52	41	
Pinic acid	1.0	35	38 ± 6	[168]
GA	1.0	41	38 ± 6	
PA	1.0	41	50 ± 9	
L	1.0	184	200 ± 34	
Norpinic acid	1.0	43	42 ± 7	
Hexadecane	1.0	>200	>200	
50% NaCl, 50%L	1.0	27–28	21 ± 4	
10% NaCl, 90%L	1.0	41–44	39 ± 7	
1% NaCl, 99%L	1.0	80–85	67 ± 11	
50% GA, 50%L	1.0	48	48 ± 8	
10% NaCl, 90% GA	1.0	36–37	36 ± 6	
10 % AS, 90 % PA	1.0	34–37	46 ± 8	
33% PA, 33% Pinic acid, 33% Norpinic acid	1.0	35–44	47 ± 8	
10% AS, 30% PA, 30% GA, 30% L	1.0	32–44	49 ± 8	

In most cases the deviation from the theoretical diameters could be attributed to the activation kinetics

[a]*AS* ammonium sulfate, *GA* glutamic acid, *L* leucine, *PA* pinonic acid

Abbatt et al. studied the ability of mixed ammonium sulfate and organic acid (malonic, azelaic, hexanoic, *cis*-pinonic, oleic, and stearic acids) particles to act as CCN [237]. Their goal was to test whether surface-tension lowering by these species would have a significant effect on particle activation. They observed highly variable results for different combinations of organics, leading them to conclude that CCN behavior of mixed inorganic–organic aerosols is not characterized solely by surface tension depression effects of the organics and that solubility is the primary factor.

Recently we studied the effect of surfactants like methylglyoxal and acetaldehyde by exposing deliquesced ammonium sulfate seed aerosols (65% RH) 8 ppb or 250 ppb of the organic gas in a 3.5-m^3 continuous flow aerosol reaction chamber [238]. The CCN activity was measured using a Continuous-Flow Streamwise

Thermal Gradient CCN Chamber (CFSTGC). Both of these organic species were observed to cause significant enhancements in CCN activity at small particle sizes. No detectable particle volume growth associated with uptake was observed, consistent with the observations of Kroll et al. [239] and with the relatively low Henry's law constants of methylglyoxal and acetaldehyde [240]. Furthermore, the particle surface tensions inferred from the CCN data using KTA were significantly lower than those measured for bulk solutions with the equivalent aqueous phase composition predicted using Henry's law. This suggests that surface adsorption is also important for determining aerosol surface tension and thus CCN activity [241].

A few recent field studies have highlighted the challenges in using current instrumentation to understand the composition dependent effects on hygroscopicity. These discrepancies in the measured hygroscopicity can have important implications for other inferred parameters such as surface tension. Good et al. measured aerosol composition, hygroscopicity, and CCN activity in the tropical Atlantic on board the RHaMBLe Discovery Cruise D319 and evaluated the ability of κ to represent water uptake [242]. They observed noticeable differences in the measured and predicted CCN activity for all three measurement periods, which can be partially attributed to limitations in measurement and analytical techniques including the use of the HTDMA to validate the applicability of the κ-model for relative humidities over 94%. In another field study, aerosol physical, chemical, and hygroscopic properties were measured during the COPS campaign in Germany [243]. They found inconsistencies between critical supersaturations derived using the CCNC and those derived using the HTDMA κ-model. Inability to resolve these differences would result in inaccurate predictions of aerosol indirect effects.

5.4   Modeling Surfactant Effects on CCN Activity

In recent years several groups have developed models to analyze the effect of surfactants on aerosol surface tension behavior [25, 32, 93, 143, 232, 244].

Seidl created a model based on the state of the surface film (e.g. expanded or condensed), the equilibrium spreading pressure, and the area per film molecule to describe organic film formation from fatty acids, then applied it to rainwater and aerosol particles [245]. He concluded that, in most cases, only dilute films (with concentrations below that necessary to form a complete monolayer) would form on aerosols and raindrops, and such films would not affect their physical or chemical properties. However, dense films were predicted to form on aerosols in the western U.S., mainly attributable to biomass burning. Mazurek and coworkers developed a model to describe structural parameters (elastic properties, etc.) of fatty acid films on rainwater without requiring knowledge of the surfactant concentration or composition by using surface pressure-area and surface pressure–temperature isochors and the rain rate and drop diameter distribution [33]. This model can be used to identify the origin of specific compounds and an approximate chemical composition based on the force–area characteristics of collected rainwater films.

Based on the thermodynamics of aggregate formation, Tabazadeh suggested that micelle formation would limit the surface tension depression capability of organics in ambient aerosols to 10 dyn cm^{-1}, but she pointed out that even this limited amount of surface tension could impact cloud activation [11].

Djikaev and Tabazadeh developed a model by including adsorption as well as Henry's law to describe trace gas uptake into cloud droplets for binary systems (water and the trace gas) [241]. Testing properties for both soluble and insoluble organic species, they found that a large fraction of the organic will remain near the gas–liquid interface if it is surface active, which could affect the surface tension and cloud physics.

Prisle and coworkers implemented parameterization of surfactant effects on cloud activation and cloud radiative properties in a global climate model [246], and found that including only surface tension parameterization gave erroneous results. They found that detailed parameterization of surfactant properties were required to achieve accurate predictions of cloud droplet number calculations (CDNC).

5.4.1 Molecular Dynamics Simulations of Surfactant Effects

Molecular dynamic simulations have also been used to study surfactant films on water droplets [247–255]. Ågren and coworkers simulated the surface-bulk partitioning of various organics in atmospheric droplets [250–253]. They studied amino acids (<50 molecules), HULIS (<162 molecules), and *cis*-pinonic acid (<243 molecules) in water droplets (<10,000 molecules). As expected, the amino acids affected the surface tension depending on their hydrophobic character, with the most amphiphilic species depressing surface tension to the greatest extent [252]. Model HULIS compounds (*cis*-pinonic acid, pinic acid, and pinonaldehyde) formed aggregates both at the surface and in the bulk of the water droplets, dependent on the number of organic molecules present [250].

Zachariah and coworkers used molecular dynamics simulations to study the effect of organic coatings on water uptake by aqueous droplets [247–249, 254]. They determined that the sticking coefficient of water decreased if an organic layer was present over a pure water surface, and that the sticking coefficient was dependent on the structure of the organic molecules and chain–chain interactions. Takahama and Russell [255] simulated the accommodation of impinging water molecules by slabs of water with and without interfacial surfactant films. Consistent with the findings of Zachariah and coworkers, they found that a surfactant film decreased the water accommodation coefficient by 70–100%, depending on the packing density and projected surface coverage of the surfactant hydrocarbon chains.

5.4.2 Modeling Surface-Bulk Partitioning

Several modeling and experimental studies have been conducted recently in order to understand the role of surface-bulk partitioning of surfactants in cloud droplet activation [256–263].

Li and coworkers modeled the surface-bulk partitioning of SDS in mixed SDS/NaCl particles using Köhler theory and chemical properties of the surfactant, allowing the solute concentration and surface tension of the aerosol to vary as the organic partitioned between the gas–aerosol interface and the particle bulk [257]. This partitioning was found to affect both the Raoult and Kelvin terms, leading to a net increase in S_c.

Sorjamaa and coworkers also demonstrated theoretically the importance of including the partitioning of the surfactant between the bulk and the surface in Köhler theory calculations [263]. This model differed from that of Li et al. in that surface effects were rigorously derived using Gibbs' surface thermodynamics. Including surface-bulk partitioning in models of the aqueous SDS/NaCl and *cis*-pinonic acid/$(NH_4)_2SO_4$ systems showed, in agreement with the conclusions of Li et al., that S_c is underestimated if partitioning is neglected, leading to decreased cloud droplet activation. The effect of surface-bulk partitioning is greater for smaller particles. In a second study, Sorjamaa et al. studied fatty acids, diols, and HULIS by varying the two surface tension parameters of the S–L equation within a specified range to control the surface-bulk partitioning of each organic [262]. They found that for slightly surface-active species, neglecting partitioning would not be a large source of error as long as the surface tension including organics was used in Köhler theory. However, for more surface-active species, partitioning was important to include. Additionally, they determined that strong surfactants might not affect the Köhler curve as much as a slightly surface-active species, because the organic would partition to the surface of the droplet more efficiently, possibly increasing the critical radius. Efforts have been made to simplify the surface-bulk partitioning model of Sorjamaa et al. in order to reduce computational expense [258, 261].

Romakkaniemi and coworkers modeled the reactive uptake of gaseous methylglyoxal to an $(NH_4)_2SO_4$ aerosol, based on Henry's law equilibrium, and also allowed aqueous phase reactions of methylglyoxal with ammonium, hydronium and OH radicals to take place [264]. They showed that by including surface-bulk partitioning of surface-active SOA products, an order of magnitude higher concentration of methylglyoxal would enter into the aqueous aerosols (for particles with $r < 200$ nm). However, even with this additional organic within the aerosol, the surface tension depression at the point of activation was predicted to be negligible.

More recently, Topping developed a methodology for an analytical solution to calculate the movement of organic material from the bulk to a surface layer, requiring only surface tension parameters from binary systems [265]. He found that the method was computationally efficient, but it must be validated by comparisons with laboratory experimental data, and then further with ambient studies and smog chambers.

5.5 Kinetic Limitations to Cloud Droplet Growth

It is assumed in Köhler theory that cloud droplet activation is a process whereby the particle instantly reaches thermodynamic equilibrium with the local supersaturation condition [266]. However, kinetic limitations on droplet growth can render this

equilibrium assumption invalid under certain realistic conditions [173, 174]. It is well known that organic films at the air–aqueous interface inhibit the mass transfer of water between the gas and liquid phases [105, 107]. Non-instantaneous dissolution of organic particulate matter can also serve as a kinetic limitation to equilibration. In this section we review theoretical, field, and experimental approaches to characterize kinetic limitations to cloud droplet growth and their impacts.

5.5.1 Theory

Chuang et al. distinguished between CCN and cloud droplet nuclei (CDN) by describing CCN as particles that activate to become droplets within a cloud chamber of fixed or prescribed supersaturation, whereas CDN are particles that activate in the atmosphere under the more relevant time-varying supersaturation conditions [173]. They compared the timescale for particle growth at equilibrium to the condensational growth timescale, and concluded that the discrepancies in empirical correlations between cloud droplet and CCN concentrations could be at least partly attributed to limitations in kinetic growth. In such cases, the equilibrium assumption can lead to an overestimation of the droplet number concentrations, causing errors in models of cloud droplet populations and consequently affecting estimates of cloud radiative climate forcing. Phinney et al. compared the cloud droplet formation and growth parameterization developed by Abdul-Razzak et al. [267] and Abdul-Razzak and Ghan [268] (ARG) [267, 268] to an adiabatic parcel model that accounts for the kinetics of droplet growth [269]. They found that there are certain conditions under which the ARG parameterization underpredicts the supersaturation and the cloud droplet number concentration, especially in highly polluted urban areas where updraft velocities are low and aerosol number concentrations are high.

Typically WSOC are the compounds in atmospheric aerosols that exhibit substantial surfactant behavior [93]. In general, the presence of WSOC can affect CCN activity by either changing the surface tension (Kelvin) or by changing the moles of solute in the droplet (Raoult). The use of a numerical model to investigate the effect of organics on cloud droplet activation has suggested that WSOC can influence droplet concentrations by increasing the amount of solute in a particle and by reducing the surface tension [270]. Nenes et al. [271] used a cloud parcel model and found numerous conditions under which chemical effects on cloud droplet number were comparable to the first indirect effect [271]. They studied various chemical effects including dissolution of soluble gases and partially soluble solutes in the growing droplet, accommodation coefficient changes from the formation of organic films at the droplet surface, and surface tension depression by dissolved organic substances. Their simulations indicated that all these effects show a strong dependence on updraft velocity. The mass accommodation coefficient has a negligible effect on the cloud droplet number for marine aerosols, but the aerosol number increased considerably for urban environments. Under marine conditions the surface tension effect can be up to 50% of the Twomey effect, whereas under

urban conditions it can exceed the Twomey effect. In this study the authors concluded that the uncertainties in the surface tension behavior are probably more influential than uncertainties in the solute concentration alone. The influence of WSOC would also be greater if they are distributed according to the CCN surface area (vs volume), as a greater mass of WSOC will be present on CCN with high S_c. Additionally, the presence of surfactants and condensable gases can act synergistically to increase cloud droplet number. Using an aerosol activation parameterization that includes surface tension effects, it has been shown that the addition of surfactants to CCN affects drastically how the CCN responds to changes in the updraft velocity [272].

Ervens et al. used an adiabatic cloud parcel model to confirm that the largest changes in droplet number due to the presence of WSOC occur at low updraft velocities and high aerosol concentration [273]. This is because, under these conditions, the kinetic effects on growth are important and the equilibrium assumption leads to an overestimate of the composition effects. Film-forming compounds have also been shown, using a cloud parcel model, to have an effect on droplet growth and they can reduce the cloud droplet number concentration, which has direct consequences for climate-cloud feedbacks [274]. Lance et al. extended this analysis to scales larger than individual updrafts and used a detailed numerical cloud parcel model to show that organic surfactants can impact cloud droplet number as much as changes in updraft velocity [275].

Khvorostyanov and Curry recently developed an alternative parameterization to calculate droplet activation kinetics that reduces the uncertainties associated with cloud parcel models and allows changes in basic assumptions like the kinetic corrections in the droplet growth rate to be accommodated more easily [276]. Their method is computationally more efficient and flexible as it eliminates the need to run numerous simulations using cloud parcel models; instead, it is based on a direct numerical solution of the integral supersaturation equation.

Asa-Awuku and Nenes developed a numerical model to investigate the effect of dissolution kinetics on CCN activity [244]. According to their parameterization, solution dissolution kinetics will not cause a change in the critical supersaturation if there are substantial amounts of inorganic electrolytes and low molecular weight organic acids present in ambient CCN. The effect of dissolution kinetics is not enough to inhibit CCN activity but, under certain conditions, affected droplets can undergo a slower growth rate and require a higher supersaturation level to activate.

5.5.2   Lab

A number of laboratory studies have shown how the presence of surfactants can affect the growth kinetics of aerosols. Figure 4 and Table 8 show theoretically and experimentally derived activation diameters for various surface-active organics. When activation is observed at a larger critical diameter than the one predicted theoretically, this can be an indication of kinetic limitations, especially those related to solubility. Additionally, in the past few years, chamber studies have

tried to study specifically the CCN activity of WSOC [25, 97, 197, 277, 278]. Most of these indicate that the presence of WSOC does not affect droplet growth kinetics, but it is important to note that the organics in these experiments are also not strong surfactants. Typically in these studies, the activated droplet diameter at each supersaturation is plotted for the different samples and compared to the activation of a pure inorganic salt. If the sample particles can grow to similar diameters as the inorganic, it implies that droplet growth kinetics are not affected, at least in the environment of the cloud chamber. For instance, SOA was generated in the 12 m^3 Carnegie Mellon University chamber from the ozonolysis of a sesquiterpene, β-caryophyllene, and online measurements were made using a Static Diffusion (SD) CCN counter and a Continuous-Flow Streamwise Thermal Gradient CCN chamber (CFSTGC) to study the droplet formation characteristics of this SOA [277]. The WSOC fraction and the droplet growth kinetics of the CCN were found to be strongly anti-correlated, implying that the insoluble material in the SOA can delay droplet growth by forming a kinetic barrier to water uptake. Additionally, the less volatile material in the SOA was not very hygroscopic, but it impacted growth kinetics. The gas phase uptake of surfactants like methylglyoxal and acetaldehyde has been observed in chamber studies to enhance CCN activity of inorganic seed aerosols but not to have an effect on activation kinetics [238].

Corrigan and Novakov [164] observed that the measured values of the critical diameter for adipic acid are around two times greater than the calculated values, unlike the more soluble succinic acid, which shows closer agreement [164]. This could possibly be due to the lower solubility of adipic acid causing a delay in the growth of the cloud droplet.

To study the importance of solubility on the activation of a cloud droplet, Shantz et al. measured the growth rates of water droplets on pure organic particles, such as succinic, glutaric, adipic, pimelic, and suberic acids, and their mixtures with ammonium sulfate, using a thermal gradient static cloud diffusion chamber (CCNc) [279]. Additionally, they used a kinetic model of droplet growth modified to account for solubility, and were able to reproduce successfully the observed delays in particle growth. Their results once again assert the importance of solubility for cloud droplet activation; the particles exhibited a short delay (1–2 s) in activation if the organic coats the ammonium sulfate and can reduce the CDNC relative to ammonium sulfate by up to 85%.

Hegg et al. studied the CCN activity of products of cyclohexane and α-pinene oxidation by ozone generated in a 600-m^3 Calspan Corporation chamber by coupling the chamber outflow to a static thermal diffusion chamber to measure the CCN activation spectrum [280]. They concluded that the presence of organic components, or at least sparingly soluble or relatively low-hygroscopicity organics, may significantly alter the CCN efficiency of the aerosol and increase the time necessary to activate.

Small amounts of salt can have a great effect on the cloud droplet activation of leucine [168]. This effect has also been observed with adipic and succinic acids [281]. Essentially, the barrier to water uptake and activation is decreased in the presence of an inorganic salt.

The effect of palmitic acid (water insoluble, surface active organic) coatings on water uptake by ammonium sulfate was studied using a combination of FTIR, Transmission Electron Microscopy (TEM), and Aerosol Mass Spectrometry (AMS) [282]. The results indicated that a thin coating will not change the kinetics of water uptake of ammonium sulfate particles greatly, but a thicker coating (~50 wt % organic) may have a discernible effect.

Andrews and Larson coated black carbon particles with organic surfactants like Tween 80 or azelaic acid and observed an enhancement in the hygroscopicity of these ordinarily hydrophobic compounds [283]. Knowing that these elemental carbon particles are quite abundant in the atmosphere, typically formed in combustion processes, this study is key in trying to understand how organic compounds on their surface can change their chemical and physical interactions in the atmosphere.

The laboratory studies discussed in this section highlight the importance of the solubility of aerosol organic material on CCN activity. As stated previously, solubility affects the Raoult term in the Köhler equation (1). The solubility limits the amount of organic material that is incorporated into the particle and thus influences the potential for the formation of a surface film and/or micelles. Hence, solubility indirectly also impacts the surface tension of the particle, thereby influencing the CCN activity via the Kelvin effect.

5.5.3   Field

CCN closure studies, where observations of ambient aerosol CCN activity are compared to the CCN concentration predicted via Köhler theory based on the particle size distribution and composition, often show discrepancies that can be attributed to kinetic limitations to droplet growth. Besides affecting cloud properties, kinetic limitations to droplet growth in the atmosphere may also impact the lifetime of aerosol particles. Changes in particle lifetime may influence the aerosol composition due to photochemical aging or heterogeneous processing of the aerosol.

In a study conducted in a semi-rural location (Egbert, Ontario) in the fall of 2005, good CCN closure was attained in most cases when it was assumed that the particulate organics were insoluble and that the growing droplet had the surface tension of water [284]. However, when organic content was high the closure was not as good. Sensitivity analyses suggested that organic solubility limitations and/or surface tension depression were important.

Shantz et al. incorporated the results from another field study conducted in Egbert in May–June 2007 into a cloud droplet model [285]. This field study compared the CCN cloud droplet water uptake by aerosol particles containing organics from anthropogenic or biogenic sources. Fresher biogenic particles, distinguished using AMS, exhibited the same initial growth rate as ammonium sulfate, but organics from anthropogenic sources delayed initial growth of particles, possibly due to film formation.

Ruehl et al. measured the rate of cloud droplet formation in August–September 2006 at four different sites in the US to represent various air masses: Houston, TX (urban), Great Smokey Mountain National Park, TN (polluted regional), Bondville, IL (background continental), and the Southern Great Plains site (Lamont, OK) [286]. They used a fully-coupled numerical flow model to transform the observed size distributions into mass accommodation coefficient (α) distributions. The mass accommodation is defined as the probability that a water vapor molecule will be incorporated into the liquid phase upon collision with a droplet. They reported that 59% of ambient CCN grew at a rate similar to ammonium sulfate and that kinetic limitations were important only for some air masses. Contradicting results were found by Lance et al. [224] where another CCN closure study in Houston, Texas around the same time showed no substantial delay in activation kinetics [224]. The origin of this discrepancy is unclear, but the use of different instruments in both studies may have contributed to the differences in observations.

In another field study near the central Californian coast in July–August 2007, persistent bimodal spectra were observed for the cloud droplets, which are attributed to the presence of kinetic limitations to droplet growth. The inferred mass accommodation coefficients for the slowly-growing mode were smaller than ammonium sulfate. Additionally, the particles with low accommodation coefficients showed a small and narrow size distribution, indicating that the observed kinetic limitations arose due to the presence of a condensed film rather than slow dissolution [287].

The first joint shipboard and airborne study related to the chemical composition and water-uptake behavior of particulates in ship emissions was conducted on emissions from a Post-Panamax class container ship off the central coast of California. The results showed that the majority of particles outside the ship plume did not show slow water uptake kinetics as compared to ammonium sulfate, but in-plume particles with critical supersaturation between 0.1% and 0.35% had slower uptake kinetics than ammonium sulfate [288].

Water-soluble organics present in Mexico City aerosols were found to act as surfactants, but they did not retard activation kinetics [289]. The ocean surface also contains significant amounts of slightly soluble surfactants, which could potentially affect activation kinetics. The CCN activity of the DOM in seawater samples collected near the Georgia coast showed growth similar to ammonium sulfate even though this DOM form compressed surface films that altered surface tension, suggesting that DOM primarily affects CCN activity through its impact on surface tension [197].

6 Summary and Outlook

It is clear that surface-active organics in atmospheric aerosols can significantly impact aerosol heterogeneous chemistry, cloud formation, and freezing. Most of these effects stem from the tendency of surface-active molecules to partition to the
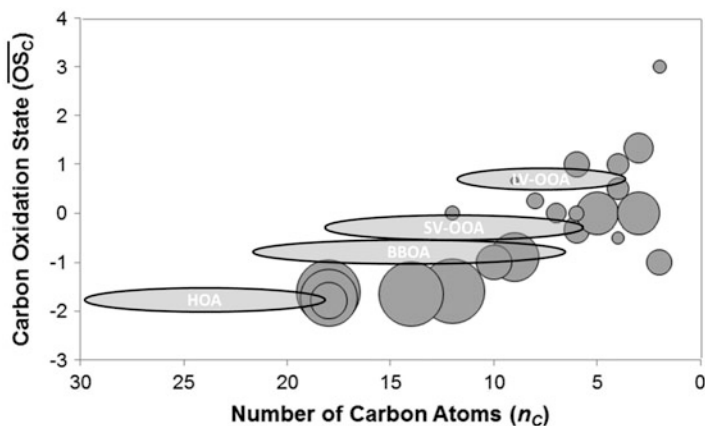
Fig. 6 Bubble diagram depicting maximum measured surface tension depression for organic surfactant species in aqueous solution (from Tables 2, 3, 4 and 7) as a function of average carbon oxidation state ($\overline{\text{OS}_\text{C}}$) in the molecule and number of carbon atoms (n_C) [296]. The size of the bubble is proportional to the maximum measured departure from the surface tension of water (72 mN m^{-1}) for each species. Also shown are typical values of ($\overline{\text{OS}_\text{C}}$) and n_C for atmospheric organic aerosol material as classified from Aerodyne Aerosol Mass Spectrometer measurements. "HOA" indicates hydrocarbon-like organic aerosol, "BBOA" is biomass burning aerosol, "SV-OOA" is semivolatile oxidized organic aerosol, and "LV-OOA" is low-volatility oxidized organic aerosol

gas–aerosol interface, forming an organic surface film and reducing the surface tension. At this time, the prevalence of organic surface films on ambient atmospheric aerosols is not completely known. There is a need for the development of new techniques capable of directly detecting organic films on ambient aerosols in situ without sample drying.

It is also not currently possible to predict reliably the formation of organic surface films on aerosols as a function of aerosol chemical composition. To this end, there is a need for more laboratory experiments to characterize phase behavior and surface tension depression for naturally occurring organic surfactants under the range of conditions typical of the aqueous aerosol environment (i.e., supersaturated salt concentrations, pH ~0–8, multiple organic species [34, 290–295]). The potential for liquid–liquid phase separation [12] and glass formation [13, 14] in aerosols containing surfactants should be evaluated, and the concomitant effects on aerosol freezing, CCN activity and heterogeneous chemistry should be explored.

Figure 6 summarizes the maximum measured surface tension depression for organic surfactant species in aqueous solution (data from Tables 2, 3, 4 and 7) in the context of the carbon oxidation state ($\overline{\text{OS}_\text{C}}$) vs carbon number ($n_\text{C}$) diagram of Kroll et al. [296]. The highest surface tension depression is observed for fatty acid salts with relatively low ($\overline{\text{OS}_\text{C}}$) and high n_C. However, significant surface tension depression potential exists for species with a wide range of ($\overline{\text{OS}_\text{C}}$) vs n_C, typical of both freshly emitted and aged primary organic aerosol, or SOA. It is also

apparent from Fig. 6 that more surface tension measurements are needed for species with ($\overline{\mathbf{OS_C}}$) and n_C values that fall within the ranges defined by Kroll et al. [296] as being typical for atmospheric organic aerosol material.

Finally, for a complete picture of the multiple roles of surface-active organic material in the chemistry and physics of aerosols, field experiments are needed which couple direct observations of aerosol heterogeneous chemistry [148], CCN, and IN activity with studies of aerosol composition, surface tension, and particle morphology. New techniques which provide speciated ambient aerosol organic composition [297] or functional group information [298] are expected to yield additional insight.

References

1. Forster P, Ramaswamy V, Artaxo P, Berntsen T, Betts R, Fahey DW, Haywood J, Lean J, Lowe DC, Myhre G, Nganga J, Prinn R, Raga G, Schulz M, Van Dorland R (2007) Changes in atmospheric constituents and in radiative forcing. In: Solomon S, Qin D, Manning M, Chen Z, Marquis M, Averyt KB, Tignor M, Miller HL (eds) Climate change 2007: the physical science basis. Contribution of working group I to the fourth assessment report of the intergovernmental panel on climate change. Cambridge University Press, Cambridge
2. Jimenez JL, Canagaratna MR, Donahue NM, Prevot ASH, Zhang Q, Kroll JH, DeCarlo PF, Allan JD, Coe H, Ng NL, Aiken AC, Docherty KS, Ulbrich IM, Grieshop AP, Robinson AL, Duplissy J, Smith JD, Wilson KR, Lanz VA, Hueglin C, Sun YL, Tian J, Laaksonen A, Raatikainen T, Rautiainen J, Vaattovaara P, Ehn M, Kulmala M, Tomlinson JM, Collins DR, Cubison MJ, Dunlea EJ, Huffman JA, Onasch TB, Alfarra MR, Williams PI, Bower K, Kondo Y, Schneider J, Drewnick F, Borrmann S, Weimer S, Demerjian K, Salcedo D, Cottrell L, Griffin R, Takami A, Miyoshi T, Hatakeyama S, Shimono A, Sun JY, Zhang YM, Dzepina K, Kimmel JR, Sueper D, Jayne JT, Herndon SC, Trimborn AM, Williams LR, Wood EC, Middlebrook AM, Kolb CE, Baltensperger U, Worsnop DR (2009) Evolution of organic aerosols in the atmosphere. Science 326:1525–1529
3. Kanakidou M, Seinfeld JH, Pandis SN, Barnes I, Dentener FJ, Facchini MC, Van Dingenen R, Ervens B, Nenes A, Nielsen CJ, Swietlicki E, Putaud JP, Balkanski Y, Fuzzi S, Horth J, Moortgat GK, Winterhalter R, Myhre CEL, Tsigaridis K, Vignati E, Stephanou EG, Wilson J (2005) Organic aerosol and global climate modelling: a review. Atmos Chem Phys 5:1053–1123
4. Ellison GB, Tuck AF, Vaida V (1999) Atmospheric processing of organic aerosols. J Geophys Res Atmos 104:11633–11641
5. Gill PS, Graedel TE, Weschler CJ (1983) Organic films on atmospheric aerosol-particles, fog droplets, cloud droplets, raindrops, and snowflakes. Rev Geophys 21:903–920
6. Cistola DP, Hamilton JA, Jackson D, Small DM (1988) Ionization and phase-behavior of fatty-acids in water – application of the Gibbs phase rule. Biochemistry 27:1881–1888
7. Leck C, Bigg EK (2005) Biogenic particles in the surface microlayer and overlaying atmosphere in the central Arctic Ocean during summer. Tellus B 57:305–316
8. Leck C, Bigg EK (2005) Source and evolution of the marine aerosol – a new perspective. Geophys Res Lett 32:L19803. doi:10.1029/2005GL023651

9. Posfai M, Gelencser A, Simonics R, Arato K, Li J, Hobbs PV, Buseck PR (2004) Atmospheric tar balls: particles from biomass and biofuel burning. J Geophys Res Atmos 109: D06213. doi:10.1029/2003JD004169

10. Reid JP, Dennis-Smither BJ, Kwamena NO, Miles REH, Hanford KL, Homer CJ (2011) The morphology of aerosol particles consisting of hydrophobic and hydrophilic phases: hydrocarbons, alcohols and fatty acids as the hydrophobic component. Phys Chem Chem Phys 13:15559–15572

11. Tabazadeh A (2005) Organic aggregate formation in aerosols and its impact on the physico-chemical properties of atmospheric particles. Atmos Environ 39:5472–5480

12. Bertram AK, Martin ST, Hanna SJ, Smith ML, Bodsworth A, Chen Q, Kuwata M, Liu A, You Y, Zorn SR (2011) Predicting the relative humidities of liquid-liquid phase separation, efflorescence, and deliquescence of mixed particles of ammonium sulfate, organic material, and water using the organic-to-sulfate mass ratio of the particle and the oxygen-to-carbon elemental ratio of the organic component. Atmos Chem Phys 11:10995–11006

13. Tong H-J, Reid JP, Bones DL, Luo BP, Krieger UK (2011) Measurements of the timescales for the mass transfer of water in glassy aerosol at low relative humidity and ambient temperature. Atmos Chem Phys 11:4739–4754

14. Zobrist B, Marcolli C, Pedernera DA, Koop T (2008) Do atmospheric aerosols form glasses? Atmos Chem Phys 8:5221–5244

15. Blanchard DC (1964) Sea-to-air transport of surface active material. Science 146:396–397

16. Buseck PR, Posfai M (1999) Airborne minerals and related aerosol particles: effects on climate and the environment. Proc Natl Acad Sci USA 96:3372–3379

17. Peterson RE, Tyler BJ (2002) Analysis of organic and inorganic species on the surface of atmospheric aerosol using time-of-flight secondary ion mass spectrometry (TOF-SIMS). Atmos Environ 36:6041–6049

18. Peterson RE, Tyler BJ (2003) Surface composition of atmospheric aerosol: individual particle characterization by TOF-SIMS. Appl Surf Sci 203:751–756

19. Russell LM, Maria SF, Myneni SCB (2002) Mapping organic coatings on atmospheric particles. Geophys Res Lett 29. doi:10.1029/2002GL014874

20. Tervahattu H, Hartonen K, Kerminen VM, Kupiainen K, Aarnio P, Koskentalo T, Tuck AF, Vaida V (2002) New evidence of an organic layer on marine aerosols. J Geophys Res Atmos 107:4053. doi:10.1029/2000JD000282

21. Tervahattu H, Juhanoja J, Kupiainen K (2002) Identification of an organic coating on marine aerosol particles by TOF-SIMS. J Geophys Res Atmos 107:4319. doi:10.1029/2001JD001403

22. Tervahattu H, Juhanoja J, Vaida V, Tuck AF, Niemi JV, Kupiainen K, Kulmala M, Vehkamaki H (2005) Fatty acids on continental sulfate aerosol particles. J Geophys Res Atmos 110. doi:10.1029/2004JD005400

23. Takahama S, Liu S, Russell LM (2010) Coatings and clusters of carboxylic acids in carbon-containing atmospheric particles from spectromicroscopy and their implications for cloud-nucleating and optical properties. J Geophys Res Atmos 115. doi:10.1029/2009JD012622

24. Pfann WG, Olsen KM (1953) Purification and prevention of segregation in single crystals of germanium. Phys Rev 89:322–323

25. Asa-Awuku A, Sullivan AP, Hennigan CJ, Weber RJ, Nenes A (2008) Investigation of molar volume and surfactant characteristics of water-soluble organic compounds in biomass burning aerosol. Atmos Chem Phys 8:799–812

26. Cavalli F, Facchini MC, Decesari S, Mircea M, Emblico L, Fuzzi S, Ceburnis D, Yoon YJ, O'Dowd CD, Putaud JP, Dell'Acqua A (2004) Advances in characterization of size-resolved organic matter in marine aerosol over the North Atlantic. J Geophys Res Atmos 109. doi:10.1029/2004JD005137

27. Decesari S, Facchini MC, Mircea M, Cavalli F, Fuzzi S (2003) Solubility properties of surfactants in atmospheric aerosol and cloud/fog water samples. J Geophys Res Atmos 108:4685. doi:10.1029/2003JD003566

28. Facchini MC, Decesari S, Mircea M, Fuzzi S, Loglio G (2000) Surface tension of atmospheric wet aerosol and cloud/fog droplets in relation to their organic carbon content and chemical composition. Atmos Environ 34:4853–4857

29. Kiss G, Tombacz E, Hansson HC (2005) Surface tension effects of humic-like substances in the aqueous extract of tropospheric fine aerosol. J Atmos Chem 50:279–294

30. Salma I, Ocskay R, Varga I, Maenhaut W (2006) Surface tension of atmospheric humic-like substances in connection with relaxation, dilution, and solution pH. J Geophys Res Atmos 111:D23205. doi:10.1029/2005JD007015

31. Taraniuk I, Graber ER, Kostinski A, Rudich Y (2007) Surfactant properties of atmospheric and model humic-like substances (HULIS). Geophys Res Lett 34:L16807. doi:10.1029/2007GL029576

32. Facchini MC, Mircea M, Fuzzi S, Charlson RJ (1999) Cloud albedo enhancement by surface-active organic solutes in growing droplets. Nature 401:257–259

33. Mazurek AZ, Pogorzelski SJ, Kogut AD (2006) A novel approach for structure quantification of fatty acids films on rain water. Atmos Environ 40:4076–4087

34. Keene WC, Pszenny AAP, Maben JR, Stevenson E, Wall A (2004) Closure evaluation of size-resolved aerosol pH in the New England coastal atmosphere during summer. J Geophys Res Atmos 109:D23202. doi:10.1029/2004JD004801

35. Zhang Q, Jimenez JL, Worsnop DR, Canagaratna M (2007) A case study of urban particle acidity and its influence on secondary organic aerosol. Environ Sci Technol 41:3213–3219

36. Buajarern J, Mitchem L, Reid JP (2007) Characterizing the formation of organic layers on the surface of inorganic/aqueous aerosols by Raman spectroscopy. J Phys Chem A 111:11852–11859

37. Voss LF, Bazerbashi MF, Beekman CP, Hadad CM, Allen HC (2007) Oxidation of oleic acid at air/liquid interfaces. J Geophys Res Atmos 112:D06209. doi:10.1029/2006JD007677

38. Voss LF, Hadad CM, Allen HC (2006) Competition between atmospherically relevant fatty acid monolayers at the air/water interface. J Phys Chem B 110:19487–19490

39. King MD, Rennie AR, Thompson KC, Fisher FN, Dong CC, Thomas RK, Pfrang C, Hughes AV (2009) Oxidation of oleic acid at the air-water interface and its potential effects on cloud critical supersaturations. Phys Chem Chem Phys 11:7699–7707

40. Rogge WF, Mazurek MA, Hildemann LM, Cass GR, Simoneit BRT (1993) Quantification of urban organic aerosols at a molecular-level – identification, abundance and seasonal-variation. Atmos Environ Part A 27:1309–1330

41. Schauer JJ, Kleeman MJ, Cass GR, Simoneit BRT (2001) Measurement of emissions from air pollution sources. 3. C-1-C-29 organic compounds from fireplace combustion of wood. Environ Sci Technol 35:1716–1728

42. Simoneit BRT, Schauer JJ, Nolte CG, Oros DR, Elias VO, Fraser MP, Rogge WF, Cass GR (1999) Levoglucosan, a tracer for cellulose in biomass burning and atmospheric particles. Atmos Environ 33:173–182

43. Hildemann LM, Markowski GR, Cass GR (1991) Chemical composition of emissions from urban sources of fine organic aerosol. Environ Sci Technol 25:744–759

44. Meyers PA, Hites RA (1982) Extractable organic compounds in midwest rain and snow. Atmos Environ 16:2169–2175

45. Rogge WF, Hildemann LM, Mazurek MA, Cass GR, Simoneit BRT (1993) Sources of fine organic aerosol. 4. Particulate abrasion products from leaf surfaces of urban plants. Environ Sci Technol 27:2700–2711

46. Simoneit BRT (1977) Organic matter in eolian dusts over the Atlantic Ocean. Mar Chem 5:443–464

47. Simoneit BRT, Mazurek MA (1982) Organic-matter of the troposphere. 2. Natural background of biogenic lipid matter in aerosols over the rural Western United-States. Atmos Environ 16:2139–2159

48. Zhang Q, Anastasio C (2003) Free and combined amino compounds in atmospheric fine particles (PM2.5) and fog waters from Northern California. Atmos Environ 37:2247–2258

49. Fraser MP, Cass GR, Simoneit BRT (1999) Particulate organic compounds emitted from motor vehicle exhaust and in the urban atmosphere. Atmos Environ 33:2715–2724
50. Grosjean D, Vancauwenberghe K, Schmid JP, Kelley PE, Pitts JN (1978) Identification of C3-C10 aliphatic dicarboxylic-acids in airborne particulate matter. Environ Sci Technol 12:313–317
51. Kawamura K, Kaplan IR (1987) Motor exhaust emissions as a primary source for dicarboxylic-acids in Los-Angeles ambient air. Environ Sci Technol 21:105–110
52. Kawamura K, Ng LL, Kaplan IR (1985) Determination of organic acids (C1-C10) in the atmosphere, motor exhausts, and engine oils. Environ Sci Technol 19:1082–1086
53. Rogge WF, Hildemann LM, Mazurek MA, Cass GR, Simoneit BRT (1993) Sources of fine organic aerosol. 2. Noncatalyst and catalyst-equipped automobiles and heavy-duty diesel trucks. Environ Sci Technol 27:636–651
54. Rogge WF, Hildemann LM, Mazurek MA, Cass GR, Simoneit BRT (1993) Sources of fine organic aerosol. 3. Road dust, tire debris, and organometallic brake lining dust: roads as sources and sinks. Environ Sci Technol 27:1892–1904
55. Schauer JJ, Kleeman MJ, Cass GR, Simoneit BRT (1999) Measurement of emissions from air pollution sources. 2. C-1 through C-30 organic compounds from medium duty diesel trucks. Environ Sci Technol 33:1578–1587
56. Schauer JJ, Kleeman MJ, Cass GR, Simoneit BRT (2002) Measurement of emissions from air pollution sources. 5. C-1-C-32 organic compounds from gasoline-powered motor vehicles. Environ Sci Technol 36:1169–1180
57. Simoneit BRT (1985) Application of molecular marker analysis to vehicular exhaust for source reconciliations. Int J Environ Anal Chem 22:203–232
58. Sodeman D, Toner SM, Prather KA (2005) Determination of single particle mass spectral signatures from light-duty vehicle emissions. Environ Sci Technol 39:4569–4580
59. Warneck P (2003) In-cloud chemistry opens pathway to the formation of oxalic acid in the marine atmosphere. Atmos Environ 37:2423–2427
60. Cheng Y, Li SM, Leithead A, Brickell PC, Leaitch WR (2004) Characterizations of cis-pinonic acid and n-fatty acids on fine aerosols in the Lower Fraser Valley during Pacific 2001 Air Quality Study. Atmos Environ 38:5789–5800
61. He LY, Hu M, Huang XF, Yu BD, Zhang YH, Liu DQ (2004) Measurement of emissions of fine particulate organic matter from Chinese cooking. Atmos Environ 38:6557–6564
62. Robinson AL, Subramanian R, Donahue NM, Bernardo-Bricker A, Rogge WF (2006) Source apportionment of molecular markers and organic aerosol. 3. Food cooking emissions. Environ Sci Technol 40:7820–7827
63. Rogge WF, Hildemann LM, Mazurek MA, Cass GR, Simonelt BRT (1991) Sources of fine organic aerosol. 1. Charbroilers and meat cooking operations. Environ Sci Technol 25:1112–1125
64. Schauer JJ, Kleeman MJ, Cass GR, Simoneit BRT (1999) Measurement of emissions from air pollution sources. 1. C-1 through C-29 organic compounds from meat charbroiling. Environ Sci Technol 33:1566–1577
65. Schauer JJ, Kleeman MJ, Cass GR, Simoneit BRT (2002) Measurement of emissions from air pollution sources. 4. C-1-C-27 organic compounds from cooking with seed oils. Environ Sci Technol 36:567–575
66. Schauer JJ, Rogge WF, Hildemann LM, Mazurek MA, Cass GR (1996) Source apportionment of airborne particulate matter using organic compounds as tracers. Atmos Environ 30:3837–3855
67. Zhao Y, Hu M, Slanina S, Zhang Y (2007) Chemical compositions of fine particulate organic matter emitted from Chinese cooking. Environ Sci Technol 41:99–105
68. Barger WR, Garrett WD (1970) Surface active organic material in the marine atmosphere. J Geophys Res 75:4561–4566
69. Bezdek HF, Carlucci AF (1974) Concentration and removal of liquid microlayers from a seawater surface by bursting bubbles. Limnol Oceanogr 19:126–132

70. Garrett WD (1967) The organic chemical composition of the ocean surface. Deep Sea Res Oceanographic Abstracts 14:221–227

71. Gershey RM (1983) Characterization of seawater organic-matter carried by bubble-generated aerosols. Limnol Oceanogr 28:309–319

72. Kawamura K, Gagosian RB (1987) Implications of [omega]-oxocarboxylic acids in the remote marine atmosphere for photo-oxidation of unsaturated fatty acids. Nature 325:330–332

73. Keene WC, Maring H, Maben JR, Kieber DJ, Pszenny AAP, Dahl EE, Izaguirre MA, Davis AJ, Long MS, Zhou XL, Smoydzin L, Sander R (2007) Chemical and physical characteristics of nascent aerosols produced by bursting bubbles at a model air-sea interface. J Geophys Res Atmos 112:D21202. doi:10.1029/2007JD008464

74. Marty JC, Saliot A, Buat-Mqnard P, Chesselet R, Hunter KA (1979) Relationship between the lipid compositions of marine aerosols, the sea surface microlayer, and subsurface water. J Geophys Res 84:5707–5716

75. Mochida M, Kitamori Y, Kawamura K, Nojiri Y, Suzuki K (2002) Fatty acids in the marine atmosphere: factors governing their concentrations and evaluation of organic films on sea-salt particles. J Geophys Res Atmos 107:4325–4334

76. Morris RJ, Culkin F (1974) Lipid chemistry of eastern Mediterranean surface layers. Nature 250:640–642

77. O'Dowd CD, Facchini MC, Cavalli F, Ceburnis D, Mircea M, Decesari S, Fuzzi S, Yoon YJ, Putaud JP (2004) Biogenically driven organic contribution to marine aerosol. Nature 431:676–680

78. Fang J, Kawamura K, Ishimura Y, Matsumoto K (2002) Carbon isotopic composition of fatty acids in the marine aerosols from the Western North Pacific: implication for the source and atmospheric transport. Environ Sci Technol 36:2598–2604

79. Gagosian RB, Zafiriou OC, Peltzer ET, Alford JB (1982) Lipids in aerosols from the tropical North Pacific: temporal variability. J Geophys Res 87:11133–11144

80. Pankow JF (1994) An absorption-model of the gas aerosol partitioning involved in the formation of secondary organic aerosol. Atmos Environ 28:189–193

81. Seinfeld JH, Pankow JF (2003) Organic atmospheric particulate material. Ann Rev Phys Chem 54:121–140

82. Ervens B, Volkamer R (2010) Glyoxal processing by aerosol multiphase chemistry: towards a kinetic modeling framework of secondary organic aerosol formation in aqueous particles. Atmos Chem Phys 10:8219–8244

83. Nopmongcol U, Khamwichit W, Fraser MP, Allen DT (2007) Estimates of heterogeneous formation of secondary organic aerosol during a wood smoke episode in Houston. Texas Atmos Environ 41:3057–3070

84. Sareen N, Schwier AN, Shapiro EL, Mitroo DM, McNeill VF (2010) Secondary organic material formed by methylglyoxal in aqueous aerosol mimics. Atmos Chem Phys 10:997–1016

85. Schwier AN, Sareen N, Mitroo DM, Shapiro EL, McNeill VF (2010) Glyoxal-methylglyoxal cross-reactions in secondary organic aerosol formation. Environ Sci Technol 44:6174–6182

86. Shapiro EL, Szprengiel J, Sareen N, Jen CN, Giordano MR, McNeill VF (2009) Light-absorbing secondary organic material formed by glyoxal in aqueous aerosol mimics. Atmos Chem Phys 9:2289–2300

87. Tan Y, Carlton AG, Seitzinger SP, Turpin BJ (2010) SOA from methylglyoxal in clouds and wet aerosols: measurement and prediction of key products. Atmos Environ 44:5218–5226

88. Cole-Filipiak NC, O'Connor AE, Elrod MJ (2010) Kinetics of the hydrolysis of atmospherically relevant isoprene-derived hydroxy epoxides. Environ Sci Technol 44:6718–6723

89. Darer AI, Cole-Filipiak NC, O'Connor AE, Elrod MJ (2011) Formation and stability of atmospherically relevant isoprene-derived organosulfates and organonitrates. Environ Sci Technol 45:1895–1902

90. Eddingsaas NC, VanderVelde DG, Wennberg PO (2010) Kinetics and products of the acid-catalyzed ring-opening of atmospherically relevant butyl epoxy alcohols. J Phys Chem A 114:8106–8113

91. Surratt JD, Chan AWH, Eddingsaas NC, Chan MN, Loza CL, Kwan AJ, Hersey SP, Flagan RC, Wennberg PO, Seinfeld JH (2010) Reactive intermediates revealed in secondary organic aerosol formation from isoprene. Proc Natl Acad Sci USA 107:6640–6645

92. Chebbi A, Carlier P (1996) Carboxylic acids in the troposphere, occurrence, sources, and sinks: a review. Atmos Environ 30:4233–4249

93. Shulman ML, Jacobson MC, Carlson RJ, Synovec RE, Young TE (1996) Dissolution behavior and surface tension effects of organic compounds in nucleating cloud droplets. Geophys Res Lett 23:277–280

94. Tuckermann R (2007) Surface tension of aqueous solutions of water-soluble organic and inorganic compounds. Atmos Environ 41:6265–6275

95. Tuckermann R, Cammenga HK (2004) The surface tension of aqueous solutions of some atmospheric water-soluble organic compounds. Atmos Environ 38:6135–6138

96. Varga Z, Kiss G, Hansson HC (2007) Modelling the cloud condensation nucleus activity of organic acids on the basis of surface tension and osmolality measurements. Atmos Chem Phys 7:4601–4611

97. Asa-Awuku A, Nenes A, Gao S, Flagan RC, Seinfeld JH (2010) Water-soluble SOA from alkene ozonolysis: composition and droplet activation kinetics inferences from analysis of CCN activity. Atmos Chem Phys 10:1585–1597

98. George I, Abbatt JPD (2010) Heterogeneous oxidation of atmospheric aerosol particles by gas-phase radicals. Nat Chem 2:713–722

99. Altieri KE, Carlton AG, Lim HJ, Turpin BJ, Seitzinger SP (2006) Evidence for oligomer formation in clouds: reactions of isoprene oxidation products. Environ Sci Technol 40:4956–4960

100. Lim HJ, Carlton AG, Turpin BJ (2005) Isoprene forms secondary organic aerosol through cloud processing: model simulations. Environ Sci Technol 39:4441–4446

101. Gelencser A, Hoffer A, Kiss G, Tombacz E, Kurdi R, Bencze L (2003) In-situ formation of light-absorbing organic matter in cloud water. J Atmos Chem 45:25–33

102. Li Z, Schwier AN, Sareen N, McNeill VF (2011) Reactive processing of formaldehyde and acetaldehyde in aqueous aerosol mimics: surface tension depression and secondary organic products. Atmos Chem Phys 11:11617–11629

103. Nozière B, Ekstrom S, Alsberg T, Holmstrom S (2010) Radical-initiated formation of organosulfates and surfactants in atmospheric aerosols. Geophys Res Lett 37:L05806. doi:10.1029/2009GL041683

104. Surratt JD, Kroll JH, Kleindienst TE, Edney EO, Claeys M, Sorooshian A, Ng NL, Offenberg JH, Lewandowski M, Jaoui M, Flagan RC, Seinfeld JH (2007) Evidence for organosulfates in secondary organic aerosol. Environ Sci Technol 41:517–527

105. Archer RJ, La Mer VK (1955) The rate of evaporation of water through fatty acid monolayers. J Phys Chem 59:200–208

106. Rideal EK (1925) On the influence of surface films in the evaporation of water. J Phys Chem 29:1585–1588

107. Rosano HL, La Mer VK (1956) The rate of evaporation of water through monolayers of esters, acids, and alcohols. J Phys Chem 60:348–353

108. Anttila T, Kiendler-Scharr A, Tillman R, Mentel TF (2006) On the reactive uptake of gaseous compounds by organic-coated aqueous aerosols: theoretical analysis and application to the heterogeneous hydrolysis of N2O5. J Phys Chem A 110:10435–10443

109. Badger CL, Griffiths PT, George I, Abbatt JPD, Cox RA (2006) Reactive uptake of N2O5 by aerosol particles containing mixtures of humic acid and ammonium sulfate. J Phys Chem A 110:6986–6994

110. Escoreia EN, Sjostedt SJ, Abbatt JPD (2010) Kinetics of N2O5 hydrolysis on secondary organic aerosol and mixed ammonium bisulfate-secondary organic aerosol particles. J Phys Chem A 114:13113–13121

111. Folkers M, Mentel TF, Wahner A (2003) Influence of an organic coating on the reactivity of aqueous aerosols probed by the heterogeneous hydrolysis of N2O5. Geophys Res Lett 30:1644–1647

112. McNeill VF, Wolfe GM, Thornton JA (2007) The oxidation of oleate in submicron aqueous salt aerosols: evidence of a surface process. J Phys Chem A 111:1073–1083

113. McNeill VF, Patterson J, Wolfe GM, Thornton JA (2006) The effect of varying levels of surfactant on the reactive uptake of N2O5 to aqueous aerosol. Atmos Chem Phys 6:1635–1644

114. Rouviere A, Ammann M (2010) The effect of fatty acid surfactants on the uptake of ozone to aqueous halogenide particles. Atmos Chem Phys 10:11489–11500

115. Stemmler K, Vlasenko A, Guimbaud C, Ammann M (2008) The effect of fatty acid surfactants on the uptake of nitric acid to deliquesced NaCl aerosol. Atmos Chem Phys 8:5127–5141

116. Thornton JA, Abbatt JPD (2005) N2O5 reaction on sub-micron sea salt aerosol: effect of surface active organics. J Phys Chem A 109:10004–10012

117. Thornton JA, Braban CF, Abbatt JPD (2003) N2O5 hydrolysis on sub-micron organic aerosols: the effect of relative humidity, particle phase, and particle size. Phys Chem Chem Phys 5:4593–4603

118. Cosman LM, Bertram AK (2008) Reactive uptake of N2O5 on aqueous H2SO4 solutions coated with 1-component and 2-component monolayers. J Phys Chem A 112:4625–4635

119. Cosman LM, Knopf DA, Bertram AK (2008) N2O5 reactive uptake on aqueous sulfuric acid solutions coated with branched and straight-chain insoluble organic surfactants. J Phys Chem A 112:2386–2396

120. Knopf DA, Cosman LM, Mousavi P, Mokamati S, Bertram AK (2007) A novel flow reactor for studying reactions on liquid surfaces coated by organic monolayers: methods, validation, and initial results. J Phys Chem A 111:11021–11032

121. Chan MN, Lee AKY, Chan CK (2006) Responses of ammonium sulfate particles coated with glutaric acid to cyclic changes in relative humidity: hygroscopicity and Raman characterization. Environ Sci Technol 40:6983–6989

122. Cruz CN, Pandis SN (1998) The effect of organic coatings on the cloud condensation nuclei activation of inorganic atmospheric aerosol. J Geophys Res Atmos 103:13111–13123

123. Cruz CN, Pandis SN (2000) Deliquescence and hygroscopic growth of mixed inorganic–organic atmospheric aerosol. Environ Sci Technol 34:4313–4319

124. Glass SV, Park SC, Nathanson GM (2006) Evaporation of water and uptake of HCl and HBr through hexanol films at the surface of supercooled sulfuric acid. J Phys Chem A 110:7593–7601

125. Lawrence JR, Glass SV, Nathanson GM (2005) Evaporation of water through butanol films at the surface of supercooled sulfuric acid. J Phys Chem A 109:7449–7457

126. Lawrence JR, Glass SV, Park SC, Nathanson GM (2005) Surfactant control of gas uptake: effect of butanol films on HCl and HBr entry into supercooled sulfuric acid. J Phys Chem A 109:7458–7465

127. Park SC, Burden DK, Nathanson GM (2007) The inhibition of N2O5 hydrolysis in sulfuric acid by 1-butanol and 1-hexanol surfactant coatings. J Phys Chem A 111:2921–2929

128. Schofield RK, Rideal EK (1926) The kinetic theory of surface films – part II. Gaseous, expanded, and condensed films. Proc R Soc 110A:167–177

129. Myers D (1988) Surfactant science and technology. VCH, New York

130. Gilman JB, Vaida V (2006) Permeability of acetic acid through organic films at the air-aqueous interface. J Phys Chem A 110:7581–7587

131. Donaldson DJ, Vaida V (2006) The influence of organic films at the air-aqueous boundary on atmospheric processes. Chem Rev 106:1445–1461

132. Donaldson DJ, Valsaraj KT (2010) Adsorption and reaction of trace gas-phase organic compounds on atmospheric water film surfaces: a critical review. Environ Sci Technol 44:865–873

133. Kolb CE, Cox RA, Abbatt JPD, Ammann M, Davis EJ, Donaldson DJ, Garrett BC, George C, Griffiths PT, Hanson DR, Kulmala M, McFiggans G, Poschl U, Riipinen I, Rossi MJ, Rudich Y, Wagner PE, Winkler PM, Worsnop DR, O' Dowd CD (2010) An overview of current

issues in the uptake of atmospheric trace gases by aerosols and clouds. Atmos Chem Phys 10:10561–10605

134. Clifford D, Bartels-Rausch T, Donaldson DJ (2007) Suppression of aqueous surface hydrolysis by monolayers of short chain organic amphiphiles. Phys Chem Chem Phys 9:1362–1369

135. Park SC, Burden DK, Nathanson GM (2009) Surfactant control of gas transport and reactions at the surface of sulfuric acid. Acc Chem Res 42:379–387

136. Burden DK, Johnson AM, Nathanson GM (2009) HCl uptake through films of pentanoic acid and pentanoic acid/hexanol mixtures at the surface of sulfuric acid. J Phys Chem A 113:14131–14140

137. Dentener FJ, Crutzen PJ (1993) Reaction of N2O5 on tropospheric aerosols – impact on the global distributions of NOx, O3, and OH. J Geophys Res Atmos 98:7149–7163

138. Evans MJ, Jacob DJ (2005) Impact of new laboratory studies of N(2)O(5) hydrolysis on global model budgets of tropospheric nitrogen oxides, ozone, and OH. Geophys Res Lett 32. doi:10.1029/2005GL022469

139. Liao H, Seinfeld JH, Adams PJ, Mickley LJ (2004) Global radiative forcing of coupled tropospheric ozone and aerosols in a unified general circulation model. J Geophys Res Atmos 109. doi:10.1029/2003JD004456

140. Dash UN, Mohanty BK (1997) Thermodynamic functions of solutions of homologous dicarboxylic acids in water + acetone mixtures from surface tension measurements. Fluid Phase Equilibria 134:267–276

141. Ekström S, Nozière B, Hansson H-C (2009) The cloud condensation nuclei (CCN) properties of 2-methyltetrols and C3-C6 polyols from osmolality and surface tension measurements. Atmos Chem Phys 9:973–980

142. Hyvarinen AR, Lihavainen H, Gaman A, Vairila L, Ojala H, Kulmala M, Viisanen Y (2006) Surface tensions and densities of oxalic, malonic, succinic, maleic, malic, and cis-pinonic acids. J Chem Eng Data 51:255–260

143. Topping DO, McFiggans GB, Kiss G, Varga Z, Facchini MC, Decesari S, Mircea M (2007) Surface tensions of multi-component mixed inorganic/organic aqueous systems of atmospheric significance: measurements, model predictions and importance for cloud activation predictions. Atmos Chem Phys 7:2371–2398

144. Finlayson-Pitts BJ, Hemminger JC (2000) Physical chemistry of airborne sea salt particles and their components. J Phys Chem A 104:11463–11477

145. Krisch MJ, D'Auria R, Brown MA, Tobias DJ, Hemminger JC, Ammann M, Starr DE, Bluhm H (2007) The effect of an organic surfactant on the liquid–vapor interface of an electrolyte solution. J Phys Chem C 111:13497–13509

146. Clifford D, Donaldson DJ (2007) Direct experimental evidence for a heterogeneous reaction of ozone with bromide at the air-aqueous interface. J Phys Chem A 111:9809–9814

147. Brown SS, Ryerson TB, Wollny AG, Brock CA, Peltier R, Sullivan AP, Weber RJ, Dube WP, Trainer M, Meagher JF, Fehsenfeld FC, Ravishankara AR (2006) Variability in nocturnal nitrogen oxide processing and its role in regional air quality. Science 311:67–70

148. Bertram TH, Thornton JA, Riedel TP (2009) An experimental technique for the direct measurement of N2O5 reactivity on ambient particles. Atmos Meas Tech 2:231–242

149. Bertram TH, Thornton JA, Riedel TP, Middlebrook AM, Bahreini R, Bates TS, Quinn PK, Coffman DJ (2009) Direct observations of N2O5 reactivity on ambient aerosol particles. Geophys Res Lett 36:L19803. doi:10.1029/2009GL040248

150. Bertram TH, Thornton JA (2009) Toward a general parameterization of N(2)O(5) reactivity on aqueous particles: the competing effects of particle liquid water, nitrate and chloride. Atmos Chem Phys 9:8351–8363

151. Riemer N, Vogel H, Vogel B, Anttila T, Kiendler-Scharr A, Mentel TF (2009) Relative importance of organic coatings for the heterogeneous hydrolysis of N(2)O(5) during summer in Europe. J Geophys Res Atmos 114. doi:10.1029/2008JD011369

152. Smoydzin L, von Glasow R (2007) Do organic surface films on sea salt aerosols influence atmospheric chemistry? A model study. Atmos Chem Phys 7:5555–5567

153. Baker MB (1997) Cloud microphysics and climate. Science 276:1072–1078
154. Gavish M, Popovitzbiro R, Lahav M, Leiserowitz L (1990) Ice nucleation by alcohols arranged in monolayers at the surface of water drops. Science 250:973–975
155. Majewski J, Popovitzbiro R, Bouwman WG, Kjaer K, AlsNielsen J, Lahav M, Leiserowitz L (1995) The structural-properties of uncompressed crystalline monolayers of alcohols CnH2n + 1OH (n = 13–31) on water and their role as ice nucleators. Chem Eur J 1:304–311
156. Majewski J, Popovitzbiro R, Kjaer K, Alsnielsen J, Lahav M, Leiserowitz L (1994) Toward a determination of the critical size of ice nuclei – a demonstration by grazing-incidence X-ray-diffraction of epitaxial-growth of ice under the C31H63OH alcohol monolayer. J Phys Chem 98:4087–4093
157. Popovitzbiro R, Wang JL, Majewski J, Shavit E, Leiserowitz L, Lahav M (1994) Induced freezing of supercooled water into ice by self-assembled crystalline monolayers of amphiphilic alcohols at the air-water-interface. J Am Chem Soc 116:1179–1191
158. Seeley LH, Seidler GT (2001) Two-dimensional nucleation of ice from supercooled water. Phys Rev Lett 87:055702. doi:10.1103/PhysRevLett.87.055702
159. Ochshorn E, Cantrell W (2006) Towards understanding ice nucleation by long chain alcohols. J Chem Phys 124. doi:10.1063/1.2166368
160. Cantrell W, Robinson C (2006) Heterogeneous freezing of ammonium sulfate and sodium chloride solutions by long chain alcohols. Geophys Res Lett 33:L07802. doi:10.1029/2005GL024945
161. Zobrist B, Koop T, Luo BP, Marcolli C, Peter T (2007) Heterogeneous ice nucleation rate coefficient of water droplets coated by a nonadecanol monolayer. J Phys Chem C 111:2149–2155
162. Zobrist B, Marcolli C, Peter T, Koop T (2008) Heterogeneous ice nucleation in aqueous solutions: the role of water activity. J Phys Chem A 112:3965–3975
163. Knopf DA, Forrester SM (2011) Freezing of water and aqueous NaCl droplets coated by organic monolayers as a function of surfactant properties and water activity. J Phys Chem A 115:5579–5591
164. Corrigan CE, Novakov T (1999) Cloud condensation nucleus activity of organic compounds: a laboratory study. Atmos Environ 33:2661–2668
165. Cruz CN, Pandis SN (1997) A study of the ability of pure secondary organic aerosol to act as cloud condensation nuclei. Atmos Environ 31:2205–2214
166. Henning S, Rosenorn T, D'Anna B, Gola AA, Svenningsson B, Bilde M (2005) Cloud droplet activation and surface tension of mixtures of slightly soluble organics and inorganic salt. Atmos Chem Phys 5:575–582
167. Prenni AJ, DeMott PJ, Kreidenweis SM, Sherman DE, Russell LM, Ming Y (2001) The effects of low molecular weight dicarboxylic acids on cloud formation. J Phys Chem A 105:11240–11248
168. Raymond TM, Pandis SN (2003) Formation of cloud droplets by multicomponent organic particles. J Geophys Res Atmos 108:4469. doi:10.1029/2003JD003503
169. Raymond TM, Pandis SN (2002) Cloud activation of single-component organic aerosol particles. J Geophys Res Atmos 107:4787. doi:10.1029/2002JD002159
170. Liu PSK, Leaitch WR, Banic CM, Li SM, Ngo D, Megaw WJ (1996) Aerosol observations at Chebogue Point during the 1993 North Atlantic Regional Experiment: relationships among cloud condensation nuclei, size distribution, and chemistry. J Geophys Res Atmos 101:28971–28990
171. Kohler H (1936) The nucleus in the growth of hygroscopic droplets. Trans Faraday Soc 32:1152–1161
172. Seinfeld JH, Pandis SN (2006) Atmospheric chemistry and physics: from air pollution to climate change, 2nd edn. Wiley, New York
173. Chuang PY, Charlson RJ, Seinfeld JH (1997) Kinetic limitations on droplet formation in clouds. Nature 390:594–596
174. Nenes A, Ghan S, Abdul-Razzak H, Chuang PY, Seinfeld JH (2001) Kinetic limitations on cloud droplet formation and impact on cloud albedo. Tellus B 53:133–149

175. Kulmala M, Laaksonen A, Korhonen P, Vesala T, Ahonen T, Barrett JC (1993) The effect of atmospheric nitric acid vapor on cloud condensation nucleus activation. J Geophys Res 98:22949–22958
176. Laaksonen A, Korhonen P, Kulmala M, Charlson RJ (1998) Modification of the Köhler equation to include soluble trace gases and slightly soluble substances. J Atmos Sci 55:853–862
177. Topping D, McFiggans G (2012) Tight coupling of particle size, number and composition in atmospheric cloud droplet activation. Atmos Chem Phys 12:3253–3260
178. Padró LT, Asa-Awuku A, Morrison R, Nenes A (2007) Inferring thermodynamic properties from CCN activation experiments: single-component and binary aerosols. Atmos Chem Phys 7:5263–5274
179. Kulmala M, Laaksonen A, Charlson RJ, Korhonen P (1997) Clouds without supersaturation. Nature 388:336–337
180. Petters MD, Kreidenweis SM (2007) A single parameter representation of hygroscopic growth and cloud condensation nucleus activity. Atmos Chem Phys 7:1961–1971
181. Washburn, E.W. (1926–1930;2003). International Critical Tables of Numerical Data, Physics, Chemistry and Technology (1st Electronic Edition). Knovel. Online version available at: http://www.knovel.com/web/portal/browse/display?_EXT_KNOVEL_DISPLAY_bookid= 735&VerticalID=0
182. Dutcher CS, Wexler AS, Clegg SL (2010) Surface tensions of inorganic multicomponent aqueous electrolyte solutions and melts. J Phys Chem A 114:12216–12230
183. Hu Y-F, Lee H (2004) Prediction of the surface tension of mixed electrolyte solutions based on the equation of Patwardhan and Kumar and the fundamental Butler equations. J Colloid Interface Sci 269:442–448
184. Li ZB, Li YG, Lu JF (1999) Surface tension model for concentrated electrolyte aqueous solutions by the Pitzer equation. Ind Eng Chem Res 38:1133–1139
185. Li ZB, Lu BCY (2001) Surface tension of aqueous electrolyte solutions at high concentrations – representation and prediction. Chem Eng Sci 56:2879–2888
186. Hu J, Zhang X, Wang Z (2010) A review on progress in QSPR studies for surfactants. Int J Mol Sci 11:1020–1047
187. Setschenow JZ (1889) Uber Die Konstitution Der Salzosungen auf Grund ihres Verhaltens zu Kohlensaure. Z Physik Chem 4:117–125
188. Matijevic E, Pethica BA (1958) The properties of ionized monolayers, part 1. Sodium dodecyl sulfate at the air/water interface. Trans Faraday Soc 54:1383–1389
189. Adamson AW, Gast AP (1997) Physical chemistry of surfaces, 6th edn. Wiley, New York
190. Booth AM, Topping DO, McFiggans G, Percival CJ (2009) Surface tension of mixed inorganic and dicarboxylic acid aqueous solutions at 298.15 K and their importance for cloud activation predictions. Phys Chem Chem Phys 11:8021–8028
191. Fainerman VB, Miller R (2001) Simple method to estimate surface tension of mixed surfactant solutions. J Phys Chem B 105:11432–11438
192. Fainerman VB, Miller R, Aksenenko EV (2002) Simple model for prediction of surface tension of mixed surfactant solutions. Adv Colloid Interface Sci 96:339–359
193. Hitzenberger R, Berner A, Kasper-Giebl A, Loflund M, Puxbaum H (2002) Surface tension of Rax cloud water and its relation to the concentration of organic material. J Geophys Res 107:4752. doi:10.1029/2002JD002506
194. Barger WR, Garrett WD (1976) Surface active organic material in air over the Mediterranean and over the eastern equatorial Pacific. J Geophys Res 81:3151–3157
195. Seidl W, Hänel G (1983) Surface-active substances on rainwater and atmospheric particles. Pure Appl Geophys 121:1077–1093
196. Capel PD, Gunde R, Zuercher F, Giger W (1990) Carbon speciation and surface tension of fog. Environ Sci Technol 24:722–727
197. Moore RH, Ingall ED, Sorooshian A, Nenes A (2008) Molar mass, surface tension, and droplet growth kinetics of marine organics from measurements of CCN activity. Geophys Res Lett 35:L07801. doi:10.1029/2008GL033350

198. Graber ER, Rudich Y (2006) Atmospheric HULIS: how humic-like are they? A comprehensive and critical review. Atmos Chem Phys 6:729–753
199. Chen Y, Schnitzer M (1978) The surface tension of aqueous solutions of soil humic substances. Soil Sci 125:7–15
200. Anderson MA, Hung AYC, Mills D, Scott MS (1995) Factors affecting the surface tension of soil solutions and solutions of humic acids. Soil Sci 160:111–116
201. Yates LM, von Wandruszka R (1999) Effects of pH and metals on the surface tension of aqueous humic materials. Soil Sci Soc Am J 63:1645–1649
202. Aumann E, Tabazadeh A (2008) Rate of organic film formation and oxidation on aqueous drops. J Geophys Res Atmos 113:D23205. doi:10.1029/2007JD009738
203. Klavins M, Purmalis O (2010) Humic substances as surfactants. Environ Chem Lett 8:349–354
204. Aumann E, Hildemann LM, Tabazadeh A (2010) Measuring and modeling the composition and temperature-dependence of surface tension for organic solutions. Atmos Environ 44:329–337
205. Frosch M, Prisle NL, Bilde M, Varga Z, Kiss G (2011) Joint effect of organic acids and inorganic salts on cloud droplet activation. Atmos Chem Phys 11:3895–3911
206. Terashima M, Fukushima M, Tanaka S (2004) Influence of pH on the surface activity of humic acid: micelle-like aggregate formation and interfacial adsorption. Colloids Surf A 247:77–83
207. Hagenhoff K, Dong J, Chowdhry B, Leharne S (2010) Aqueous solution of anionic surfactants mixed with soils show a synergistic reduction in surface tension. Water Air Soil Pollut 209:3–13
208. Gaman AI, Kulmala M, Vehkamaki H, Napari I, Mircea M, Facchini MC, Laaksonen A (2004) Binary homogeneous nucleation in water-succinic acid and water-glutaric acid systems. J Chem Phys 120:282
209. Vanhanen J, Hyvarinen A-P, Anttila T, Viisanen Y, Lihavainen H (2008) Ternary solution of sodium chloride, succinic acid, and water – surface tension and its influence on cloud droplet activation. Atmos Chem Phys 8:4595–4604
210. Riipinen I, Koponen IK, Frank GP, Hyvärinen AP, Vanhanen J, Lihavainen H, Lehtinen KEJ, Bilde M, Kulmala M (2007) Adipic and malonic acid aqueous solutions: surface tensions and saturation vapor pressures. J Phys Chem A 111:12995–13002
211. Langmuir I (1917) The shapes of group molecules forming the surfaces of liquids. Proc Natl Acad Sci USA 3:251–257
212. Langmuir I (1917) The constitution and fundamental properties of solids and liquids. J Am Chem Soc 39:1848–1906
213. De Mul MNG, Davis HT, Evans DF, Bhave AV, Wagner JR (2000) Solution phase behavior and solid phase structure of long-chain sodium soap mixtures. Langmuir 16:8276–8284
214. Johann R, Vollhardt D (1999) Texture features of long-chain fatty acid monolayers at high pH of the aqueous subphase. Mater Sci Eng C 8–9:35–42
215. Slauenwhite DE, Johnson BD (1996) Effect of organic matter on bubble surface tension. J Geophys Res 101:3769–3774
216. Schwier AN, Mitroo DM, McNeill VF (2012) Surface tension depression by low-solubility organic material in aqueous aerosol mimics. Atmos Environ 54:495–500
217. McNeill VF, Yattavelli RLN, Thornton JA, Stipe CB, Landgrebe O (2008) The heterogeneous OH oxidation of palmitic acid in single component and internally mixed aerosol particles: vaporization, secondary chemistry, and the role of particle phase. Atmos Chem Phys 8:5465–5476
218. Svenningsson B, Rissler J, Swietlicki E, Mircea M, Bilde M, Facchini MC, Decesari S, Fuzzi S, Zhou J, Mønster J, Rosenørn T (2006) Hygroscopic growth and critical supersaturations for mixed aerosol particles of inorganic and organic compounds of atmospheric relevance. Atmos Chem Phys 6:1937–1952
219. Grosjean D (1982) Formaldehyde and other carbonyl in Los Angeles ambient air. Environ Sci Technol 16:254–262

220. Novakov T, Penner JE (1993) Large contribution of organic aerosols to cloud-condensation-nuclei concentrations. Nature 365:823–826
221. Rivera-Carpio CA, Corrigan CE, Novakov T, Penner JE, Rogers CF, Chow JC (1996) Derivation of contributions of sulfate and carbonaceous aerosols to cloud condensation nuclei from mass size distributions. J Geophys Res Atmos 101:19483–19493
222. Novakov T, Corrigan CE (1996) Cloud condensation nucleus activity of the organic component of biomass smoke particles. Geophys Res Lett 23:2141–2144
223. Mochida M, Kuwata M, Miyakawa T, Takegawa N, Kawamura K, Kondo Y (2006) Relationship between hygroscopicity and cloud condensation nuclei activity for urban aerosols in Tokyo. J Geophys Res Atmos 111:D23204. doi:10.1029/2005JD006980
224. Lance S, Nenes A, Mazzoleni C, Dubey MK, Gates H, Varutbangkul V, Rissman TA, Murphy SM, Sorooshian A, Flagan RC, Seinfeld JH, Feingold G, Jonsson HH (2009) Cloud condensation nuclei activity, closure, and droplet growth kinetics of Houston aerosol during the Gulf of Mexico Atmospheric Composition and Climate Study (GoMACCS). J Geophys Res Atmos 114:D00F15. doi:10.1029/2004JD004596
225. Broekhuizen K, Kumar PP, Abbatt JPD (2004) Partially soluble organics as cloud condensation nuclei: role of trace soluble and surface active species. Geophys Res Lett 31:L01107. doi:10.1029/2003GL018203
226. Shilling JE, King SM, Mochida M, Worsnop DR, Martin ST (2007) Mass spectral evidence that small changes in composition caused by oxidative aging processes alter aerosol CCN properties. J Phys Chem A 111:3358–3368
227. Schwier AN, Sareen N, Lathem T, Nenes A, McNeill VF (2011) Ozone oxidation of oleic acid films decreases aerosol CCN activity. J Geophys Res Atmos 116. doi:10.1029/2010JD015520
228. VanReken TM, Ng NL, Flagan RC, Seinfeld JH (2005) Cloud condensation nucleus activation properties of biogenic secondary organic aerosol. J Geophys Res 110. doi:10.1029/2004JD005465
229. Varutbangkul V, Brechtel FJ, Bahreini R, Ng NL, Keywood MD, Kroll JH, Flagan RC, Seinfeld JH, Lee A, Goldstein AH (2006) Hygroscopicity of secondary organic aerosols formed by oxidation of cycloalkenes, monoterpenes, sesquiterpenes, and related compounds. Atmos Chem Phys 6:2367–2388
230. Dinar E, Taraniuk I, Graber ER, Katsman S, Moise T, Anttila T, Mentel TF, Rudich Y (2006) Cloud condensation nuclei properties of model and atmospheric HULIS. Atmos Chem Phys 6:2465–2482
231. Dinar E, Taraniuk I, Graber ER, Anttila T, Mentel TF, Rudich Y (2007) Hygroscopic growth of atmospheric and model humic-like substances. J Geophys Res Atmos 112:D05211. doi:10.1029/2006JD007442
232. Wex H, Hennig T, Salma I, Ocskay R, Kiselev A, Henning S, Massling A, Wiedensohler A, Stratmann F (2007) Hygroscopic growth and measured and modeled critical super-saturations of an atmospheric HULIS sample. Geophys Res Lett 34:L02818. doi:10.1029/2006GL028260
233. Fors EO, Rissler J, Massling A, Svenningsson B, Andreae MO, Dusek U, Frank GP, Hoffer A, Bilde M, Kiss G, Janitsek S, Henning S, Facchini MC, Decesari S, Swietlicki E (2010) Hygroscopic properties of Amazonian biomass burning and European background HULIS and investigation of their effects on surface tension with two models linking H-TDMA to CCNC data. Atmos Chem Phys 10:5625–5639
234. Riipinen I, Koponen IK, Frank GP, Hyvaerinen AP, Vanhanen J, Lihavainen H, Lehtinen KEJ, Bilde M, Kulmala M (2007) Adipic and malonic acid aqueous solutions: surface tensions and saturation vapor pressures. J Phys Chem A 111:12995–13002
235. Pradeep Kumar P, Broekhuizen K, Abbatt JPD (2003) Organic acids as cloud condensation nuclei: laboratory studies of highly soluble and insoluble species. Atmos Chem Phys 3:509–520
236. Hori M, Ohta S, Murao N, Yamagata S (2003) Activation capability of water soluble organic substances as CCN. J Aerosol Sci 34:419–448

237. Abbatt JPD, Broekhuizen K, Kumal PP (2005) Cloud condensation nucleus activity of internally mixed ammonium sulfate/organic acid aerosol particles. Atmos Environ 39:4767–4778

238. Sareen N, Schwier AN, Lathem T, Nenes A, McNeill VF (2012) Gas-phase surfactants may enhance aerosol cloud nucleation. In press, Proc. Natl. Acad. Sci. USA

239. Kroll JH, Ng NL, Murphy SM, Varutbangkul V, Flagan RC, Seinfeld JH (2005) Chamber studies of secondary organic aerosol growth by reactive uptake of simple carbonyl compounds. J Geophys Res Atmos 110:D23207. doi:10.1029/2005JD006004

240. Betterton EA, Hoffmann MR (1988) Henry's law constants of some environmentally important aldehydes. Environ Sci Technol 22:1415–1418

241. Djikaev YS, Tabazadeh A (2003) Effect of adsorption on the uptake of organic trace gas by cloud droplets. J Geophys Res Atmos 108:4869. doi:10.1029/2003JD003741

242. Good N, Topping DO, Allan JD, Flynn M, Fuentes E, Irwin M, Williams PI, Coe H, McFiggans G (2010) Consistency between parameterisations of aerosol hygroscopicity and CCN activity during the RHaMBLe discovery cruise. Atmos Chem Phys 10:3189–3203

243. Irwin M, Good N, Crosier J, Choularton TW, McFiggans G (2010) Reconciliation of measurements of hygroscopic growth and critical supersaturation of aerosol particles in central Germany. Atmos Chem Phys 10:11737–11752

244. Asa-Awuku A, Nenes A (2007) Effect of solute dissolution kinetics on cloud droplet formation: extended Köhler theory. J Geophys Res Atmos 112:D22201. doi:10.1029/2005JD006934

245. Seidl W (2000) Model for a surface film of fatty acids on rain water and aerosol particles. Atmos Environ 34:4917–4932

246. Prisle NL, Asmi A, Topping D, Partanen AI, Romakkaniemi S, Dal Maso M, Kulmala M, Laaksonen A, Lehtinen KEJ, McFiggans G, Kokkola H (2012) Surfactant effects in global simulations of cloud droplet activation. Geophys Res Lett 39:L05802. doi:10.1029/2011GL050467

247. Chakraborty P, Zachariah MR (2007) "Effective" negative surface tension: a property of coated nanoaerosols relevant to the atmosphere. J Phys Chem A 111:5459–5464

248. Chakraborty P, Zachariah MR (2008) Sticking coefficient and processing of water vapor on organic-coated nanoaerosols. J Phys Chem A 112:966–972

249. Chakraborty P, Zachariah MR (2011) On the structure of organic-coated water droplets: from "net water attractors" to "oily" drops. J Geophys Res 116:D21205. doi:10.1029/2011JD015961

250. Hede T, Li X, Leck C, Tu Y, Ågren H (2011) Model HULIS compounds in nanoaerosol clusters - investigations of surface tension and aggregate formation using molecular dynamics simulations. Atmos Chem Phys 11:6549–6557

251. Li X, Hede T, Tu Y, Leck C, Ågren H (2011) Glycine in aerosol water droplets: a critical assessment of Köhler theory by predicting surface tension from molecular dynamics simulations. Atmos Chem Phys 11:519–527

252. Li X, Hede T, Tu Y, Leck C, Ågren H (2011) Amino acids in atmospheric droplets: perturbation of surfact tension and critical supersaturation predicted by computer simulations. Atmos Chem Phys Discuss 11:30919–30947

253. Li X, Hede T, Tu Y, Leck C, Ågren H (2010) Surface-active cis-pinonic acid in atmospheric droplets: a molecular dynamics study. J Phys Chem Lett 1:769–773

254. Ma X, Chakraborty P, Henz BJ, Zachariah MR (2011) Molecular dynamic simulation of dicarboxylic acid coated aqueous aerosol: structure and processing of water vapor. Phys Chem Chem Phys 13:9374–9384

255. Takahama S, Russell LM (2011) A molecular dynamics study of water mass accommodation on condensed phase water coated by fatty acid monolayers. J Geophys Res Atmos 116. doi:10.1029/2010JD014842

256. Kokkola H, Sorjamaa R, Peraniemi A, Raatikainen T, Laaksonen A (2006) Cloud formation of particles containing humic-like substances. Geophys Res Lett 33:L10816. doi:10.1029/2006GL026107

257. Li Z, Williams AL, Rood MJ (1998) Influence of soluble surfactant properties on the activation of aerosol particles containing inorganic solute. J Atmos Sci 55:1859–1866

258. Prisle NL, Dal Maso M, Kokkola H (2011) A simple representation of surface active organic aerosol in cloud droplet formation. Atmos Chem Phys 11:4073–4083

259. Prisle NL, Raatikainen T, Laaksonen A, Bilde M (2010) Surfactants in cloud droplet activation: mixed organic–inorganic particles. Atmos Chem Phys 10:5663–5683

260. Prisle NL, Raatikainen T, Sorjamaa R, Svenningsson B, Laaksonen A, Bilde M (2008) Surfactant partitioning in cloud droplet activation: a study of C8, C10, C12 and C14 normal fatty acid sodium salts. Tellus B 60:416–431

261. Raatikainen T, Laaksonen A (2011) A simplified treatment of surfactant effects on cloud drop activation. Geosci Model Dev 4:107–116

262. Sorjamaa R, Laaksonen A (2006) The influence of surfactant properties on critical supersaturations of cloud condensation nuclei. J Aerosol Sci 37:1730–1736

263. Sorjamaa R, Svenningsson B, Raatikainen T, Henning S, Bilde M, Laaksonen A (2004) The role of surfactants in Kohler theory reconsidered. Atmos Chem Phys 4:2107–2117

264. Romakkaniemi S, Kokkola H, Smith JN, Prisle NL, Schwier AN, McNeill VF, Laaksonen A (2011) Partitioning of semivolatile surface-active compounds between bulk, surface, and gas-phase. Geophys Res Lett 38:L03807. doi:10.1029/2010GL046147

265. Topping D (2010) An analytical solution to calculate bulk mole fractions for any number of components in aerosol droplets after considering partitioning to a surface layer. Geosci Model Dev 3:635–642

266. Ghan SJ, Chung CC, Penner JE (1993) A parameterization of cloud droplet nucleation part I: single aerosol type. Atmos Res 30:198–221

267. Abdul-Razzak H, Ghan SJ, Carpio CR (1998) A parameterization of aerosol activation 1. Single aerosol type. J Geophys Res Atmos 103:6123–6131

268. Abdul-Razzak H, Ghan SJ (2000) A parameterization of aerosol activation 2. Multiple aerosol types. J Geophys Res Atmos 105:6837–6844

269. Phinney LA, Lohmann U, Leaitch WR (2003) Limitations of using an equilibrium approximation in an aerosol activation parameterization. J Geophys Res Atmos 108:4371. doi:10.1029/2002JD002391

270. Anttila T, Kerminen VM (2002) Influence of organic compounds on the cloud droplet activation: a model investigation considering the volatility, water solubility, and surface activity of organic matter. J Geophys Res 107:4662. doi:10.1029/2001JD001482

271. Nenes A, Charlson RJ, Facchini MC, Kulmala M, Laaksonen A, Seinfeld JH (2002) Can chemical effects on cloud droplet number rival the first indirect effect? Geophys Res Lett 29:1848. doi:10.1029/2002GL015295

272. Rissman TA, Nenes A, Seinfeld JH (2004) Chemical amplification (or dampening) of the Twomey effect: conditions derived from droplet activation theory. J Atmos Sci 61:919–930

273. Ervens B, Feingold G, Kreidenweis SM (2005) Influence of water-soluble organic carbon on cloud drop number concentration. J Geophys Res Atmos 110:D18211. doi:10.1029/2004JD005634

274. Feingold G, Chuang PY (2002) Analysis of the influence of film-forming compounds on droplet growth: implications for cloud microphysical processes and climate. J Atmos Sci 59:2006–2018

275. Lance S, Nenes A, Rissman TA (2004) Chemical and dynamical effects on cloud droplet number: implications for estimates of the aerosol indirect effect. J Geophys Res Atmos 109:D22208. doi:10.1029/2004JD004596

276. Khvorostyanov VI, Curry JA (2008) Kinetics of cloud drop formation and its parameterization for cloud and climate models. J Atmos Sci 65:2784–2802

277. Asa-Awuku A, Engelhart GJ, Lee BH, Pandis SN, Nenes A (2009) Relating CCN activity, volatility, and droplet growth kinetics of beta-caryophyllene secondary organic aerosol. Atmos Chem Phys 9:795–812

278. Engelhart GJ, Asa-Awuku A, Nenes A, Pandis SN (2008) CCN activity and droplet growth kinetics of fresh and aged monoterpene secondary organic aerosol. Atmos Chem Phys 8:3937–3949

279. Shantz NC, Leaitch WR, Caffrey PF (2003) Effect of organics of low solubility on the growth rate of cloud droplets. J Geophys Res Atmos 108. doi:10.1029/2002JD002540

280. Hegg DA, Gao S, Hoppel W, Frick G, Caffrey P, Leaitch WR, Shantz N, Ambrusko J, Albrechcinski T (2001) Laboratory studies of the efficiency of selected organic aerosols as CCN. Atmos Res 58:155–166

281. Bilde M, Svenningsson B (2004) CCN activation of slightly soluble organics: the importance of small amounts of inorganic salt and particle phase. Tellus B 56:128–134

282. Garland RM, Wise ME, Beaver MR, Dewitt HL, Aiken AC, Jimenez JL, Tolbert MA (2005) Impact of palmitic acid coating on the water uptake and loss of ammonium sulfate particles. Atmos Chem Phys 5:1951–1961

283. Andrews E, Larson SM (1993) Effect of surfactant layers on the size changes of aerosol-particles as a function of relative-humidity. Environ Sci Technol 27:857–865

284. Chang RYW, Liu PSK, Leaitch WR, Abbatt JPD (2007) Comparison between measured and predicted CCN concentrations at Egbert, Ontario: focus on the organic aerosol fraction at a semi-rural site. Atmos Environ 41:8172–8182

285. Shantz NC, Chang RYW, Slowik JG, Vlasenko A, Abbatt JPD, Leaitch WR (2010) Slower CCN growth kinetics of anthropogenic aerosol compared to biogenic aerosol observed at a rural site. Atmos Chem Phys 10:299–312

286. Ruehl CR, Chuang PY, Nenes A (2008) How quickly do cloud droplets form on atmospheric particles? Atmos Chem Phys 8:1043–1055

287. Ruehl CR, Chuang PY, Nenes A (2009) Distinct CCN activation kinetics above the marine boundary layer along the California coast. Geophys Res Lett 36. doi:10.1029/2009GL038839

288. Murphy SM, Agrawal H, Sorooshian A, Padró LT, Gates H, Hersey S, Welch WA, Jung H, Miller JW, Cocker DR, Nenes A, Jonsson HH, Flagan RC, Seinfeld JH (2009) Comprehensive simultaneous shipboard and airborne characterization of exhaust from a modern container ship at sea. Environ Sci Technol 43:4626–4640

289. Padró LT, Tkacik D, Lathem T, Hennigan CJ, Sullivan AP, Weber RJ, Huey LG, Nenes A (2010) Investigation of cloud condensation nuclei properties and droplet growth kinetics of the water-soluble aerosol fraction in Mexico City. J Geophys Res 115:D09204. doi:10.1029/2009JD013195

290. Fridlind AM, Jacobson MZ (2000) A study of gas-aerosol equilibrium and aerosol pH in the remote marine boundary layer during the first aerosol characterization experiment (ACE 1). J Geophys Res Atmos 105:17325–17340

291. Keene WC, Savoie DL (1998) The pH of deliquesced sea-salt aerosol in polluted marine air. Geophys Res Lett 25:2181–2184

292. Pszenny AAP, Moldanov J, Keene WC, Sander R, Maben JR, Martinez M, Crutzen PJ, Perner D, Prinn RG (2004) Halogen cycling and aerosol pH in the Hawaiian marine boundary layer. Atmos Chem Phys 4:147–168

293. Takahama S, Davidson CI, Pandis SN (2006) Semicontinuous measurements of organic carbon and acidity during the Pittsburgh air quality study: implications for acid-catalyzed organic aerosol formation. Environ Sci Technol 40:2191–2199

294. Tang IN, Munkelwitz HR (1994) Water activities, densities, and refractive-indexes of aqueous sulfates and sodium-nitrate droplets of atmospheric importance. J Geophys Res Atmos 99:18801–18808

295. Tang IN, Tridico AC, Fung KH (1997) Thermodynamic and optical properties of sea salt aerosols. J Geophys Res Atmos 102:23269–23275

296. Kroll JH, Donahue NM, Jimenez JL, Kessler SH, Canagaratna MR, Wilson KR, Altieri KE, Mazzoleni LR, Wozniak AS, Bluhm H, Mysak ER, Smith JD, Kolb CE, Worsnop DR (2011) Carbon oxidation state as a metric for describing the chemistry of atmospheric organic aerosol. Nat Chem 3:133–139

297. Yatavelli RLN, Thornton JA (2010) Particulate organic matter detection using a micro-orifice volatilization impactor coupled to a chemical ionization mass spectrometer (MOVI-CIMS). Aerosol Sci Technol 44:67–74
298. Russell LM, Bahadur R, Ziemann PJ (2011) Identifying organic aerosol sources by comparing functional group composition in chamber and atmospheric particles. Proc Natl Acad Sci USA 108:3516–3521
299. McFiggans G, Artaxo P, Baltensperger U, Coe H, Facchini MC, Feingold G, Fuzzi S, Gysel M, Laaksonen A, Lohmann U, Mentel TF, Murphy DM, O'Dowd CD, Snider JR, Weingartner E (2006) The effect of physical and chemical aerosol properties on warm cloud droplet activation. Atmospheric Chemistry and Physics 6: 2593–2649.

Index